EXTENDED ABSTRACTS

of the 4th International Congress of
Croatian Society of Mechanics

held in Bizovac, Croatia
September 18-20, 2003

CIP – Katalogizacija u publikaciji
Nacionalna i sveučilišta knjižnica, Zagreb

UDK 531 / 534 (063)

INTERNATIONAL Congress of Croatian Society of Mechanics
(4 ; 2003 ; Bizovac)
Extended Abstracts of the
4thInternational Congress of Croatian Society of Mechanics held in Bizovac,
September 18-20, 2003. / edited by Franjo Matejiček.
Zagreb: Croatian Society of Mechanics, 2003.

Bibliografija iza svakog rada.

ISBN 953 - 96243 – 4 – 7

I. Mehanika -- Zbornik

430905170

Edited by
Franjo Matejiček

Published by

CROATIAN SOCIETY OF MECHANICS
Head Office:
Faculty of Mechanical Engineering and Naval Architecture
University of Zagreb
Ivana Lučića 5, HR-10000 Zagreb, Croatia

Design by:
Franjo Matejiček

Printed by:
"Grafika" Osijek, Croatia

Issues: 150

ISBN 953-96243-4-7

4th INTERNATIONAL CONGRESS OF CROATIAN SOCIETY OF MECHANICS

ORGANIZING COMMITTEE

Ivo ALFIREVIC	University of Zagreb
Nenad BICANIC	University of Glasgow
Lidija FRGIC	University of Zagreb
Dražan KOZAK	University of Osijek
Ivica KOŽAR	University of Rijeka
Pavao MAROVIC	University of Split
Franjo MATEJICEK	University of Osijek, President
Jurica SORIC	University of Zagreb
Vicko ŠIMIC	University of Zagreb
Zdravko VIRAG	University of Zagreb

Organiser of the Congress:

CROATIAN SOCIETY OF MECHANICS
Head Office:
Faculty of Mechanical Engineering and Naval Architecture
University of Zagreb
Ivana Lučića 5, HR-10000 Zagreb, Croatia
http://www.csm.hr

Secretary's Office
Jasminka Biondić
Faculty of Mechanical Engineering and Naval Architecture
University of Zagreb
Ivana Lučića 5, HR-10000 Zagreb, Croatia
☏ +385-1-61 68 540
Fax –385-1-61 68 187
e-mail: jasna.biondic@csm.hr

CENTRAL EUROPEAN ASSOCIATION FOR COMPUTATIONAL MECHANICS
(CEACM)

Under the auspices of

The Ministry of Science and Technology of the Republic of Croatia

The Extended Abstracts and Full-text Paper on CD-ROM
was Published with the support of

The Ministry of Science and Technology of the Republic of Croatia

Sponsored by:

University of Zagreb
Faculty of Mechanical Engineering and Naval Architecture in Zagreb
Faculty of Civil Engineering in Zagreb

University J.J. Strossmayer in Osijek
Mechanical Engineering Falculty in Slavonski Brod
Faculty of Civil Engineering in Osijek

University of Rijeka
Technical Faculty in Rijeka
Faculty of Civil Engineering in Rijeka

University of Split
Faculty of Electrical Engineering, Mechanical Engineering and
Naval Architecture in Split
Faculty of Civil Engineering in Split

INTERNATIONAL SCIENTIFIC COMMITTEE

Ivo ALFIREVIĆ	University of Zagreb
Nenad BIĆANIĆ	University of Glasgow
Claudio BORRI	University of Florence
René de BORST	Delft University of Technology
Josip BRNIĆ	University of Rijeka
James W. DALLY	University of Maryland
Elmar FICKER	Technical University München
Alessandro FREDDI	University of Bologna
Stjepan JECIĆ	University of Zagreb
Vinko JOVIĆ	University of Split
Michal KLEIBER	Polish Academy of Sciences, Warsaw
Vladimir KOMPIŠ	University of Žilina
Ivica KOŽAR	University of Rijeka
Wilfried B. KRÄTZIG	Ruhr - University of Bochum
Željan LOZINA	University of Split
Herbert A. MANG	Vienna Technical University
Pavao MAROVIĆ	University of Split
Franjo MATEJIČEK	University of Osijek
Ante MIHANOVIĆ	University of Split
Zoran MRŠA	University of Rijeka
Osman MUFTIĆ	University of Zagreb
Maks OBLAK	University of Maribor
Eugenio OŃATE	Polytechnic University of Catalonia
Roger J. OWEN	University of Wales, Swansea
Bernhard SCHREFLER	University of Padua
Jurica SORIĆ	University of Zagreb
Yoichi SUMI	Yokohama National University
Vicko ŠIMIĆ	University of Zagreb
Leopold ŠKERGET	University of Maribor
Boris ŠTOK	University of Ljubljana
Masao TOYODA	University of Osaka
Nikola VRANKOVIĆ	University of Zagreb
Michael P. WNUK	University of Wisconsin - Milwaukee
Peter WRIGGERS	University of Hannover

INTERNATIONAL REVIEW COMMITTEE

Ivo ALFIREVIĆ	University of Zagreb
Mirko HUSNJAK	University of Zagreb
Stjepan JECIĆ	University of Zagreb
Ivica KOŽAR	University of Rijeka
Željan LOZINA	University of Split
Pavao MAROVIĆ	University of Split
Franjo MATEJIČEK	University of Osijek
Zoran MRŠA	University of Rijeka
Maks OBLAK	University of Maribor
Zdravko VIRAG	University of Zagreb
Damir SEMENSKI	University of Zagreb
Ivo SENJANOVIĆ	University of Zagreb
Vladimir SIGMUND	University of Osijek
Luka SOPTA	University of Rijeka
Jurica SORIĆ	University of Zagreb
Leopold ŠKERGET	University of Maribor

P R E F A C E

The 4th International Congress of Croatian Society of Mechanics, which is organized by Croatian Society of Mechanics and Central European Association for Computational Mechanics (CEACM), is the fourth in the series of organized gathering of scientists and researchers in the field of general mechanics, mechanics of solids, mechanics of fluid and computational mechanics.

These Extended abstracts contains 4 invited lectures and 80 extended abstracts as well as attached CD-ROM with all of 84 session papers presented at the Congress in Hotel Termia in Bizovac during the period September 18 -20, 2003.

The overwhelming majority of papers deals with topics of computational mechanics but the papers from other areas of mechanics are included, too. Although, all contributing papers have been reviewed, they are printed and writhed from camera-ready copies supplied by the authors and the editors cannot accept responsibility for any errors or inconsistencies contained in the papers.

Editors and organizers are very grateful to all reviewers and participants for their contributions in making this Congress a success. They also wish to thank our sponsors for their financial support and all those who helped in any way in organizing this Congress.

Franjo Matejiček

Zagreb, September 2003.

CONTENTS

Invited lectures

Session papers

Invited lectures

4th International Congress
of Croatian Society of Mechanics
September, 18-20, 2003
Bizovac, Croatia

4thICCSM

NUMERICAL MODELING AND IMPLEMENTATION OF R-C FRACTURING THROUGH THE FEM

Claudio Borri, Luca Salvatori and Wolfhard Zahlten

Keywords: Fracture Mechanics, Finite Element Method, Reinforced Concrete.

Abstract

This contribution deals with the specific FE formulations of two distinct three-dimensional continuum models for the simulation of fracturing in concrete and quasi-brittle materials: an isotropic scalar damage model (SDM) and a rotating crack model (RCM).

According to the isotropic SDM, the loss of integrity of the material is controlled through a single scalar parameter. The resulting damaged stiffness tensor is a scalar multiple of the elastic stiffness tensor, so it decreases proportionally in every direction, independently of the direction of the loading. On the other hand, the RCM reproduces the anisotropic behaviour of cracking. The implemented version allows the formation of up to three mutually orthogonal cracks, which keep aligned with the principal directions (of both stresses and strains).

For both models, some implementation devices and numerical algorithms (also useful for other constitutive laws) are described. The models are implemented into an 8-node isoparametric volume element and tested in the analysis of simple but representative structures, for which experimental tests and different numerical simulations are available.

1. Introduction

The present paper, originated within a thorough study for a final degree thesis [5], deals with the modelling of fracturing concrete, through the Finite Element Method.

The non-linearities of reinforced-concrete result from the non-linear behaviour of its individual components and of their interaction (concrete cracking in tension, concrete plasticity in compression, steel plasticity, etc.). In the present study, the attention focuses on concrete behaviour and in particular on cracking (even though the models are formulated in such a way as to easily allow the combination of cracking and plasticity). In particular, two different cracking concrete continuum models, namely a single parameter isotropic damage model (SDM) and a rotating crack model (RCM), are analysed, developed and implemented into an existing modular computer program (FEMAS, Finite Element Modulus of Arbitrary Structures, Ruhr-Universität Bochum, Germany). These models are of interest not only for concrete but also for other – so-called quasi-brittle – materials (such as masonry, rocks and some kind of soils), which are frequently used by civil engineers.

2. Physical parameters characterizing tensional cracking

Cracking and consequent loose of mechanical properties occur due to the proliferation and the coalescence of micro-defects and micro-voids, which exist in concrete even before the application of any external action. The directions of principal local stresses are unpredictable because of the randomness of heterogeneity but, on a larger scale, experimental tests have shown that macro-cracks open on the plane orthogonal to the maximum principal nominal (average) stress.

2.1 Uni-axial traction test

In the material models of the present study, the three-dimensional fracturing behaviour of concrete is traced back to the uni-dimensional behaviour, which can be more easily deduced from experimental uni-axial traction tests. The traction-separation law (fig. 2a), relating the stress σ to the fracture opening w, is considered the true physical (gauge-independent) property of the fracturing material. The experimental traction-separation curve can be analytically expressed, e.g. by means of an exponential function

$$\sigma = f_{\mathrm{w}}(w) = f_{\mathrm{t}} \exp\left(-w/w_{\mathrm{G}}\right) \tag{1}$$

whose characterizing physical parameters are the tensile strength f_{t} and the specific fracture energy G_{t} (i.e. the area under the traction-separation curve). The parameter $w_{\mathrm{G}} = G_{\mathrm{t}}/f_{\mathrm{t}}$ is evaluated by imposing the correct energy dissipation.

2.2 Definition of strain during fracturing

Due to the cracking-zone localization, it is indeed not possible to give a physically meaningful definition of strain during fracturing, as it depends on the length along which it is measured. Therefore, experiments always deal with elongations. On the other hand, continuum constitutive models need to define strain-like quantities, which could be obtained by choosing a characteristic length h, along which to smear the elongations. In FE analysis, h is usually the actual finite element length projected along the considered direction. In this study, the dependence of h on the direction is neglected and an equivalent element size $h = \sqrt[3]{V_{\mathrm{elem}}}$ is assumed, where the volume of the element V_{elem} is computed through Gauss' numerical integration.

3. Isotropic Scalar Damage Model (SDM)

The isotropic SDM represents the simplest version of the damage model and the immediate extension of the uni-axial case to a general three-dimensional stress state. The loss of integrity is controlled through a single scalar parameter and the resulting damaged stiffness tensor is a scalar multiple of the elastic stiffness tensor, so it decreases proportionally in every direction, independently of the direction of the loading. As the isotropic linear elastic material is characterized by two scalars (usually Young's modulus E and Poisson's ratio ν), the most general isotropic SDM should deal with two independent parameters. For the presented single-parameter version, Poisson's ratio is assumed as constant.

3.1 Hypothesis

The basic assumptions of the isotropic SDM are the following:

1) Damage is isotropic and it does not affect Poisson's ratio, i.e. the damaged material stresses $\boldsymbol{\sigma}$ are obtained by multiplying the bulk material stresses $\boldsymbol{\sigma}_{\mathrm{b}}$ by the scalar factor $1-\omega$:

$$\boldsymbol{\sigma} = (1-\omega)\boldsymbol{\sigma}_{\mathrm{b}} \tag{2}$$

The damage parameter ω represents a scalar measure of the damage level. Initially, it is set to 0 for the undamaged material, then it starts increasing as soon as the elastic limit is reached, growing asymptotically to the limit value of 1, which corresponds to the completely damaged material, unable to transmit any stress (fig. 1c).

2) Bulk material is isotropic linear elastic:

$$\boldsymbol{\sigma}_{\mathrm{b}} = \mathbf{D}_{\mathrm{e}}\boldsymbol{\varepsilon} \tag{3}$$

where $\mathbf{D}_{\mathrm{e}}$ is the isotropic linear elasticity tensor and $\boldsymbol{\varepsilon}$ is the strain tensor. The combination of tensional cracking and compressive plasticity can be introduced by modifying this relationship.

3) Damage evolution is characterized by a dependence of the damage parameter on the applied strain. In order to automatically take into account the unloading-reloading conditions

(assuming linear unloading-reloading without residual deformation), the damage parameter is chosen as a function

$$\omega = \omega(\kappa) \tag{4}$$

of the strain tensor through the maximum strain level reached in the material history κ.

4) The damage increases monotonically (no "repairing" is allowed):

$$\kappa(t) = \max_{\tau \le t} \varepsilon_{\text{eq}}(\tau) \tag{5}$$

is the maximum historically reached value at time t (not necessary the physical time) of the equivalent strain ε_{eq}, which is a scalar measure of the reached strain-level.

5) A strain-tensor "norm" is provided:

$$\varepsilon_{\text{eq}} = \varepsilon_{\text{eq}}(\boldsymbol{\varepsilon}) \tag{6}$$

The way equivalent strain ε_{eq} is defined affects the shape of the elastic domain. As concrete fracture grows mainly when the material is stretched, only the positive normal strains $\varepsilon_{\text{eq}}^{\text{pos}}(\boldsymbol{\varepsilon}) = \left\| \langle \boldsymbol{\varepsilon} \rangle \right\| = \sqrt{\sum_{I=1}^{3} \langle \varepsilon_I \rangle^2}$ should be taken into account (fig. 1a). In this study, Rankine's criterion of maximum principal stress is used and the equivalent strain is defined as $\varepsilon_{\text{eq}}^{\text{Rank}} = \frac{1}{E} \max_{I=1,2,3} \langle \sigma_{\text{b},I} \rangle$ (fig. 1b). In the previous formulas, ε_I and $\sigma_{\text{b},I}$ are the I^{th} principal strain and principal bulk-stress respectively and the angular brackets denote the "positive part" operator, i.e. $\langle x \rangle = \max(0, x)$.

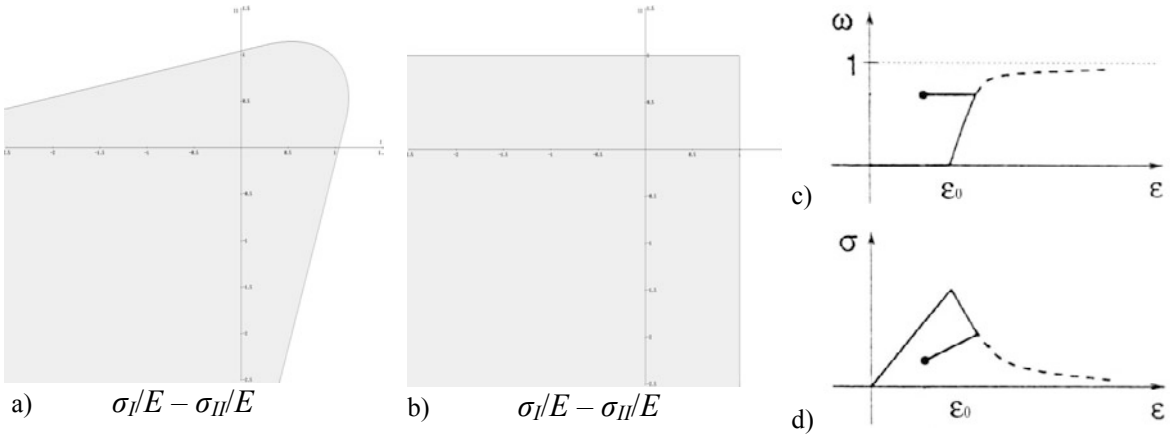

Figure 1: Young-modulus-normalized 2-D elastic domain shapes for $\varepsilon_{\text{eq}}^{\text{pos}} = 1$ (a) and $\varepsilon_{\text{eq}}^{\text{Rank}} = 1$ (b) in principal stress space, for $\nu = 0.2$. Evolution of the damage parameter for the uni-axial test (c) and corresponding stress-strain diagram (d).

3.2 Damage evolution law

In order to keep the model as simple as possible, a stress-strain relationship is explicitly defined, instead of deducing it from (1), as it will be done for the RCM, and an exponential softening is chosen (fig. 1d):

$$\sigma = \begin{cases} E\varepsilon & \text{if } \varepsilon \le \varepsilon_0 \\ f_{\text{t}} \exp\left(-\dfrac{\varepsilon - \varepsilon_0}{\varepsilon_{\text{G}}} \right) & \text{if } \varepsilon > \varepsilon_0 \end{cases} \tag{7}$$

where $\varepsilon_0 = f_{\text{t}}/E$ is the strain at elastic limit and the value of ε_{G} can be determined by imposing the correct energy dissipation. Comparing (7) with the uni-axial version of damage model $\sigma = (1-\omega)E\varepsilon$ (and substituting κ to uni-axial strain ε), the damage evolution law

$$\omega(\kappa)=\begin{cases}0 & \text{if } \kappa \le \varepsilon_0 \\ 1-\dfrac{\varepsilon_0}{\kappa}\exp\left(-\dfrac{\kappa-\varepsilon_0}{\varepsilon_G}\right) & \text{if } \kappa > \varepsilon_0\end{cases} \tag{8}$$

is obtained. Imposing the correct energy dissipation and smearing the strain along the crack-band width h, the parameter $\varepsilon_G = \dfrac{G_t - G_e}{f_t h}$ can be evaluated, where $G_{el} = f_t \varepsilon_0 / 2$ is the energy at the elastic limit.

3.3 Formulation and implementation

The formulation and the implementation of the isotropic SDM are straightforward from the hypothesis, as an explicit stress-strain relationship can be obtained by successive substitution of (6), (5), (4), (3) and (2).

4. Rotating Crack Model (RCM)

The basic idea of the RCM is to keep the principal axis of stresses and strains aligned and to allow the cracks to rotate with them. In this way, each crack always opens in pure mode-I, being only subjected to normal stress and normal strain, and the relationship obtained for uni-axial case is sufficient for the description of the model. The objections about the physical meaning of "crack rotation" have been overtaken in [2]. In the following description, the formulation presented in [3] is considered.

4.1 Hypothesis

The RCM is based on the following assumption:

1) Strains $\boldsymbol{\varepsilon}$ are decomposed into a bulk material part $\boldsymbol{\varepsilon}_b$ and a cracking part $\boldsymbol{\varepsilon}_c$:
$$\boldsymbol{\varepsilon} = \boldsymbol{\varepsilon}_b + \boldsymbol{\varepsilon}_c \tag{9}$$
2) Bulk material behaves as isotropic linear elastic, i.e. stresses $\boldsymbol{\sigma}$ are related to bulk-material strains through linear elasticity tensor (the combination with plasticity modifies this hypothesis):
$$\boldsymbol{\sigma} = \mathbf{D}_e \boldsymbol{\varepsilon}_b \tag{10}$$
3) Cracking strains are produced by up to three mutually orthogonal cracks, which keep aligned with the principal directions (of both stresses and strains):
$$\boldsymbol{\varepsilon}_c = \mathbf{T}_n^T \mathbf{e}_c \tag{11}$$
4) For the i^{th} principal direction, the principal cracking strain e_i^c is assumed to depend only on the relevant principal stress s_i (and on its history). This relationship can be expressed through a function $e_i^c = g_i(s_i)$, which describes all the possible material statuses (namely uncracked, softening and unloading-reloading). In vector notation, it reads:
$$\mathbf{e}_c = \mathbf{g}(\mathbf{s}) = \left[g_1(s_1), g_2(s_2), g_3(s_3)\right]^T \tag{12}$$

In the previous formulas $\mathbf{e}_c = \left[e_1^c, e_2^c, e_3^c\right]^T$ and $\mathbf{s} = \left[s_1, s_2, s_3\right]^T$ denote the 3-component column vector of principal cracking strains and principal stresses respectively and

$$\mathbf{T}_n^T = \begin{bmatrix} n_{11}^2 & n_{12}^2 & n_{13}^2 & n_{11}n_{12} & n_{12}n_{13} & n_{13}n_{11} \\ n_{21}^2 & n_{22}^2 & n_{23}^2 & n_{21}n_{22} & n_{22}n_{23} & n_{23}n_{21} \\ n_{31}^2 & n_{32}^2 & n_{33}^2 & n_{31}n_{32} & n_{32}n_{33} & n_{33}n_{31} \end{bmatrix} \tag{13}$$

is the transformation matrix for second order tensors from principal coordinates into global coordinates, being n_{ij} the j^{th} component of the i^{th} principal unit-vector in the global coordinate system.

4.2 Formulation

Rewriting (9) in principal coordinates and substituting the normal components of inverted (10) and of (12) leads to:

$$\mathbf{e} = \tilde{\mathbf{C}}_{\mathrm{e}}\mathbf{s} + \mathbf{g}(\mathbf{s}) \tag{14}$$

where $\mathbf{e}$ is the principal strains vector and $\tilde{\mathbf{C}}_{\mathrm{e}}$ is the 3×3 normal component sub-matrix of the elastic compliance. Equations (14) are in general non-linear, so they must be linearized and an iterative solution is required. At the n^{th}, incremental step, $\boldsymbol{\varepsilon}^{(n)}$ (and consequently $\mathbf{e}^{(n)}$) is given and the corresponding $\mathbf{s}^{(n)}$ must be computed. From the $(n\text{-}1)^{\mathrm{th}}$ step, both $\mathbf{e}^{(n-1)}$ and $\mathbf{s}^{(n-1)}$ are known. Assuming as first tentative value $\mathbf{s}^{(n,0)} = \mathbf{s}^{(n-1)}$, the linearized (14) $\mathbf{e}^{(n)} = \tilde{\mathbf{C}}_{\mathrm{e}}\left(\mathbf{s}^{(n,0)} + \delta\mathbf{s}^{(1)}\right) + \mathbf{g}\left(\mathbf{s}^{(n,0)}\right) + \tilde{\mathbf{C}}_{\mathrm{c}}\left(\mathbf{s}^{(n,0)}\right)\delta\mathbf{s}^{(1)}$ can be obtained, where

$$\tilde{\mathbf{C}}_{\mathrm{c}}\left(\mathbf{s}^{(n,0)}\right) = \left.\frac{\partial\mathbf{g}}{\partial\mathbf{s}}\right|_{\mathbf{s}^{(n,0)}} = \begin{bmatrix} \mathrm{d}g_1/\mathrm{d}s_1\left(s_1^{(n,0)}\right) & 0 & 0 \\ 0 & \mathrm{d}g_2/\mathrm{d}s_2\left(s_2^{(n,0)}\right) & 0 \\ 0 & 0 & \mathrm{d}g_3/\mathrm{d}s_3\left(s_3^{(n,0)}\right) \end{bmatrix} \tag{15}$$

denotes the normal component sub-matrix of cracking compliance. Introducing the normal block of the tangent material stiffness matrix in principal coordinates $\tilde{\mathbf{D}}_{\mathbf{n}}\left(\mathbf{s}^{(n,0)}\right) = \left(\tilde{\mathbf{C}}_{\mathrm{e}} + \tilde{\mathbf{C}}_{\mathrm{c}}\left(\mathbf{s}^{(n,0)}\right)\right)^{-1}$, the principal stress correction $\delta\mathbf{s}^{(1)} = \tilde{\mathbf{D}}_{\mathrm{n}}^{(0)}\delta\mathbf{e}^{(0)}$ can be computed from the increment of principal strains $\delta\mathbf{e}^{(0)} = \mathbf{e}^{(n)} - \tilde{\mathbf{C}}_{\mathrm{e}}\mathbf{s}^{(n,0)} - \mathbf{g}\left(\mathbf{s}^{(n,0)}\right)$. Therefore, the updated tentative principal stresses $\mathbf{s}^{(n,1)}=\mathbf{s}^{(n,0)}+\delta\mathbf{s}^{(1)}$ can be computed. The iterative procedure:

$$\left.\begin{aligned} \delta\mathbf{s}^{(i)} &= \left(\tilde{\mathbf{C}}_{\mathrm{e}} + \tilde{\mathbf{C}}_{\mathrm{c}}\left(\mathbf{s}^{(n,i-1)}\right)\right)^{-1}\left(\mathbf{e}^{(n)} - \tilde{\mathbf{C}}_{\mathrm{e}}\mathbf{s}^{(n,i-1)} - \mathbf{g}\left(\mathbf{s}^{(n,i-1)}\right)\right) \\ \mathbf{s}^{(n,i)} &= \mathbf{s}^{(n,i-1)} + \delta\mathbf{s}^{(i)} \end{aligned}\right\} \quad i = 1,2,\ldots \tag{16}$$

can be repeated until the desired precision δs_{toll} is obtained, i.e. $\left\|\delta\mathbf{s}^{(i)}\right\| < \delta s_{\mathrm{toll}}$. Finally, the stress vector is transformed into global coordinates:

$$\boldsymbol{\sigma} = \mathbf{T}_{\mathrm{n}}\mathbf{s} \tag{17}$$

4.3 Relationship between principal cracking strain and principal stress

Considering the i^{th} principal direction, the functions $e_i^{\mathrm{c}} = g_i\left(s_i\right)$ of (12) have to distinguish the different material statuses (fig. 2b). The analysis begins with undamaged material and no cracking strain is present:

$$g_i^{\mathrm{uncracked}}\left(s_i\right) = 0 \tag{18}$$

As soon as the principal stress s_i reaches the tensile strength, a crack opens and g_i describes the softening law. Assuming constant cracking strains over the finite element, i.e. $e_i^{\mathrm{c}} = w_i/h_i$, and considering (1), during softening

$$g_i^{\mathrm{softening}}\left(s_i\right) = f_{\mathrm{w}}^{-1}\left(s_i\right)/h_i \tag{19}$$

holds.

During unloading and reloading a linear law without residual deformations is assumed (keeping in mind that crack surfaces can not overlap):

$$g_i^{\text{un-/re-loading}}\left(s_i\right) = \begin{cases} \left(e_i^{\mathrm{c,max}}/s_i^{\max}\right)s_i & \text{if } s_i > 0 \\ 0 & \text{if } s_i < 0 \end{cases} \tag{20}$$

As the stress is unknown, also the material status cannot be known in advance. In particular, to decide whether a softening direction keeps in softening or starts unloading, an additional assumption-

verification loop must be provided. At the beginning of each iterative step (16), "softening" status is assumed for each previously-softening direction and the relevant g_i is evaluated accordingly. As during both softening and unloading stress should decrease, a positive stress correction means a wrong assumption. So, if a previously-softening direction exhibits a positive stress correction, the material status for that direction must be changed to "unloading" and the iterative step must be repeated.

On the other hand, if a direction status is "unloading-reloading", positive stress corrections are allowed (reloading), unless the total stress exceeds the maximum previously-reached softening stress. In that case, and the status switches to "softening" again.

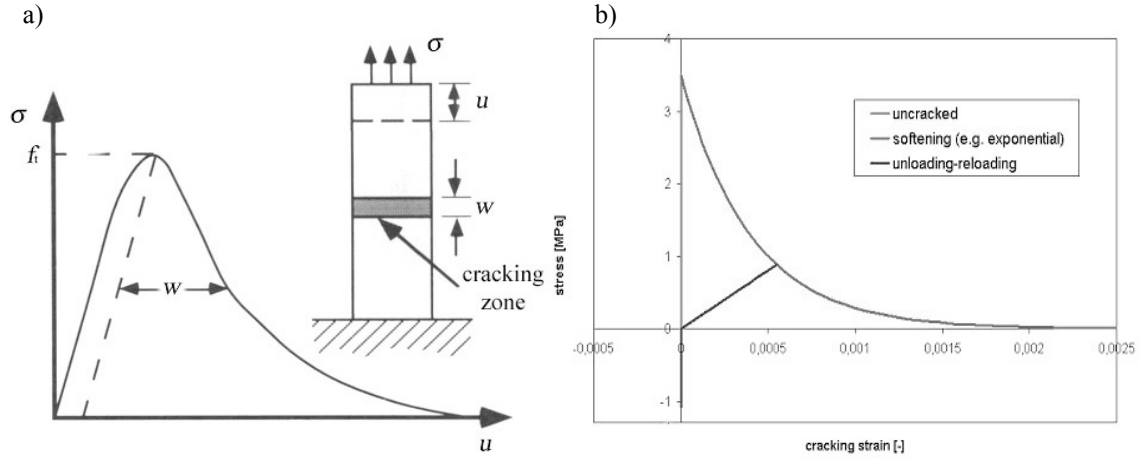

Figure 2: Uni-axial traction test and typical stress-elongation diagram (a). Diagram of the relationship between stress and cracking strain, illustrating the possible material statuses (b).

4.4 Implementation and computational devices

To compute the stress vector the following steps have been implemented:

1. From the given strains $\boldsymbol{\varepsilon}$, the principal directions (i.e. n_{ij}) and the principal strains $\mathbf{e}$ are computed.
2. The current principal directions are compared with those at previous step and, if necessary, reordered in such a way as to maximize the scalar products (in absolute value) of the current principal unit-vectors and the relevant ones at the previous step. If a scalar product is negative, the sign of the current unit-vector is changed.
3. The iterative procedure begins:
   3.1. For each principal direction, an assumption on material status is made.
   3.2. The principal stresses correction $\delta\mathbf{s}$ is evaluated, accordingly with the assumptions.
   3.3. For each principal direction, the material-status assumption is checked and, if necessary, modified.
   3.4. If at least one assumption is changed, the program flow jumps to 3.2.
   3.5. The principal stresses $\mathbf{s}$ are updated.
   3.6. The convergence criterion is checked and, if it is not satisfied, another iteration begins.
4. The stress vector is rotated into global coordinate system through (17).
5. The stress vector and the principal directions are stored as "old" values for next subroutine-call.

5. Numerical example

The developed constitutive laws hold for each material point of the continuum. The FE formulation aims at substituting the infinite number of material points by a finite numerically manageable number of sampling points. Thus, non-linear equations are evaluated only at the integration points and a "homogeneous crack state" is postulated in their neighbourhood. Therefore, a crack opening at an integration point in the numerical model should not be confused with a fracture observed in

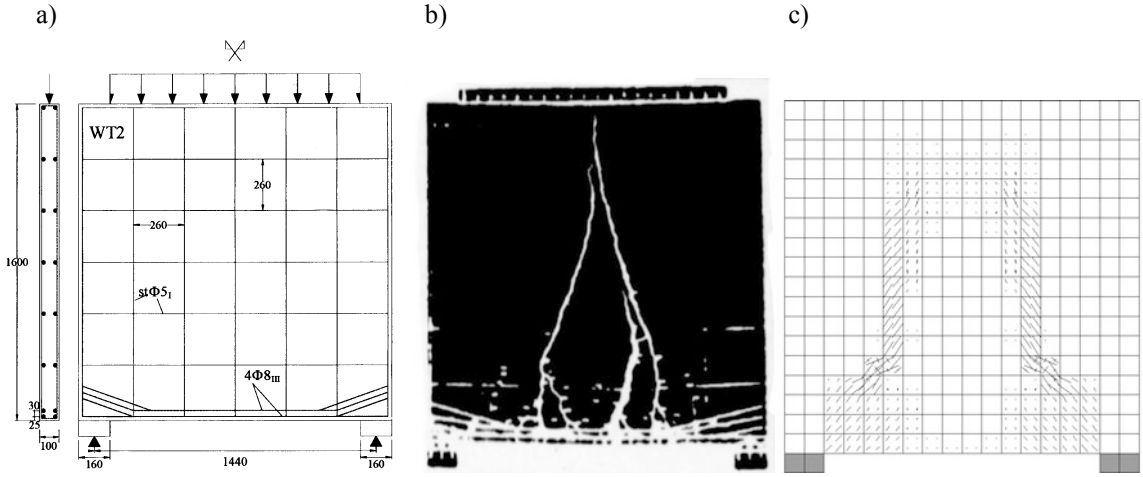

Figure 3: Geometry of Leonhardt and Walther's "WT3" deep beam (a); comparison between experimental cracking (b) and numerical simulation with the RCM (c).

an experimental test: a zone of cracked integration points defines instead a region where a macroscopically visible crack is likely to open in the actual structure.

In this study, a standard 8-node isoparametric element has been used for implementing the material models, with a $2\times2\times2$ integration scheme. The non-linear static analysis have followed an incremental-iterative procedure.

The deep beam "WT3" (fig. 3a), experimentally tested by Leonhardt and Walther [4], has been modelled and analyzed. For this structure, comparison with different numerical modelling (i.e. fixed crack modelling through the code DIANA) is also available [1]. The uniform load has been applied through constant increments (both in the experiment and in the numerical analysis).

For the modelling of concrete, both isotropic SDM and RCM have been tested. For the modelling of reinforcements, the discrete approach, with the assumptions of perfect bond and of negligible plasticity in steel, has been adopted. Consequently, the reinforcement bars have been modelled through 2-node linear elastic truss elements, which share the nodes with the three-dimensional continuum elements modelling concrete. The material parameters used for the model are $E_c = 24000\,\mathrm{N/mm^2}$, $\nu = 0.2$, $f_t = 3.65\,\mathrm{N/mm^2}$ and $G_f = 60\,\mathrm{J/m^2}$ for concrete and $E_s = 210000\,\mathrm{N/mm^2}$ and $\nu = 0.3$ for steel.

Numerical cracking scheme at failure for the RCM (fig. 3c) substantially matches with the experimental cracking path (fig. 3b).

Comparing the load-displacement diagrams (fig. 4) as from the experimental test and from different numerical analysis, it appears that all numerical models initially overestimate the actual

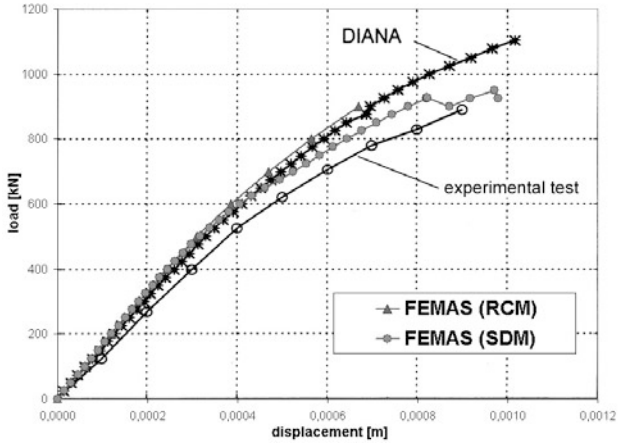

Figure 4: Load-displacement diagram for the "WT3" deep beam: comparison between experimental results and simulations with DIANA (fixed crack model) and FEMAS (SDM and RCM).

stiffness (likely because of an overestimated concrete Young's modulus). After cracking, the RCM and the fixed crack model of DIANA behave almost identically, whereas the SDM shows a faster softening due to the isotropy of the damage. In the isotropic SDM, the elements with wide opening cracks are indeed virtually removed from the structure (as their stiffness is multiplied by a vanishing factor), while they should keep transferring normal stresses parallel to the crack plane.

6. Concluding remarks

Two different continuum models for the FE analysis of fracturing concrete have been analyzed, developed and numerically tested.
The single-parameter isotropic SDM proved to be very fast in the analysis (because of its explicit expression for the stress tensor, which does not require additional iterations) and numerically very stable, even in advanced cracking stage.

The RCM presents a more complicate formulation and implementation and it requires several numerical devices (principal direction re-ordering, iterative stress-evaluation procedure, material-status assumption-verification loop) but it shows a more consistent behaviour. Its continuum formulation allows indeed the implementation into standard FE codes and its properties can be defined from the uni-axial test.

Future steps of this research work will focus on the development of different more sophisticated fracturing models (e.g. with discontinuities embedded in the element shape-functions), on the combination of tension cracking with compression plasticity, as well as on the development of element-embedded reinforcements capable of bond-slip simulation.

References

[1] Angotti, F., Galano, L., Orlando, M. and Vignoli, A., Modellazione agli elementi finiti di strutture in c.a. in campo non lineare, in *Bollettino Ingegneri*, n. 7-8 and 9 (1997).

[2] Bažant, Z, Comment on Orthotropic Models for Concrete and Geomaterials, in *Journal of Engineering Mechanics*, n. 109, ASCE (1983), 849-865.

[3] Jirásek, M. and Zimmermann, T., Analysis of Rotating Crack Model, in *Journal of Engineering Mechanics*, vol. 124, ASCE (1998), 842-851.

[4] Leonhardt, F. and Walther, R., Wandartige Träger, *Deutscher Ausschuss für Stahlbeton*, n. 178, Berlin (1966).

[5] Salvatori, L., *Modelli di fessurazione nel calcestruzzo attraverso il metodo degli elementi finiti*, Thesis, Università degli Studi di Firenze, Florence (2002).

Claudio Borri, Prof. Dr. Eng. Dr. Eng h. c., University of Florence, Department of Civil Engineering, via S. Marta 3, 50139, Firenze, Italy, tel.: +39-055-479-6217, fax: +39-055-495333, cborri@dicea.unifi.it

Luca Salvatori, Eng., University of Florence, Department of Civil Engineering, via S. Marta 3, 50139, Firenze, Italy, tel.: +39-333-1491544, fax: +39-055-495333, luca.salvatori@dicea.unifi.it

Wolfhard Zahlten, Prof. Dr. Eng., University of Wuppertal, Department of Structural Mechanics and Numerical Methods, Pauluskirchstr. 7, 42285, Wuppertal, Germany, tel.: +49-202-439-4105, fax: +49-202-439-4104, wolfhard@vodka.bau.uni-wuppertal.de

4th International Congress
of Croatian Society of Mechanics
September, 18-20, 2003
Bizovac, Croatia

4thICCSM

NUMERICAL SIMULATION OF FABRIC REINFORCED HYDRAULIC HOSES

Herbert Rattensperger, Josef Eberhardsteiner and Herbert A. Mang

Keywords: *hydraulic hose, hyperelasticity, woven material, fabric lattice model*

1. Introduction

Hydraulic hoses with woven reinforcements are widely used in industry, e.g. for power transmission and for fluid transport. Such hydraulic hoses are composite structures where the fabric reinforcement consisting of steel wire or textile materials lead to a flexible hose behaviour as well as to a high resistance against inside pressure. Rubber as base material guarantees the tightness of high-pressure hydraulic hoses. The reinforcement is arranged in braided form with plaited fibre bundles. The interaction between the individual fibre bundles influences the global stiffness of the reinforcement significantly.

The purpose of this work is to develop a realistic numerical simulation model for high-pressure hydraulic hoses with woven wire or textile reinforcement. The aims of research are realistic predictions of the deformation and stress response under service loads, determination of the bursting pressure, and optimisation of the crimping of fittings (see Figure 1). For that purpose, well-suited experimental tests for identification of the material parameters of rubber are essential. Concerning rubber, the main objective is to provide reliable material data for realistic loading conditions. For that reason, biaxial membrane tests in addition to the standard uniaxial tests are recommended for identification of material parameters.

(a) 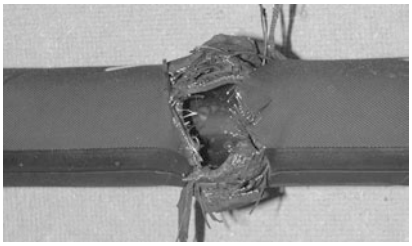 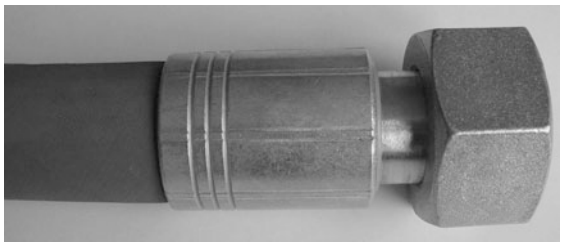 (b)

Figure 1. Analysis goals: (a) prediction of bursting pressure, (b) simulation of the crimping of fittings

The main topic of this paper is the mathematical description of the mechanical behaviour of the fabric reinforcement. Its stiffness and strength has a significant influence on global hose behaviour. The research concept is based on a trapezoidally-shaped fabric lattice model where the single fibres are represented by a spatial structure of rods. In addition to material and geometrical nonlinearities, this constitutive model also takes into account the increase of the fabric stiffness because of the mutual obstruction of crossing textile fibre bundles. For consideration of the latter, a concept based on the Hertzian theory was used. The stress state in the reinforcement layer, including lateral compression of single fibres or fibre bundles, and the tangent stiffness according to this stress state, are

determined by means of an incremental-iterative procedure within the framework of the finite element (FE) method.

2. Constitutive Modelling of textile braid reinforcement

Textile reinforcements of hydraulic hoses usually consist of a braid. Internal pressure leads to a complex load-carrying mechanism in the textile reinforcement. Several concepts are available for consideration of the mechanical behaviour of a braid in a numerical simulation, including the interaction between textile fibre bundles. In this paper a macro-mechanical concept for the description of the composite structure is used.

The assumption of a homogenised composite material is one mode of treatment of woven fabric reinforcements in FE analysis. This concept is based on the choice of a suitable anisotropic constitutive model. The equivalent material parameters are identified by means of experiments with fabric composites or by the so-called unit-cell method. In the latter case, a representative volume element is discretised using the mechanical properties of the different materials. Numerical analyses of characteristic deformation states yield equivalent material parameters, which are then introduced into a constitutive law for a homogeneous anisotropic material used in a global FE model. In general, this concept is restricted either to a linear constitutive behaviour, or to an orthotropic composite material. A unit-cell concept considering nonlinear material behaviour was suggested by Reese [9].

The fundamental idea of the concept used in this work is separate consideration of the matrix material (rubber) and reinforcement (textile or wire braid). Thereby, rebar elements represent the braided reinforcement which is embedded in the matrix material. The stiffness of the rebar layers is determined by the so-called fabric lattice model. In a paper by Kato et al. [4] the stiffness of the textile braid was integrated analytically at the integration point level. This resulted in restrictions regarding consideration of nonlinearities. In this work, a fabric lattice model based on a numerical formulation allows the taking of many forms of nonlinear material behaviour into account. It also permits numerical treatment of complex geometric situations, e.g., the simulation of the crimping of fittings.

2.1 Mechanical concept of fabric lattice model

In [9] the proposed fabric lattice model is used to represent wire reinforcements. In this paper textile braids have been considered. Two rebar layers, each with stiffness in only one of the two plaiting directions of the braid, represent the properties of the fabric lattice in the FE analysis. Respective rebar layers are interacting. For the calculation of stiffness and stress in the rebar layers by means of the proposed fabric lattice model, the following topics have to be considered:

- structural details of the textile braid and its mapping to the fabric lattice model,
- implementation of the fabric lattice model into the global FE analysis procedure,
- transfer of global quantities from the rebar layer to local quantities of the fabric lattice model,
- analysis of the fabric lattice model by means of a local nonlinear FE procedure, and
- back-transfer of local quantities from the fabric lattice model to global quantities of the rebar layer.

2.1.1 Mapping of the textile braid to the fabric lattice model

Details of the structure of a textile braid, shown in Figure 2a, illustrate the interaction of the fibre bundles. The forces acting in the fibres of one plaiting direction are influenced by the fibre forces in the other direction. This is reflected by notations such as F_x (F_y) in Figure 2a.

The shaded quarter of the detail in Figure 2a is treated as a representative cell. One half of a fibre bundle of this representative cell is treated as a bar in the fabric lattice model, as shown in Figure 2b. The mutual obstruction of the fibre bundles is represented by nonlinear springs between the respective bars. The fabric lattice cannot carry shear forces. These forces are carried entirely by the surrounding rubber material. The proposed fabric lattice model is not restricted to an orthogonal ar-

rangement of fabrics. This is important for realistic numerical simulations of high-pressure hydraulic hoses, reinforced by textile braids.

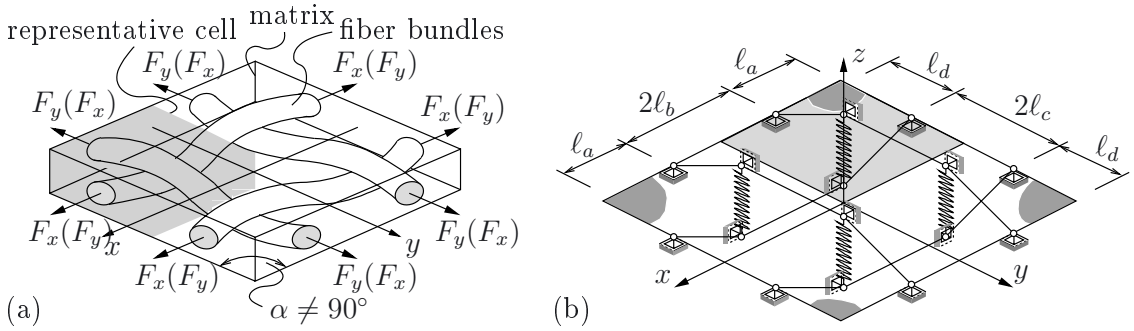

Figure 2. (a) Details of the structure of a textile braid, (b) mechanical system of the fabric lattice model

2.1.2 Implementation of the fabric lattice model

Regarding the implementation of the fabric lattice model in a global FE analysis procedure, the model shown in Figure 2b can be reduced to the system illustrated in Figure 3. Thereby, the symmetry of the lattice model was utilised. Using this system, the tangent stiffness and the stresses in the textile braid are determined by means of a local analysis. Consideration of plastic deformations in the textile reinforcement and of a nonlinear spring behaviour requires an incremental-iterative solution algorithm for the local fabric lattice model. This local nonlinear analysis is performed at the integration point level of the global nonlinear FE analysis.

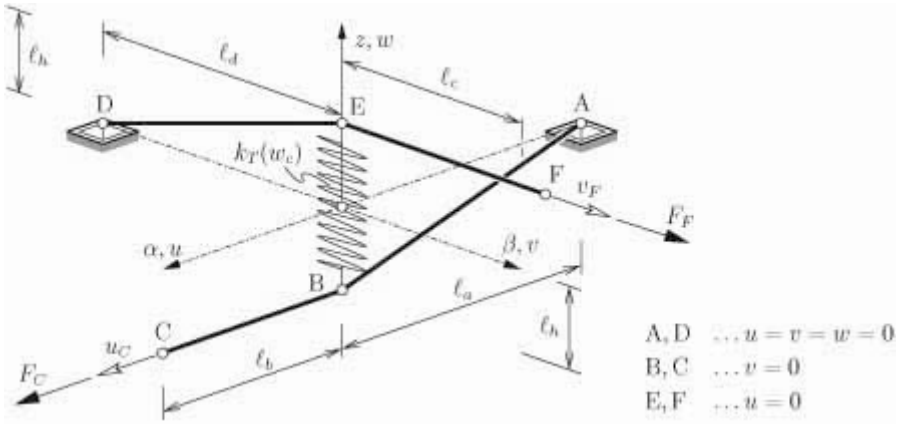

Figure 3. Considered quarter of fabric lattice model

2.1.3 Transfer from global to local quantities

The state variables of a geometric nonlinear global FE analysis on the integration point level depends on the formulation of the FE program. This paper is based on a formulation using the Cauchy stress tensor $\boldsymbol{\sigma}$ and the logarithmic strain tensor $\boldsymbol{\varepsilon}$. The first step of the numerical simulation of the textile braid is the transfer of state variables from the rebar layers of the global FE analysis ($\boldsymbol{\varepsilon}$, $\Delta\boldsymbol{\varepsilon}$, $\boldsymbol{\sigma}$) to the corresponding quantities of the local fabric lattice model (vector of nodal displacements $\mathbf{u}$, $\Delta\mathbf{u}$, force vector $\mathbf{F}$). In the situation for the iteration steps i and i+1 of increment k of the global nonlinear FE analysis is shown. The superscript of the local quantities n and n+1, respectively, refers to the increment of the fabric lattice analysis.

Table 1. Fabric lattice model – global and local variables

global		local		local		global
$\varepsilon^{k,i}$		$\boldsymbol{u}^{n}$	nonlinear	$\boldsymbol{F}^{n+1}$		$\boldsymbol{\sigma}^{k,i+1}$
$\boldsymbol{\sigma}^{k,i}$	⇨	$\boldsymbol{F}^{n}$	local analysis	$\Delta\boldsymbol{F}^{n+1}$	⇨	$\Delta\boldsymbol{\sigma}^{k,i+1}$
$\Delta\boldsymbol{\varepsilon}^{k,i}$		$\Delta\boldsymbol{u}^{n+1}$	(increm./iter)	$\boldsymbol{K}^{n+1}$		$\boldsymbol{C}^{k,i+1}$

The uniaxial stress state in a rebar layer is characterized by $\boldsymbol{\sigma} \equiv \sigma_{11} = \sigma_1$. The corresponding strain quantities are $\boldsymbol{\varepsilon} \equiv \varepsilon_{11} = \varepsilon_1$, $\Delta\boldsymbol{\varepsilon} \equiv \Delta\varepsilon_{11} = \Delta\varepsilon_1$, and λ_1, denoting the longitudinal stretch. Hence, standard transfer relations between tensor components and the respective components of nodal displacements and forces of the fabric lattice model can be used.

2.1.4 Components of the local fabric lattice model

(i) Material behaviour of fibres

The components of the local fabric lattice model are bars and a nonlinear spring (Figure 3). The bars represent the fibres of the woven braid, made of textile materials like polyester or Kuralon®. The nonlinear elastic spring is used to consider the mutual obstruction of the fibre bundles. A characteristic stress-strain diagram for the textile material Kuralon® is shown in Figure 4. The constitutive relation for the textile materials is based on a hyperelastic formulation. The energy function has the form

$$W = \frac{1}{2}\left(K - \frac{2}{3}G\right)\,(\ln J)^2 + G\,\left[(\ln\lambda_1)^2 + 2\,(\ln\lambda_2)^2\right]. \qquad \textbf{(1)}$$

It was proposed in [5] and is used for determination of the constitutive law for Kuralon®. In Eq. (1) K and G correspond to the bulk and shear modulus, respectively. J denotes the Jacobian determinant, λ_1 the axial stretch and λ_2 the transverse stretch of the textile fibre. This model is suitable for moderately large strains and provides a very good approximation of the true situation.

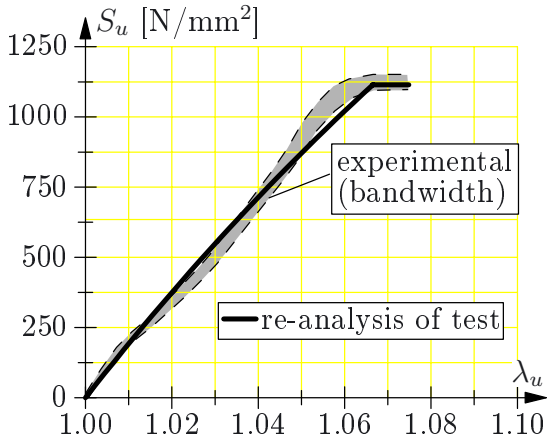

Figure 4. Bandwidth of S_1 –λ_1-diagrams of Kuralon® fibres

The partial derivative of W with respect to the Green strain component in the axial direction, E_1, results in the corresponding component of the Second Piola-Kirchhoff stress tensor,

$$S_1 = \frac{\partial W}{\partial E_1} = \frac{\partial W}{\partial \lambda_1}\frac{\partial \lambda_1}{\partial E_1} = \frac{9GK}{3K+G}\frac{\ln\lambda_1}{\lambda_1^2} = E\frac{\ln\lambda_1}{\lambda_1^2}\,. \qquad \textbf{(2)}$$

S_1 is acting in the textile fibre. E denotes the initial elastic modulus. Equation (2) represents a linear relation between the Cauchy stress and the logarithmic strain. The second partial derivative of W with respect to E_1 yields the tangential modulus

$$E_T = \frac{\partial^2 W}{\partial E_1^2} = \frac{\partial S_1}{\partial \lambda_1}\frac{\partial \lambda_1}{\partial E_1} = E\left(\frac{1 - ln\,\lambda_1}{\lambda_1^4}\right). \tag{3}$$

With Eqs. (2) and (3) the material behaviour of Kuralon® can be represented in the local FE analysis of the fabric lattice model.

(ii) Characterisation of the nonlinear spring

For consideration of the mutual obstruction of the fibre bundles a nonlinear spring is used to connect points B and E of the fabric lattice model (Figure 3). Based on the Hertzian theory [2], which describes the contact of two elastic bodies with curved surfaces, the stiffness of the nonlinear spring is evaluated. The mechanical behaviour of the nonlinear spring is defined by

$$F_c = k_T(w_c)\ w_c \qquad \text{and} \qquad \frac{\partial F_c}{\partial w_c} = k_T\ , \tag{4}$$

where F_c denotes the spring force, w_c stands for the displacement and k_T is the tangent stiffness of the spring. Evaluating the equations for the interaction of two cylindrical elastic bodies [1] yields the relative displacement of the cylinders

$$w_c = \sqrt[3]{C\ \left(1-\nu^2\right)^2 \frac{\overline{F}_c^{\,2}}{E^2}\frac{r_1 + r_2}{r_1\ r_2}}\ , \qquad C = 1.03421, \tag{5}$$

with r_1 and r_2 denoting the radii of the cylinders, and $\overline{F}_c$ standing for the force acting at a single intersection point of the fibre bundles. This force is defined by $\overline{F}_q = 4\ F_c\ /(n_{fb}.n_{fb})$, where n_{fb} denotes the number of fibres in a bundle [7]. Equation (5) is specified for a plaiting angle of 55°. In general, this value determines the orientation of the reinforcement of hydraulic hoses. Specification of Eq. (5) for two fibres with equal diameter d_f yields

$$F_c = \frac{C}{8}\ \ {n_{fb}}^2 \sqrt{d_f}\ \ \frac{E}{1-\nu^2}\ \ \sqrt{{w_c}^3}\ . \tag{6}$$

The partial derivative of F_c with respect to the displacement w_c results in the tangent stiffness of the nonlinear spring

$$k_T = \frac{\partial Fc}{\partial w_c} = \frac{3C}{16}\ \ {n_{fdb}}^2 \sqrt{d_f}\ \ \frac{E}{1-\nu^2}\ \ \sqrt{w_c}\ . \tag{7}$$

(iii) Determination of ultimate load

The maximum loading of a textile braid occurs at the contact area of two crossing fibres (Figure 5a). The stress states in the textile fibres of these parts of a braid is characterised by a combination of a longitudinal tensile stress and of the transverse compressive stress. For the evaluation of this stress state as well as for the determination of the ultimate load state, a semi-analytical method is used within the local fabric lattice model [7].

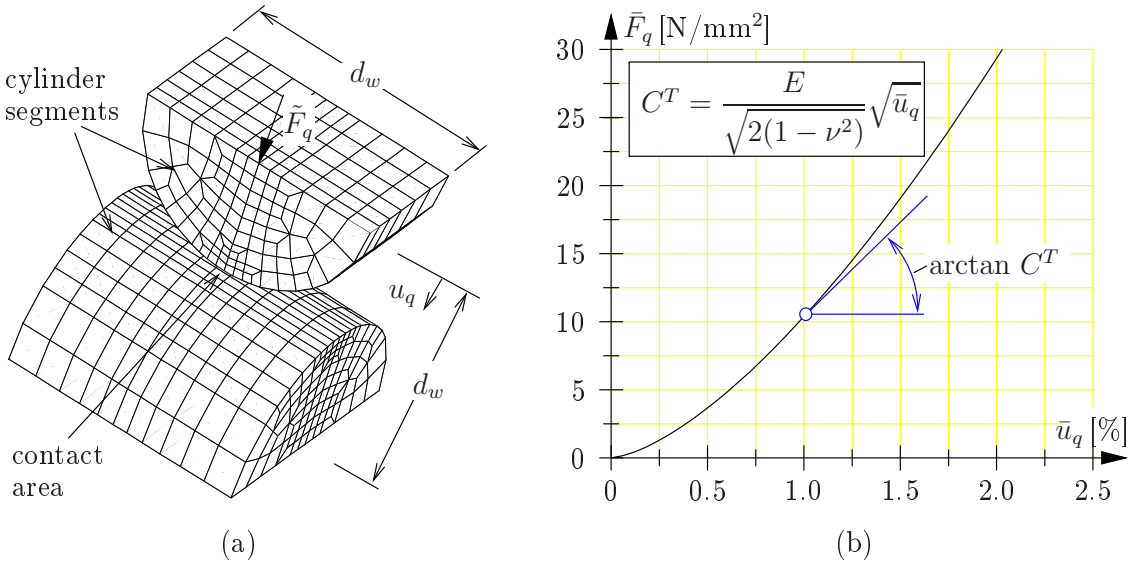

Figure 5. (a) contact area of two cylindrical bodies – contour plot of transverse stresses, (b) force-displacement diagram of the nonlinear spring

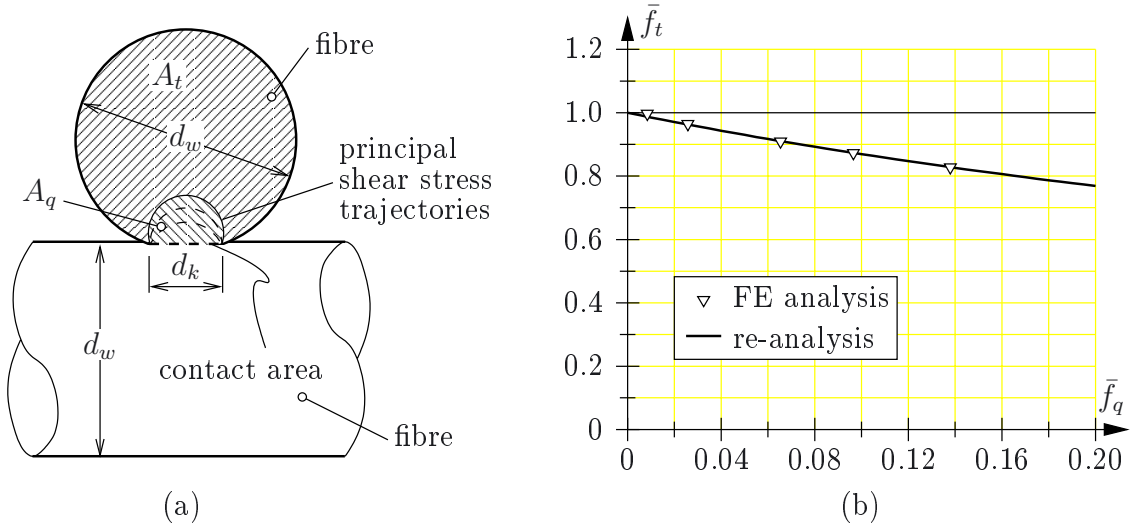

Figure 6. (a) characteristics of the principal shear stress trajectories, (b) $\bar{f}_t - \bar{f}_q$ -interaction

The failure mechanism of the fibres is illustrated in Figure 6a. The cross section of the fibre is divided into two parts, A_t and A_c. The former carries longitudinal tension and the latter transverse compression. Based on this assumption, the ultimate fibre force $\overline{F}_u$ is defined as

$$\overline{F}_u = \left(\frac{{d_f}^2 \pi}{4} - {d_c}^2 \zeta \right) f_{tu}\,, \tag{8}$$

where f_{tu} denotes the uniaxial tensile strength, d_c is the diameter of the contact area (Figure 6a), and ζ stands for the parameter representing influence of the transverse compression. The latter depends on the individual plastic behaviour of the respective fibre material. It is determined by numerical analysis at the level of the intersection point (Figure 5a). For vanishing transverse compression ($d_c = 0$), the maximum ultimate fibre force yields

$$\max \overline{F}_u = \left(\frac{{d_f}^2 \pi}{4} \right) f_{tu} . \tag{9}$$

When reaching the limit load $\overline{F}_t = max\, \overline{F}_u$, the pressure in the contact area is assumed to be equal to f_{tu}. From this, the diameter d_c is obtained as

$$d_c = \sqrt{\frac{4\overline{F}_c}{\pi f_{tu}}} . \tag{10}$$

Inserting Eq. (10) into Eq. (8) and introducing the dimensionless quantity $\bar{f}_t$, yields

$$\overline{f}_t = \frac{\overline{F}_u}{max\, \overline{F}_u} = \left(1 - \frac{4\varsigma \overline{f}_c}{\pi + 4\varsigma \overline{f}_c} \right), \tag{11}$$

where $\bar{f}_c = \overline{F}_c / \overline{F}_t$ represents the ratio of the axial force and the transverse force. Figure 6b shows a comparison of results from FE analysis and results obtained by Eq. (11). Thereby, ζ was identified by one of the FE results. Parallel to the local analysis of the fabric lattice model, the failure criterion for the fibres,

$$\overline{F}_t \le \bar{f}_t \, max\, \overline{F}_u , \tag{12}$$

was checked.

3. Numerical Examples

The fabric lattice model is used for the numerical simulation of (i) a representative part of a high-pressure hydraulic hose under internal pressure, and (ii) the crimping of a hose fitting.

Figure 7 illustrates the axisymmetric model with the boundary conditions of the considered part of the hose. Four rebar layers represent the two textile braid reinforcement. The axial tension force F_x depends on the internal pressure *pi*, which is increased until the bursting pressure is reached. During the simulation the change of the hose volume, the stress state and the change of the plaiting angle of the reinforcement are observed.

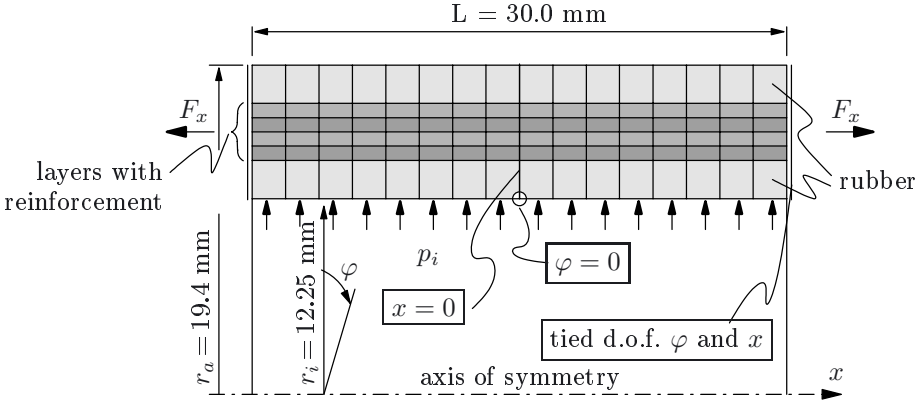

Figure 7. FE model of a representative part of a hydraulic hose

Figure 8a shows the fibre stresses in the two layers of textile braid, as a function of the internal pressure. The inner textile braid has higher stress levels. Therefore, the bursting pressure of the hose is determined by the strength of the inner textile braid. The change of the braid angle in consequence of growing internal pressure is shown in Figure 8b. The theoretical optimum of the plaiting angle is $\vartheta = 54.74°$ [8]. The value of ϑ is a little higher when the bursting pressure is reached.

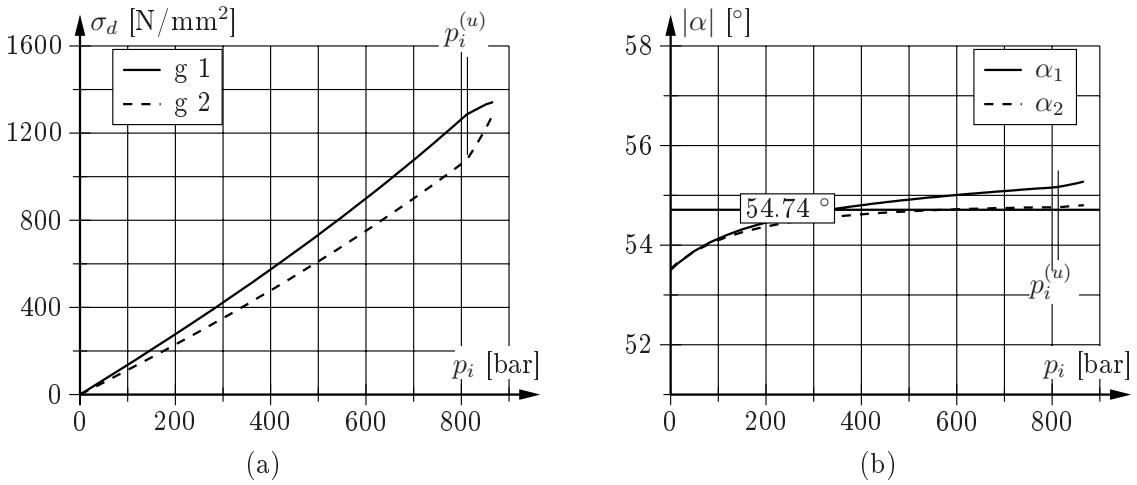

Figure 8. Representative part of a hose: (a) Cauchy stress of the fibres vs. internal pressure for two layers of textile braid, (b) change of the plaiting angle ϑ vs. internal pressure p_i

In a more complex numerical simulation the crimping of a hose fitting and the interaction between the fitting, rubber, and reinforcement are investigated. An axisymmetric deformed model of a textile hose with a crimped fitting is shown in Figure 9. For the crimping process, the hose is partially peeled at its end. Then a cylindrical metallic ferrule is pushed over this end and a nipple is inserted in the hose. Thereafter the ferrule is pressed onto the hydraulic hose by means of a press die. The resulting axial stresses of the fibres are shown in Figure 9 in the form of a contour plot. The peaks of the stresses are under the ribs of the ferrule. In case of a too strong pressing process in this area rupture of fibres will occur. A comparison of the deformation of the structure, as obtained from the numerical simulation, with the respective experimental observation shows very good agreement.

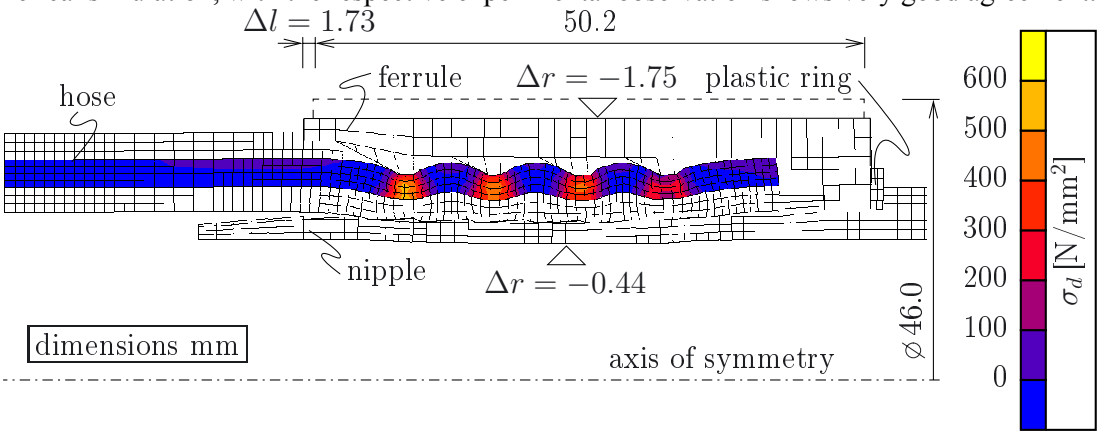

Figure 9. Deformed FE model of the crimping of a hose fitting

4. Conclusions

The objective of the presented work was to develop a realistic numerical simulation model for high-pressure hydraulic hoses with textile reinforcement in order to predict the deformation and stress response under service loads and the bursting process of such hoses. For consideration of textile woven reinforcements a local nonlinear fabric lattice model was developed. This model was applied to a special type of rebar layers. For the verification of the model the results from numerical analysis of a representative part of a hose under internal pressure and from simulation of the crimping of a hose fitting were used. Good agreement with experimental results has confirmed the usefulness of the proposed model for numerical investigation of textile braids.

References

[1] Geckeler, J., "Handbuch der Physik", Band 6, Kapitel 3: "Elastostatik". Springer, Berlin, 1928.

[2] Hertz, H., "Über die Verteilung der Druckkräfte in einem elastischen Kreiszylinder", Zeitschrift für-Mathematik und Physik, XXVIII Jahrgang, 1883. Verlag von B.G. Teubner, Leibzig.

[3] Johannknecht , R.; Jerrams, S.J., "The need for equi-biaxial testing to determine elastomeric material properties", Proceeding of the First European Conference on Constitutive Models for Rubber, 1999, Vienna, Austria

[4] Kato, S.; Yoshino, T.; Minami, H., "Formulation of constitutive equations for fabric membranes based on the concept of fabric lattice model", Engineering Structures, **21**, 1999, pp. 691-708.

[5] Meschke, G.; Helnwein, P., "Large-strain 3D-analysis of fibre-reinforced composites using rebar elements: hyperelastic formulations for cords", Computional Mechanics, **13**, 1994, pp. 241-254.

[6] Ogden, R.W., "Non-linear elastic deformations", John Wiley & Sons, New York, 1984.

[7] Rattensperger, H., "Berechnungsmodelle für verstärkte Elastomere und deren Anwendung für Hochdruckhydraulikschläuche". PhD thesis, Vienna University of Technology, 2003.

[8] [6] Rattensperger, H.; Eberhardsteiner, J.; Mang, H.A., "Numerical Investigation of High-Pressure Hydraulic Hoses Reinforced With Steel Wire Braid", *Proceedings of IUTAM-Symposium Computational Mechanics of Solid Materials at Large Strains,* Stuttgart 2001 (Ed.: Chr. Miehe), Kluwer Academic Publishers, 2003, pp 407-416.

[9] Reese, S., "Meso-macro modelling of fibre-reinforced composites exhibiting elastoplastic material behaviour", CD-ROM Proceedings of the European Conference on Computational Mechanics 2001 (ECCM), 2001, Cracow, Poland.

Herbert Rattensperger, Dipl.-Ing. Dr. techn.
Josef Eberhardsteiner, Ao.Univ.-Prof. Dipl.-Ing. Dr. techn.
Herbert A. Mang, O.Univ.-Prof. Dipl.-Ing. Dr. techn. Dr. h.c. mult. Ph.D.

Vienna University of Technology, Institute for Strength of Materials, Karlsplatz 13, A-1040 Vienna, Austria
Telephone: +43 1 58801-20212, Telefax: +43 1 58801-20282, e-mail: ej@fest.tuwien.ac.at

4th International Congress
of Croatian Society of Mechanics
September, 18-20, 2003
Bizovac, Croatia

4thICCSM

ON NUMERICAL DETERMINATION OF MECHANICAL RESPONSE IN PROBLEMS OF COUPLED MULTI-PHYSICS

Boris ŠTOK, Nikolaj MOLE

Keywords: *coupled problems, thermo-elasto-viscoplasticity, heat conduction, electro-magnetic induction, numerical modelling, finite & boundary elements*

1. Introduction

From a consideration of structural mechanics problems, in particular those regarding civil engineering constructions and a considerable part of mechanical components in mechanical engineering supposed to behave elastically, an incontestable conclusion could be made. In particular, when external actions are exclusively of mechanical origin the physical framework is quite clear, and the mathematics describing the respective problems rather simple and easy manageable, with solutions obtainable in a well defined way. Also, the material constitutive behaviour being usually linear and constant in time, the corresponding structural responses are linear as well, i.e. proportional to the applied loads. But, this image should not induce us to generalize the actual situation to problems of continuum mechanics, especially those met in industrial environment [1-8]. Such an induction, when referred to manufacturing and technology processes, would definitely be most erroneous.

The above stated physical simplicity attributed to structural mechanics problems can be rather quickly abnegated even for simple structures. Constructions in nuclear and process (chemical & pharmaceutical) engineering, like pipelines, pressure vessels, pumps and other structural components, are actually exposed, in addition to mechanical loads, to another source of loading, originating from experienced temperature variation with respect to the ambient temperature at which a construction was installed. Direct consequence of the temperature difference being volume expansion it can result, in case of unhomogeneous temperature field and obstructed free dilatation, in origination of additional stresses, called thermal stresses. Though possibly thermal stresses zero, it is indisputable that presence of the temperature difference affects the mechanical state anyway, by giving rise to thermal strains and corresponding variation of the displacement field.

Of importance in the above discussion is that actions not necessarily of mechanical origin can contribute significantly to a development of mechanical state in a structure. A similar behaviour as proven in case of temperature can be attributed also to humidity, in particular with regard to wood and polymeric materials. But, since only metallic materials will be considered in this paper the temperature will remain the basic non-mechanical state variable that we focus on. In fact, beside the considered structural mechanics problems there is a variety of physical applications, in their essence quite diverse such as heat treatment and hot metal forming, which are based exclusively upon established temperature variation. The problem of temperature field determination in a body of interest is definitely a heat conduction problem. However, considering that from an isothermal temperature field a respective variation is obtained only by applying external heat agents, the problem solution can rather quickly go beyond the respective physical framework. Such a case is encountered in induction heating where the principal physical mechanism generating heat is electromagnetic induction.

Each of the three addressed physical problems - the mechanical, heat conduction and the electromagnetic one are *per se* physically rather pretty clarified and mathematically well determined,

irrespective of eventual complexities characterizing their description [8]. In principle, provided the respective boundary conditions and domain distributed actions are known in time each of the considered problems can be solved on its own. In reality, however, interdependence between individual physical phenomena always exist in physically complex problems, causing that time evolution of a primary field variable in one physical system cannot be determined without prior knowledge of a respective primary field variable in the other physical system. This characteristic, which is very often mutual with physical interdependence exhibited in both directions, demands for a coupled solution strategy.

Another type of coupling, not primarily characterized by physical dissimilarity, is encountered when a problem domain consists of several interacting subdomains. Within the same physical framework, again, physical response of a subsystem can be determined only upon simultaneous knowledge of respective physical behaviour of those subsystems that are adjacent to a considered one. Which obviously demands for a coupled solution strategy, as well [8,9].

Simplifications, which are rather frequently used in traditional engineering approach in order to reduce the complexity of physically complex, and eventually multi-domain problems, are always disputable. Adoption of such simplifications is namely prone to loss of physical objectivity, which is however not permissible for a reliable problem analysis. Indeed, while multi-physics coupling affects the actions distributed over the problem domain, it is via boundary interface conditions that multy-domain coupling is manifested. Two study-cases, that will be considered numerically for the purpose of this presentation, contain all the characteristcs discussed. In the first case a workpiece is heated by induction, and afterwards, when a required nonuniform temperature distribution is attained, it is quenched in order to obtain specific mechanical properties. In the second case induction is used to heat a billet to a required nearly uniform temperature distribution, bringing it thus in a mushy-state, which is followed by a corresponding metal forming operation. Potential industrialization of the both cases is rather evident.

Strategies for a solution of physically coupled nonlinear problems will be considered in the paper, along with the discussion on the selection of appropriate space and time discretization methods that will result in a computationally efficient solution. Three physical problems, the thermomechanical, heat conduction and the electromagnetic problem respectively, will be considered in detail, and their coupling effects will be discussed upon results of the corresponding computer simulations of two study-cases.

2. Coupled field problems – Formulation & Solution

2.1 Definition of a certain class of boundary value problems

For the sake of simplicity let us consider first a one domain problem that is characterized by a single physical phenomenon. With x denoting Cartesian coordinates $x_i=x,y,z$ of a point in space, let $x\in\Omega$ and $x\in\Gamma$ denote respectively the domain of interest and its boundary, while $u=u(x)$ denotes a primary variable of the problem which can be either scalar or vector quantity, and real or complex. In general, field distribution $u=u(x)$ may change with time, therefore $u=u(x,t)$, where t stays for the time variable. Time evolution of the field distribution is governed by the corresponding problem equation, in accordance with given initial and boundary conditions, which can be written as

$$\begin{aligned} &A\,u = f \;,\; x \in \Omega \\ &u = u_0 \,,\; x \in \Omega \;;\; t = 0 \;\wedge\; B\,u = g \;,\; x \in \Gamma \;;\; t > 0 \quad . \end{aligned} \tag{1}$$

Here, $u_0=u_0(x)$ is the initial field distribution at time $t=0$, while $f=f(x,t)$ and $g=g(x,t)$ are the applied external actions, acting within the domain Ω and on the boundary Γ, respectively. For the class of physical problems we are going to address A and B are differential operators of the following general form

$$A = \sum_{\mathrm{i}} \sum_{\mathrm{j}} \frac{\partial}{\partial x_{\mathrm{i}}} \left(a_{\mathrm{ij}} \frac{\partial}{\partial x_{\mathrm{j}}} \right) + b \frac{\partial}{\partial t} + c \frac{\partial^2}{\partial t^2} \; ; \; \mathrm{i,j} \in \{x, y, z\}$$
$$B = \{B_{\mathrm{u}}, B_{\mathrm{q}}\}; \; B_{\mathrm{u}} = 1 \; , \; B_{\mathrm{q}} = \sum_{\mathrm{i}} d_{\mathrm{i}} \frac{\partial}{\partial x_{\mathrm{i}}} \; ; \; \mathrm{i} \in \{x, y, z\} \quad . \tag{2}$$

In the formulation of the boundary condition operator B nature of the possible boundary conditions has been taken into account, resulting thus in the splitting of the operator B into B_{u} and B_{q}, which give respectively the operational structure of corresponding essential and natural boundary conditions. Because of conjugacy of the primary and secondary problem variables entering the two types of boundary conditions the boundary Γ can be accordingly split in two parts, Γ_{u} and Γ_{q}, respectively, fulfilling $\Gamma_{\mathrm{u}} \cup \Gamma_{\mathrm{q}} = \Gamma$ and $\Gamma_{\mathrm{u}} \cap \Gamma_{\mathrm{q}} = \varnothing$.

Coefficients a_{ij}, b, c and d_{i} are the problem constitutive parameters that depend to a great degree on material physical properties. The most simple case regarding the corresponding problem solution is undoubtedly encountered when those parameters are constant in time. However, very often the field distribution $u=u(x)$ does affect the physical properties, therefore

$$C_{\mathrm{p}} = C_{\mathrm{p}}(u) \quad , \tag{3}$$

where symbolics C_{p} is introduced to represent the whole set of the above discussed constitutive parameters. This characteristic renders the problem solution definitely nonlinear, but, in the context of the assumed single physical phenomenon one domain problem, with domain and boundary actions, $f(x,t)$ and $g(x,t)$ respectively, fully independent, it is still self-consistent.

In other words, having in view physically coupled problems we are going to address in the next subsection, self-consistency of a problem may be considered as equivalence to physical uncoupleness. Considering dependence (3) in the problem equations (1) the uncoupled problem may be represented symbolically in the form of

$$P(u) = 0 \quad \vee \quad P(u, \dot{u}) = 0 \quad \vee \quad P(u, \dot{u}, \ddot{u}) = 0 \quad , \tag{4}$$

where the three forms arise with regard to the established degree of the time derivatives, that are active in the governing equation operator A (2).

2.2 Where coupleness comes from?

In a multi-physics problem each individual physical phenomenon could be considered roughly in the same way as presented above. Let us consider, for the sake of simplicity, a problem that is characterized by two physical phenomena within a common material domain Ω, and $u_1=u_1(x,t)$ and $u_2=u_2(x,t)$ being the respective primary variables. The respective field evolutions are governed by the same type of equations as given by (1), provided all the appertaining quantities entering the definition equations (1) and (2) are supplemented by the respective indeces, i.e. 1 or 2 for the considered cases. Which is certainly not enough for the multi-physics problem to be considered as a coupled one. Then, where the coupleness comes from?

In the same way as in a single physical phenomenon problem the appertaining constitutive parameters can be affected by the respective field distribution (3), it is quite possible that in a physically coupled problem the constitutive parameters, determining individual physical problems, are affected, apart from the proper field distribution, also from the corresponding field distribution of the companion physical problem. Since this interaction can be exhibited, in general, in both directions, the following relations can be established

$$C_{\mathrm{p}}^{(1)} = C_{\mathrm{p}}^{(1)}(u_1, u_2) \; , \; C_{\mathrm{p}}^{(2)} = C_{\mathrm{p}}^{(2)}(u_2, u_1) \quad , \tag{5}$$

which definitely brings coupleness between the considered physical phenomena into force.

In some problems coupleness can be demonstrated also by the companion field distribution specifying directly the applied domain actions $f(x,t)$, experiencing thus the following functional relations

$$f_1 = f_1(u_1, u_2)\ ,\ \ f_2 = f_2(u_2, u_1)\quad .\qquad (6)$$

Here, the highest degree of functional dependence, including also eventual dependence of the proper field distribution, has been taken into account. In contrast to the established physical interdependence, which is manifested through the whole domain, the companion field distribution may affect also the applied boundary actions $g(x,t)$. For this particular case, which can actually arise in a multi-domain problem, the following functional relations can be written

$$g_1 = g_1(u_1, u_2)\ ,\ \ g_2 = g_2(u_2, u_1)\quad .\qquad (7)$$

In analogy to the formulation (4) the coupled multi-physics problem can be formulated by defining the corresponding two equations sets, symbolically written as

$$\begin{aligned} &P_1(u_1, u_2) = 0\ ,\ \ P_2(u_2, u_1) = 0 \quad \vee \\ &P_1(u_1, \dot{u}_1, u_2, \dot{u}_2) = 0\ ,\ \ P_2(u_2, \dot{u}_2, u_1, \dot{u}_1) = 0 \quad \vee \\ &P_1(u_1, \dot{u}_1, \ddot{u}_1, u_2, \dot{u}_2, \ddot{u}_2) = 0\ ,\ \ P_2(u_2, \dot{u}_2, \ddot{u}_2, u_1, \dot{u}_1, \ddot{u}_1) = 0 \quad . \end{aligned} \qquad (8)$$

Each of the particular functional relationships, i.e. $P_1(u_1,...)=0$ and $P_2(u_2,...)=0$ respectively, expresses a unique condition governing the respective single physical phenomenon under consideration. In particular, the relationship $P_1(u_1,...)=0$ governs the field variable $u_1=u_1(x,t)$ whilst $P_2(u_2,...)=0$ is responsible for the field variable $u_2=u_2(x,t)$.

2.3 Strategies for solution of coupled problems

Solving of the complete coupled problem, as determined by functional relations (8), requires use of iteration techniques to couple the respective partial solutions. In the solution strategy different aspects, the problem is characterized with, are to be properly addressed. First, although the simplest case, not containing any time rates of the variables $u_1=u_1(x,t)$, $u_2=u_2(x,t)$, is considered, its solution may be required at several time/load steps in connection with an incremental continuation procedure if the history of the field variables is requested for timely variable boundary conditions and/or in order to facilitate the numerical analysis of strongly nonlinear problems. In contrast to the referred time-independent problems, transient processes, on the other hand, are characterized by the appearance of the time rates of the primary variables in the governing equations. Both the variables $u_1=u_1(x,t)$, $u_2=u_2(x,t)$ and their time rates are unknown quantities that are linked via the integration in time

$$u_\alpha = \int \dot{u}_\alpha \,\mathrm{d}t\ ,\ \ \dot{u}_\alpha = \int \ddot{u}_\alpha \,\mathrm{d}t\ \ ;\quad \alpha = 1,2\quad ,\qquad (9)$$

which is usually performed by approximation following an incremental scheme.

When dynamic effects are not pronounced the single step formula

$$w(\tau + \Delta\tau) = w(\tau) + \left[(1-\zeta)\dot{w}(\tau) + \zeta\,\dot{w}(\tau + \Delta\tau)\right]\Delta\tau\quad ,\ (10)$$

may be considered as sufficient to allow stepping of a field variable $w=w(x,t)$ in time. Here, notation $w=w(x,t)$ is used to represent in turn either $u_\alpha = u_\alpha(x,t)$ or its time rate $\dot{u}_\alpha = \dot{u}_\alpha(x,t)$. Provided the respective field values at time $t=\tau$ are known, the time integration formula allows to calculate the corresponding values at time $t=\tau+\Delta\tau$. Regarding the selected magnitude of the collocation parameter ζ which can take the value within the range $0\le\zeta\le1$ either explicit ($\zeta=0$) or implicit ($\zeta\neq0$) time integration scheme is obtainable.

In contrast to the time integration formula (10), where time rate $\ddot{w} = \ddot{w}(x,t)$ does not enter in the scheme, there exist for the solution of dynamically characterized problems a series of integration schemes, either explicit or implicit. From the computational point of view explicit methods are particularly attractive since they require, in principle, less computational work. Here, we will make use of a modified constant acceleration method with $\ddot{w} = \ddot{w}(x,t)$ assumed constant during time interval $[\tau,\tau+\Delta\tau]$, and having the magnitude as determined at the start of the considered time interval. In consequence, the corresponding values of integrated fields $\dot{w}(x,t)$ and $w(x,t)$ at the end of the considered time interval can be found in accordance with

$$\dot{w}(\tau+\Delta\tau)=\dot{w}(\tau)+\ddot{w}(\tau)\Delta\tau \quad , \qquad w(\tau+\Delta\tau)=w(\tau)+\dot{w}(\tau)\Delta\tau+\ddot{w}(\tau)\frac{\Delta\tau^2}{2} \quad . \qquad (11)$$

The just discussed time/load integration aspect of the problem solution deals with the time dimension, covering thus the history of the respective field variables. The considered time integration algorithms are general, and can be used in the solution of uncoupled as well as coupled problems. The second aspect is however specific for coupled problems. It actually deals with the issue of achieving a physically consistent coupled solution that will provide each individual partial solution to be in agreement with the appertaining governing equations, and at the same time taking full account of the impact the companion field evolution exerts on it.

In conjunction with the suitable approximate time integration scheme, (10) or (11), the governing equations (8) provide a system for the field computation of either the state variables or their time rates at each time instant, in the sequel denoted by $v_1=v_1(x,t)$, $v_2=v_2(x,t)$ for convenience. In this context, the essential problem is considered to be the solution of a system of equations

$$F_1(v_1,v_2)=0 \quad , \qquad F_2(v_2,v_1)=0 \quad , \qquad (12)$$

at distinct time instants during the course of an incremental continuation procedure. At this stage, analytical field solution of the considered system being not feasible, let us transform the problem (12) into a corresponding discretized matrix form

$$\mathbf{F}_1(\boldsymbol{V}_1,\boldsymbol{V}_2)=\mathbf{0} \quad , \qquad \mathbf{F}_2(\boldsymbol{V}_2,\boldsymbol{V}_1)=\mathbf{0} \quad . \qquad (13)$$

The introduced vectors $\boldsymbol{V}_1$ and $\boldsymbol{V}_2$ represent the finite sets that are assembled from the respective nodal values at discrete points of the domain Ω, used for the spatial approximation of $v_1=v_1(x,t)$, $v_2=v_2(x,t)$ fields at considered time instant. Correspondingly, the coupled problem formulation (13) represents actually two systems of linear equations for the unknowns $\boldsymbol{V}_1$ and $\boldsymbol{V}_2$, respectively. The coupleness between the two systems is manifested implicitly since impact of the companion field distribution, e.g. $\boldsymbol{V}_2$ in the equations set $\mathbf{F}_1(\boldsymbol{V}_1,\boldsymbol{V}_2)=0$ for the unknowns $\boldsymbol{V}_1$, is entering the system coefficients of the equations set $\mathbf{F}_1(\boldsymbol{V}_1,\boldsymbol{V}_2)=\mathbf{0}$. This characteristic complicates the systems solution by rendering it nonlinear and requiring an iterative procedure.

Considering the way how coupleness is manifested it proves advantageous to handle each of the equations set in (13) individually. A feasible technique involves then the consecutive solution of (13), applying an adequate iteration procedure with one of the sets of unknowns $\boldsymbol{V}_1$ and $\boldsymbol{V}_2$ assumed temporary fixed. Among different ways of how performing the required iteration loop in order to reach the coupled solution at considered time instant, two of them, respectively Jacobi iteration and Gauss-Seidel iteration procedure, are rather familiar and easy to implement.

If in the *i*-th cycle of the iteration loop estimate $\boldsymbol{V}^{\mathrm{i}}$ is supposed to be known, then $\boldsymbol{V}^{\mathrm{i+1}}$ is a new estimate. Seeing that in Jacobi iteration, applied to the solution of (13)

$$\mathbf{F}_1(\boldsymbol{V}_1^{\mathrm{i+1}},\boldsymbol{V}_2^{\mathrm{i}})=\mathbf{0} \quad , \qquad \mathbf{F}_2(\boldsymbol{V}_2^{\mathrm{i+1}},\boldsymbol{V}_1^{\mathrm{i}})=\mathbf{0} \quad , \qquad (14)$$

the considered systems of equations are actually uncoupled with respect to the temporary unknowns $\boldsymbol{V}_1^{\mathrm{i+1}},\boldsymbol{V}_2^{\mathrm{i+1}}$, the respective systems solutions within an iteration cycle may be treated also concurrently. On the contrary, in Gauss-Seidel iteration, when applied to the solution of (13)

$$\mathbf{F}_1(\boldsymbol{V}_1^{\mathrm{i+1}},\boldsymbol{V}_2^{\mathrm{i}})=\mathbf{0} \quad , \qquad \mathbf{F}_2(\boldsymbol{V}_2^{\mathrm{i+1}},\boldsymbol{V}_1^{\mathrm{i+1}})=\mathbf{0} \quad , \qquad (15)$$

the iteration solution procedure must be performed consecutively. The iteration namely starts with an estimate to one of the sets of unknowns, say $\boldsymbol{V}_2^{\mathrm{i}}$. The first equation in (15) is then solved for the other set of unknowns, $\boldsymbol{V}_1^{\mathrm{i+1}}$, and this updated information is used in the second equation to provide the new estimate $\boldsymbol{V}_2^{\mathrm{i+1}}$.

3. Physical & Mathematical description of considered physically coupled problems

3.1 Description of Electromagnetic-Thermal-Mechanical coupling

Beside cutting processes, heat treatment and metal forming are among the most frequently encountered processes in materials processing technologies. Both are characterized by the presence of different physical phenomena which contribute decisively by their coupling to the resulting mechanical/metallurgical state of a manufactured product. In the sequel, we will consider such processes in which electromagnetic – thermal – mechanical coupling is established.

In heat treatment both the chemical composition and a kind of heat treatment, that a workpiece is subjected to, allows for a great variety of properties to be obtained. Since kinetics of structural changes in a material of a specified chemical composition is exclusively conditioned with a time variation of the temperature field it is of fundamental importance in any heat treatment process to achieve controlled heating and cooling. The temperature field time variation, though generating structural changes in a direct and independent way, depends itself on the external factors above all. On one side it is the energy entering the system, and on the other side it is the heat leaving the system that determine the heat transfer. The major trouble of such a thermal analysis consists in the field determination of the energy sources and the corresponding time variation in the heating phase, while in the cooling phase it consists in the identification of real boundary conditions, taking the amount of heat leaving the system properly into account. When electromagnetic induction is used for heating, strong coupleness between the thermal and electromagnetic phenomena is proven. On the other hand, the imposed cooling rate gives rise to significant changes of the metallurgical/ mechanical state, which is characterized by quite similar intensity of coupleness between the thermal and mechanical phenomena.

In hot metal forming pretty the same physical phenomena can be evidenced, but with rather different degree of coupleness proven. In order to bring a workpiece to a desired temperature distribution again electromagnetic induction can be applied, while in the metal forming phase the heated workpiece is exposed to a considerable change of its initial geometry. In contrast to the established strong electromagnetic – thermal coupling, coupleness between the mechanical and thermal phenomena may not be so intensive. Of course, in connection with the irreversible plastic work heat may be generated, the amount of it and its impact on the temperature field distribution being dependent on a great number of factors, that will not be considered here.

In order to distinguish in the following mathematical descriptions the dimensional structure of a considered quantity let us introduce in the sequel the following convention: scalar, vector and tensor variables will be denoted respectively by italic, italic bold and simple bold notations, e.g. a, A for scalars, $\boldsymbol{a}$, $\boldsymbol{A}$ for vectors and $\mathbf{a}$, $\mathbf{A}$ for tensors.

3.2 Description of electromagnetic eddy current problem

In an electromagnetic field (emf) problem with a relatively slow time variation, i.e. $\sigma << \omega\,\varepsilon$, where σ and ε are respectively the electrical conductivity and permitivity, and ω is the source frequency, the conducting currents dominate the problem, therefore, the displacement currents can be neglected. In consequence, the steady-state approximation may be used which simplifies the problem considerably [10]. Maxwell's equations, which govern the emf distribution, read for the considered case as follows

$$\text{curl}\,\boldsymbol{H} = \boldsymbol{J} \quad , \quad \text{curl}\,\boldsymbol{E} = -\frac{\partial \boldsymbol{B}}{\partial t} \quad , \quad \text{div}\,\boldsymbol{B} = 0 \quad , \quad (16)$$

with $\boldsymbol{H}$, $\boldsymbol{E}$ being vectors of magnetic and electric strength, $\boldsymbol{B}$ being vector of magnetic flux density, and $\boldsymbol{J}$ being vector of the conduction current density. These quantities are further related by the following constitutive relationships

$$\boldsymbol{B} = \mu\,\boldsymbol{H} \quad , \quad \boldsymbol{J} = \boldsymbol{J}_{\text{source}} + \boldsymbol{J}_{\text{eddy}} = \sigma\,\boldsymbol{E} \quad , \quad (17)$$

with μ being the magnetic permeability, and $\boldsymbol{J}_{\text{source}}$, $\boldsymbol{J}_{\text{eddy}}$ being respectively the source and eddy current densities.

In order to give a complete mathematical description of the emf problem, in which a workpiece that is made of an electrically conducting material is passed in an induction heating process through coils carrying an alternating electric current, the whole space domain must be considered. Accordingly, the infinite domain Ω in which the emf exists can be decomposed in three non-overlapping subdomains Ω_α; $\alpha \in \{\mathrm{I,W,A}\}$ with indices I,W,A referring to the corresponding domains, occupied respectively by the inductor, the workpiece and the air. The physical consistency of the emf, which exists in all three subdomains Ω_α; $\alpha \in \{\mathrm{I,W,A}\}$, is achieved, apart from obeying the governing domain equations (16) and (17), by fulfilment of the corresponding continuity relations at the boundaries Γ_α; $\alpha \in \{\mathrm{I,W}\}$. At these boundaries, which are actually common interfaces to the adjacent electrically nonconductive air domain, the continuity of the normal component of magnetic flux density and the tangential component of magnetic field intensity is implied

$$\left(\boldsymbol{B}_\alpha - \boldsymbol{B}_\mathrm{A}\right)\cdot\boldsymbol{n}_\alpha = 0\ ,\ \left(\boldsymbol{H}_\alpha - \boldsymbol{H}_\mathrm{A}\right)\times\boldsymbol{n}_\alpha = \boldsymbol{0}\ ;\quad \alpha\in\left\{\mathrm{I,W}\right\}\quad , (18)$$

where vector $\boldsymbol{n}_\alpha$ is exterior normal to the boundary Γ_α; $\alpha \in \{\mathrm{I,W}\}$. The behaviour of the emf at infinity is characterized by

$$\boldsymbol{B}_\mathrm{A} \to \boldsymbol{0} \quad \text{as} \quad |\boldsymbol{x}| = \sqrt{x^2+y^2+z^2} \to \infty \quad . \qquad (19)$$

The magnetic flux being divergence free it can be expressed in terms of a vector magnetic potential $\boldsymbol{A}$ which is itself, according to the Coulomb gauge, divergence free

$$\boldsymbol{B} = \mathrm{curl}\,\boldsymbol{A}\ ,\ \ \mathrm{div}\,\boldsymbol{A} = 0 \quad . \qquad (20)$$

In consequence, a solution to the stated emf problem (16)-(19) can be found by the corresponding transformation of the governing equations. By assuming linear and isotropic materials with constant permeability the transformation yields

$$\Delta\boldsymbol{A} - \mu\sigma\frac{\partial\boldsymbol{A}}{\partial t} = -\mu\,\boldsymbol{J}_\mathrm{source}\ ,\quad \boldsymbol{J}_\mathrm{eddy} = -\sigma\frac{\partial\boldsymbol{A}}{\partial t}\quad , (21)$$

with associated interface and boundary conditions in terms of the vector potential $\boldsymbol{A}$. Here, potential $\boldsymbol{A}$ takes the role of the mathematically defined primary variable, instead of $\boldsymbol{H}$ or $\boldsymbol{E}$, the magnetic and electric strength respectively, which are actually the physical primary variables of the problem.

If the applied source potential is assumed harmonic in time all the associated field quantities are time harmonic functions as well. Their distribution therefore depends only on the position and phase delay at each point in space, which can be mathematically managed in a simple way by introducing complex notation. The time variation of the potential $\boldsymbol{A}(\boldsymbol{x},\mathrm{t})$ at any point $\mathrm{P}(\boldsymbol{x})$ can be obtained as the real part of a corresponding complex function

$$\boldsymbol{A}(\boldsymbol{x},t) = \boldsymbol{A}_0(\boldsymbol{x})\,\cos(\omega t + \varphi(\boldsymbol{x})) = \mathrm{Re}[\hat{\boldsymbol{A}}_0(\boldsymbol{x})\exp(\mathrm{j}\,\omega t)]\quad , (22)$$

where the introduced complex magnetic vector potential $\hat{\boldsymbol{A}}_0(\boldsymbol{x})$ includes the information about the field amplitude and its time delay with respect to the imposed source excitation.

With respect to the introduced complex framework all physical quantities associated with the emf problem, which were considered above as real vector functions, can be understood from now on as complex functions. Their behaviour is still determined by the same system of equations, which however has now to be treated as a system of complex equations.

The emf, produced by the current-carrying coils, induces eddy currents in the workpiece, which is in consequence heated resistively by the Joule effect. The electric power q_V, induced in a unit volume of a workpiece by eddy currents, is proportional to the intensity of the actual emf, and its effective value, when expressed in terms of the vector potential $\hat{\boldsymbol{A}}_0(\boldsymbol{x})$, is as follows

$$q_\mathrm{V} = \frac{\sigma\omega^2}{2}\left|\hat{\boldsymbol{A}}_0(\boldsymbol{x})\right|^2 \quad . \qquad (23)$$

This electric power acts as an imposed heat source in the associated thermal problem within the subdomain Ω_W, and is actually the key driving force.

3.3 Description of heat conduction thermal problem

Heat transfer in a continuum, that occupies an isotropic material domain Ω and is exposed to volume distributed heat source q_V and eventual boundary heat flux q_S, is governed by thermodynamic equilibrium. With ρc and k being respectively the thermal capacity and thermal conductivity, the corresponding temperature field $T(\boldsymbol{x},t)$ in the body is then subject to time variation in accordance with the heat conduction equation

$$\rho c \frac{\partial T}{\partial t} = \operatorname{div}(k \ \operatorname{grad} T) + q_V \quad , \quad (24)$$

and associated initial and boundary conditions

$$T(\boldsymbol{x},0) = T^0(\boldsymbol{x}) \ , \quad \boldsymbol{x} \in \Omega \ ; \ t = 0$$
$$T(\boldsymbol{x},t) = T^*(\boldsymbol{x},t) \ , \quad \boldsymbol{x} \in \Gamma_T \ \wedge \ -k \ \operatorname{grad} T(\boldsymbol{x},t) \,.\, \boldsymbol{n} = q^*(\boldsymbol{x},t) \ , \quad \boldsymbol{x} \in \Gamma_q \ ; \ t > 0 \quad . \quad (25)$$

Here, it has been assumed that on the part Γ_T of the boundary Γ essential boundary conditions with prescribed temperature variation T^* are given, whilst on the remaining part Γ_q natural boundary conditions, i.e. convection and radiation heat fluxes q^*, are known.

The key driving force for the temperature field evolution, temperature T being the primary variable of the problem, is the application of external agents q_V and q_S. Considering the induction heating and subsequent rapid cooling, that will be addressed in the context of heat treatment process investigation, the intensities of those actions are provided by knowledge of respective companion physical processes, namely, electromagnetic induction on one hand and heat exchange between the workpiece and a quenchant on the other hand. In this regard heat source intensity, as determined by (23), will be taken into account. Also, it is worth mentioning that in contrast to the emf analysis, where the whole space domain composed of three material subdomains had to be fully taken into consideration, the thermal analysis can be performed just by considering a subdomain that is occupied by the workpiece.

3.4 Description of elastoplasticity & viscoplasticity contact mechanics problem

Mechanical response of a deformable continuum, occupying an isotropic elasto-plastic material domain Ω and being exposed to volume and surface distributed forces, $\boldsymbol{f}$ and $\boldsymbol{p}^*$ respectively, and to eventual variation of the initially isothermal state T_0, is governed by the set of equilibrium, deformation and constitutive equations

$$\operatorname{div} \boldsymbol{\sigma} + \boldsymbol{f} = \boldsymbol{0}$$
$$\boldsymbol{\varepsilon} = \frac{1}{2}\left[\operatorname{grad} \boldsymbol{u} + (\operatorname{grad} \boldsymbol{u})^T\right] \quad (26)$$
$$\boldsymbol{\sigma} = \mathbf{H} : \boldsymbol{\varepsilon} - \frac{E\,\alpha}{1 - 2\upsilon}(T - T_0)\,\boldsymbol{\delta} \quad ,$$

where $\boldsymbol{u}$ is the displacement vector, and $\boldsymbol{\varepsilon}$ and $\boldsymbol{\sigma}$ are respectively the strain and stress tensor. Material properties E, υ and α are in turn Young's modulus, Poisson's ratio and coefficient of thermal expansion. The fourth order tensor $\mathbf{H}$ is actually the stress-strain constitutive tensor which is composed in case of pure elastic response from the elastic coefficients E and υ, whilst in case of inelastic response it is enlarged by incorporation of parameters characterizing such behaviour, e.g. hardening modulus H. Finally, $\boldsymbol{\delta}$ is the Kronecker tensor.

Physical consistency of the mechanical response is achieved, in addition to (26), by fulfilment of corresponding initial and boundary conditions, which read for the assumed initially stress-strain free mechanical state as follows

$$\boldsymbol{\sigma}(\boldsymbol{x},0) = \boldsymbol{\sigma}^0(\boldsymbol{x}) = \mathbf{0} \ , \ \boldsymbol{\varepsilon}(\boldsymbol{x},0) = \boldsymbol{\varepsilon}^0(\boldsymbol{x}) = \mathbf{0} \ , \ \boldsymbol{u}(\boldsymbol{x},0) = \boldsymbol{0} \ , \ \boldsymbol{x} \in \Omega \ ; \ t = 0$$
$$\boldsymbol{u} = \boldsymbol{u}^*(\boldsymbol{x},t) \ , \ \boldsymbol{x} \in \Gamma_u \ \wedge \ \boldsymbol{\sigma} \,.\, \boldsymbol{n} = \boldsymbol{p}^*(\boldsymbol{x},t) \ , \quad \boldsymbol{x} \in \Gamma_\sigma \ ; \ t > 0 \quad . \quad (27)$$

Here, it has been assumed that on the part Γ_u of the boundary Γ essential boundary conditions with prescribed displacements are given, whilst on the remaining part Γ_σ natural boundary conditions, expressed in terms of applied tractions, are known.

Since displacement field $\boldsymbol{u}(\boldsymbol{x},t)$ acts as the primary variable of the mechanical problem, the set of governing equations (26) can be adequately reduced. By considering the decomposition of the strain tensor $\boldsymbol{\varepsilon}$ into elastic and inelastic part, $\boldsymbol{\varepsilon} = \boldsymbol{\varepsilon}^{\mathrm{e}} + \boldsymbol{\varepsilon}^{\mathrm{p}}$, and assuming material properties constant this reduction yields vector equation governing time evolution of the displacement field.

$$\mu \operatorname{div}(\operatorname{grad} \boldsymbol{u}) + (\lambda + \mu) \operatorname{grad}(\operatorname{div} \boldsymbol{u}) - (2\mu + 3\lambda)\, \alpha \operatorname{grad}(T - T_0) - 2\mu \operatorname{div} \boldsymbol{\varepsilon}^{\mathrm{p}} + \boldsymbol{f} = \boldsymbol{0} \quad . \tag{28}$$

The above equation introduces, in regard to the Navier-Lame equilibrium equation, a modification due to presence of the inelastic response.

The key driving force for the variation of mechanical quantities in the above stated heat treatment process investigation will definitely be thermal expansion, in fact, its unhomogeneous and possibly abrupt distribution through the body. Therefore, occurrence of plastic deformation at least in a part of the body is rather expected. In order to enable, at any stage of the process evolution, proper identification of the respective material response, i.e. either elastic or inelastic, in the constitutive equation of (26) the thermomechanical state function F, referred also as a yield function, is introduced in accordance with

$$F(\boldsymbol{\sigma} - \boldsymbol{\alpha}, T, \varepsilon_{\mathrm{p}}) = f(\boldsymbol{\sigma} - \boldsymbol{\alpha}) - K_{\mathrm{p}}(T, \varepsilon_{\mathrm{p}}) \quad . \tag{29}$$

The defined yield function depends directly on the actual state of stress $\boldsymbol{\sigma}$ and accumulated plastic strain ε_{p}, and indirectly on temperature T and eventual nonisotropic hardening, expressed by the so called back stress tensor $\boldsymbol{\alpha}$. As indicated, temperature affects the yield parameter K_{p} which is definitely of great importance. Yield function F is actually an uniaxial equivalent for the corresponding characterization of the otherwise spatial stress state. Accordingly, the loading function $f(\boldsymbol{\sigma} - \boldsymbol{\alpha})$ is the corresponding mapping to uniaxial stress representation and yield parameter K_{p} becomes uniaxial yield stress.

With respect to (29), where only non-positive values of the yield function F are admissible by definition, i.e. $F \leq 0$, characterization of the current material response that corresponds to eventual change of the applied loads can be uniquely determined. Accordingly, the mechanical states, proving at some level of loading $F<0$, are characterized by elastic response, irrespective of either loading or unloading is applied. If hardening materials are considered, which means $\partial K/\partial \varepsilon_{\mathrm{p}} > 0$, then occurrence of plastic deformation is conditioned by the stress state corresponding to $F=0$ and stress change, associated with the given change of the applied loads, corresponding to $\mathrm{d}F=0$.

In order to describe properly conditions met in metal forming processes the above description of boundary conditions should be enlarged. Because in metal forming a change of initial workpiece geometry is imposed by direct action of tooling, i.e. punch and die, on the formed workpiece, the considered mechanical problem actually belongs to a class of contact mechanics problems. Accordingly, the usual division of the boundary Γ should be correspondingly enlarged by taking contact conditions at the common interface, say Γ_c, between the contacting bodies into account. This enlargement yields $\Gamma_u \cup \Gamma_\sigma \cup \Gamma_c = \Gamma$, by fulfilling simultaneously $\Gamma_u \cap \Gamma_\sigma = \Gamma_u \cap \Gamma_c = \Gamma_\sigma \cap \Gamma_c = \varnothing$.

In contrast to essential and natural boundary conditions that are defined explicitly, at the contact boundary Γ_c none of the problem variables are given explicitly. Since at that boundary stress-displacement compatibility between the variables of the respective bodies in contact must be respected, this relationship is established implicitly by considering coupling with the contacting body. This compatibility namely implies that kinematic and stress variables at material points on the adjacent surfaces follow the non-penetrability condition, kinematic stick-slip relations according to the actual frictional law, and contact stresses continuity [11].

If the two bodies in contact are denoted respectively by $\doteq_{\mathrm{A}}$ ($\boldsymbol{x} \in \Omega_{\mathrm{A}}$) and $\doteq_{\mathrm{B}}$ ($\boldsymbol{x} \in \Omega_{\mathrm{B}}$), and their common boundary by $\Gamma_c = \Gamma_{\mathrm{A}} \cap \Gamma_{\mathrm{B}}$, then the compatibility of respective contact stresses (α=A,B) is imposed by

$$\boldsymbol{p}_A + \boldsymbol{p}_B = \boldsymbol{0} \;\; ; \quad \boldsymbol{p}_\alpha = \boldsymbol{\sigma}_\alpha . \boldsymbol{n}_\alpha \;\; , \quad \boldsymbol{x} \in \Gamma_c \quad , \; (30)$$

while consistency of the contact status poses additional constraints on the contact tractions

$$\sigma_\alpha = \boldsymbol{p}_\alpha . \boldsymbol{n}_\alpha \le 0 \quad \wedge \quad \tau_\alpha = \left| \boldsymbol{p}_\alpha - \sigma_\alpha \boldsymbol{n}_\alpha \right| \le \mathrm{P}(\mu, \sigma_\alpha) \;\; , \boldsymbol{x} \in \Gamma_c \quad , \qquad (31)$$

where σ_α and τ_α are respectively the normal and tangential component of the traction vector $\boldsymbol{p}_\alpha$. The constraint posed on τ_α establishes actually its relation with respect to frictional resistance $\mathrm{P}(\mu,\sigma_\alpha)$, with μ being coefficient of friction.

Kinematic compatibility of the contacting points $\boldsymbol{x}_A = \boldsymbol{x}_B$, which occupy at a given stage of loading the same position, is directly related to the actually established relationship of τ_α in (31). By an additional loading established inequality in the considered relationship imposes equality of displacements, while established equality imposes equality of displacements in the direction normal to the actual contact area, which can be formulated as follows

$$\mathrm{d}\boldsymbol{u}_A = \mathrm{d}\boldsymbol{u}_B \quad \vee \quad \mathrm{d}u_A^n = \mathrm{d}u_B^n \;\; ; \quad \mathrm{d}u_\alpha^n = \mathrm{d}\boldsymbol{u}_\alpha . \boldsymbol{n}_A \;\; , \quad \boldsymbol{x} \in \Gamma_c \quad . \quad (32)$$

In principle, a solution to the contact problem can be then achieved by coupling the two single domain solutions, provided compatibility (30)-(32) of the two mechanical states is respected.

Another type of mechanical problem can be formulated with respect to hot metal forming, where elastic deformation is negligible and viscoplastic response dominates. In principle, governing equations (26) are fully applicable, provided that the stress and strain tensor, $\boldsymbol{\sigma}$ and $\boldsymbol{\varepsilon}$, are substituted by their deviatoric parts, $\mathbf{s}$ and $\mathbf{e}$ respectively, and rate form of the respective equations is considered. The constitutive equation in (26) is adequately substituted by a corresponding viscoplastic one [12]. Often, the Norton-Hoff law in the form of

$$\mathbf{s} = 2K \left(\sqrt{3}\, e_{vp}\right)^{m-1} \dot{\mathbf{e}} \qquad (33)$$

is successfully applied. The physical parameters K and m are respectively the consistency of the material and the rate sensitivity index, while e_{vp} is the equivalent strain rate, similar to the previously mentioned equivalent plastic strain ε_p. Their respective definitions are

$$\varepsilon_p = \int \sqrt{\frac{2}{3} \dot{\boldsymbol{\varepsilon}}^p : \dot{\boldsymbol{\varepsilon}}^p}\, \mathrm{d}t \;\; ; \quad e_{vp} = \sqrt{\frac{2}{3} \dot{\mathbf{e}} : \dot{\mathbf{e}}} \quad . \qquad (34)$$

In the viscoplastic problem, as well as in elastoplastic one, material incompressibility is assumed with regard to inelastic deformation, yielding

$$\mathrm{tr}\, \mathrm{d}\boldsymbol{\varepsilon}^p = 0 \;\; ; \quad \mathrm{div}\, \dot{\boldsymbol{u}} = 0 \quad , \quad (35)$$

where tr stays for the trace of differential of plastic strain tensor $\boldsymbol{\varepsilon}^p$. The time evolution of the velocity field $\boldsymbol{v}(\boldsymbol{x},t)$ or equivalently $\dot{\boldsymbol{\varepsilon}}(\boldsymbol{x},t)$, the strain rate tensor $\dot{\boldsymbol{\varepsilon}} = \dot{\mathbf{e}}$ is namely primary variable of the viscoplastic problem, is then obtained by considering, along with the considered domain governing equations, the respective rate forms of initial, boundary and contact conditions.

3.5 Governing equations for axisymmetric case

In cases with cylindrical symmetry the problem quantities are invariant with respect to the circumferential direction, the property that affects also the structure of the involved non-scalar physical quantities. Several components of the vector primary variables, such as displacement component u_φ in the mechanical problem, and magnetic and electric strength components H_φ, E_r and E_z, respectively, in the electromagnetic problem are null by definition. From the computational point of view the most significant consequence of cylindrical symmetry is evidenced in the electromagnetic problem, because of the corresponding transformation of a rather complex vector problem to easy manageable scalar problem. On the other hand, the governing equations of the remaining two physical problems preserve their form.

To enable further mathematical manipulations with respect to the new framework a cylindrical coordinate system (r,θ,z) with $\boldsymbol{e}_r$, $\boldsymbol{e}_\theta$, $\boldsymbol{e}_z$ as unit basis vectors will be used. Regarding the emf problem, it can be stated that the current density $\hat{\boldsymbol{J}}(r,z,t)$ of the form

$$\hat{\boldsymbol{J}}(r,z,t) = \hat{\boldsymbol{J}}_0(r,z)\, \exp(\mathrm{j}\omega t) \;\; , \quad \hat{\boldsymbol{J}}_0(r,z) = \hat{J}_\theta(r,z)\, \boldsymbol{e}_\theta \; (36)$$

gives rise to the emf the structure of which is on the contrary rotationally planar

$$\hat{\boldsymbol{H}}(r,z,t) = \hat{\boldsymbol{H}}_0(r,z)\ \exp(\mathrm{j}\omega t)\ ,\quad \hat{\boldsymbol{H}}_0(r,z) = \hat{H}_\mathrm{r}(r,z)\ \boldsymbol{e}_\mathrm{r} + \hat{H}_\mathrm{z}(r,z)\ \boldsymbol{e}_\mathrm{z}\quad , \qquad (37)$$

while the corresponding magnetic potential $\hat{\boldsymbol{A}}(r,z,t)$ is circumferential

$$\hat{\boldsymbol{A}}(r,z,t) = \hat{\boldsymbol{A}}_0(r,z)\ \exp(\mathrm{j}\omega t)\ ,\quad \hat{\boldsymbol{A}}_0(r,z) = \hat{A}_\theta(r,z)\ \boldsymbol{e}_\theta\quad . \qquad (38)$$

The considered emf problem can be thus expressed in terms of a single complex scalar function $\hat{A}_\theta(r,z)$, which on the central axis always vanishes due to cylindrical symmetry of the problem. By setting $\hat{A}_\theta(r,z) \equiv A(r,z)$, $\hat{J}_\theta(r,z) \equiv J(r,z)$ for brevity, and considering the above functional structure the governing differential equation (21) reduces to

$$\Delta A - g\left(A, J_\mathrm{source}, \sigma\right) = 0\ ,\ g\left(A, J_\mathrm{source}, \sigma\right) = \left(\frac{1}{r^2} + \mathrm{j}\mu\omega\sigma\right) A - \mu J_\mathrm{source}\quad , \qquad (39)$$

the solution of which yields, by fulfilment of the associated continuity conditions

$$\begin{aligned} &A_\alpha = A_\mathrm{A}\ ,\ \frac{1}{\mu_\alpha}\left[\frac{\partial \mathrm{A}_\alpha}{\partial \boldsymbol{n}_\alpha} + \frac{A_\alpha}{r} n_\mathrm{r}\right] = \frac{1}{\mu_\mathrm{A}}\left[\frac{\partial A_\mathrm{A}}{\partial \boldsymbol{n}_\alpha} + \frac{A_\mathrm{A}}{r} n_\mathrm{r}\right]\ ,\ \boldsymbol{x} \in \Gamma_\alpha\ ;\ \alpha \in \{\mathrm{I}, \mathrm{W}\} \\ &|\boldsymbol{x}| = \sqrt{r^2 + z^2} \to \infty\ \ \Rightarrow\ \ A_\mathrm{A} \to 0 \end{aligned}\quad , \qquad (40)$$

the space distribution and time variation of the vector magnetic potential $\hat{\boldsymbol{A}}(r,z,t)$.

Contrary to the vector quantities characterizing the emf problem, in the thermal problem the temperature field $T(r,z,t)$ is a scalar field whose initial value is specified by the initial conditions. The time evolution of the temperature field is determined by the governing domain equation (24) and specified boundary conditions (25). In case that material properties are assumed constant the transformation of (24) yields

$$\Delta T + \frac{q_\mathrm{V}}{k} = \frac{\rho c}{k}\frac{\partial T}{\partial t}\quad . \qquad (41)$$

This equation can be further transformed to the same form as obtained for the emf problem. In fact, from the numerical viewpoint any approximation of the considered field time derivative will be realized by an adequate combination of the corresponding field values $T^*(r,z)=T(r,z,t^*)$ computed at previous time instant, i.e. at time t^*, and unknown field values $T(r,z,t)$ at the actual time t considered. For the explicit time scheme the following equation is obtained

$$\Delta T - g\left(T, q_\mathrm{V}, T^*\right) = 0\ ,\ \ g\left(T, q_\mathrm{V}, T^*\right) = \left(\frac{1}{t - t^*}\ \frac{\rho c}{k}\right) T - \left(\frac{q_\mathrm{V}}{k} + \frac{1}{t - t^*}\frac{\rho c}{k} T^*\right)\quad , \qquad (42)$$

the solution of which yields, by fulfilment of the associated boundary conditions the space distribution and time variation of the temperature field $T(r,z,t)$.

Similar conclusions can be made with respect to the governing equation of mechanical problem. For the two non-zero components of the displacement vector, u_r and u_z, equation (28) can be written in the componental scalar form

$$\Delta u_\alpha + \frac{1}{\mu}\left\{(\lambda + \mu)\,\mathrm{grad}(\mathrm{div}\boldsymbol{u}) - (2\mu + 3\lambda)\,\alpha\,\mathrm{grad}(T - T_0) - 2\mu\,\mathrm{div}\,\boldsymbol{\varepsilon}^\mathrm{p} + \boldsymbol{f}\right\}_\alpha = 0,\ \alpha = r, z\quad , \qquad (43)$$

where notation $\{...\}_\alpha$ is used to denote the corresponding vectorial component. Also those equations can be further transformed to the above obtained forms, (39) and (42). Symbolically, we obtain

$$\Delta u_\alpha - g\left(u_\alpha, f_\alpha, u_\alpha^*\right) = 0\ ,\ \alpha = r, z\quad , \qquad (44)$$

where in the term u_α^* the respective contributions of the displacement component adjacent to u_α, temperature T and plastic strain $\boldsymbol{\varepsilon}^\mathrm{p}$ are assembled. The above equations yield, by fulfilment of the associated boundary conditions the space distribution and time variation of the displacement field $\boldsymbol{u}(r,z,t)$.

4. Finite element & Boundary element numerical implementation

4.1 Integral variational formulations

In view of an approximative solution of the governing equations, respectively equation (39) in the emf problem, equation (42) in the thermal problem and equations (44) in the mechanical problem, the problem can be mathematically reformulated. Taking advantage of formally identic structure, and introducing instead of $A(r,z)$, $T(r,z,t)$ and $u_\alpha(r,z,t)$ a generalized variable $u(r,z)$, the following integral equation

$$\int_\Omega \left[\Delta u - g(u, f_V, w^*)\right] v \, d\Omega = 0 \quad , \quad (45)$$

can be obtained, its equivalence with the above stated governing equations being established on the basis of arbitrary selection of admissible function $v(r,z)$. The function $g(u,f_V,w^*)$ represents the corresponding g-terms in the respective governing equations. By applying Green's theorems the above equation can be further reformulated to yield respectively a weak

$$-\int_\Omega \nabla u \, \nabla v \, d\Omega + \int_\Gamma v \frac{\partial u}{\partial \boldsymbol{n}} d\Gamma - \int_\Omega g(u, f_V, w^*) \, v \, d\Omega = 0 \quad , \quad (46)$$

and inverse variational form of the basic integral formulation

$$\int_\Omega u \, \Delta v \, d\Omega + \int_\Gamma \left(v \frac{\partial u}{\partial \boldsymbol{n}} - u \frac{\partial v}{\partial \boldsymbol{n}} \right) d\Gamma - \int_\Omega g(u, f_V, w^*) \, v \, d\Omega = 0 \quad . \quad (47)$$

These two integral equations are fundamental equations for the finite element (FEM) and boundary element (BEM) methodologies that will be applied in the approximative solution of the problem.

To allow general treatment of the both approximation approaches we take again the generalized variable $u(r,z)$ as our primary variable, which will be in accordance to the applied approach adequately discretized.

4.2 Finite element approximation

Field approximation of the generalized variable $u(r,z)$ in the finite element domain $\Omega^F=\sum\Omega_e$ is based on the respective nodal values U_k^F and corresponding local polynomial approximation within each finite element Ω_e

$$U_e^F(r,z) = \sum_{k=1}^{N_{fe}} \Phi_k^e(r,z) U_k^F \ , \ \Phi_k^e(r_i, z_i) = \delta_{ik} \ ; \ (r,z) \in \Omega_e \quad . \quad (48)$$

In order to obtain the corresponding FEM discrete formulation of the considered physical problems we subject, considering the specified approximation (48), the weak variational formulation (46) to the application of a finite series of test functions $v_k(r,z) \in \{v_k^F; v_k^F \equiv \Phi_k^e\}$ that are associated to the given FE discretization nodes. The result of the test functions application is a corresponding system of linear equations with U_k^F as unknowns. Its matrix structure, where internal domain nodal quantitities are separated from the contour ones for convenience, regarding subsequent coupling with the corresponding BE set of equations when considering a multi-domain problem, is as follows

$$\begin{bmatrix} \mathbf{S}_{II}^F & \mathbf{S}_{IC}^F \\ \mathbf{S}_{CI}^F & \mathbf{S}_{CC}^F \end{bmatrix} \begin{Bmatrix} \boldsymbol{U}_I^F \\ \boldsymbol{U}_C^F \end{Bmatrix} = \begin{Bmatrix} {}^{\Omega}\boldsymbol{F}_I^F \\ {}^{\Omega}\boldsymbol{F}_C^F + {}^{\Gamma}\boldsymbol{F}_C^F \end{Bmatrix} \quad . \quad (49)$$

In a single domain problem this system is solved by considering the corresponding essential and boundary conditions.

4.3 Boundary element approximation

Alternatively, the field approximation of the generalized variable $u(r,z)$ can be performed exclusively upon respective approximation of its boundary distribution. Then, the approximation of the primary variable $u(r,z)$ on the domain's boundary $\Gamma^{\mathrm{B}}=\sum\Gamma_{\mathrm{e}}$ is based on the respective nodal values $U_{\mathrm{k}}^{\mathrm{B}}$ and corresponding local polynomial approximation along each boundary element Γ_{e}

$$U_{\mathrm{e}}^{\mathrm{B}}(r,z)=\sum_{\mathrm{k=1}}^{\mathrm{N_{be}}}\psi_{\mathrm{k}}^{\mathrm{e}}(r,z)U_{\mathrm{k}}^{\mathrm{B}}\ ,\ \psi_{\mathrm{k}}^{\mathrm{e}}(r_{\mathrm{i}},z_{\mathrm{i}})=\delta_{\mathrm{ik}}\ ;\ (r,z)\in\Gamma_{\mathrm{e}}\quad .\qquad (50)$$

In addition, in the BE approach also normal derivative must be approximated on the boundary. This approximation is based on the respective nodal values and corresponding local polynomial approximation along each boundary element Γ_{e}

$$\left(\frac{\partial U}{\partial \boldsymbol{n}}\right)_{\mathrm{e}}^{\mathrm{B}}(r,z)=\sum_{\mathrm{k=1}}^{\mathrm{N_{beq}}}\chi_{\mathrm{k}}^{\mathrm{e}}(r,z)Q_{\mathrm{k}}^{\mathrm{B}}\ ,\ \chi_{\mathrm{k}}^{\mathrm{e}}(r_{\mathrm{i}},\mathrm{z}_{\mathrm{i}})=\delta_{\mathrm{ik}}\ ;\ (r,z)\in\Gamma_{\mathrm{e}}\quad .\qquad (51)$$

In order to obtain the corresponding BEM discrete formulation of the considered physical problems we subject, considering the specified approximations (50) and (51), the inverse variational formulation (47) to the application of a finite series of test functions $v_{\mathrm{k}}(r,z)\in\{v_{\mathrm{k}}^{\mathrm{B}};v_{\mathrm{k}}^{\mathrm{B}}\in\Delta v_{\mathrm{k}}^{\mathrm{B}}-g(v_{\mathrm{k}}^{\mathrm{B}},0,0)=-\delta(r-r_{\mathrm{k}},z-z_{\mathrm{k}})\}$ that are associated to the given BE discretization nodes. The result of the test functions application is a corresponding system of linear equations with $U_{\mathrm{k}}^{\mathrm{B}}$ and $Q_{\mathrm{k}}^{\mathrm{B}}$ as unknowns, which reads

$$\mathbf{S}_{\mathrm{U}}^{\mathrm{B}}\boldsymbol{U}_{\mathrm{C}}^{\mathrm{B}}+\mathbf{S}_{\mathrm{Q}}^{\mathrm{B}}\boldsymbol{Q}_{\mathrm{C}}^{\mathrm{B}}={}^{\Omega}\boldsymbol{F}_{\mathrm{C}}^{\mathrm{B}}\quad .\ (52)$$

In a single domain problem this system is solved by considering the corresponding essential and boundary conditions.

4.4 Coupled Finite element & Boundary element approximation

Coming back to our particular case of modelling the considered emf problem there are two major reasons to use mixed FE-BE approach in a numerical solution to the considered multi-domain problem [10]. The domain of a workpiece could experience significant nonlinear material behaviour, while the surrounding air domain, which is in principle infinite, is characterized by constant physical parameters. In addition, the relative position between the inductor and a workpiece is continuously changing during the induction process. In respective local reference frames the physical components, i.e. the coil and the heated piece, can be discretized through volume uniquely by finite elements, their varying relative position in the absolute reference frame not affecting the finite element structure within the local domain. On the contrary, as a linear domain problem can be always transformed to a boundary problem, the respective air domain can be considered in an associated absolute reference frame just by a corresponding discretization of its boundary. Due to the established behaviour of emf at infinity the only boundaries to be considered are those appertaining to the coil and the piece. Modelling of an infinite domain is so avoided in an elegant manner, but the greatest advantage to use boundary elements is certainly a facilitated management of the boundaries space variation which can be done solely by considering it locally, i.e. within the air subdomain. Therefore, no finite element remeshing is needed.

In accordance to the most appropriate discretization methodology applied the investigated multi-domain problem can be solved by finding a solution of individual subdomain problems in terms of nodal domain/boundary values of the respective physical variables, the physical consistency of the overall solution being ensured by imposing the continuity conditions (40) across the subdomain interfaces.

In principle, in a multi-domain problem two uncoupled systems of equations, regardless of whether FEM or BEM is used, can be built upon given discretization. Because of existing interdomain coupleness their physically consistent solution is however attained only by simultaneous consideration of the corresponding interface continuity conditions. In view of direct application to the

particular induction heating problem, we are considering, the coupling of a FEM discretized domain with a BEM discretized domain is of interest. Accordingly, the respective FEM and BEM systems of equations, as determined by (49) and (52)

$$\begin{bmatrix} \mathbf{S}_{II}^{F} & \mathbf{S}_{IC}^{F} \\ \mathbf{S}_{CI}^{F} & \mathbf{S}_{CC}^{F} \end{bmatrix} \begin{Bmatrix} \boldsymbol{U}_{I}^{F} \\ \boldsymbol{U}_{C}^{F} \end{Bmatrix} = \begin{Bmatrix} {}^{\Omega}\boldsymbol{F}_{I}^{F} \\ {}^{\Omega}\boldsymbol{F}_{C}^{F} + {}^{\Gamma}\boldsymbol{F}_{C}^{F} \end{Bmatrix} \quad , \quad \mathbf{S}_{U}^{B}\boldsymbol{U}_{C}^{B} + \mathbf{S}_{Q}^{B}\boldsymbol{Q}_{C}^{B} = {}^{\Omega}\boldsymbol{F}_{C}^{B} \equiv \boldsymbol{0} \qquad \cdot (53)$$

are to be solved simultaneously. Here, reference is made directly to the considered emf problem, therefore, ${}^{\Omega}\boldsymbol{F}_{C}^{B} = \boldsymbol{0}$. The fulfilment of the continuity conditions (40) imposes coupling of the two systems, which is established in discretized form by corresponding connectivity matrices $\mathbf{C}_{\alpha}$

$$\boldsymbol{U}_{C}^{B} = \mathbf{C}_{U}\boldsymbol{U}^{F} \equiv \mathbf{C}_{UC}\boldsymbol{U}_{C}^{F} \quad , \quad {}^{\Gamma}\boldsymbol{F}_{C}^{F} = \mathbf{C}_{QU}\boldsymbol{U}_{C}^{B} + \mathbf{C}_{Q}\boldsymbol{Q}_{C}^{B} \qquad \cdot \quad (54)$$

The solution of the resulting coupled system of equations

$$\begin{bmatrix} \mathbf{S}_{II}^{F} & \mathbf{S}_{IC}^{F} & \mathbf{0} \\ \mathbf{S}_{CI}^{F} & \mathbf{S}_{CC}^{F} - \mathbf{C}_{QU}\mathbf{C}_{UC} & -\mathbf{C}_{Q} \\ \mathbf{0} & \mathbf{S}_{U}^{B}\mathbf{C}_{UC} & \mathbf{S}_{Q}^{B} \end{bmatrix} \begin{Bmatrix} \boldsymbol{U}_{I}^{F} \\ \boldsymbol{U}_{C}^{F} \\ \boldsymbol{Q}_{C}^{B} \end{Bmatrix} = \begin{Bmatrix} {}^{\Omega}\boldsymbol{F}_{I}^{F} \\ {}^{\Omega}\boldsymbol{F}_{C}^{F} \\ {}^{\Omega}\boldsymbol{F}_{C}^{B} \end{Bmatrix} \quad (55)$$

yields nodal values of the magnetic vector potential $\boldsymbol{A}$ ($\boldsymbol{U}=\boldsymbol{A}$) upon which the heat generation over the volume of the workpiece can be computed.

5. Numerical simulation of physically coupled study cases

5.1 Case 1 – Induction heating – quenching simulation

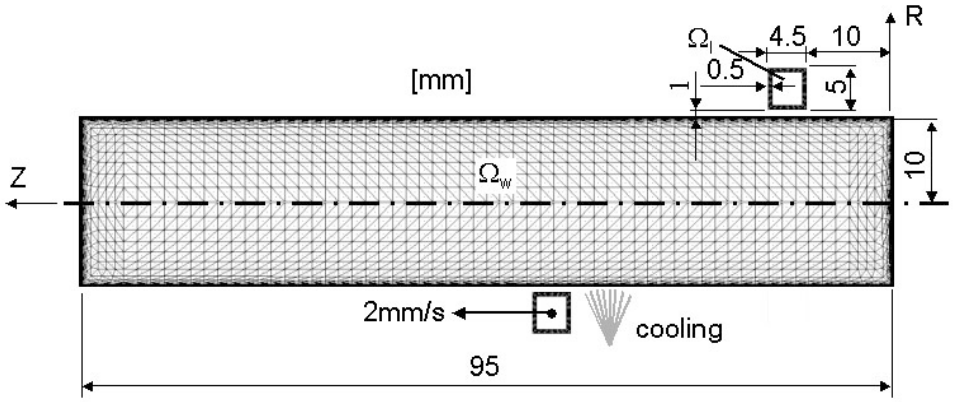

Figure 1: Numerical model of induction heating - quenching set-

In the induction heating – quenching set-up (Fig. 1), where induction heating is followed by immediate quenching, the high frequency electric source (ω=400kHz) with the effective current variation, as shown in Fig. 2a, is applied for 70s on a moving copper coil ($\sigma=60.10^{6}\,(\Omega m)^{-1}$, $\mu_r=1$) which encloses a workpiece of initial temperature 22^{0}C, the latter having the Curie point at temperature 768^{0}C. The coil displacement in the axial direction is realized according to the given velocity profile (Fig. 2a). Because of large variation of the temperature field due to the induced emf the physical properties are considered as temperature dependent, and when actual also magnetic field dependent (Fig. 2b).

In the thermal part of computation thermal convection and radiation is taken into account, with convection heat transfer coefficient being $10W/m^2K$ on the workpiece surface exposed to heating. Quenching of the workpiece, which is applied immediately after passing of the inductor, is performed corresponding to two different intensities of cooling, the respective heat transfer coefficients being $10W/m^2K$ (quenching on air) and $1000W/m^2K$ (quenching by water). Emissivity coefficient of the workpiece is taken as 0.92.

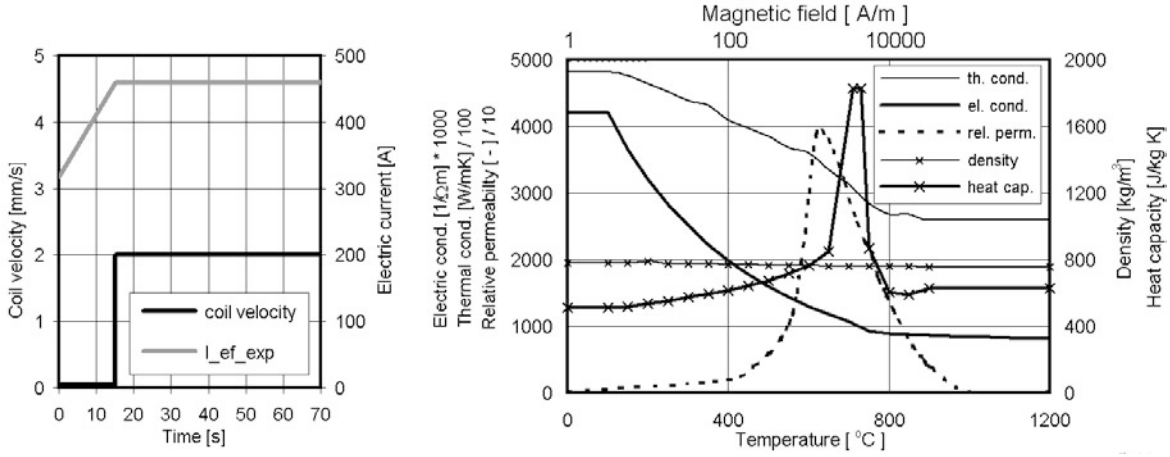

Figure 2: Time variation of induction heating process parameters & Temperature dependence of material properties

In the mechanical part thermo-elasto-plastic material response with linear temperature independent hardening ($H = 23333$MPa), and constant Young's modulus and Poisson's ratio, their values being respectively 210000MPa and 0.3, is assumed. The yield stress and coefficient of thermal expansion are taken, however, as temperature dependent, obeying functional relations

$$\sigma_{\mathrm{p}}(\tilde{T}) = 279 + 6.616\,\tilde{T} - 5.855\,\tilde{T}^2 + 0.042\,\tilde{T}^3 + 0.025\,\tilde{T}^4 \text{ [MPa]}$$

$$\alpha(\tilde{T}) = [12.0842 - 0.8601\,\tilde{T} + 0.1811\,\tilde{T}^2 + 0.0169\,\tilde{T}^3 - 0.0027\,\tilde{T}^4].10^{-6} \text{ [K}^{-1}\text{]}$$

where dimensionless temperature parameter $\tilde{T}$ stays for $\tilde{T} = T.10^{-2}$, and temperature T is to be taken in ^{0}C.

In the actual numerical model (Fig. 1) a triangular FE discretization of the workpiece domain with a quadratic field approximation for the primary variable has been used in the electro-magnetic, thermal and mechanical analysises. In electro-magnetic analysis the inductor and air domain is taken into account, too. For discretization of the inductor domain we used the same FE as for the workpiece domain, while the air domain has been discretizated by BE with a quadratic function approximation, coinciding in nodes with boundary edges of the workpiece and inductor. For the approximation of the BE normal derivative on the boundary a sectionally constant approximation has been assumed.

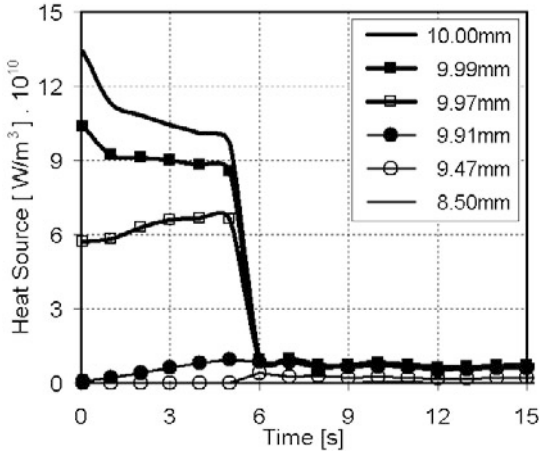

Figure 3: Heat source time evolution

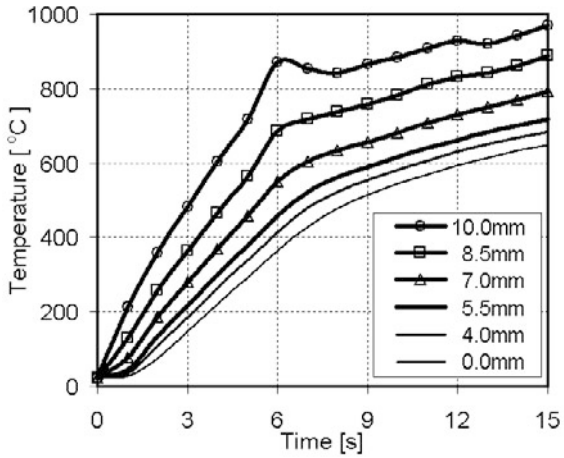

Figure 4: Temperature time evolution

From the displayed computed results in Figs 3-4, showing the time evolution of the generated heat source and the corresponding temperature variation across the workpiece's cross-section beneath the coil during first 15s, that is when the coil is fixed, the impact of several parameters affect-

ing the magnetic induction can be clearly revealed, despite the fact that high source frequency causes sharp localization of the emf near the surface. Most evident is certainly the passing beyond the Curie point with abrupt change in the magnetic permeability, in consequence of which the emf spreads from a very thin surface layer (about 0.05mm) with large heat source intensity into interior of the workpiece (to the depth of about 0.5mm), which is characterized by a significant decrease of the generated heat (Fig. 3). This behaviour is directly reflected in the evolution of the temperature field as it can be seen from the corresponding plots in Fig. 4.

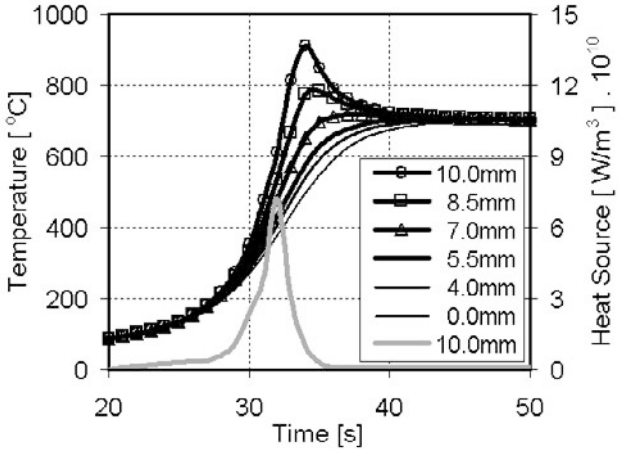

Figure 5: Temperature time evolution

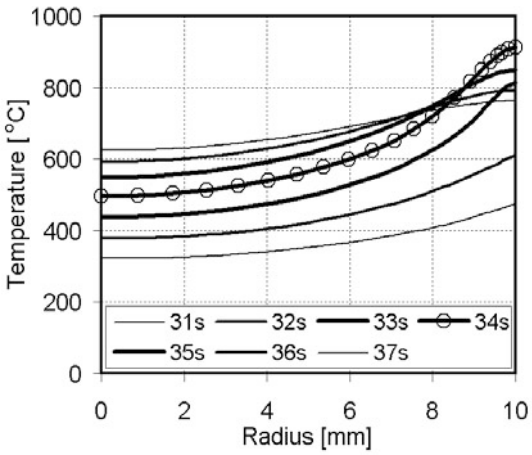

Figure 6: Temperature radial distribution

Later on, with the coil in movement, the above behaviour is not manifested so abundantly. There are several reasons for a remarkable decrease of the intensity of generated heat source on the surface (Fig. 5), all of them being a consequence of mutual interacting effects. First, there is a significant impact of the temperature field variation, established in the part of the workpiece in front of the inductor, on the electric conductivity, and in consequence on the induced eddy currents. Also, much broader region is affected by exceeding of the Curie temperature, diminuishing thus the intensity of the electromagnetic field at the surface. Finally, because of shorter exposure time of the surface points to the high emf less heat is generated by induced electric power, and consequently a smaller temperature variation is realized. The basis for the aforementioned discussion can be revealed by a careful inspection of the temperature time evolution (in case of air cooling) in a workpiece's cross-section in Fig. 5, taken in a position that corresponds to passing of the coil at time 34s. Since influence of end effects on the emf response can be excluded, this position can be considered as a characteristic one. Therefore, this evolution is similar for all the cross-sections coming under the coil during its movement along the workpiece. From Figs 5-6 it is evident that cross-section points close to the surface temperature are subject to much faster change than those in the interior. Temperature time evolution is actually affected by the nature of the considered process which consists of two phases, the heating one with the coil moving toward and over the observed cross-section, and the cooling one, when the coil is moving away from the observed cross-section. Direct impact of the both is most evidenced just at the surface. Characteristic for the first phase is a rapid increase of the surface temperature, while in the second phase the respective temperature decrease can be regulated by a corresponding cooling rate. Fig. 7 displays a comparison of the temperature time evolution for two cases, when, the coil being removed from the observed cross-section, the workpiece is chilled by air or water, the considered cases clearly demonstrating strong dependence of temperature on the cooling intensity.

In quenching processes the most important goal is to obtain a proper mechanical state in a workpiece. Influence of temperature time evolution on the stress-strain field in the workpiece after quenching can be seen from Figs 8-9. Although the accumulated equivalent plastic strain in case of water quenching is higher than in air quenching, the resulted residual stresses are smaller. Smaller residual stresses are the result of more intensive cooling, where, in contrast to air quenching, additional plastic deformation occures with opposite sign of deformation than in the heating phase.

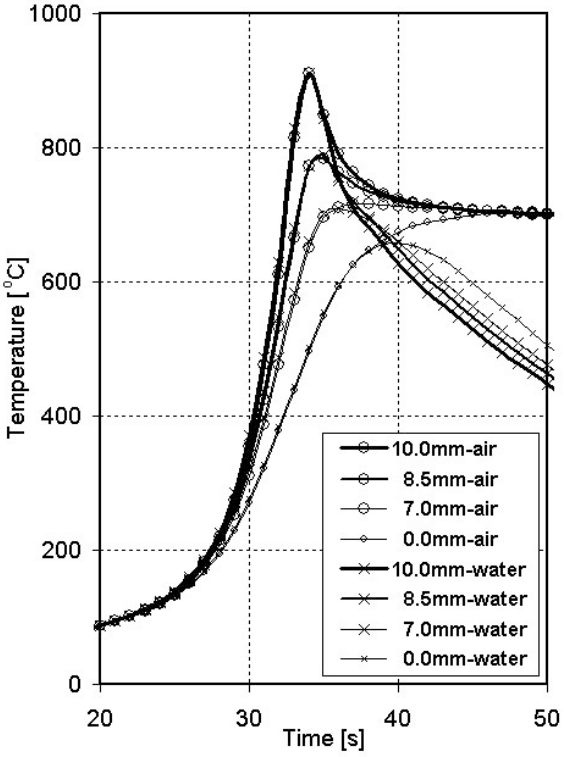

Figure 7: Temperature time evolution in dependence of cooling intensity

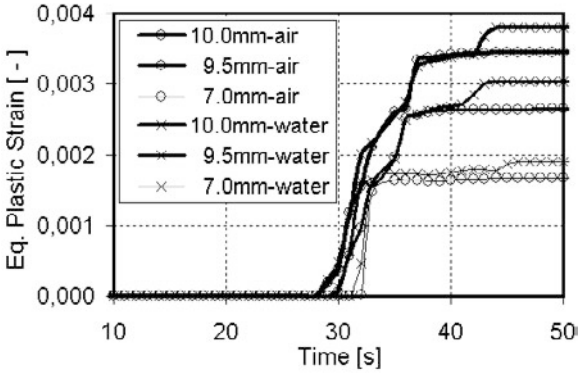

Figure 8: Equivalent plastic strain

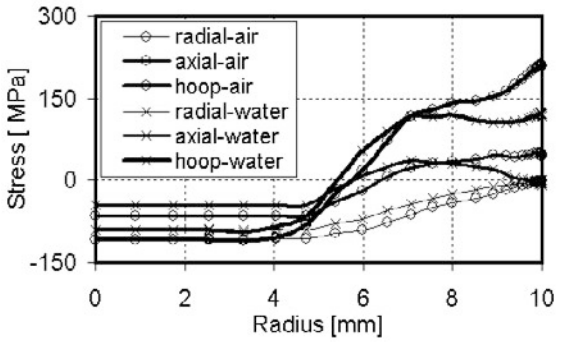

Figure 9: Residual stresses due to different cooling rates

5.2 Case 2 – Induction heating – forging simulation

Induction heating is used also in connection with metal forming. In order to facilitate the forming operation a workpiece is often preheated to a desired temperature, thus diminuishing considerably its resistance to forming. In the considered case a workpiece of initial temperature 20^0C, its Curie point being at temperature 768^0C, is heated by means of the low frequency electric source (ω=60Hz), applied on a fixed copper inductor that consists of 164 coil turns ($\sigma=60.10^6$ $(\Omega m)^{-1}$, μ_r=1). The respective effective current time variation is shown in Fig. 11. Same material properties are assumed as in the previous case with temperature and magnetic field dependence taken fully into account, since the experienced variation of the temperature field is even greater.

Due to thermal insulation of the workpiece during heating no thermal convection and radiation at the workpiece's surface is taken into account in thermal part of computation.

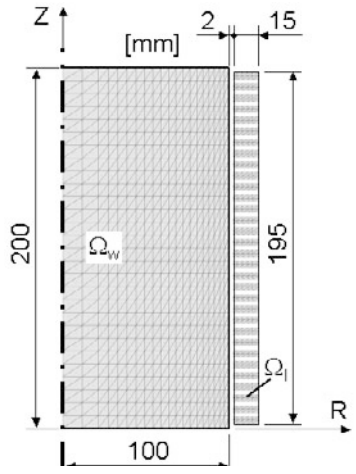

Figure 10: Numerical model

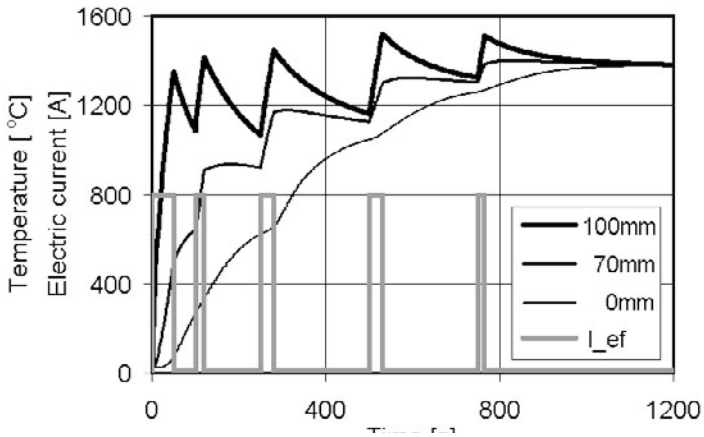

Figure 11: Time variation of the effective electric current and temperature time evolution in the workpiece

Because uniform temperature field, obtained in the workpiece before forging is high enough to

ensure a semi-solid material state, the visco-plastic material response according to Norton-Hoff's law ($K = 1\,\mathrm{Pa\,s^m}$, $m = 0.1$) is assumed. Since presence of mushy state essentially reduces the friction between the workpiece and the forging tool, a friction free contact is considered. Also, no temperature variation in the workpiece during forging is considered, due to short duration (Fig. 12).

The same combined FE – BE discretization, as used in case 1, has been applied in computer simulation of induction heating of the workpiece and subsequent forging (Fig. 10). Also, in order to reduce the computational time, the inductor domain has been divided in 32 subdomains.

Advantage of induction heating with low frequency electric source is that emf spreads into interior of the workpiece, thus generating heat through the whole domain. This behaviour is reflected in more homogeneous temperature field evolution, with temperature difference between the workpiece's surface and its interior being not so large, as when using a high frequency electric source. As evident from Fig. 11 an optimal time variation of the electric current resulting in efficient heating can be obtained, based exclusively on the corresponding computer simulation of induction heating. In the considered case we succeeded to heat the workpiece to the domain uniform temperature $1390^{o}C \pm 10^{o}C$ in 20 minutes.

The subsequent forging is decisevely characterized by the strain rate distribution which, due to its direct relation with the stresses, determines actually the resistance to forming. Such a strain rate field distribution, taken at a position near the end of forging, is displayed in Fig. 13.

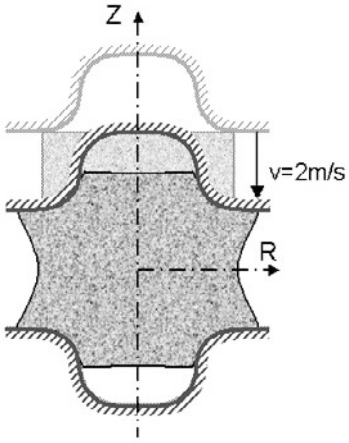

Figure 12: Forging

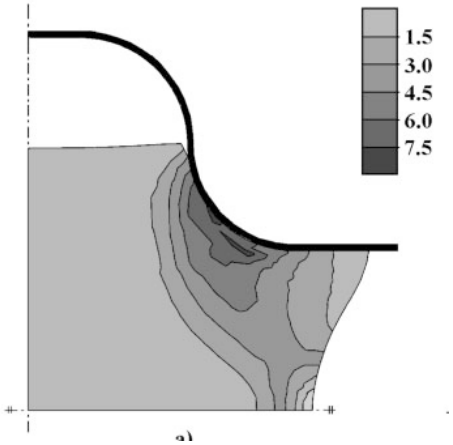

Figure 13: Equivalent strain rate

6. Conclusion

Merely qualitative estimation of technological parameters, based otherwise on a logical, but simplified manner of thinking, is often misleading and can result in false conclusions. This is particularly true in phenomenologically complex technology processes, with time evolution of the thermomechanical fields and simultaneous development of diverse physical phenomena being interdependent. Resulting from the human limited capability to analyse such complex problems intuitively, using of computer aided analyses in engineering, and the possibilities given thereby, is of great importance. For this purpose a reliable and computationally effective numerical modelling of mathematically modelled physical relationships is needed. Providing, that by its corresponding implementation into a computer code such a model is subsequently also experimentally validated, then it can be given at the user's disposal for his further exploitation.

In the paper issues regarding solution of physically coupled nonlinear problems and respective solution strategies have been considered, along with the discussion on the selection of appropriate space and time discretization methods that result in a computationally efficient solution. In particular, three physical problems: the thermomechanical, heat conduction and the electromagnetic problem, respectively, have been considered in detail, including their coupling effects. Results, obtained upon the corresponding computer simulations of two study-cases, have been thorougly discussed in view of its physical background.

References

[1] Štok B., Mole N., "Finite element modelling and simulation of electroslag remelting process". Proc. of the Third Int. Conf. on Tech. of Plasticity, 2 : 1013-1019, Kyoto, Japan, July 1990.

[2] Štok B., Mole N., "Matematično modeliranje rotacijskega litja – analiza termomehanskega stanja v orodju = Mathematical Modelling of Rotary Casting - Thermomechanical Analysis of a Mould", Kovine Zlitine Tehnologije, 27-1/2 : 175-180, 1993.

[3] Mihelič A., Štok B., "Optimization of Single and Multistep Wire Drawing Processes with Respect to Minimization of the Forming Energy". Struct. Optim., 12-2/3 : 120-126, 1996.

[4] Štok B., "Računalniško simuliranje – podpora učinkovitejšemu načrtovanju tehnoloških procesov = Computer Simulation – a Means for Improving the Efficiency of Technology Processes Design", Strojniški vestnik, 43-11/12 : 463-482, 1997.

[5] Koc P., Štok B., "Computer-Aided Identification of the Yield Curve of a Sheet Metal after Onset of Necking", Computational Materials Science, (to be printed), 2003.

[6] Poje J., Štok B., Mole N., "By Interconnecting and Integration of Knowledge Toward a New Technological Quality". Proc. of IDDRG 2003 Conf., pp. 233-240, Bled, Slovenia, May 2003.

[7] Rojc T., Štok B., "About Finite Element Sensitivity Analysis of Elastoplastic Systems ate Large Strains", Computer & Structures, 81 : 1795-1809, 2003.

[8] Mole N., "Računalniška simulacija procesa preoblikovanja kovin v testastem stanju – Computer Simulation of Metal Forming in Semi-Solid State", PhD. thesis, University of Ljubljana, 2002.

[9] Rus P., Štok B., Mole N., "Parallel Computing with Load Balancing on Heterogeneous Distributed Systems", Adv. Eng. Softw., 34-4 : 185-201, 2003.

[10] Štok B., Mole N., "Coupling FE and BE Approach in Axisymmetric Eddy Current Problems Solution". Proc. of the Int. Conf. on Comp. Eng. & Sci., 6 p., Puerto Vallarta, Mexico, August 2001.

[11] Štok B., Hudoklin A., "How to Tuckle the Compatibility Constraints in a Computational Solution of Frictional Contact Problem", Finite Elem. Anal. Design, 18 : 111-119, 1994.

[12] Mole N., Chenot J.L., Fourment L., "A Velocity Based Approach Including Acceleration to the Finite Element Computation of Viscoplastic Problems", Int. J. for Num. Meth. in Eng., 39 : 3439-3451, 1996.

PhD. Boris Štok, Professor, Faculty of Mechanical Engineering, University of Ljubljana, Aškerčeva 6, Ljubljana, Slovenia, +386-1-4771-425, boris.stok@fs.uni-lj.si

PhD. Nikolaj Mole, Assistant, Faculty of Mechanical Engineering, University of Ljubljana, Aškerčeva 6, Ljubljana, Slovenia, +386-1-4771-425, nikolaj.mole@fs.uni-lj.si

4th International Congress
of Croatian Society of Mechanics
September, 18-20, 2003
Bizovac, Croatia

4thICCSM

MESOMECHANICS OF QUASISTATIC FRACTURE

Michael P. Wnuk

ABSTRACT

A tri-axiality dependent cohesive zone model for a stationary and a quasistatic crack is proposed. The model is rooted in the mesomechanical approach to Fracture Mechanics and it is inspired by the quantum law concerning emission of light, which was postulated by Max Planck at the end of 19th century.

The model provides an extension of the early concepts of Barenblatt, Dugdale and the Bilby-Cotrell-Swinden team. It also incorporates the experimental observations of the pre-fracture states due to Panin and his school in Tomsk. Relations between micro- and macro-parameters that characterize the deformation and fracture processes in dissipative media are described in detail.

The analysis suggests that the ratio of the "true" work of fracture to the total energy dissipated during the course of the irreversible deformation contained within the end zone can be used as a measure of material resistance to a quasistatically propagating fracture. This ratio, evaluated for various sets of microstructural parameters that define the distribution of the restraining stresses within the cohesive zone, provides both conceptual and quantitative foundation for a better understanding of the phenomena essential during the early stages of fracture in non-elastic solids. Some of the by-products of the analysis are novel physical interpretations of the fracture toughness enhancement that leads to a developed R-curve.

Keywords: *cohesive zone, J-integral, specific work of fracture, cohesive tractions, microstructure, triaxiality, local constraints, ductile-brittle transition, surface tension, plastic work, ductility, overstress, dissipation.*

0. Introduction

Now, at the onset of the 21st century we are facing a few paradoxes of somewhat different nature. Fundamentally, though, these paradoxes are analogous to the problem encountered a century ago. If we decide to use symbol λ to denote the distance from the boundary of the "separation surface" in a solid body, usually identified with the crack front in the Fracture Mechanics context, then right away we observe certain peculiar predictions resulting from the theory based in the Continuum Mechanics. Singularities of all kinds abound; the classic Griffith-Irwin singular stress field of $\lambda^{-1/2}$ type for a crack contained in a perfectly brittle solid. Then there are the HRR kind of singularities of the type $\lambda^{-1/(1+n)}$ for a stress field, and $\lambda^{-n/(1+n)}$ for the strain field in a power hardening medium of Ramberg - Osgood kind. Note that the product $\boldsymbol{\sigma}.\boldsymbol{\varepsilon}$ yields a singularity of the λ^{-1} type, which upon

integration over the volume of the body yields finite strain energy. This is so for a stationary crack. In case of quasi-statically extending crack, the singularity changes to log(λ), while for dynamically moving defects the nature of the singularities becomes velocity dependent. One important aspect of the proposed study will be to focus on the transition from slow to fast motion of a propagating crack. In what follows we provide a very concise abstract of the entities and relations used in dealing with discontinuities and crack-like defects. First, we consider the approaches suggested by the Continuum Mechanics, show their shortcomings, and then elaborate on the alternative "quantum" mechanical description that opens novel possibilities in research into mesomechanics of fracture.

It has been shown that the variations in the microstructural parameters strongly affect the process zone along with the associated work of separation. The other important factors that influence the cohesive stress distribution and all the resulting fracture parameters, specifically those that are responsible for a ductile-to-brittle transition of fracture mode, are the characteristics of the state of stress induced in the vicinity of the crack front. These 3D effects are best represented by the triaxiality parameter, defined as the ratio of the mean stress to the von Mises effective stress.

As it turns out, when we consider deformation, local pre-fracture states as defined by Panin, and finally, the fracture processes at the micro- or meso-levels and the associated dissipation energies that characterize these irreversible events, none of these concepts work. They all break down at the distances less than a certain critical length, which equals the size of the process zone and cannot be determined by the macroscopically measured material constants alone. The very fact that one must introduce into the mathematical model the finite entity, called "process zone", adjacent to the crack front, provides an evidence of breakdown of the classic field theories. This breakdown occurs at the distances, which are only fractions of the material characteristic length, defined by such constants as fracture toughness and the yield stress. Of course, these two constants are macroscopically "observable" parameters and they provide a convenient link between the standard Mechanics of Fracture, as the one used in Engineering, and a more refined science of Mesomechanics. Here we deal with three length measures, R, Δ and the increment $\widehat{\delta}$, or a "quantum" of the CTOD, the quantity known as the "final stretch", used in the criterion of continuing crack growth in the early stages of fracture. Only the first of the length parameters mentioned here is susceptible to the experimental techniques used in the standard laboratory equipped for Fracture Mechanics tests. The other two, crack growth step Δ and the increment $\widehat{\delta}$ must be determined by certain very subtle and frequently indirect measurements of microstructural nature. Note that the ratio $\widehat{\delta}/\Delta$ is directly proportional to the CTOA, a useful parameter when dealing with nonelastic fracture.

This is the domain of mathematical modeling founded on the premises of Mesomechanics. Development of new concepts and mathematical approaches compatible with Mesomechanics that departs from substantially from the "classic" continuum approaches, is the primary objective of work.

1. Mathematical Model

Whenever a cohesive crack model is applied to explain the phenomena such as onset of fracture and its quasistatic growth in dissipative media, an assumption regarding the so-called "separation law" must be made in addition to the employed constitutive equations that define behavior of a given material. Using an analogy with Planck's law for the radiation of light emitted by a black body at high frequencies, when the wavelength λ approaches zero, Wnuk and Legat (2002) proposed a certain distribution of the cohesive stress within the end zone preceding the crack front. In what follows this end zone is endowed with an internal structure: within the zone of length R there is a small region, say Δ, which represents the process zone, where the final act of decohesion takes place. This region is attached to the physical tip of the crack. As it turns out, the ratio R/Δ plays an important role in relating the micro- and macro-fracture parameters.

If the distance from the physical tip of the crack is measured by a nondimensional coordinate

$$\lambda = \frac{x_1}{R}, \quad 0 \le x_1 \le R, \qquad 0 \le \lambda \le 1 \tag{1.1}$$

then the Wnuk-Legat equation reads

$$S(\lambda,\alpha,n) = S_0\lambda^n \exp\left[\alpha(1-\lambda)\right] \tag{1.2}$$

Here S_0 denotes the reference stress, while α and n are yet undetermined microstructural parameters. An example of a normalized S-distribution, normalization constant being S_0, is given in Fig.1. The figure was drawn for the set α=1 and n=0.2. It is noticed that the maximum in the curve shown in Fig.1, S_{max}/S_0, occurs at the distance $\lambda_{max} = n/\alpha = 0.2$ from the tip of the crack. This point coincides with the outer edge of the process zone Δ embedded within the end zone R, namely

$$\lambda = \left(\frac{x_1}{R}\right)_{x_1=\Delta} = \frac{\Delta}{R} \tag{1.3}$$

The reciprocal of this variable, R/Δ, was shown by Wnuk and Mura (1981) to equal the ratio of the strain at fracture, ε_f, to the yield strain ε_0. Therefore, the quantity R/Δ has been named the "ductility index", and denoted by ρ. For ductile materials the process zone is a small fraction of the end zone, leading to large ρ. For the other extreme material behavior, resulting in brittle fracture, the quantities Δ and R are almost equal, thus ρ-> 1. In the limit of perfectly brittle material behavior (i.e., elastic response up to the point of failure) both Δ and R shrink to a point, and the present model of failure reduces to the Griffith theory.

One may ask a question: does the curve shown in Fig.1 represent a separation law of the material? The answer is "no", because the cohesive law requires that the stress S should be shown as a function of the opening displacement, say δ, not as a function of the distance from the leading edge of the crack (as it is in Fig.1). The model provides sufficient information, though, to transform the curve S vs. λ, shown in Fig.1, into the separation law S vs. δ. When the appropriate boundary value problem is solved, cf. Wnuk and Legat (2002), a certain expression results for the opening displacement within the R-zone due to the action of stresses of type (1.2) – treated as an applied stress in the Sneddon's integrals. This expression reads

$$v(\lambda,\alpha,n) = \frac{n+\alpha}{\alpha+1}\left[\Lambda_1(\lambda)\right]^{(\alpha+n)} - \frac{n-1}{\alpha+1}\left[\Lambda_0(\lambda)\right]^{(\alpha+1)} \tag{1.4}$$

Here the functions Λ_0 and Λ_1 are defined as follows

$$\Lambda_0(\lambda) = \sqrt{1-\lambda} - \frac{\lambda}{2}\ln\left[\frac{1+\sqrt{1-\lambda}}{1-\sqrt{1-\lambda}}\right]$$

$$\Lambda_1(\lambda) = \sqrt{1-\lambda}\left(1-\frac{\lambda}{2}\right) - \frac{\lambda^2}{4}\ln\left[\frac{1+\sqrt{1-\lambda}}{1-\sqrt{1-\lambda}}\right] \tag{1.5}$$

Note that v = 1 for λ = 0, and v equals zero for λ = 1, which designates the outer edge of the R-zone. The normalization constant for the displacement v is the opening displacement at the tip of the crack, $v_{tip} = 4S_0R/\pi E$. The function v = v(λ,α,n) with α = 1, and n = 0.2, is depicted in Fig. 2b. With these equations available to us it is possible to re-plot the graph of Fig.1, in such a way that it will be v (=0.5δ) shown as the independent variable rather than λ. To make this plot we shall be using normalized S and normalized v. To understand the plot shown in Fig.2a, we follow the history of deformation of a fixed material particle. The sequence of events begins at v = 0, where a material cell is yet unbroken, thus the cohesion is not compromised. There S = S_0, and as we move toward the right side of the graph, S passes through a maximum and then falls to zero when v

reaches the critical value. The value of the maximum S can be easily evaluated from Eq. (1.2), and it is

$$S_{\max} = S_0 \left(\frac{n}{\alpha} \right)^n \exp\left[\alpha - n \right] \tag{1.6}$$

Now, we shall apply these equations to a description of the onset of fracture and its slow stable growth that precedes the catastrophic failure.

2. Relationship Between Micro and Macro Material Parameters

Direct measurement of the microstructural constants α and n appears to be an impossible task. However, one can resolve the problem by introducing two macro-variables, accessible in a laboratory test, namely
the over-stress factor, $k = S_{max}/S_0$, and
the ductility index, $\rho = R/\Delta$.
The first of these quantities can be easily deducted from Eq. (1.6), namely

$$k = \frac{S_{\max}}{S_0} = \left(\frac{n}{\alpha} \right)^n \exp\left(\alpha - n \right) \tag{2.1}$$

Experimental determination of the k-factor defined above was described by Siegmund and Brocks (1993), and by Brocks (2001).The second parameter, ρ, is identified with the reciprocal of λ_{max}, i.e.,

$$\frac{R}{\Delta} = \rho = \frac{1}{\lambda_{\max}} = \left(\frac{n}{\alpha} \right)^{-1} = \frac{\alpha}{n} \tag{2.2}$$

Experimental determination of this quantity presents no problem. In fact, it is a part of a standard strength of materials test. As noted in Section 1, for ductile materials we expect ρ>>1. This will be reflected by the proper choice of the parameters α and n, suitable to account for the dissipative nature of the material response. The opposite is true for the quasi-brittle and brittle end of the spectrum of material behavior, when ρ -> 1, and thus we should choose sets in which $\alpha \approx n$.

When Eqs. (2.1) and (2.2) are combined, the following transcendental equation results

$$\ln\left[k \rho^n \right] - n\left(\rho - 1 \right) = 0 \tag{2.3}$$

This equation is elementary and it can be solved for n explicitly, namely

$$n = \frac{\ln k}{\rho - 1 - \ln \rho} \tag{2.4}$$

Also, we have a second equation

$$\alpha = \frac{\alpha \ln k}{\rho - 1 - \ln \rho} \tag{2.5}$$

With these two relations we are prepared to determine unknown microstructural parameters α and n using the input data provided by the macroscopically observable quantities, k and ρ. Let us try this approach for ρ = 10 and k = 5. Substituting these values into Eqs. (2.3) and (2.4) yields

$$n = \frac{\ln 5}{9 - \ln 10} = 0.2403$$
$$\alpha = \frac{10 \ln 5}{9 - \ln 10} = 2.4031 \tag{2.6}$$

It presents no problem to show graphically the dependence of the variables k and ρ on the micro-parameters α and n, or vice versa. This has been done and illustrated in Figs. 3a and 3b. It is noteworthy that since the ductility index satisfies an inequality ρ 1, the denominator of Eq. (2.4) is always positive or it equals zero. Therefore, we expect no negative values for the parameter n. Since α = ρn, the same conclusion holds for α. The limiting case of α = n = 0 corresponds to the Dugdale model, while the set α = 0, n = 1, describes the S-distribution assumed in the Knauss' model, cf. Ungsuwarungsri and Knauss (1987a,b and c).

A more useful representation would involve expressing all the pertinent functional relationships in terms of the ductility index, which is the most accessible variable obtained in laboratory testing. Using equations (2.3) and (2.4) the graphs were constructed as shown in Figs. 4a and 4b.

This representation provides an additional advantage. Since the variable ρ = R/Δ can also be used to represent the material resistance to crack propagation associated with the quasistatic growth (within the small scale yielding range considered here R is proportional to CTOD and also to J_R). For the early stages of non-elastic fracture the parameter ρ becomes a certain function of the increment in the current crack length, say $z = \Delta a/R_{ss}$. Here the steady-state value of the length of the end zone, R_{ss}, has been used as a normalizing constant for the increment of crack length, Δa. If we now combine the results shown in Figs. 4a and 4b with the function z = z(ρ), which is determined by the governing equation of the R-curve, we shall be able to follow the changes in the parameter k (the over-stress) and the variations in the true work of fracture, W, as the crack propagates. This type of analysis is continued in the next section.

It is noteworthy that since the R-curve is a macroscopic manifestation of the subcritical crack growth, some researchers, cf. Cherapanov and Halmanov (1972,1974), Wnuk (1977, 1992) and Bolotin (1990) have attempted to apply the concept to describe the mechanism of fatigue processes. Other modifications of the cohesive zone model were suggested by Kolednik et al. (1997), who studied the influence of the energy dissipation rate on geometry and size effects. Hutchinson (1997) and Goldstein and Perelmuter (1999) have applied the model to evaluate the specific work of fracture associated with an interface crack.

3. Variations in Material Properties Due to Crack Extension. Energy Screening Phenomenon as Source of the R-Curve for Dissipative Media

It can be shown that the specific choice of the microstructural parameters has an insignificant effect on the shape of the R-curve. Therefore, to simplify the mathematics, we shall invoke the Wnuk-Rice-Sorensen differential equation, which defines an R-curve in a ductile solid. The condition of the small scale yielding (ssy) range of material behavior has been assumed in the derivation of this equation, cf. Wnuk (1972, 1974), Rice and Sorensen (1978) and Rice et al. (1980). From entirely two different ways of approach, the following equation emerged

$$\frac{dR}{da} = M - \frac{1}{2} - \frac{1}{2}\ln\left(4R/\Delta\right) \tag{3.1}$$

With the tearing modulus M assumed to be 15% greater than its minimum value, below which there is no stable crack growth, M_{min}, we have

$$M = 1.15M_{\min} = 1.15\left[\frac{1}{2} + \frac{1}{2}\ln\left(4\rho_{ini}\right)\right] \tag{3.2}$$

Now, equation (3.1) can be recast into the form

$$\frac{d\rho}{dz} = \frac{1}{2}\ln\left(\frac{\rho_{ss}}{\rho}\right) \tag{3.3}$$

Numerical integration of this nonlinear differential equation leads to an R-curve shown in Fig. 5. It is seen that the curve initiates at the fracture toughness threshold $(R/\Delta)_{ini} = \rho_{ini}$, assumed as 10, and it levels off at the steady-state value of the toughness measure $(R/\Delta)_{ss} = \rho_{ss} = 20.205$. This upper asymptote of the R-curve is established by a simple relation, compare Wnuk (1974, 1990),

$$\rho_{ss} = \frac{1}{4}\exp\left[2M - 1\right] \tag{3.4}$$

which indicates that the upper level of the universal R-curve increases exponentially with the tearing modulus M.

Once the function R = R(Δa), or – expressed in terms of the nondimensional variables – ρ = ρ(z), is determined, one can proceed with an analysis aimed at the study of variations of the material properties, such as ductility index and the over-stress factor, both strongly influenced by the history of deformation associated with the early stages of fracture. The resistance curve for the case under consideration is shown in Fig. 5.

It turns out that both ρ and k undergo a continuous change in the course of quasistatic crack growth, as shown in Figs. 4. This in turn implies the variations in the microstructural parameters, α and n, which are related to k and ρ via equations (2.3) and (2.4). When the functions shown in Figs. 4a and 4b are re-plotted using the increment of the current crack length z as an independent variable, the new graphs result, and they are shown in Figs. 6a and 6b.

The variations in α and n, as the crack propagates, lead to a gradual modification of the shape of the S-stress distribution, which was to be expected. For three chosen points of the curve shown in Fig. 5, corresponding to ρ equal to 10, 15, and 19, the S-graph are visibly altered, as shown in Fig. 7.

From the point of view focused on the physics of the quasistatic crack growth process perhaps the most significant characteristic parameter is the specific work of fracture, compare Wnuk and Read (1985). When dealing with failure in elastic-plastic solids one should distinguish between the "true" and "apparent" work of fracture. The first one is defined as the energy dissipated within the process zone during the final act of fracture, while the second is identified as the total work performed by the restraining stress S against the opening displacement within the end zone. This quantity, in addition to the work of separation (another name for the true work of fracture) includes the plastic work. Thus, we have two expressions, which describe these two work terms, namely

$$W_{true}(\alpha, n) = C\int_0^{\lambda_{max}} S(\lambda, \alpha, n)\frac{d}{dx}\left[-v(\lambda, \alpha, n)\right]dx, \qquad \lambda_{max} = n/\lambda$$

$$W_{total}(\alpha, n) = C\int_0^1 S(\lambda, \alpha, n)\frac{d}{dx}\left[-v(\lambda, \alpha, n)\right]dx \tag{3.5}$$

The constant C is defined as the product of the tip displacement (1/2 of the CTOD) and the reference stress, thus $C = v_{tip}S_0$. We note that in the limiting case of brittle material response, when $\lambda_{max} = \Delta/R \to 1$, W_{true} approaches W_{total}, while the latter becomes the familiar surface tension γ, introduced by Griffith in his energy balance criterion for the onset of catastrophic fracture.

In ductile materials, though, W_{true} and W_{total} are quite different, and usually $W_{true} \ll W_{total}$. It is of interest to study the ratio of these two quantities, compare Broberg (1979, 1999). Before we formulate the definition, let us consistently replace the parameter n by the ratio α/ρ. This will convert both functions defined in (3.5) into the functions of α and ρ, namely

$$\widehat{W}(\alpha, \rho) = C\int_0^{1/\rho} \overline{S}(\lambda, \alpha, \rho)\frac{d}{dx}\left[-\bar{v}(\lambda, \alpha, \rho)\right]dx \tag{3.6}$$

$$W(\alpha, \rho) = C\int_0^{1/\rho} \overline{S}(\lambda, \alpha, \rho)\frac{d}{dx}\left[-\bar{v}(\lambda, \alpha, \rho)\right]dx$$

Note that the subscripts "true" and "total" have been omitted, while the symbols such as hat and a bar have been added for mathematical correctness. Now, we are ready to define the so-called energy transmission ratio (ETR), namely

$$ETR = w(\alpha, \rho) = \widehat{W}(\alpha, \rho) / W(\alpha, \rho) \tag{3.7}$$

As ρ increases during the quasistatic crack extension, the ETR decreases monotonically, meaning that less and less of the energy available reaches the process zone. This interesting phenomenon is illustrated in Fig. 8, and we shall refer to it as the "energy screening effect" associated with motion of a quasistatic crack.

Because of such screening, material becomes tougher while the crack propagates, and this is reflected by the shape common to all universal, meaning geometry independent, R-curves. In fact, one could propose a reciprocal of the ETR to represent an R-curve, compare Fig. 9, in where three such $(ETR)^{-1}$ curves are plotted vs. the increment of the crack length. Such a definition would provide yet another physically meaningful interpretation of the resistance curve, and it would be added to the set of other quantities commonly used to represent an R-curve, such as K_R, J_R or $CTOD_R$.

The more ductile is the material, the more pronounced is the decrease in the w-ratio as the crack growth progresses. This effect is illustrated in Fig. 10, where two results obtained from two entirely different physical models are plotted side by side. The top curve represents the screening effect derived from the Kanuss's cohesive model that is appropriate for more brittle solids, while the lower curve resulted from the Dugdale model which was designed for rather ductile solids.

In the limiting case of zero ductility, when n -> α and ρ -> 1, the classic theory of Griffith is not capable to account for the stable quasistatic crack extension. Without the energy screening the initial instability and the terminal instability points (visibly distant on any R-curve) merge into a single point, and thus the resistance curve disappears.

4. Conclusions

The proposed distribution of the cohesive forces, which restrain the separation process in the vicinity of the crack front, are analogous to the Max Planck law used to explain radiation given off by a perfectly black body at very short wavelength of the visible light spectrum.

In an attempt to correlate the micro and macro material properties, a mesomechanical model of cohesive stress zone is employed. Both stationary and quasistatical cracks have been considered, and it has been shown that as the crack propagates during the early stages of failure, there is an interplay between the material parameters of both micro and macro nature. These variations are shown to depend on the initial state of the material and the nature of irreversible deformation phenomena that take place within the end zone preceding the crack.

Due to the assumed inner structure of the end zone associated with a crack in a dissipative medium, true fracture energy is separated from the total energy dissipated within the end zone. The ratio of these two energy terms has been defined as a measure of the energy screening phenomenon, while the reciprocal of the same ratio could be used as yet another characteristic of the material resistance to quasistatic fracture.

Although the essential parameters in the model are tri-axiality dependent, the results obtained so far are based on the assumption of the existence of a universal R- curve, which remains geometry independent. In addition, the validity of all the results presented here is subject to the requirement that the range of small scale yielding condition is not exceeded.

REFERENCES

[13] M. P. Wnuk, 1972, "Accelerating Crack in a Viscoelastic Solid Subject to Subcritical Stress Intensity", in *Proceedings of the International Conference on Dynamic Crack Propagation*, pp. 273 – 280, Lehigh University, Editor George C. Sih, publ. by Noordhoff, Leiden.

[14] M. P. Wnuk, 1974, "Quasi-Static Extension of a Tensile Crack Contained in a Viscoelastic-Plastic Solid", J. Appl. Mechanics, Vol. 41, No. 1, pp. 234 – 242.

[15] M. P. Wnuk, 1990, "Mathematical Modeling of Nonlinear Phenomena in Fracture Mechanics", in *Nonlinear Fracture Mechanics*, Editor M. P. Wnuk, published by Springer-Verlag, Wien – New York, CISM Course and Lecture No. 314, International Centre for Mechanical Sciences, Udine, Italy.

[16] M. P. Wnuk, 2001, "Effect of Cohesive Stress Distributions on the Specific Work of Fracture. Triaxiality Dependent Cohesive Zone Model", plenary lecture presented at the 2001 MESOMECHANICS and CADAMT Int. Conference, Tomsk, March 2001, Russian Federation.

[17] M. P. Wnuk and Janko Legat, "Work of Fracture and Cohesive Stress Distributions Resulting From Triaxiality Dependent Cohesive Zone Model", Int. J. Fracture, 2002, in print.

[18] T. Siegmund and W. Brocks, 2000, "The Role of Cohesive Strength and Separation Energy for Modeling of Ductile Fracture", ASTM STP 1360, pp. 139 – 151.

[19] W. Brocks, private communication given at the Int. CTOA Conference at GKSS, Geestacht near Hamburg, Germany, May 2001,

[20] J. R. Rice and E. P. Sorensen, 1978, "Continuing Crack-Tip Deformation and Fracture for Plane-Strain Crack Growth in Elastic-Plastic Solids", J.Mech.Phys.Solids, Vol. 26, pp. 263 – 286.

[21] J. R. Rice, W. J. Drugan and T. L. Sham, 1980, "Elastic-Plastic Analysis of Growing Cracks", in ASTM STP 700, ASTM, Philadelphia, pp. 189 – 221.

[22] M. P. Wnuk and T. Mura, 1981, "Comparative Study of Models for Quasi-Static Tensile Fracture", in Special Volume on *Recent Contributions to Mechanics of Solids*, editor Eringen.

[23] M. P. Wnuk and T. Mura, 1983, "Effect of Microstructure on the Upper and Lower Limit of Material Toughness in Elastic-Plastic Fracture", J. Mech. of Materials, Vol. 2, No. 1, pp. 33 – 46.

[24] M. P. Wnuk, 1990, "Mathematical Modeling of Nonlinear Phenomena in Fracture Mechanics", M. P. Wnuk – Editor, CISM Colloquia Series, Springer Verlag, pp. 359 – 451.

[25] O. Kolednik, G. Shan and F. D. Fisher, 1997, "The Energy Dissipation Rate – A New Tool to Interpret Geometry and Size Effects", in *Fatigue and Fracture Mechanics; 27th Volume*, ASTM STP 1296, R. S. Piascik, J. C. Newman and N. E. Dowling – Editors, pp. 126 – 151.

[26] K. B. Broberg, 1977, "On the Treatment of the Fracture Problem at Large Scale Yielding", in *Fracture Mechanics and Technology – Proceedings of an International Conference*, held at Hong Kong, Vol. 2, Eds. G. C. Sih and C. L. Chow, pp. 837 – 859, based on GALCIT Report, Caltech 1976.

[27] K. B. Broberg, 1999, "Cracks and Fracture", Academic Press.

[28] M. P. Wnuk and D. Read, 1986, "Essential Work of Fracture vs. Energy Dissipation Rate in Plane Stress Ductile Fracture", Int. J. Fracture, Vol. 31, pp. 161 – 171.

[29] T. Ungsuwarungsri and W. G. Knauss, 1987a, "The Role of Delayed-Softened Material Behavior in the Fracture of Composites and Adhesives", Int. J. Fracture, Vol. 35, pp. 221 – 241.

[30] T. Ungsuwarungsri and W. G. Knauss, 1987A, "A Nonlinear Analysis of EquilibriumCraze", Part I: Problem Formulation and Solution", J. Appl. Mech., Vol. 110, pp. 44- 51

[31] T. Ungsuwarungsri and W. G. Knauss, 1987c, "Part II: Simulation of Craze and Crack Growth", ibid., pp. 52 – 58.

[32] J. W. Hutchinson, 1997, "The Role of Plasticity in Toughening of Ductile Metals and Interfaces", seminar at Northwestern University in the series "Colloquia on Modern Mechanics", March 1997, Evanston, IL.

[33] R. V. Goldstein and M. N. Perelmuter, 1999, "Modeling of Bonding at an Interface Crack", Int. J. Fracture, Vol. 99, pp.53-79.

[34] G. P. Cherepanov and H. Halmonov, 1972, "On the Theory of Fatigue Crack Growth", Engineering Fracture Mech., Vol. 4, pp. 219-230.

[35] G. P. Cherepanov and H. Halmonov, 1974, "Fatigue Crack Growth Below K_{ISCC}, Int. J. of Fracture, Vol. 3, pp. 159-164.

[36] M. P. Wnuk, 1977, "Introduction to Fracture Mechanics", a textbook written in Polish, published by the Academy of Mining and Metallurgy Press, Krakow, Poland.

[37] M. P. Wnuk, 1992, "Fatigue Process Viewed as Superposition of Subcritical Crack Growth Events", 14th IUTAM Symposium on Theoretical and Applied Mechanics, Technion, Haifa, Israel.

[38] V. V. Bolotin, 1990, "Mechanics of Fatigue Fracture", in text on "Nonlinear Fracture Mechanics", CISM Series of Courses and Lectures on Mechanics, No. 314, edited by M. P. Wnuk, publ. by Springer-Verlag.

[39] M. P. Wnuk, 1990, "Mathematical Modeling of Nonlinear Fracture Phenomena", ibid, pp. 395-451.

Michael P. Wnuk Department of CE and Mechanics, University of Wisconsin – Milwaukee
Milwaukee, WI 53201, ph.414.229.5846, fax 414.229.6958, E-mail: mpw@uwm.edu

APPENDIX A

Work of fracture and the energy transmission ratio (ETR) are evaluated here for the two limiting cases of material behavior: (1) ductile, and (2) brittle. For the first one we shall use the Dugdale model (S = const.), while the second one will be represented by the Knauss model, which assumes a linear distribution of the S-stress within the end zone R. Both models are then augmented by the Wnuk "final stretch criterion" in order to establish the resistance curves, R = R(Δa), appropriate for each cohesive stress distribution. The purpose of such operation is to show the variations of the energy transmission ratio in the course of quasistatic crack extension.

Following Eqs. (3.5) we partition the total energy dissipated within the end zone into the true work of fracture, i.e., the energy dissipated within the process zone

$$W_{true} = v_{tip} \int_0^{\Delta/R} S(\lambda) \frac{d}{d\lambda}\left[-v(\lambda)\right] d\lambda \tag{A1}$$

and the remainder of the irreversible work

$$W_{irr} = v_{tip} \int_{\Delta/R}^{1} S(\lambda) \frac{d}{d\lambda}\left[-v(\lambda)\right] d\lambda \tag{A2}$$

Here, S denotes the cohesive stress restraining the decohesion process within the end zone, while $v(\lambda)$ is the normalized opening displacement against which the work is being done. The normalizing constant for $v(\lambda)$ is $v_{tip} = 4S_0/\pi E$.

Of course, the total energy dissipation W is defined as the sum of the two terms defined above, namely

$$W_{tot} = W_{true} + W_{irr} = v_{tip} \int_0^{1} S(\lambda) \frac{d}{d\lambda}\left[-v(\lambda)\right] d\lambda \tag{A3}$$

The energy transmission ratio is determined as follows

$$ETR = w = \frac{W_{true}}{W_{tot}} = \frac{\int_0^{\Delta/R} S(\lambda) v'(\lambda) d\lambda}{\int_0^{1} S(\lambda) v'(\lambda) d\lambda} \tag{A4}$$

Here, the prime indicates differentiation with respect to the nondimensional coordinate $\lambda = x_1/R$, in which x_1 is the distance measured from the crack tip. At the outer edge of the process zone, $x_1 = \Delta$, and there the variable λ assumes the physically meaningful value of Δ/R, which is the reciprocal of the ductility index ρ (=R/Δ).

ETR for the Dugdale Model

We shall now evaluate the integrals in Eq. (A4). Let us first consider the ductile case, described by the model of Dugdale, who assumed a constant S-stress, $S = S_0$. Here within the range of small scale yielding, the normalized opening displacement within the end zone is given by

$$v_D(\lambda) = \Lambda_0(\lambda) = \sqrt{1-\lambda} - \frac{\lambda}{2} \ln \frac{1+\sqrt{1-\lambda}}{1-\sqrt{1-\lambda}} \tag{A5}$$

Total work of fracture, defined by Eq. (A3), reads

$$W_{tot}^{D} = v_{tip} S_0 \int_0^1 \frac{d}{d\lambda}\left[-\Lambda_0(\lambda)\right] d\lambda = -v_{tip} S_0 \left[\Lambda_0(\lambda)\right]_0^1 = v_{tip} S_0 \tag{A6}$$

The true work of fracture, defined by Eq. (A1), is

$$W_{true}^{D} = v_{tip} S_0 \int_0^{1/\rho} \frac{d}{d\lambda}\left[-\Lambda_0(\lambda)\right] d\lambda = -v_{tip} S_0 \left[\Lambda_0(\lambda)\right]_0^{1/\rho} = v_{tip} S_0 \left[1 - \Lambda_0\left(\frac{1}{\rho}\right)\right] \tag{A7}$$

Dividing this expression by the total work of fracture, we obtain the energy transmission ratio as a function of the ductility index ρ, namely

$$ETR_D(\rho) = 1 - \Lambda_0(1/\rho) = \frac{\sqrt{\rho} - \sqrt{\rho - 1}}{\sqrt{\rho}} - \frac{1}{2\rho} \ln\left[\frac{\sqrt{\rho} + \sqrt{\rho - 1}}{\sqrt{\rho} - \sqrt{\rho - 1}}\right] \tag{A8}$$

This function is illustrated in Fig.10a. Now, if the Wnuk-Rice-Sorensen equation of the R-curve, see Eq. (3.3), is employed, the ETR_D can be plotted in terms of the increment of the quasistatic crack extension, $z = \Delta a/R_{ss}$. The result is shown in Fig. 10b.

ETR for the Knauss Model

Let us evaluate the integrals which appear in Eq. (A4). Now, the cohesive stress for this representation of material behavior is assumed to increase linearly from zero at $x_1 = 0$ to S_0 at $x_1 = R$. Substituting $S(\lambda) = \lambda S_0$ and the expression for the normalized opening displacement

$$v_K(\lambda) = \Lambda_1(\lambda) = \sqrt{1-\lambda}\left(1 - \frac{1}{2}\lambda\right) - \frac{\lambda^2}{4} \ln\left[\frac{1 + \sqrt{1-\lambda}}{1 - \sqrt{1-\lambda}}\right] \tag{A9}$$

into the integral defined by Eq. (A3), we obtain

$$\begin{aligned} W_{tot}^{K} &= v_{tip} S_0 \int_0^1 \lambda \frac{d}{d\lambda}\left[-\Lambda_1(\lambda)\right] d\lambda = \\ &= v_{tip} S_0 \left\{\left[-\lambda \Lambda_1(\lambda)\right]_0^1 + \int_0^1 \Lambda_1(\lambda)\, d\lambda\right\} = \\ &= v_{tip} S_0 \int_0^1 \Lambda_1(\lambda)\, d\lambda = \frac{v_{tip} S_0}{2.25} \end{aligned} \tag{A10}$$

In a similar way the true work of fracture is evaluated. Applying Eq. (A1) to the Knauss model, yields

$$W_{true}^{K} = v_{tip} S_0 \int_0^{1/\rho} \lambda \frac{d}{d\lambda}\left[-\Lambda_1(\lambda)\right] d\lambda =$$

$$= v_{tip} S_0 \left\{ \left[-\lambda \Lambda_1(\lambda)\right]_0^{1/\rho} + \int_0^{1/\rho} \Lambda_1(\lambda) d\lambda \right\} =$$

$$= v_{tip} S_0 \left\{ -\frac{1}{\rho}\Lambda_1\left(\frac{1}{\rho}\right) + \int_0^{1/\rho} \Lambda_1(\lambda) d\lambda \right\} \tag{A11}$$

Dividing this expression by W_{tot}^{K}, given in Eq. (A10), results in

$$ETR_K(\rho) = 2.25 \left\{ \int_0^{1/\rho} \Lambda_1(\lambda) d\lambda - \frac{1}{\rho}\Lambda_1(1/\rho) \right\} \tag{A12}$$

A plot of this function is shown in Fig. 10a, while Fig. 10b illustrates the dependence of the energy transmission ratio on the extent of quasistatic crack growth. To convert the ETR vs. ρ plot shown in Fig. 10a into the one shown in Fig. 10b, the following equation of the resistance curve (derived from the Wnuk's "final stretch" criterion) has been used

$$\frac{dR}{da} = M1 - 1 - \frac{\Delta}{4R}\ln\left(\frac{4\Delta}{R}\right) \tag{A13}$$

The tearing modulus M1, which appears in this equation, is assumed to be somewhat higher than the minimum tearing modulus (below which a stable crack growth does not exist), namely

$$M1 = 1.5\left[1 + \frac{1}{4\rho_{ini}}\ln\left(\frac{4}{\rho_{ini}}\right)\right] \tag{A14}$$

An example of the resulting R-curve is shown in Fig. A1. We note that this curve and all other results pertaining to the Knauss model are valid for ρ->1, and thus a direct comparison with the results pertinent to the Dugdale model, where ρ>>1, is not possible.

One may, however, compare the numbers. The ETR_K shown in Fig.10 vary between one and 0.59, while the ETR_D shown in the same figure varies between 0.4 and 0.14. This indicates a more substantial energy screening effect for the ductile material, reflected by the lower value of the ETR.

Finally, when Eq. (A12) is examined in the limiting case of ρ approaching 1, which corresponds to a perfectly brittle behavior, we see that the second term in the curly bracket disappears, while the integral assumes the value1/2.25, reducing the entire expression for the ETR to one. This results in zero energy screening, meaning that the entire energy available for fracture is delivered to the crack tip. One would expect such an effect for the brittle fracture.

Session lectures

4th International Congress
of Croatian Society of Mechanics
September, 18-20, 2003
Bizovac, Croatia

4thICCSM

MICROMECHANICS BY DISCRETE ELEMENT METHOD

Ante Agić

Keywords: Discrete Element Method, Micromechanics

In order to understand new materials and processes, micromechanical modeling is in intensive use by engineering comunity. The macroscopic modeling approaches leads to the construction of continuum-based phenomenological constitutive models, while the microscopic modeling bring behaviour from micro discrete nature to the macroscopic equivalent level. Discrete Element Method (DEM) is the term given to the numerical analysis procedure that simulates the behaviour within discontinue mechanics framework. DEM treats particles as an assemblage of individual or distinct bodies with adequate interrelationship. By applying their known individual constitutive properties, contact laws, velocities, displacements, and body forces, their dynamic behaviour can be studied over a selected period in time. From a computational point of wiew, there are two basic aspects in large multibody system behaviour simulation, namely contact detection and contact interaction. The contact interaction laws must relate to the distances between particles, interactions of particle structure, particle shape, unit's distribution and substance properties. Contact detection is responsible for detecting couples of discrete element close to each other. The spatial sorting and contact resolution contact are two phases of the detection process. Contact resolution detects overlap of the two objects, determined through an analysis of the objects surface geometries. The new micromechanical models and procedures come from innovative thinking and use powerful computational resources [4]. Circular disks and mono-spheres are most frequently studied due to the simplified contact detecting algorithms. Polygonal and superquadric shapes have also been studied, but are impractical for large numbered particle models due to the complexity of the contact patterns. Ellipses and clusters of spheres, in proper size arrangement, provide a realistic model for many engineering materials. For solution real micromechanical problems 3-D models of non-circular shapes will be required, and some of them are shortly described. Suspension of discrete fibres in a Newtonian fluid is another discrete element structure. In order to optimise properties and processing conditions suspension media, numerical simulation of the flow including interaction between suspended discrete objects are required. When the Reynolds number of the suspension is small, boundary integral method can be used to describe fibre motion in the fluid flow field [3]. The equilibrium equations for each of the fibres, are balance of the hydrodinamic forces and torques. This **e**quations are direct simulation model of the interaction among N fibers in an unbound suspension. In order to model the N fibres in a unit cell, the periodic solution of the Stokes flow equation must be accounted. Some special large-scale simulation algorithm are used, such as Particle Mesh Method, Multipole-based Ewald Summation. The numerical results under unit cell are averaged to produce macroscopic properties of the suspension (diffusivity tensor, structure functions, reduced viscosity). This direct calculation of fibre

motion require lot of computational power. In order to overcome this problem, the fiber orientation state is defined by orientation tensors [1]

$$a_{ij} = \int \vec{p}_i \vec{p}_j \psi(\vec{p}) d\vec{p} \tag{1}$$

$$a_{ijkl} = \int \vec{p}_i \vec{p}_j \vec{p}_k \vec{p}_l \psi(\vec{p}) d\vec{p} \tag{2}$$

where is $\vec{p}$ unit vector defining orientation and ψ is probability distribution function. The scatter data from direct simulation are fitted by kriging in order to recive aceptable functional relationship structural tensors on fiber aspect ratio and relative fibre volume. The simple kriging must be conected with evolution equation, in order to replace mathematical interpolations with physicaly based interpolators. For the center-gated disk numerical results was obtained. The polypropilene fiber suspension are chosen as model example, as described in [2]. In order to predict fiber orientation in injection-molded composite, the melt is assumed to be incompressible Stokes flow. Macroscopic equation with evolution equation for orientation tensor, on every time step solved by incremental procedure using finite elements. Figure 1 show contour line plot of tensor component a_{11} of orientation tensor in radial cross-section (B half gap thickness). The influence of the fountain flow and gate region transients on distribution orientation tensor are clear visible.

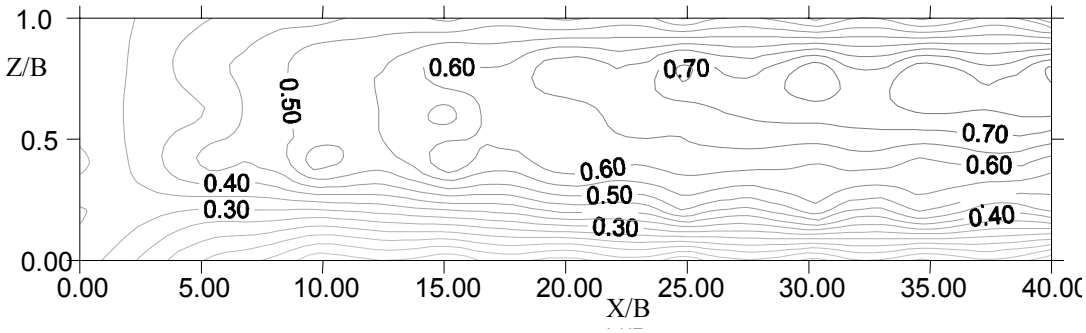

Fig. 1 The contur plot isoline of the komponent a_{11}

References

[1] Advani, S. G. and Tucker III, C. L., Closure Approximations for Three-dimensional Structure Tensors, J. of Rheology, Vol. 34, pp. 367-383.

[2] Agić, A., The Numerical Simulation Flow Moulding Processes of Short Fibre Composites, Proceedings of IV Int. Conference on Flow Processes in Composite Materials, (Ed. Jones, N.), Aberystwyth, 1996, pp. 59-69.

[3] Fan, X., Phan-Thien, N, and Zheng, R., A Direct Simulation of Fibre Suspensions, J. of Non-Newtonian Mechanics, Vol. 74, 1998, pp. 113-135.

[4] Kun, F. and Herrmann, H. J., A Study of Fragmentation Processes Using a Discrete Element Method, Int. Journal of Modern Physics C, No. 7, 1995, pp. 1342-1361.

[5] O'Connor, R. M, A Distributed Discrete Element, Modelling Environment, Algorithms, Implementation and Applications, Ph.D., MIT, 1996.

Agić Ante, Assistant Prof.
Faculty of Chemical Engineering and Technology
Marulicev trg 19, Zagreb, University of Zagreb
E-Mail: aagic@marie.fkit.hr

4th International Congress
of Croatian Society of Mechanics
September, 18-20, 2003
Bizovac, Croatia

ON THE INVARIANTS OF ORTHOTROPIC ELASTIC CONSTANTS

Ivo Alfirević, Ivica Skozrit

Keywords: Generalized Hooke's law, Orthotropic, Engineering constants, Tensor invariants

1. Introduction

Recenty the use of composite orthotropic materials in engineering structures have been increased steadily. Usually generalized Hookes law for orthotropic plates in plane stress is given. In this paper the generalized Hookes law for the three-dimensional state of stress in terms of engineering orthotropic elastic constants is proposed. Some invariants of the fourth order elasticity tensor in terms of engineering constants are considered.

$$
\begin{aligned}
\varepsilon_x &= \frac{1}{E_x}\sigma_x - \frac{\nu_{yx}}{E_x}\sigma_y - \frac{\nu_{zx}}{E_x}\sigma_z + \eta_{xxxy}\tau_{xy} + \eta_{xxyz}\tau_{yz} + \eta_{xxzx}\tau_{zx}\,,\\
\varepsilon_y &= -\frac{\nu_{xy}}{E_y}\sigma_x + \frac{1}{E_y}\sigma_y - \frac{\nu_{zy}}{E_y}\sigma_z + \eta_{yyxy}\tau_{xy} + \eta_{yyyz}\tau_{yz} + \eta_{yyzx}\tau_{zx}\,,\\
\varepsilon_z &= -\frac{\nu_{xz}}{E_z}\sigma_x - \frac{\nu_{yz}}{E_z}\sigma_y + \frac{1}{E_z}\sigma_z + \eta_{zzxy}\tau_{xy} + \eta_{zzyz}\tau_{yz} + \eta_{zzzx}\tau_{zx}\,,\\
\gamma_{xy} &= \eta_{xyxx}\sigma_x + \eta_{xyyy}\sigma_y + \eta_{xyzz}\sigma_z + \frac{\tau_{xy}}{G_{xyxy}} + \frac{\tau_{yz}}{G_{xyyz}} + \frac{\tau_{zx}}{G_{xyzx}}\,,\\
\gamma_{yz} &= \eta_{yzxx}\sigma_x + \eta_{yzyy}\sigma_y + \eta_{yzzz}\sigma_z + \frac{\tau_{xy}}{G_{yzxy}} + \frac{\tau_{yz}}{G_{yzyz}} + \frac{\tau_{zx}}{G_{yzzx}}\,,\\
\gamma_{zx} &= \eta_{zxxx}\sigma_x + \eta_{zxyy}\sigma_y + \eta_{zxzz}\sigma_z + \frac{\tau_{xy}}{G_{zxxy}} + \frac{\tau_{yz}}{G_{zxyz}} + \frac{\tau_{zx}}{G_{zxzx}}\,.
\end{aligned}
\tag{1}
$$

The type of engineering constant depends on the number of different indices as shown in Table 1.

2. Linear invariants

$$
\frac{1-2\nu_{yx}}{E_x} + \frac{1-2\nu_{zy}}{E_y} + \frac{1-2\nu_{xz}}{E_z} = \text{const.} \tag{2}
$$

$$
\frac{1}{E_x} + \frac{1}{E_y} + \frac{1}{E_z} + \frac{1}{2}\left(\frac{1}{G_{xy}} + \frac{1}{G_{yz}} + \frac{1}{G_{zx}}\right) = \text{const.} \tag{3}
$$

$$
\frac{1}{4}\left(\frac{1}{G_{xy}} + \frac{1}{G_{yz}} + \frac{1}{G_{zx}}\right) + \frac{\nu_{yx}}{E_x} + \frac{\nu_{zy}}{E_y} + \frac{\nu_{xz}}{E_z} = \text{const.} \tag{4}
$$

Table 1. Types of the engineering orthotropic elastic constants

Indices in the			Engineering orthotropic elastic constant	Number of different indices	Typical symbol of	
1st pair	2nd pair	2 pairs mutually			tensonial component	engineering constant
equal	equal	equal	Modulus of elasticity	1	$1/S_{1111}$	E_x
equal	equal	different	Poisson's ratio divided by modulus of elasticity	2	S_{1122}	$-\nu_{yx}/E_x$
equal	different	different	Normal - shearing coefficient	2	S_{1112}	η_{xxxy}
different	different	equa	Shearing modulus of elasticity	2	S_{1212}	$1/G_{xy}$
different	different	different	Coupled shearing modulus of elasticity	3	S_{1223}	$1/G_{xyyz}$

3. Quadratic invariants

$$\frac{1}{E_x^2}+\frac{1}{E_y^2}+2\frac{\nu_{yx}}{E_x}\frac{\nu_{xy}}{E_y}+\frac{1}{4G_{xy}^2}+\left(\eta_{xxxy}^2+\eta_{yyyx}^2\right)=\text{const.} \tag{5}$$

$$\frac{1}{E_x^2}+\frac{1}{E_y^2}+2\frac{\nu_{yx}}{E_x}\frac{\nu_{xy}}{E_y}-\left(\frac{1}{E_x}+\frac{1}{E_y}\right)\left(\frac{\nu_{yx}}{E_x}+\frac{\nu_{xy}}{E_y}\right)+\frac{1}{2}\left(\eta_{xxxy}+\eta_{yyyx}\right)^2=\text{const.} \tag{6}$$

$$\left(\frac{1}{E_x}+\frac{1}{E_y}\right)\left(\frac{\nu_{yx}}{E_x}+\frac{\nu_{xy}}{E_y}\right)+\frac{1}{4G_{xy}^2}+\frac{1}{2}\left(\eta_{xxxy}-\eta_{yyyx}\right)^2=\text{const.} \tag{7}$$

4. Cubic invariant

$$\frac{1}{E_x^3}+\frac{1}{E_y^3}+\frac{1}{8G_{xy}^3}+3\frac{\nu_{yx}}{E_x}\frac{\nu_{xy}}{E_y}\left(\frac{1}{E_x}+\frac{1}{E_y}\right)-\frac{3}{2}\left(\frac{\nu_{yx}}{E_x}+\frac{\nu_{xy}}{E_y}\right)\eta_{xxxy}\eta_{yyyx}+$$
$$+\frac{3}{2}\left(\frac{1}{E_x}\eta_{xxxy}^2+\frac{1}{E_y}\eta_{yyyx}^2\right)+\frac{1}{4G_{xy}}\left(\eta_{xxxy}^2+\eta_{yyyx}^2\right)=\text{const.} \tag{8}$$

5. Conclusion

Among the known engineering constants, i.e. moduli of elasticity, shearing moduli of elasticity. Poisson's ratios and normal-shearing coefficients, there exist also the coupled shearing moduli of elasticity.

Several linear, quadratic and cubic invariants in terms of engineering orthotropic elastic constants are derived.

General Hooke's law in terms of engineering constant for 3D has been proposed.

References

[6] 1. Alfirević, I.: Uvod u tenzore i mehaniku kontinuuma, Golden marketing, Zagreb 2003.

[7] 2. Hyer, M. W.: Stress Analysis of Fiber-Reinforced Composite Materials, McGraw Hill, New York 1998.

Dr. Ivo Alfirević, Professor

Faculty of Mechanical Engineering and Naval Architecture/University of Zagreb, Institute of Applied Mechanics, Ivana Lučića 5, Zagreb, Croatia, ++385 1 6168 240, ++385 1 6168 187, jasna.biondic@fsb.hr

Ivica Skozrit , Assistant

Faculty of Mechanical Engineering and Naval Architecture/University of Zagreb, Institute of Applied Mechanics, Ivana Lučića 5, Zagreb, Croatia, ++385 1 6168 450, ++385 1 6168 187, ivica.skozrit@fsb.hr

4th International Congress
of Croatian Society of Mechanics
September, 18-20, 2003
Bizovac, Croatia

4thICCSM

LOCALIZATION OF INELASTIC DEFORATION IN PROBLEMS FREE OF INITIAL STRESS CONCENTRATORS

Miroslav Audy, Jiři Krček, Michal Šejnoha and Jan Zeman

Keywords: *Localization, strong discontinuity approach, Partition of Unity method, finite element modelling*

Localization of inelastic deformation caused by strain softening has been the subject of intense study for several decades. Usually, the attention has been limited to a single crack or slip line that propagates from a predefined weak spot (notch, defect, material point with reduced stiffness, etc.). The starting point has just been naturally chosen a priory. However, situations where more than one crack may initiate at the same time still exist, e.g., the four point bending. In such a specific example the conventional use of the finite element method based solely on the concept of equilibrium would inevitably predict cracks distributed over a certain region. Clearly, the number of cracks developed at the onset of damage would depend on the selected finite element mesh. If no action was taken the subsequent damage growth would continue in the distributed manner. In case of post peak softening such a solution, however, might not be unique and bifurcation of equilibrium might occur. The proper solution thus requires to supply the standard finite element analysis with the stability analysis to select among all possible solutions the stable one. As pointed out by Brocca [4], such a solution is usually localized, although the actual damage localization depends on the size and shape of a structure, type of loading and other factors.

The problem just introduced has been already addressed by Brocca [4]. In his approach the search for the localized region is performed by minimizing the global potential energy providing a certain localization or bifurcation condition is met. In particular, one has to judge whether the solution derived from the discrete system of equilibrium equations is stable or will bifurcate (localization will take place). Following [6, 4] the equilibrated solution becomes unstable when the Hessian matrix of the total energy functional looses the positive definiteness. This approach is explored in the present study. The subsequent minimization process then results into a set of increments of crack openings of existing cracks for a given load increment. The present approach just generates two tasks: in the framework of finite element method we are required to formulate a suitable element that allows natural splitting of elastic and inelastic displacements associated with the crack opening and introducing the minimization part into a suitable optimization environment. The first task is resolved by introducing the partition of unity method [2, 3, 1, 5], to cite a few, which allows incorporation of the discontinuous part of the displacement field thus naturally splits the continuous and discontinuous parts of the total displacement such that

$$\boldsymbol{u}(\mathbf{x},t) = \widehat{\boldsymbol{u}}(\mathbf{x},t) + H_{\Gamma_d}(\mathbf{x})\widetilde{\boldsymbol{u}}(\mathbf{x},t),$$

where $H_{\Gamma_d}(\mathbf{x})$ is the Heaviside function centered at the discontinuity surface Γ_d and $\widehat{\boldsymbol{u}}$ and $\widetilde{\boldsymbol{u}}$ are continuous functions on Ω. Note that the discontinuity is introduced by the Heaviside function $H_{\Gamma_d}(\mathbf{x})$ at the discontinuity surface Γ_d and that the magnitude of the displacement jump $[\![\boldsymbol{u}]\!]$ at the discontinuity

surface is given by $\widetilde{\boldsymbol{u}}$. The second task should be resolved by employing genetic algorithms in the minimization problem.

Our objective here is to revisit the above problem in attempt of solving a number of drawbacks linked to the original approach [4]. It is expected that combining the partition of unity method for the solution of fundamental equilibrium problem of a medium impaired by cracks and the minimization procedure based on genetic algorithms for generating the stable solution when bifurcation of equilibrium takes place will provide a reliable tool for solving the underlying problem.

A detailed one-dimensional demonstrative example is presented to illustrate the principles, main ideas and applicability of the present method. First, the results demonstrate several drawbacks associated with constraining the enhanced degrees of freedom for elements impaired by cracks. Such particular drawbacks are expected to progress into higher dimensions and should be accounted for when solving more realistic problems. On the contrary, the solution of the localization problem in problems free of initial stress concentrators presented in this contribution in the framework of partition of unity method confirm the applicability of the proposed approach and advocate the use of the partition of unity method in higher dimensions.

Acknowledgement

This work was sponsored by GAČR grants GP103/01/D052 and 106/02/0678.

References

[1] M. Audy. *Localization of inelastic deformation in problems free of initial stress concentrators*. Master thesis, Czech Technical University in Prague, Faculty of Civil Engineering, Prague, 2003.

[2] I. Babuška, U. Banerjee, and J. E. Osborn. *On principles for the selection of shape functions for the generalized finite element method*. Tech. Report 01-16, TICAM, 2001.

[3] I. Babuška and J. M. Melenk. *The partition of unity method*. International Journal for Numerical Methods in Engineering **40** (1997), 727–758.

[4] M. Brocca. *Analysis of cracking localization and crack growth based on thermomechanical theory of localization*. Ph.D. thesis, University of Tokyo, 1997.

[5] K. de Proft. *Combined experimental-computational study to discrete fracture of brittle materials*. PhD thesis, Vrije Universiteit Brussel, Brussel, 2003

[6] Q. S. Nguyen. *Bifurcation and post-bifurcation analysis in plasticity and brittle fracture*. Journal of the Mechanics and Physics of Solids **35** (1987), 303–324.

Ing. Miroslav Audy
Czech Technical University in Prague, Faculty of Civil Engineering, Department of Structural Mechanics, Thákurova 7, 166 29 Prague 6, Czech Republic, Tel:+420-2-24354472, Fax:+420-2-24310775,
e-mail:miroslav.audy@seznam.cz
Ing. Jiří Krček
Czech Technical University in Prague, Faculty of Civil Engineering, Department of Structural Mechanics, Thákurova 7, 166 29 Prague 6, Czech Republic, Tel:+420-2-24354472, Fax:+420-2-24310775,
e-mail:jiri.krcek@fsv.cvut.cz
Doc. Ing. Michal Šejnoha, Ph.D.
Czech Technical University in Prague, Faculty of Civil Engineering, Department of Structural Mechanics, Thákurova 7, 166 29 Prague 6, Czech Republic, Tel:+420-2-24354494, Fax:+420-2-24310775,
e-mail:sejnom@fsv.cvut.cz
Ing. Jan Zeman
Czech Technical University in Prague, Faculty of Civil Engineering, Department of Structural Mechanics, Thákurova 7, 166 29 Prague 6, Czech Republic, Tel:+420-2-24354482, Fax:+420-2-24310775,
e-mail:zemanj@cml.fsv.cvut.cz

4th International Congress
of Croatian Society of Mechanics
September, 18-20, 2003
Bizovac, Croatia

FIRE SAFETY OF STEEL STRUCTURES

Ivica Boko and Bernardin Peroš

Keywords: large compartment, actual fire load, zone model, temperature curves.

1. Introduction

According to current scientific research findings in the field of fires, their breakout and growth, it is not possible to predict the where and when a fire might break out. Fires in industrial objects can be caused by various factors, the most significant being man. The products of a fire are: the development of high temperatures and great quantities of smoke in enclosures. High temperatures influence the supporting structure of the building, while smoke threatens humans, since most loss of life in fires is caused by smoke inhalation. This paper deals only with the effect of high temperatures upon the load-bearing steel structure.

During the last few years significant efforts have been made in scientific research to understand the process of the breakout of fires and their growth so that there is a specific scientific discipline referred to as "Fire Science". These problems have been dealt with in ENV 1991-2-2: 1995, wherein fire action is classified as heat action, i.e. accidental action in the classification of various actions. Heat actions are defined by: nominal temperature-time curve and parametric fire exposure. Parametric fire exposures have been only initiated and it has been left to each country to solve this within the National Application Documents which is one of the main tasks of this paper.

2. Short description of the paper

The paper presents the analysis of the influence of various types of actual fire loads upon the given industrial structure - a warehouse steel hall. The simulation included several different fire loads with different quantities of combustible material and different floor surfaces of the structure covered with combustible material. By applying the model of zones (Figure 1.), based on an approximate formulation [1], for different fire loads, obtained by varying the surface of ventilation openings, it was possible to obtain the temperature curves as a function of time which were used as the extreme temperature influence upon the load-bearing steel structure.

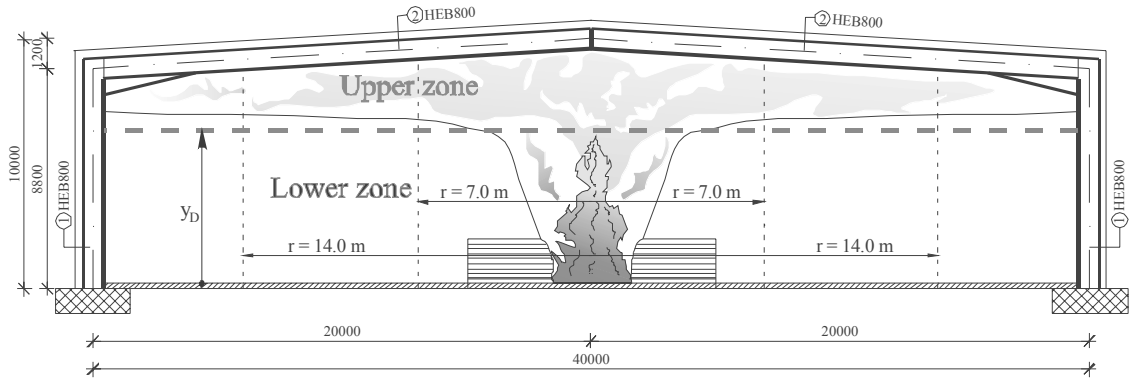

Figure 1. Presentation of the load-bearing steel structure

The obtained temperature curves were compared to a Standard temperature curve. It was proved that for large closed spaces (e.g. industrial halls) [2] the action of actual fire loads cannot be computed by applying the standard curve but by determining actual temperature curves as a function of time.

Heat transfer through the basic material was modelled by using a transient, non-linear model [3] according to the obtained values of extreme temperature curves.

The paper also includes the analysis of the state of extreme temperatures in the case of steel structure protection by incombustible mineral plates.

3. Conclusions

The fire action for a steel hall with dimensions 40 x 60 x 7.5 m was simulated by applying the zone model, based on an approximate formulation. The results obtained by employing the zone model in 6 cases of the real fire load show that the temperature in the compartment depends primarily upon the combustible material quantity, the floor surface covered by combustible material, the surface of ventilation openings and the radial distance from the fire centre.

It has been proved that the application of the Standard temperature curve [4]; [5] is not acceptable for large compartments since it is evident that the temperature action differs in space and depends upon the mentioned parameters so that it is necessary to perform computations for each actual fire load.

It has been determined that for each fire load, depending upon the required fire resistance (e.g. 30 min), the temperature in the hall does not exceed 300°C, so that the protection of the structure is not necessary in such cases.

These investigations of the actual time-temperature parameter curves in large industrial halls for different fire loads have been carried out within the NAD (National Application Documents) in the field of fire action.

References

[1] Davis, W. D. “The Zone Fire Model JET: A Model for the Prediction of Detector Activation and Gas Temperature in the Presence of a Smoke Layer”, NIST - National Institute of Standards and Tehnology, 1999

[2] Boko, I. “Safety of Steel Structures Under the Influence of Fire Loads”, M.Sci. Thesis, Faculty of Civil Engineering, University of Split, Croatia, 2001 (in Croatian)

[3] Sterner, E. and Wickstrőm, U. “TASEF - Temperature Analysis of Structures Exposed to Fire”, Swedish National Testing Institute, 1990

[4] ....., Eurocode 1, “Basis of design and actions on structures - Part 2-2: Actions on structures - Action on structures exposed to fire”, European Committee for Standardization, Brussels, 1995

[5] ....., Eurocode 3, “Design of steel structures - Part 1-2: General rules - Structural fire design”, European Committee for Standardization, Brussels, 1995

Ivica Boko, Mr. sc., CEng, Assistent
University of Split, Faculty of Civil Enginering, Matice Hrvatske 15, HR-21000 Split, Croatia,
tel: + 385 21 303330, fax: + 385 21 465117, e-mail: Ivica.Boko@gradst.hr

Bernardin Peroš, Prof. dr. sc., CEng, Associated Professor
University of Split, Faculty of Civil Enginering, Matice Hrvatske 15, HR-21000 Split, Croatia,
tel: + 385 21 303331, fax: + 385 21 465117, e-mail: Bernardin.Peros@gradst.hr

4th International Congress
of Croatian Society of Mechanics
September, 18-20, 2003
Bizovac, Croatia

FINITE PLASTIC STRAINS WITHIN NONISOTHERMAL CONTEXT

Marko Čanađija, Josip Brnić

Keywords: finite strains, thermoplasticity, finite element method

1. Introduction

Thermomechanical behaviour is frequently met in practice. In a wide variety of mechanical problems, thermal effects are usually neglectable. From other point of view, in large variety of thermal problems, mechanical effects are also neglectable. In some problems, like linear thermoelasticity, these effects are considered. However, thermal effects influence the mechanical ones, but mechanical effects have no effect on thermal behaviour.

In analysis of plastic deformation, work applied to achieve permanent deformation is in a large amount dissipated as heat. This heat source cannot be neglected even in the infinitesimal context. For the finite plastic strains this is particularly true. Temperature change causes several effects interesting from the mechanical side. One of them is, for example, softening of the material in question, i. e. lowering of yield stress with the increase of temperature.

Computational tasks involving finite thermoplastic strains are almost exclusively solved numerically. A most popular numerical tool is certainly the finite element method. Since isochoric behaviour of plastic deformation causes numerical difficulties with pure displacement based finite element method, mixed finite element method is preferred.

The coupled problems in general can be approached by simultaneous solution or some sort of staggered approach. In the context of thermoplasticity at finite strains, simultaneous solution leads toward larger and nonsymmetrical systems. Integration is unconditionally stable. Usual decoupling into mechanical and thermal phase yields smaller and symmetrical systems. But, obtained scheme lacks unconditional stability and is only conditionally stable. In analysis of metal materials this not represent a problem and such decoupling is often used.

2. Kinematics

The fundamental measure of deformation in continuum mechanics is deformation gradient **F**. It is defined as derivative of configuration. We separate elastic and plastic part of deformation through multiplicative decomposition of deformation gradient:

$$\mathbf{F}(\mathbf{X}) = \mathbf{F}^e(\mathbf{X})\mathbf{F}^p(\mathbf{X}). \tag{1}$$

3. Balance and constitutive laws

We use basic laws of continuum mechanics [7]. Helmholtz free energy represents a basis for stress calculations in hyperelastic formulation used in this work. Mechanical dissipation is calculated as fraction of plastic power $\mathcal{P}^p_{mech}$ [3, 4]:

$$\mathcal{D}_{mech} = \chi \mathcal{P}^p_{mech} = \chi \sqrt{\frac{2}{3}} \lambda \left(-\partial_\xi K - \sigma_y(\theta) \right). \tag{2}$$

4. Numerical model overview

As a numerical tool, we use the mixed finite element method [2, 5]. This is efficient way of circumventing numerical difficulties associated with incompressibility of plastic deformation.

We decouple problem into two smaller sub-problems: mechanical, in which temperature is held constant and thermal, in which displacements are held constants. Such approach is usually addressed as isothermal split.

5. Example

In this example we consider necking of the rectangular bar. Specimen is stretched very fast. This causes that heat convection to the environment and heat conduction from warmer toward colder parts of the specimen can be practically neglected. Therefore, problem can be in essence treated as adiabatic. As a result, strong local heating of the specimen occurs due to dissipation of heat from plastic deformation. The rise in temperature and accompanying plastic strain is particularly evident through occurrence of the so-called Lüder's shear bands [6]. These shear bands occur at approximately 45^{o} degrees to the longitudinal axis of specimen, what corresponds to the planes of maximal shear stresses, Figure 1. Problem is frequently addressed to as the adiabatic shear banding and could be placed in the field of material instability.

This problem was already analysed in the past, see Armero and Simo [1] in the case of material properties independent of temperature. However, to the author's knowledge, this problem with material properties as functions of temperature has not been previously analysed in relevant literature.

6. Conclusions

Paper presented a formulation for associative coupled thermoplasticity. Such approach efficiently deals with coupling between thermal and mechanical effects that occur during plastic deformation. However, this work is far from finished. Further work in this field should be directed toward coupling between damage/failure effects and micro-macro phenomena. Rate effects should be included. Of further interest is introduction of solid-solid phase change effects.

References

[1] Armero, F., Simo, J. C., “A Priori Stability Estimates and Unconditonally Stable Product Formula Algorithms for Nonlinear Coupled Thermoplasticity”, International Journal of Plasticity, Vol. 9, 1993, pp 749-782.

[2] Čanađija, M.:,"Numerical Analysis of Nonlinear Isothermal and Nonisothermal Processes of Plastic Deformation of Metals", (in croatian), Ph. D. Thesis, Faculty of Engineering, University of Rijeka, 2002.

[3] Kamlah, M., Haupt, P.,”On the Macroscopic Description of Stored Energy and Self Heating During Plastic Deformation”, International Journal of Plasticity, Vol. 13, 1998, pp 893-911.

[4] Rosakis, P., Rosakis, A.J., Ravichandran, G., Hodowany, J.,” A Thermodynamic Internal Variable Model for the Partition of Plastic Work into Heat and Stored Energy in Metals”, Journal of the Mechanics and Physics of Solids, Vol. 48, 2000, pp 581-607.

[5] Simo, J. C., Miehe, C., “Associative Coupled Thermoplasticity at Finite Strains: Formulation, Numerical Analysis and Implementation”, Computer Methods in Applied Mechanics and Engineering, Vol. 98, 1992, pp 41-104.

[6] Schey, J. A. :”Introduction to Manufacturing Processes”, McGraw-Hill, Boston, 2000.

[7] Truesdell, C., Noll, W.: “ The Nonlinear Field Theories”, in Handbuch der Physik, vol. III/3, ed. Flügge, S., Springer – Verlag, Berlin, 1965.

Assist. Prof. Marko Čanađija
University of Rijeka, Faculty of Engineering, Department of Engineering Mechanics, Vukovarska 58, HR-51000 Rijeka, Croatia, ++385 51 651 496, ++385 51 651 490, markoc@riteh.hr
Prof. Josip Brnić
University of Rijeka, Faculty of Engineering, Department of Engineering Mechanics, Vukovarska 58, HR-51000 Rijeka, Croatia, ++385 51 651 491, ++385 51 651 490, brnic@riteh.hr

4th International Congress
of Croatian Society of Mechanics
September, 18-20, 2003
Bizovac, Croatia

4thICCSM

COMPLETE FRANCIS TURBINE FLOW SIMULATION FOR THE WHOLE RANGE OF DISCHARGES

Z. Čarija and Z. Mrša

Keywords: *CFD, Numerical simulation, Francis turbine, Fluent, Parallel computing, Linux cluster*

1. Introduction

Computational Fluid Dynamic (CFD) is widely used today in design, research and development of hydraulic turbines. This is a process where fluid flow domain is divided into many small volumes where governing equations are converted into algebraic equations, which can be solved. Computational result strongly depends on methods used for converting governing to algebraic equations and on the choice of the fluid flow domain. Chosen technique depends on available computer resources and on possibility to simplify domain of interest.

Due to the nonuniform distribution of the incoming water from the spiral casing, no periodicity is applied in the tandem cascade and runner fluid flow simulation was done for the complete Francis turbine. Another reason for simulating entire flow is the strong interactions between the components (especially between guide vanes, runner and draft tube). For more accurate results it is inevitable to take care of these interactions into the fluid flow numerical simulation, which can only be done by unsteady flow simulation [6].

2. Investigated geometry, computational grid and numerical model

Francis turbine fluid flow numerical simulation will be presented. The investigated turbine consists of spiral casing, tandem cascade with 10 stay vanes and 20 guide vanes channels, runner with 15 blades and draft tube. Geometry definition and grid generation was carried out with the FLUENT preprocessor GAMBIT. Final grid is huge and it is decomposed for the parallel processing. Fluid flow analysis of the entire Francis turbine was done with the commercial computer code FLUENT, where Reynolds averaged Navier-Stokes equations are applied on finite volumes. Turbulence is taken into account with the standard k-ε model. The computational mesh of the complete turbine is shown in Fig.1 where different colours represent different processors.

Figure 1. Computational grid

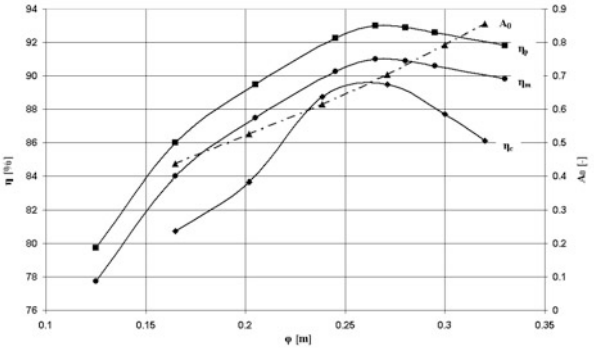

Figure 2. Measured and calculated efficiencies

3. Results

Numerical simulation and measurements were done for the same specific head ψ (prototype at the head H=125m) and different specific flow rates φ. Calculated, model and prototype efficiency are shown on Fig.2 with the wicket gate opening curve. Calculated results show in average 2% lower efficiency then measured ones. This is due to the still coarse grid and limitation of the applied turbulence model.
Numerical simulation of entire Francis turbine flow for different points of operation shows clearly the influence of the wicket-gate opening on the draft tube vortex existence and direction at the inlet part of draft tube. Vortex changes its direction from clockwise to counter clockwise (Fig.3) when going from small to height discharges. It disappears at optimal point of operation lowering draft tube and overall turbine losses. Another vortexes are generated in horizontal part of draft tube due to influence of elbow type draft tube. The main part of the whole turbine losses are draft tube losses.

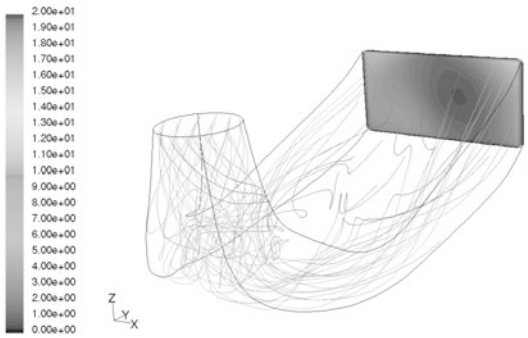

Figure 3. Path lines in draft tube (A_0=0.86)

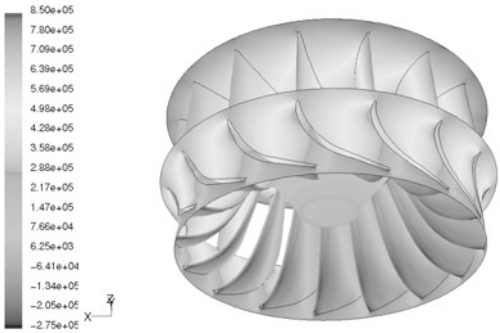

Figure 4. Runner static pressure distribution (A_0=0.86)

Pressure and suction sides of runner blades are clearly visible and stagnation places on runner blades (Fig.4). Pressure differences from the pressure and suction sides are higher at the higher load and these differences result in torque on the shaft. The lowest pressures are on the suction side near the trailing edge where cavitations can occurs at the high.

4. Conclusion

Using CFD it is possible to get significant insight into issues such as energy transfer and fluid flow details in hydraulic turbines. Only the last fine-tuning has to be done experimentally.

References

[1] Čarija Z, Mrša Z. Complete Francis Turbine Fluid Flow Simulation. Proceedings of the 13th Interntional DAAAM Symposium 2002; ISBN 3-901509-13-5

[2] Eisinger R, Ruprecht A. Automatic Shape Optimisation of Hydro Turbine Components based on CFD. Seminar "CFD for turbomachinery applications" 2001.

[3] Heitele, M., Helmrich, T., Maihofer, M., Ruprecht, A. "Hew Insight ito an Old Product by High Performance Computing". 5th European SGI/CRAY MPP Workshop, Bologna, 1999..

[4] Lipej A, Poloni C. "Design of Kaplan Runner Using Multiobjective genetic algorithm optimisation", Journal of Hydraulic Research 2000; Vol. 38.

[5] Mrša Z, Sopta L, Vuković S. "Shape optimisation method for Francis turbine spiral casing design", ECCOMAS 2000.

[6] Ruprecht A, Eisinger R. "Numerical Simulation of a Complete Francis Turbine including unsteady rotor/stator interactions", 20th IAHR Symposium on Hydraulic Machinery and Systems 2001.

[7] Ruprecht A, Eisinger R, Göde E, Rainer D. "Virtual Numerical Test Bed for Intuitive Design of Hydro Turbine Components", IHA 1999.

Zoran Čarija, assist. and Zoran Mrša prof.dr.sc.
Faculty of Engineering, University of Rijeka, Department of Fluid Mechanics and Comp. Engineering
Vukovarska 58, Rijeka, Croatia, Phone: 0038551 651554, Fax.: 0038551 651-490, e-mail: zcarija@rijeka.riteh.hr
Zoran Mrša prof.dr.sc.
Faculty of Engineering, University of Rijeka, Department of Fluid Mechanics and Computational Engineering, Vukovarska 58, Rijeka, Croatia, Phone: 0038551 651554, Fax.: 0038551 651-490, e-mail: mrsa@rijeka.riteh.hr

4th International Congress
of Croatian Society of Mechanics
September, 18-20, 2003
Bizovac, Croatia

4thICCSM

ON NUMERICAL TREATMENT OF SHALLOW WATER FLOW OVER THE DRY BED INCLUDING BALANCING

N. Črnjarić-Žic, S. Vuković and L. Sopta

Keywords: *Shallow-water equations, finite volume method, source term, dry bed, unstructured grid.*

1. Introduction

The shallow water equations are accepted in many practical applications as the governing equations for the unsteady water flow in natural watercourses and in the case of flooding. For modelling a realistic problem it is necessary to use this nonhomogeneous system that includes source terms relevant to the varying bed topography.

The first emphasis of this work is on using the numerical scheme in which the source term is appropriately discretized, so that the balance between the flux gradient and the source term is obtained. The first order scheme developed by Hubbard and Garcia-Navarro in [5] by an extension of the standard upwind finite volume numerical scheme based on the Roe's approximate solver, satisfies that balancing property, so we present it and use it in this work. The scheme is applied here to both one- and two-dimensional problems. Besides the problem of the correct source term discretisation an additional problem arises if the propagation over the dry bed occurs. We propose here a numerical technique that is necessary for appropriate treatment of this problem. This technique is crucial for the water flow computations over the natural watercourses. Simulation results corresponding to the test problems in the last section illustrate that the proposed numerical treatment successfully handles complex flow domains.

2. Application of the first order upwind schemes to the shallow water equations

The first order upwind Q scheme is used in the paper. The main advantage of the presented scheme applied over the irregular bed topography against some other numerical schemes lies in the fact that the balancing between the flux gradient and the source term can be obtained. Particularly, in the shallow water case the scheme is constructed in such way that it preserves the quiescent steady state exactly. The described numerical procedure can be applied to the cells of the wetted domain where the hyperbolic conservation law is valid. The problem arises on the moving boundaries of the wetted domain that are, in the numerical sense, made from the cells that are not completely surrounded by other wet cells. In that sense, the additional problem we consider is the numerical treatment of the wetting front that advances over upward slope. In such a situation some adaptations of the numerical scheme are necessary. The corrections we propose are based on the idea of a global balancing between the flux gradient and the source term.

3. Numerical results

With the numerical tests presented in this section we want to illustrate the improvements obtained when using the balanced scheme against the non-balanced scheme and additionally by the correct treatment of the wet/dry boundary. In the paper we present two one-dimensional and two two-dimensional test problems.

4. Conclusion

A first order upwind numerical scheme is used for the water flow evaluation over the varying riverbed in one- and two-dimensional cases. To avoid difficulties that arise in numerical computations when the water flow propagates over the dry bed an additional technique is presented here. Because such situations are natural in the real water flow simulations, the proposed numerical treatment is necessary in the practical applications.

References

[1] Brufau, P., Vazquez-Cendon, M.E., Garcia-Navarro, P., "A numerical model for the flooding and drying of irregular domains", Int. J. for Numerical Methods in Fluids, Vol. 39, 2002, pp 247-275

[2] Vazquez-Cendon, M. E., "Improved Treatment of Source Terms in Upwind Schemes for the Shallow Water Equations in Channels with Irregular Geometry", J. of Computational Physics, Vol. 148, 1999, pp 497-526.

[3] Bermudez, A., Derviex, A., Desideri, J.-A., Vazquez, M. E., "Upwind Schemes for the Two-Dimensional Shallow Water Equations with Variable Depth Using Unstructured Meshes", Rapport de recherché No 2738, INRIA, 1995.

[4] Zhou, J.G., Causon, D.M., Mingham, C.G., Ingram, D.M., Smith, A.D., "The Surface Gradient Method for the Treatment of Source Terms in the Shallow Water Equations", J. of Computational Physics, Vol. 168, 2001, pp 1-25

[5] Hubbard, M.E., Garcia-Navarro, P., "Flux Difference Splitting and the Balancing of Source Terms and Flux Gradients", J. of Computational Physics, Vol. 165, 2000, pp 89-125

[6] LeVeque J.R., "Balancing Source Terms and Flux Gradients in High-Resolution Godunov Methods: The Quasi-Steady Wave-Propagation Algorithm", J. of Computational Physics, Vol. 146, 1998, pp 346-365

[7] Vuković S., Sopta L., "ENO and WENO Schemes with The Exact Conservation Property for One-Dimensional Shallow Water Equations", J. of Computational Physics, Vol. 179, 2002, pp 593-621

[8] Kurganov A., Levy D., "Central-Upwind Schemes for the Saint-Venant System", Mathematical Modelling and Numerical Analysis , Vol. 36, 2002, pp. 397-425

Assist. Mr. Sc. Nelida Črnjarić-Žic, dipl. Ing.
Faculty of Engeneering, University of Rijeka, Department of Mathematics, Vukovarska 58, Rijeka, Croatia, tel: +385 51 651 484,
e-mail: nelida@riteh.hr
Asoc. Prof. D. Sc. Senka Vuković, prof.
Faculty of Engeneering, University of Rijeka, Department of Fluid Mechanics and Computational Engineering, Vukovarska 58, Rijeka, Croatia, tel: +385 51 651 494,
e-mail: senka.vukovic@ri.hinet.hr
Prof. D. Sc. Luka Sopta, dipl. Ing.
Faculty of Engeneering, University of Rijeka, Department of Fluid Mechanics and Computational Engineering, Vukovarska 58 Rijeka, Croatia, tel: +385 51 651 493,
e-mail: luka.sopta@riteh.hr

4th International Congress
of Croatian Society of Mechanics
September, 18-20, 2003
Bizovac, Croatia

4thICCSM

ANALYSIS OF POTENTIAL FLOW AROUND WING-BODY CONFIGURATIONS

I. Cvitanović, Z. Virag and S. Krizmanić

Keywords: Potential Flow, Panel Method, Missile and Aircraft Aerodynamics

Although remarkable advances are being made in flow field calculations using finite difference, finite element and also finite volume methods, the surface integral approach of panel methods coupled with corrections for compressibility and viscous effects still offers certain advantages [1]. For most of high-Reynolds-number flows of interest in aircraft aerodynamics viscous effects are confined to thin boundary layers, i.e. the global flow features weakly depend on the Reynolds number. If the configuration causes only small perturbations and there are no strong shocks, the linearized model of potential flow is applicable. Such flow is governed by the Prandtl-Glauert equation:

$$\left(1-M_\infty^2\right)\Phi_{xx}+\Phi_{yy}+\Phi_{zz}=0 \tag{1}$$

where M_∞ is the free stream Mach number and Φ is potential of the perturbation velocity. At the impermeable surface the following boundary condition is applied

$$\partial\Phi/\partial\vec{n}+\vec{V}_\infty\cdot\vec{n}=0 \tag{2}$$

In this paper, Prandtl-Glauert equation is transformed to Laplace's equation using affine coordinate transformation and solved by a panel method, where singularities are distributed over the surface of the configuration [1,3,4]. The wing incidence is represented by vortex distributions corresponding to pressure differences across the wing. The wing thickness effect is given by source and sinks located over the wing reference plane. The body thickness and incidence are simulated by line sources and doublets placed along the body reference axis. Finally, the interference effects of the wing on the body are cancelled by a vortex distribution on the body surface.

Computer program, based on presented method was tested on a wing-body-canard aerodynamic configuration, in uniform flow at Mach number M_∞=0.1. Geometry of the configuration and experimental results for lift and moment coefficients were taken from the reference [5]. Two cases were studied: body-wing configuration and body-wing-canard configuration. The body of configuration was modelled using 50 line sources and doublets, while for cancellation of wing and canard-induced velocities on the body, 4 x 10 surface vortex panels were used. Both, wing and canard were modelled using 6 x 8 surface vortex panels.

The results were obtained for both configurations at five angles of attack and given in Fig. 1. The results are presented in the form of the lift and moment coefficients versus angle of attack. In addition, each diagram contains experimental data taken from reference [5], as well as the results obtained by methods of project aerodynamics, taken from reference [2].

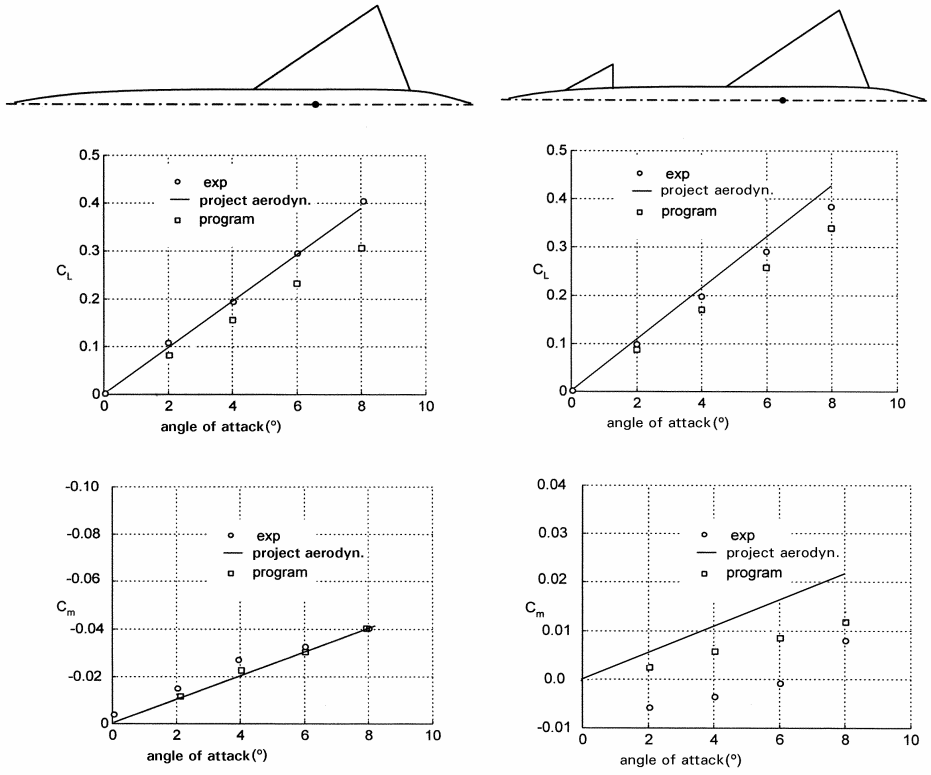

Figure 1. Results for the two configurations

It is clear that project aerodynamics gives slightly better results for the standard wing-body configuration and in the case of wing-body-canard configuration the results obtained by the proposed method are in better agreement with experimental data than the results of project aerodynamics. The discrepancies between obtained results and experimental data rise with angle of attack, due to the simplifications in the mathematical model.

It can be concluded that the in the case of the non-standard (body-wing-canard) configurations, the application of more sophisticated methods is required. Thus, the presented method is expected to give better results than the project aerodynamics methods.

References

[1] Hunt, B., "The Panel Method for Subsonic Aerodynamic Flows: A survey Of Mathematical Formulations and Numerical Models and an Outline of the New British Aerospace Scheme", Computational Fluid Dynamics, Hemisphere Publishing Corporation, 1980.

[2] Janković, S., "Mehanika leta zrakoplova", Fakultet strojarstva i brodogradnje, Zagreb, 2002.

[3] Katz, J., Plotkin, A., "Low-Speed Aerodynamics", McGraw-Hill, New York,1991.

[4] Morino, L., "Computational Methods in Potential Aerodynamics", Springer-Verlag, Berlin, 1985.

[5] Pitts, W.C., Nielsen, J.N., Kaattari,G.E., "Lift and Center of Pressure of Wing-Body-Tail Combination at Subsonic, Transsonic and Supersonic Speeds.", NACA Report, 1957.

Ivan Cvitanović, M. sc.
JANAF, Ulica grada Vukovara 14, 10000 Zagreb, Hrvatska, 01/3039-397, icvitan@lycos.com

Zdravko Virag, Ph. D.
Faculty of Mechanical Engineering and Naval Architecture, Chair of Fluid Mechanics,
I. Lučića 5, 10000 Zagreb, Hrvatska, 01/6168-137, zdravko.virag@fsb.hr
Severino Krizmanić, B.sc
Faculty of Mechanical Engineering and Naval Architecture, Chair of Fluid Mechanics,
I. Lučića 5, 10000 Zagreb, Hrvatska, 01/6168-156, severino.krizmanic@fsb.hr

4th International Congress
of Croatian Society of Mechanics
September, 18-20, 2003
Bizovac, Croatia

MODELLING FLEXIBLE MULTIBODY SYSTEMS USING BOND GRAPH TECHNIQUE

V. Damić, M. Čohodar

Keywords: flexible multibody systems, bond graphs, differential- algebraic equations

1. Introduction

The paper explores application of bond graph technique to modelling of multibody systems consisting of interconnected rigid and deformable bodies, each of which may undergo large translational and rotational displacements. In this paper co-rotational approach is used because of its good properties [3,4,6].

But why bond graphs? Strength of bond graphs lies in its multidisciplinary paradigm and visual expressiveness [5]. It is power flow modelling technique well suited for modelling of mechatronic systems.

2. Co-rotational approach in Bond Graph settings

We will start analysing a typical slender multibody link. It will be represented as collection of straight plane beam finite elements. Bond Graph model of a beam element is shown in Figure 1.

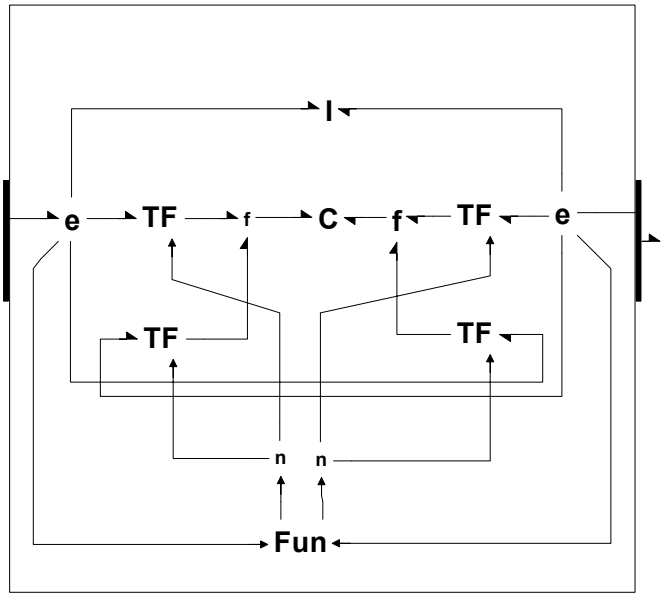

Figure 1. Bond Graph model of a beam finite element based on co-rotational approach

Bond Graph model of beam element can be used as building blocks for developing complex flexible multibody system models. We will illustrate this point in the next section.

3. Model of Kanes's spin up experiment

In order to analyse capabilities of Bond Graph approach a problem known as Kanes's spin-up experiment was analysed. It is often used as test problem for different flexible bodies models formulations.

The model is developed using the component model approach of [5]. The system level model is shown in Figure 2. The rotating beam was discretized using ten finite Bond Graph elements.

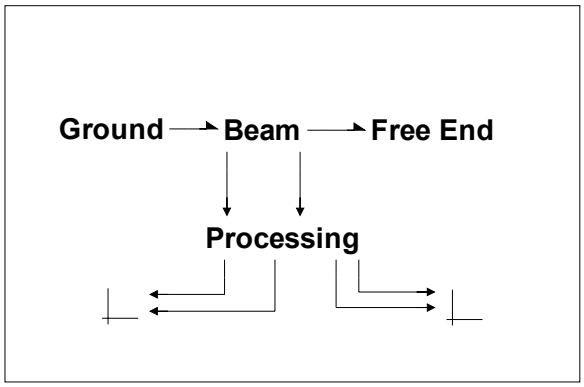

Figure 2. System model of Kanes's spin-up experiment

The model was developed using BondSim program [5]. After some experimentation the simulation was executed using rather tight error control. The results obtained are in excellent agreement with the results reported in literature.

4. Conclusions

The aim of present work is to show capabilities of the bond graph approach in simulation of structural component that is often used in industrial and technological applications. Using co-rotational approach a Bond Graph model of a two dimensional beam finite element was developed, which can be used with confidence for constructing models of planar flexible multibody systems.

References

[1] AA Shabana (1998), Dynamics of Multibody Systems, 2nd edn., Cambridge University Press, Cambridge

[2] JC Simo, L Vu-Quoc (1986) On the Dynamics of Flexible Beams Under Large Overall Motion – The Planar Case, Part I & II, J of Applied Mechanics, Vol. 53, pp. 849-863

[3] CC Rankin, FA Brogan (1986), An Element Independent Co-rotational Procedure for Treatment of Large Rotations, ASME J. Pressure Vessel Technology, Vol. 105, pp. 165-174

[4] MA Crisfield, GF Mota (1996), A Unified Co-rotational Framework for solids, shells and beams, Int. J. Solids Structures, Vol. 33, pp. 2969-2992

[5] V Damic and J Montgomery (2003), Mechatronics by Bond Graphs, Springer-Verlag, Heidelgerg-Berlin

[6] M Branderberger, M Clerici (1999), Modeling Nonlinear Flexible Mechanisms Using ADAMS/Flex and Nonlinear Co0rotational FE-Techniques, International ADAMS Users' Conference, Berlin, Nov. 17-19, 1999

[7] JS Przemieniecki (1985), Theory of Matrix Structural Analysis, Reprint Dover Publications, New York

[8] AA and G de Jalon, E Bayo (1991), Dynamics of Flexible Multibody Systems Using Cartesian Co-ordinates and Large Displacement Theory, Int. J. Numer. Methods Eng., Vol 32, pp. 1543-1563

[9] TR Cane, RR Ryan, AK Banerjee (1987), Dynamics of a Cantilever Beam Attached to a Moving Base, J. of Guidance, Control and Dynamics, Vol. 13(2), pp. 139-151

Vjekoslav Damic, Prof. Dr.Sc., The Polytechnic of Dubrovnik, Cira Carica 4, 20000 Dubrovnik, Croatia, +385 20 445 713, vdamic@vdu.hr

Majda Cohodar, M. Sc , Faculty of Mechanical Engineering University of Sarajevo, Vilsonovo Setaliste 9, Sarajevo, Bosnia i Herzegovina, +385 33 656 562, fax. +385 33 653 055, cohodar@mef.unsa.ba

4th International Congress
of Croatian Society of Mechanics
September, 18-20, 2003
Bizovac, Croatia

4thICCSM

PREDICTING RESIDUAL STRESSES DUE TO SOLIDIFICATION IN CAST PLASTIC PLATES

I. Demirdžić, Ejub Džaferović and Alojz Ivanković*

Keywords: *visco-elastic, residual stresses, finite volume method*

The problem of residual stresses in viscoelastic materials has received considerable attention in the past. Full mathematical description of viscoelastic processes were published in 1960s, inspired by the glass industry. However, the mathematical models were very complex and rarely solvable even for the simplest one-dimensional situations.

Thermal processing is the dominant mechanism of inducing residual stresses into polymeric materials, since most are manufactured at elevated temperatures and then cooled to room temperature. During this cooling process, the material solidifies and the strain becomes 'frozen-in'. These frozen-in strains produce stresses in the material after the processing is complete.

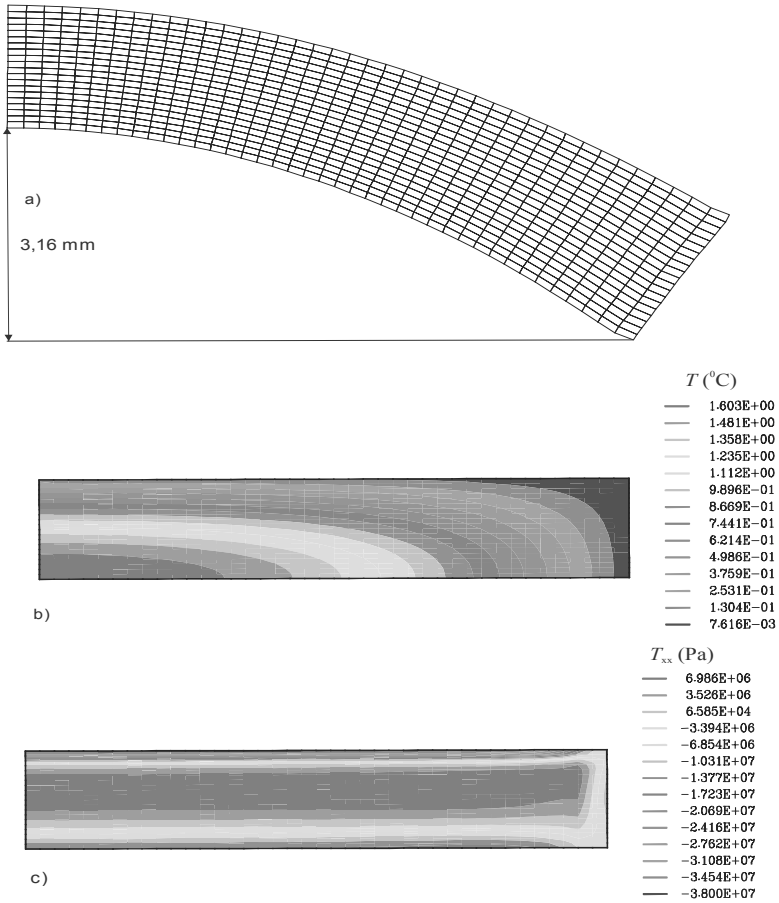

Figure 1. Asymetrical cooling a) deformed shape, b) temperature distribution, c) stress distribution after 1100 s.

In this work a method is described for the quantitative prediction of thermally induced residual stresses in polymeric materials. A linear viscoelastic constitutive law and the time-temperature superposition principle are used to describe the material behaviour. The convolution integrals arising from the constitutive law are solved numerically using the Finite Volume Method to discretise the governing equations. In this paper an incremental formulation of the constitutive relations is used.

As an example of the method application, the behaviour of a plate shaped polymeric product cooled in two different ways is analysed. The test plate was cooled from the fully softened state to the room temperature in a controlled environment. The accuracy of the method is demonstrated through the comparison with published numerical results.

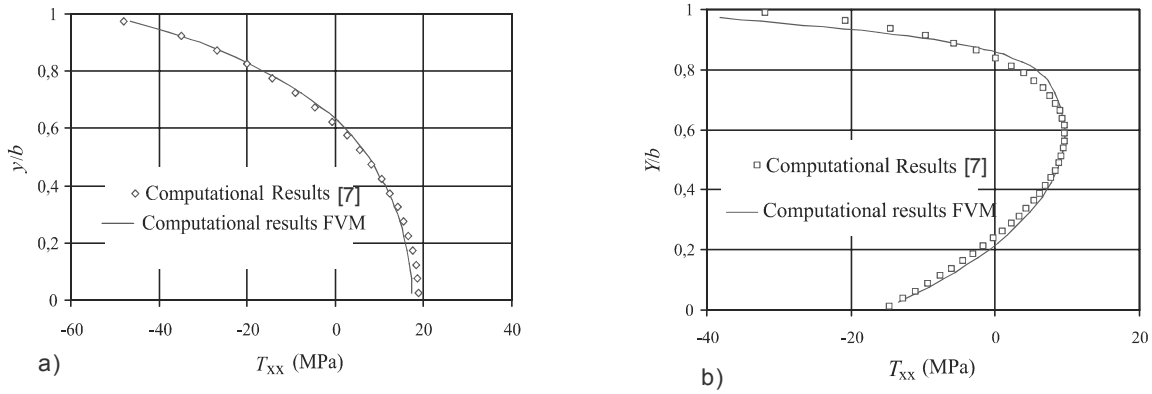

Figure 2. Stress distribution at the symmetry cross section

References

[1] Chow, P., Cross, M., "An enthalpy control volume unstructured mesh (CV-UM) algorithm for solidification by conduction only", Int. J. Numer. Methods Engrg, 35 (1992) 1849–1870.

[2] Christensen, R.M., "Theory of Viscoelasticity, an Introduction", Academic press, New York, 1971.

[3] Demirdžić, I., Muzaferija, S., "Numerical method for coupled fluid flow, heat transfer and stress analysis using unstructured moving meshes with cells of arbitrary topology", Comput. Methods Appl. Mech. Eng., 125 (1995) 235–255.

[4] Džaferović, E., "Interaction between viscoplastic fluid and viscoelastic solid-Numerical modelling", PhD Thesis, University of Sarajevo, 2002 (in Bosnian).

[5] Teskeredžić, A., Demirdžić, I., and Muzaferija, S., "Numerical method for heat transfer, fluid flow, and stress analysis in phase-change problems", Numerical Heat Transfer, Part B, 42(2002) 437–459.

[6] Tropsa, V., "Predicting residual stresses due to solidification in cast plastic plates", PhD thesis, University of London, 2001.

[7] Voller, V. R., "An overview of numerical methods for solving phase change problems in W. J. Minkowycz and E. M. Sparrow (eds.)", Advances in numerical heat transfer, chap. 9, Taylor & Francis, Philadelphia, 1997.

I. Demirdžić(i.demirdzic@de.cd-adapco.com), Ejub Džaferović (dzaferovic@mef.unsa.ba)
Mašinski fakultet u Sarajevu,
Vilsonovo šetalište 9, 71000 Sarajevo
Bosnia and Herzegovina

* Dr. Alojz Ivankovic MEng, PhD
Imperial College London, Mechanical Engineering Department
Exhibition Road; London SW7 2AZ; United Kingdom
Telephone : ++44 (0)207 594 7134; Fax : ++44 (0)207 594 7017
Email: a.ivankovic@imperial.ac.uk

Adress correspondence to I. Demirdžić, CD adapco, Dürenhofstrasse 4, D-90402 Nürnberg, Germany,
E-mail: i.demirdzic@de.cd-adapco.com

4th International Congress
of Croatian Society of Mechanics
September, 18-20, 2003
Bizovac, Croatia

4thICCSM

FATIGUE DAMAGES AND REPAIR OF A CEMENT MILL GEAR WHEEL

Ž. Domazet, T. Piršić, M. Stupalo

Keywords: *Fatigue cracks, repair welding, FEM*

1. Introduction

In spite of numerous and expensive researches in the field of fatigue, cracks and failures caused by fatigue occur every day in all fields of human activity. Because of that, special attention should be paid to fatigue crack repairs as well as fatigue crack avoidance. A lucky circumstance with many fatigue failures is a relatively long crack propagation period from its origin to the final failure and crack can be discovered easily. What to do with discovered fatigue cracks is a well known question in such situations. As the complete replacement can be time consuming and expensive, and reduction of service loads with existing fatigue crack is dangerous and mostly unacceptable, fatigue crack repairs seem to be the best solution. The necessary steps for a successful repair of fatigue cracked component and application of this procedures is presented with example from cement industry.

2. Failure description

The gear wheel was fabricated from cast steel and mounted in two ring parts at the front side of the cement mill. After twenty years in service, the great gear wheel failed due to fatigue (Stupalo [3]). When the whole mill plant was stopped and inspected, additional seventeen fatigue cracks have been found at the tooth fillets. Joint efforts of alternating stresses, casting errors (sized several millimetres to several centimetres) and most likely existence of tensile residual stresses caused fatigue cracks initiation and propagation at the critical positions. At several positions, very close to the surface, a lot of casting errors (pores, slag inclusions, etc.) have been found. The cross section of the gear rim where complete fatigue failure occurred (fatigue crack No.2), was additionally weakened by decreasing the rim thickness due to connecting bolts. The position of the cracks is shown on Figure 1. The surface crack length varied from 20 mm to 600 mm (total failure). Position and size (surface length) of each discovered crack were estimated by means of non-destructive testing (magneto-flux method). In order to determine the complete data on crack shape and size and to perform repair welding, voluminous work (crack removal by arc-air grooving) has been undertaken.

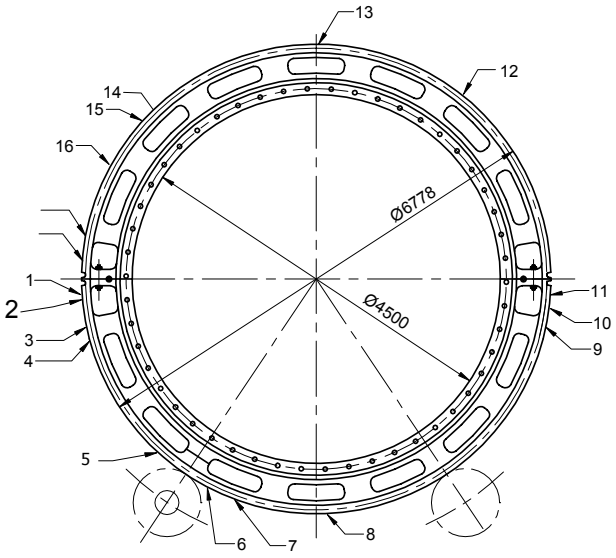

Figure 1: Detected cracks on cement mill

3. Stress analysis

Numerical method (FEM) was used to determine the stress distribution at the gear rim. Linear elastic model with mesh refinement in high stress gradient areas (tooth fillets) were used. FEM mesh and calculated stresses are shown on Figure 2 and Figure 3.

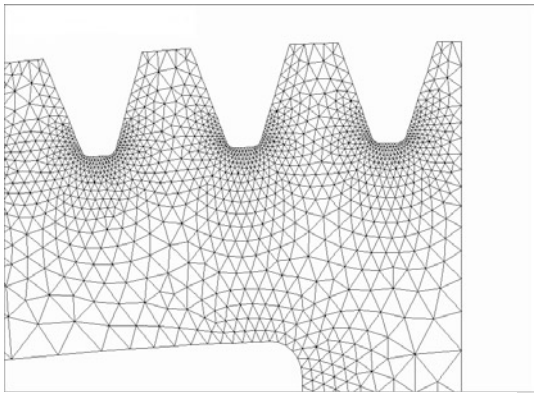

Figure 2: FEM - mesh

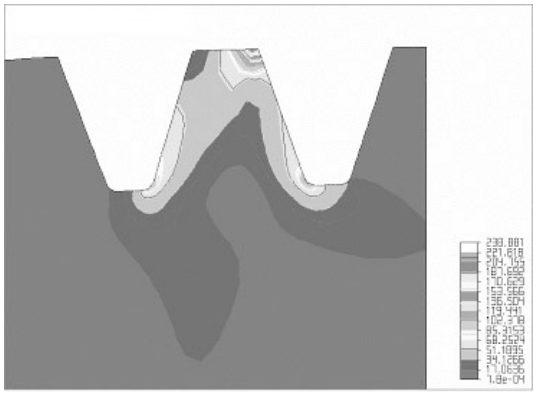

Figure 3: Calculated stress distribution

Calculated maximum stress amplitudes have been found at the tooth fillet, approximately 50 - 115 MPa, depending on their positions at the surface. These stress values could not be the only reason for cracks' initiation and propagation, but in existence of casting errors, weakened rim and residual stresses fatigue cracks occurred and propagated from the surface to the depth of the rim.

4. Repair procedure

At several positions, very close to the surface, a lot of casting errors (pores, slag inclusions, etc.) have been found, Fig.1. The cross section of the gear rim where complete fatigue failure occurred (fatigue crack No.2), Figure 1, was additionally weakened by decreasing the rim thickness due to connecting bolts.

In spite of great number of cracks and one complete failure of gear ring, repair welding was performed. All necessary steps for the best quality insurance (best welders, best welding rods, preheating, very slow cooling conditions, NDT inspection following every layer, hammering of all layers, etc.) have been respected and documented.

All described activities took two months and cost approx. $50 000, instead of $300 000 for new gear ring and four months for its delivery and montage. Three years after repair and frequent controls during the service, no further cracks have been reported.

References

[1] Domazet, Ž., “Fatigue crack retarding methods”, Ph.D Thesis, University of Zagreb, 1993.
[2] Domazet, Ž., "Engineering Failure Analysis", Vol. 3, No. 2, 1996., pp. 137-147.
[3] Stupalo, M., "Report on repair welding of gear wheel", Dalmacijacement, 1993.

dr. sc. Željko Domazet, Professor
Faculty of Electrical Engineering, Mechanical Engineeting and Naval Architecture
University of Split, R. Boškovića bb, 21000 Split Croatia,
tel. (+385 21) 305777, fax. (+385 21) 305877, zeljko.domazet@fesb.hr

dr. sc. Tonči Piršić, Assistant Professor
Faculty of Electrical Engineering, Mechanical Engineeting and Naval Architecture
University of Split, R. Boškovića bb, 21000 Split Croatia,
tel. (+385 21) 305777, fax. (+385 21) 305877, tpirsic@fesb.hr

Mladen Stupalo, Salona – Var, Kaštelanska cesta 39a, 21210 Solin, Croatia

4th International Congress
of Croatian Society of Mechanics
September, 18-20, 2003
Bizovac, Croatia

4thICCSM

INFLUENCE OF THE OUTFLOW BOUNDARY CONDITIONS IN THE OPEN CHANNEL AND SHALLOW WATER MODELS

Siniša Družeta, Nelida Črnjarić-Žic and Lado Kranjčević

Keywords: open channel flow, shallow water, outflow boundary conditions, domain size

1. Introduction

Boundary conditions can have an important effect on the simulation results. Inappropriate use of boundary conditions can significantly distort the results, which could in case of open channel and shallow water models lead to seriously over or under-estimated water levels and flooded areas.

As it is always necessary to choose the appropriate boundary condition type, it is sometimes also very important to have them sufficiently distant from the domain areas of specific interest (noted also in [2]). This means the computational domain sometimes needs to be larger than the physical domain, so the modeler could be assured that no possible specific boundary-condition-based effects would alter the result at the domain area of interest.

The outflow boundary conditions used for the survey presented in this paper were discharge - water depth dependency function for 1D open channel model and nonreflecting (transmissive) boundary condition for 2D shallow water model. Simulations were carried out with software package SOPEX STRIPP12, used for river flow and flooding simulation.

Since the principal aim was to examine the influence of the outflow boundary and referent point vicinity in the process of practical modeling, a real test-case was used. Section of the river Kupa in the Kuželj village (near Brod na Kupi, Croatia), originally modeled for the purpose of a technical report [3], was chosen as a suitable geometry.

In order to avoid other possible modeling problems, only steady states were computed, the numerical scheme used was balanced Q-scheme (one of the most robust and extensively tested currently available) and the flow was always subcritical.

2. Outflow boundary condition in 1D open channel model

A cross-section positioned in the middle of the domain was chosen as the location of interest. Its distance from domain end (i.e. outflow boundary) was varied by domain shortening and the influence on the computed water levels was observed.

Outflow boundary condition used for 1D model was discharge - water depth dependency function given by Manning formula ([1]). Analyzing Manning formula and the results presented in the paper showed that only when the domain outflow is placed at the beginning of a long channel section with constant geometry (for example man-made channel) the computed results would not be influenced by outflow boundary position. For the test-case used in the paper, the results were notably influenced by the outflow boundary condition along the downstream 2/3 of the domain.

It was concluded that the increase in the domain length would principally stabilize the computed water levels, which could help the modeler to iteratively determine the adequate domain length for which the water level would settle. This method would still be quite impractical and the results probably still shouldn't be taken without caution.

3. Outflow boundary condition in 2D shallow water model

2D model of the selected section of river Kupa was considerably bigger and built with more detail than the 1D model. A single numerical node in the middle part of the domain was chosen as the location of interest and simulations for three domains with different sizes were performed. Analogously as in 1D open channel testing, the domain was progressively shortened in the downstream part of river Kupa.

Outflow boundary condition used was nonreflecting boundary condition, which inserts fictive cells along the domain boundary, i.e. outside of it. In these cells extrapolation of the zero order is applied, meaning the values of water depth and velocity in them are kept equal to the values in neighboring cells inside the domain.

Since the computed water levels at the location of interest were dramatically influenced by the domain size, outflow boundary cells for each of the 2D domains were checked up. The investigation showed that the computation results could only be regarded as reliable when the domain slope at the outflow boundary cells is nearly equal to the slope of the channel geometry downstream of the outflow boundary. If riverbed geometry has a varying, irregular slope (as in natural open channels), the only solution is to somewhat enlarge the numerical domain and consequently distance the domain area of interest from the outflow boundary.

4. Conclusion

The results shown in the paper indicate that discharge - water depth dependency function for 1D open channel and nonreflecting outflow boundary condition for 2D shallow water models strikingly influence the computed water levels almost along the whole of the domain.

Since both 1D and 2D outflow conditions used in this paper fictionally generate uniform flow downstream of the domain boundary, outflow boundary should be positioned either in the lengthy channel section along which the actual flow is predominantly uniform, or sufficiently away from the location of interest. Results presented in this paper suggest that sufficient distance for this would be huge, which indicates that further investigation of this problem is needed.

References

[1] Chaudry, M. H., “Open Channel Flow”, Prentice Hall, New Jersey, 1993

[2] Hubbard, M. E., “On the accuracy of one-dimensional models of steady converging/diverging open channel flow”, Int. J. Numer. Meth. Fluids, Vol. 35, 2001, pp 785-808

[3] Sopta, L., Vuković, S., Črnjarić-Žic, N., Družeta, S., Škifić, J., Bukovac, O., “Matematički model rijeke Kupe i V. Belice u mjestu Kuželj”, Sopex d.o.o. – Faculty of Civil Engineering University of Rijeka, Rijeka, 2003

Siniša Družeta, Young Assist.
Faculty of Engineering University of Rijeka, Department of Fluid Mechanics and Computational Engineering, Vukovarska 58, Rijeka, Croatia, 00385 (0)51 651497, 00385 (0)51 651490,
sinisa.druzeta@riteh.hr

Nelida Črnjarić-Žic, Assist. M. Sc.
Faculty of Engineering University of Rijeka, Department of Mathematics, Vukovarska 58, Rijeka, Croatia, 00385 (0)51 651481, 00385 (0)51 651490,
nelida.crnjaric@riteh.hr

Lado Kranjčević, Assist. M. Sc.
Faculty of Engineering University of Rijeka, Department of Fluid Mechanics and Computational Engineering, Vukovarska 58, Rijeka, Croatia, 00385 (0)51 651554, 00385 (0)51 651490,
lado.kranjcevic@riteh.hr

4th International Congress
of Croatian Society of Mechanics
September, 18-20, 2003
Bizovac, Croatia

4thICCSM

THE INFLUENCE OF THE REDUNDANT MOVING ON THE PRESSURE MAGNITUDE VARIATION BY MEN SITTING

Ergić, T.; Vnučec, Z.; Muftić, O.

Keywords: redundant moving, human sitting, measurement, magnitude variation of pressure

1 Introduction

One of the basic characteristics of the comfortable sitting is the magnitude of the pressure with its distribution in the contact regions. The sitting pressure takes effect to the bulked muscles and long bones. Its influence trough long-time duration can cause changes in soft tissues and skeleton. It is known that magnitude variations of pressure on contacting surfaces have influence on blood circulatory system of sitting surfaces. A lot of jobs demand continuous sitting or the standstill position of any body parts. During static measurement of sitting pressure it is noticed that even very small displacements of any human body parts cause significant pressure variation [1 - 6]. The influence of redundant movements on the magnitude and distribution of sitting pressures has been determined.

2 The force-measuring equipment

The measurements of the sitting pressure were performed on the specially developed seat, with the pressure transducers in form of an indentor with diameter of 8 mm. The measurements were performed with the one-axial strain gauges type FLA –3-11, length 3 mm; three-channels amplifier type KWS 3082A (HBM); and an analogous/digital converter Multifunction Board PCI 20428-3A.

3 Results of measurements

The measurements of the magnitude variations of sitting pressure caused by movements of arms, legs, head and body even caused by speaking were carried out. Applying Microsoft Excel, and own developed software application for analysis of the recorded data calculated the measured forces. The results are shown as function "force-time" in figures. For example, the results that are obtained in the sitting posture by moving of legs "forward-backward" are shown in Fig. 1; and by moving of legs to "under seat" in Fig. 2. Influence of speaking on the magnitude variation of the sitting force is measured by pronunciation of words ″dobar dan″ ("good day") and the results are shown in Fig. 3; and by words ″tik-tak″ in Fig. 4.

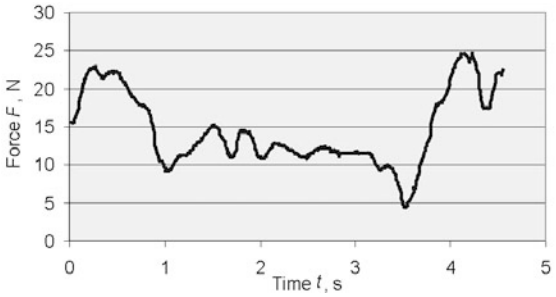

Figure 1. Moving of legs "forward-backward"

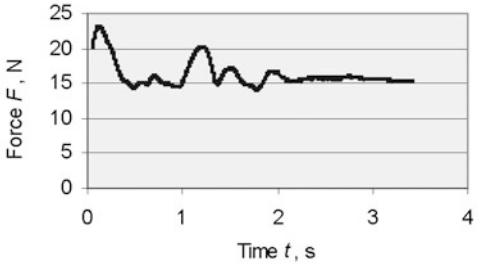

Figure 2. Moving of legs to "under seat"

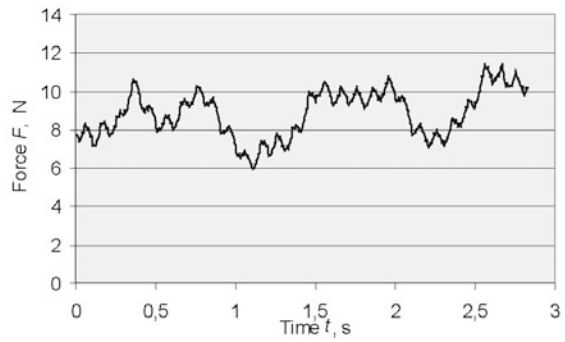

Figure3. Pronouncing the words ″dobar dan″ with sound intensity of max. 75 dB

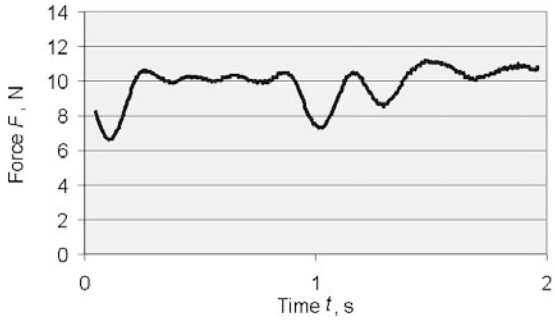

Figure 4. Pronouncing the words ″tik tak″ with sound intensity of max. 71 dB

4 Conclusions

The influence of the redundant moving on the magnitude variations and distribution of sitting pressure should be obtained from the measurements on the full sitting surface. From conducted research and measured results it can be concluded:

- Movements of arms and head have relatively small influences on the magnitude variations of the sitting pressure.
- It is very interesting fact that the magnitude variations of the sitting pressure caused by loud speaking and deep respiration were bigger than the magnitude variations of the sitting pressure caused by quickly movements of arms and head.
- At passive sitting, the isometric loading of the leg muscles has a significant influence on the magnitude variations of the sitting pressure.

References

[1] Guohao Dai, Gertler, J. P, Kamm, R. D.: The Effects of External Compression on Venous Blood Flow and Tissue Deformation in the Lower, Journal of Biomechanical Engineering, 1999, Vol. 121 No. 6, pp 557 - 564

[2] Stranden, E.: Dynamic leg volume changes when sitting in a locked and free floating tilt office chair, Ergonomics, 2000,Vol.43, No.3, pp 421 – 433

[3] Ergić, T., Ivandić Ž., Kozak, D.: The Significance of Contact Pressure Distribution on the Soft Tissue by Men Sitting, Proceedings of the 7th International Design Conference, DESIGN 2002, Dubrovnik, 2002, 743-748

[4] Cholewicki, J. Polzhofer, K.G. Radebold, A.: Postural Control of Trunk During Unstable Sitting, Journal of Biomechanical Engineering, 2000, Vol. 33, pp 1733 - 1737

[5] Vander, V.,Sherman, J., Luciano: Human Physiology the Mehanisms of Body Function, McGraw-Hill 1998

[6] Van Deursen L.D., Lengsfeld, M., Snijders, J.C., Evers, M.J.J. Goossens M.H.R.: Mechanical Effects of Continuous Passive Motion on the Lumbar Spine in Seating, Journal of Biomechanical Engineering, 2000, Vol. 33, pp 695-699

Dr.sc. Todor Ergić, Higher Research Assistant
University of Osijek, Mechanical Engineering Faculty
Trg Ivane Brlić-Mazuranić 18, HR-35000 Slavonski Brod, Croatia
Tel. +385 35 446 188, Fax: +385 35 446 446, E-mail: tergic@sfsb.hr
Dr.sc. Zdravko Vnučec, Associate Professor
University of Osijek, Mechanical Engineering Faculty
Trg Ivane Brlić-Mazuranić 18, HR-35000 Slavonski Brod, Croatia
Tel. +385 35 446 188, Fax: +385 35 446 446, E-mail: zvnucec@sfsb.hr
Dr.sc. Osman Muftić, Full Professor
University of Zagreb, Faculty of Mechanical Engineering and Naval Architecture,
Ivana Lučića 5, HR-10000 Zagreb, Croatia
Tel. +385 1 6168113, Fax: +385 1 6156940, E-mail: omuftic@fsb.hr

4th International Congress
of Croatian Society of Mechanics
September, 18-20, 2003
Bizovac, Croatia

3D FINITE ELEMENT FOR MODELLING REINFORCED AND PRESTRESSED CONCRETE STRUCTURES

Mirela Galić, Pavao Marović and Željana Nikolić

Keywords: *numerical analysis, concrete structures, 3D model, reinforcing bar, prestressing tendon.*

1. Introduction

In civil engineering practice, numerical modelling of reinforced concrete and prestressed concrete structures is mainly used as a tool for the assessment of the structural safety of non-standard reinforced and prestressed concrete structures and has been studied by many authors. This paper presents a numerical treatment of reinforcing bars and prestressing tendons in three-dimensional (3D) numerical modelling of reinforced and prestressed concrete structures according to the work performed in Ref. [1]. The equations of the finite element method have been obtained from the incremental form of the principle of virtual work [2]. The influence of the prestressing tendon on the concrete is modelled by distributed normal and tangential load along the tendon and the two forces concentrated on the anchors. Tendon can be prestressed on one end or at both ends. The prestressed equivalent nodal forces are computed to get the contribution of the prestressing to the global stiffness. The developed model makes it possible to compute the friction losses which result from concrete deformation and losses in the anchorage zone.

The described modelling of the reinforcing bars and prestressing tendons in 3D is implemented in the computer programme PRECON3D, Ref. [1].

2. Short description of the proposed model

The proposed model for the numerical treatment of reinforced and prestressed concrete structures consists of 3D concrete elements with embedded reinforcing bars and/or prestressing tendons. The 3D isoparametric 20-node elements are used for concrete modelling and 1D isoparametric 3-node elements are used for reinforcing bars and prestressing tendons modelling.

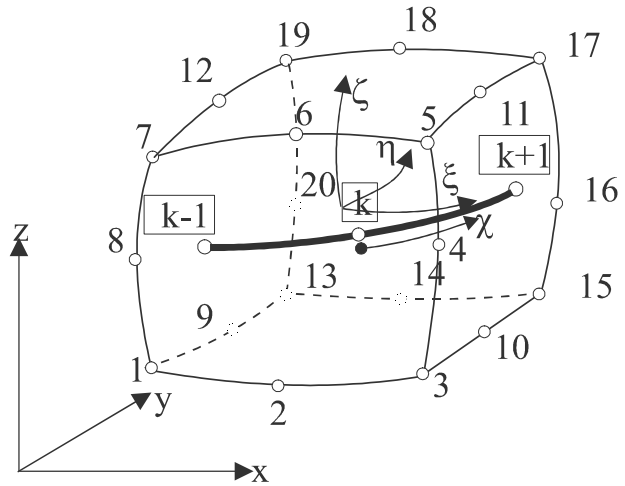

Figure 1. 3D concrete element with embedded 1D bar or tendon element

The reinforcing bars and prestressing tendons are treated as separate 1D elements embedded into 3D concrete elements so that their displacements are consistent with the parent element. Within this modelling the basic assumptions are: (1) the reinforcing bars or prestressing tendons are modelled with 1D isoparametric element whose node coordinates are defined in the global coordinate system; (2) the bond between concrete and bars or tendons is perfect, i.e. the slip behaviour is neglected; (3) the bar or tendon element can take only axial force.

The tendon position is determined by nodes whose coordinates are defined in a global coordinate system. In order to ensure the continuity between tendon elements, the boundary nodes have to be placed at the intersection point of the tendon and boundary plane of 3D concrete element. The 1D tendon element geometry is described by space function of the second order.

The prestressing forces depend on the intensity of the prescribed forces on the anchorages and instantaneous as well as time-dependent prestressing losses. In the actual model, implemented in the computer programme PRECON3D, only the losses due to the friction between the tendon and concrete is taken into account. The prestressing force values on the ends are known, so, the influence of the prestressing in the internal points of the tendon should be determined. In accordance with the finite element method approach [3] the acting forces, continuously distributed normal and tangential load along the tendon and the two forces concentrated on the anchors, have to be transferred into the nodes of the 3D concrete element. So, we have to determine equivalent nodal forces due to anchorage forces and due to the distributed load along the tendon. The described modelling of the reinforcing bars and prestressing tendons in 3D is implemented in the computer programme PRECON3D. The performance of the proposed model is illustrated by the solution procedure of one example, published in Ref. [4].

3. Conclusions

This paper presents a numerical treatment of reinforcing bars and prestressing tendons in 3D numerical modelling of reinforced and prestressed concrete structures. The advantage of the proposed modelling is complete freedom in prescribing the location and geometry of reinforcing bars and prestressing tendons.

The described modelling of the reinforcing bars and prestressed tendons in 3D is implemented in the computer programme PRECON3D [1]. The numerical example, prestressed girder clamped at one end and freely supported at the other end is given to illustrate some of the possibilities of the developed model. The obtained results show good agreement with the published one, analytical and numerical, in Ref. [4].

References

[1] Galić, M., "Numerical 3D Model of Prestressed Concrete Structures", M.Sci. Thesis, University of Split, Faculty of Civil Engineering, Split, 2002 (in Croatian)

[2] Zienkiewicz, O.C. and Taylor, R.L., "The Finite Element Method - Volume 1: The Basis", 5th edition, Butterworth Heinemann, Oxford, 2000

[3] Hofstetter, G. and Mang, H.A., "Computational Mechanics of Reinforced Structures", Friedr. Vieweg & Sohn Verlagsgesellschaft mbH, Braunschweig/Wiesbaden, 1995

[4] Antoniak, D. and Konderla, P., "General FEM Model of Prestressing Tendons", Computer Assisted Mechanics and Engineering Sciences,Vol. **7**, 2000, pp 435-448.

Mirela Galić, Mr. sc., CEng, Assistent
University of Split, Faculty of Civil Enginering, Matice Hrvatske 15, HR-21000 Split, Croatia,
tel: + 385 21 303334, fax: + 385 21 465117, e-mail: mirela.galic@gradst.hr
Pavao Marović, Prof. dr. sc., CEng, Full Professor
University of Split, Faculty of Civil Enginering, Matice Hrvatske 15, HR-21000 Split, Croatia,
tel: + 385 21 303334, fax: + 385 21 465117, e-mail: marovic@gradst.hr
Željana Nikolić, Prof. dr. sc., CEng, Associated Professor
University of Split, Faculty of Civil Enginering, Matice Hrvatske 15, HR-21000 Split, Croatia,
tel: + 385 21 303332, fax: + 385 21 465117, e-mail: zeljana.nikolic@gradst.hr

4th International Congress
of Croatian Society of Mechanics
September, 18-20, 2003
Bizovac, Croatia

CYCLICALLY LOADED WELDED PLATE DURING THE CENTER-CRACK PROPAGATION

Vladimir Gliha, Danilo Rojko

Keywords: WP specimen, plate, welded joint, crack, stiffness, crack-opening, cyclic loading, control mode, loading range, stress intensity range, crack propagation rate

Abstract

A residual stress field caused by welding influences the fracture resistance of welded joints in the as-welded condition. Residual stresses are not present on small-scale fracture-toughness specimens cut from welded joints. Wide plate (WP) specimen is designed to be sample of a pre-cracked welded joint were the residual stresses are included, too. Therefore, the fracture toughness data which are experimentally determined on WP specimens reflect the effects of residual stresses. For all that small-scale fracture-toughness specimens are usually used for the experimental fracture toughness determination of welded joints in the laboratory practise.

According to the recommendations and standards cracks on CT and SENB specimens should be prepared by using cyclic loading in the displacement-control mode. A reliable control of the loading amplitude is possible and so the control of fatigue-crack progression because stiffness of these specimens decrease to a high degree when crack propagate. It was necessary to find out how the stiffness of a WP specimens would change if fatigue crack propagated during cyclic loading of WP specimens. Therefore the stiffness of a plate due to crack propagation was analysed in order to prepare cracks on WP specimens with a multi-pass butt-welded joint in the as-welded condition. Loadings in the load- and in the displacement-control mode were taken into account.

WP specimen and the model of this specimen used in the research were as follows

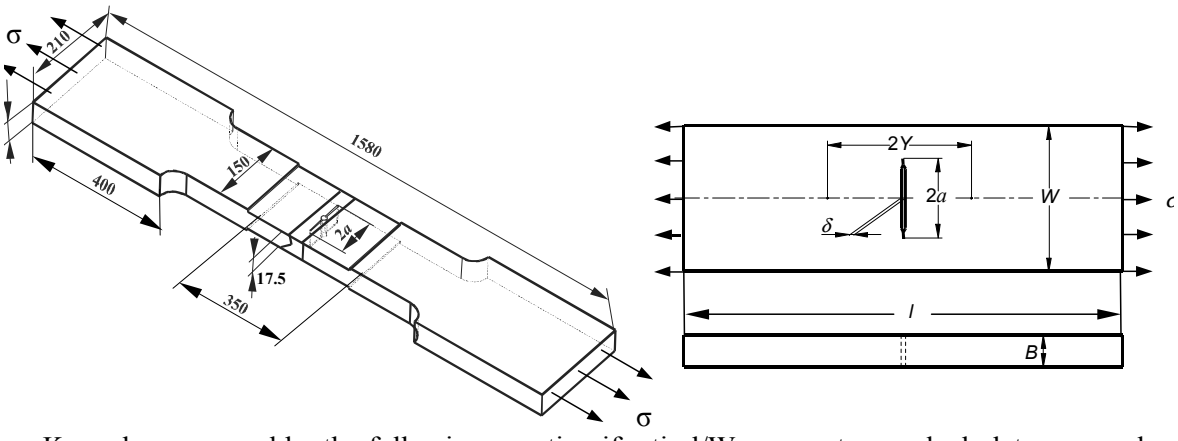

K can be expressed by the following equation if ratio l/Won a center-cracked plate approaches infinity:

$$K = \sigma\sqrt{\pi\, a}\,\sqrt{\sec\frac{\alpha\,\pi}{2}}\cdot(1-0{,}025\alpha^2+0{,}06\alpha^4)$$

where a is the crack size and $\alpha = 2a/W$ is its relative size.

SENB specimen was used to determine allowable stress level on WP specimens during precracking

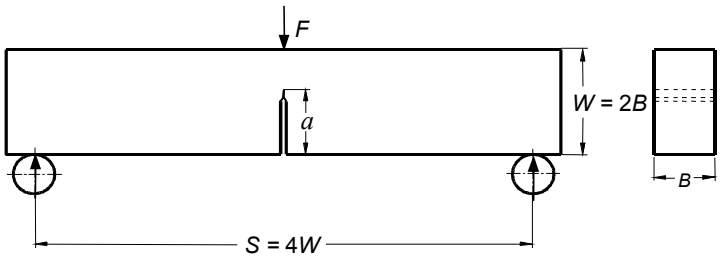

The stiffness of WP specimen is defined as

$$k = \frac{\delta F}{\delta u}$$

F is loading while u is displacement at the point where loading is applied to the center-cracked plate.

The stiffness of a 17.5 mm thick, 150 mm wide and 350 mm long center-cracked plate against the crack size $a - a_0$ at three different assumptions is shown in the figure. The initial crack size is $\alpha_0 = 34.5$ mm while the final one $a_0 + 3$ mm = 37.5 mm.

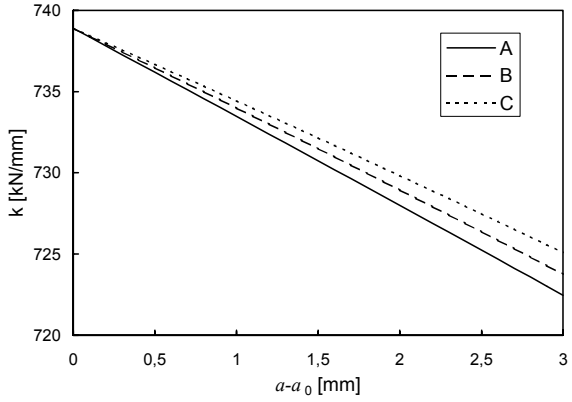

The stress intensity range and crack propagation rate increase during cyclic loading of the plate because stiffness decreases when cracks propagate. The loading range is constant if the plate is loaded in the load-control mode, whereas it decreases if the plate is loaded in the displacement-control mode. The stress intensity range and crack propagation rate increase in the displacement-control mode but by one third less than in the load-control mode. Crack propagation control on WP specimens will be, therefore, easier.

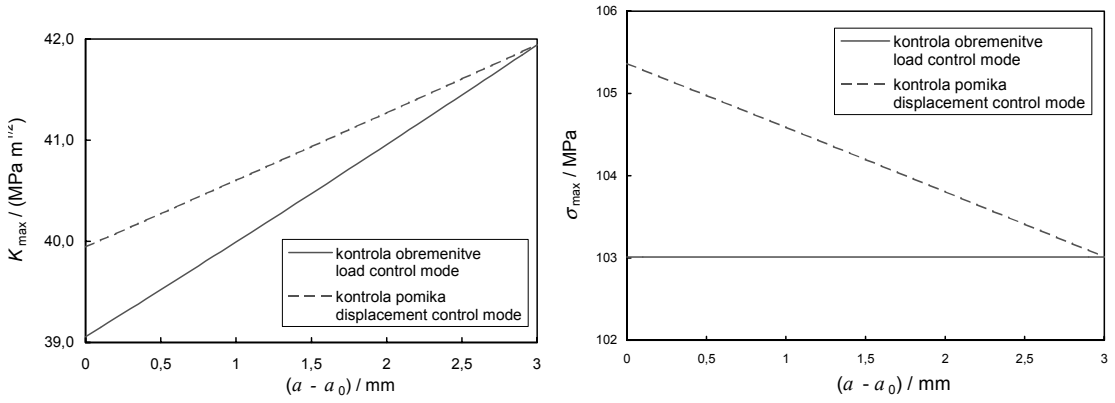

Vladimir Gliha, dr Danilo Rojko, dr
University of Maribor, Faculty of Mechanical Engineering, Smetanova 17, 2000 Maribor, Slovenia, E-mails: vladimir.gliha@uni-mb.si, danilo.rojko@uni-mb.si

4th International Congress
of Croatian Society of Mechanics
September, 18-20, 2003
Bizovac, Croatia

PRECISION BENDING IN TWO STAGES

B. Grizelj, M. Math and D. Grizelj

Keywords: bending, tool, part geometry, bending in two stages

1. Introduction

The important criteria in evaluation of bent components is the bending angle. The relative bending angle error may represent the measure of angle accuracy of the bent parts.

$$O_a = \frac{\alpha_2 - \alpha_{wz}}{\alpha_{wz}}$$

where we have: $\alpha_2 -$ bending angle after withdrawal of pressure; $\alpha_{wz} -$ die angle
There are three types of die bending: opened, half-opened and closed, see Fig. 1

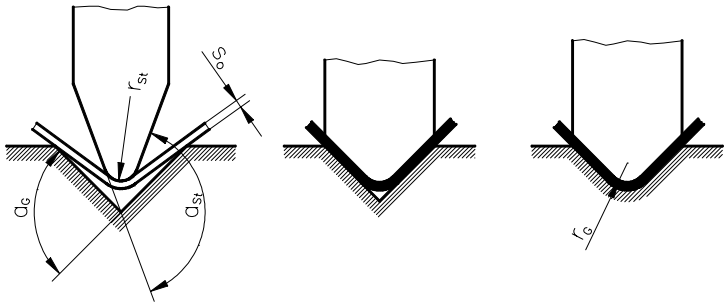

Figure 1. Die designation

2. Precision bending in two stages

The precise bending in two phases is presented on the figure 2.

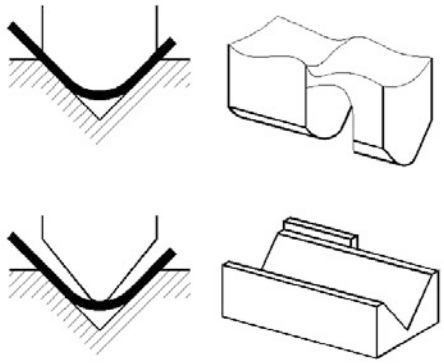

Figure 2. The precise bending in two stages

In the first stage the workpiece has greater radii then it is needed (early stage of bending), but after that, the workpiece is bended with demanded radii (final stage of bending).
Although is the cost of bending in two stage greater then in one bending stage, this has advantage in economical sense by small and medium series, because there is no supplementary finishing of the tool. By great series, it is accomplished through corresponding disposition of the tools (figure 2). The punches for early stage of bending and final bending are side by side. The width of the punch is equal to the width of the workpiece. After early stage of bending the workpiece is put beneath the punch for final bending. In next phases i.e. punch motion the both operation are performed simultaneously (on one workpiece the early stage of bending, while on the other the final bending). On this way it is reduced the time that it almost as by bending in one stage.
The dependency of relativ error of the bending angle O_a from specific maximum force F_{max}/b are presented by bending in two stages on the figure 3. The width of the tool is w=20 mm, material St 1403 and thickness is s_o= 0.75 mm.

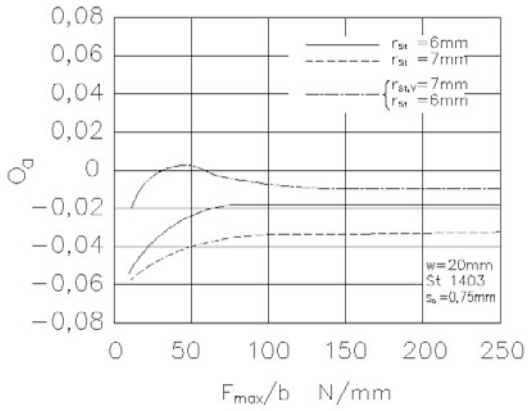

Figure 3. The dependence of relative error the bending angle from specific maximum force by bending in one stage as well as in precise bending in two stages by bending in half open tool 90^0-V

When the workpiece is bended with the radii r_{St}= 6 mm (full line), where this correspond with the radii of the workpiece, then the relative error changes as it is expected by bending with the width of the tool $w<w_{opt}$. It is decreased in the field of lesser specific force, firstly very strong, and later achieved constant value by F_{max}/b = 80 N/mm.
If it is applied r_{St}=7mm instead of r_{St}=6, then the form of the curve is similar (dotted line). All the same, the relative error is significantly greater. If that workpiece is firstly bended
With F_{max}/b = 50 N/mm and bending radii r_{St}=7mm and after that it comes the final bending with radii r_{St}=6 mm the curve has form of that dot line on figure 3.

3. Conclusion

Bending die geometry is obtained out of requirements regarding geometry of the bent components and their size. These parameters give in advance minimal and maximal sizes of the bent components. Shape of die, its width, curvature of the bottom die part, upper die angle and its radius and width exert influence on accuracy of bending.
This paper analysis the influence precision bending in two stages

Branko Grizelj Ph.D. Professor
University of Osijek, Faculty of Mechanical Engineering in Slavonski Brod, Trg. I.B.Mažuranić 18, 35000 Slavonski Brod Croatia 035 446-188, 035 446-446, e-mail: branko.grizelj@sfsb.hr
Miljenko Math Ph d. Professor
University of Zagreb, Faculty o Mechanical Engineering and Naval Arhitecture, Zagreb Ivana Lučića 5, 10000 Zagreb, Croatia e-mail: math.miljenko@fsb.hr
B.Sc. Dejan Grizelj, “Simens”, 10000 Zagreb Croatia

4th International Congress
of Croatian Society of Mechanics
September, 18-20, 2003
Bizovac, Croatia

EXPERIMENTAL AND NUMERICAL ANALYSIS OF CRACK TIP POSITION EFFECT LOCATED IN HAZ

Nenad Gubeljak, Dražan Kozak, Franjo Matejiček, Maks Oblak

Keywords: Fracture toughness testing, weld joint, heat affected zone, finite element analysis

Abstract

In the last decade the extensive fracture toughness testing of welded joints with the crack located in the heat-affected zone of structural steels was performed [1, 2]. Many investigations of fracture behaviour show that unpredictable fracture behaviour of specimen with crack tip located in HAZ can occur. The reason for such behaviour may lie in the HAZ microstructure heterogeneity and existing of local brittle zones (coarse-grained heat affected zone - CGHAZ). The spreading of stress and strain fields in the vicinity of crack tip, which is located in the HAZ, may be analysed very effective by finite element calculation [3]. The aim of this paper is to determine the effect of different crack tip position in HAZ on crack driving force and consequently on fracture behaviour of strength mismatch fracture toughness specimen.

High strength low alloyed HSLA steel (with thickness of 40 mm), corresponding to the grade HT80, was used as the base metal (BM) in a quenched and tempered condition (Q+T). Three different overmatched X-grooved multi-pass welded joints are studied (so-called mismatch factor $M=R_{p0.2WM}/R_{p0.2BM}$). The first was pure homogeneous with 21% higher yield strength related to BM (Fig. 1a). The second and the third joint were heterogeneous with two root passes welded by wire, which ensures 13% overmatch with the root height of 9 mm (Fig. 1b) and 14 mm (Fig. 1c), respectively. The rest passes were filled also by electrode with 21% overmatch.

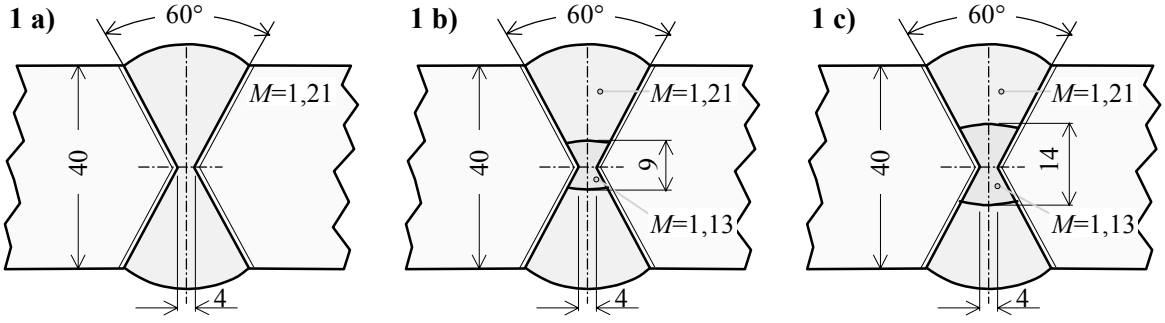

Fig. 1 Homogeneous 1 a), inhomogeneous 1 b) and 1 c) strength overmatch X-welded joints

Three-point bend test specimens (a/W=0.3) with 36 mm of thickness were extracted from the welded joints. Fracture toughness tests were performed according to BS 7448 [4]. Finite element analyses were performed to calculate the magnitude of maximum principal stress, what may serve as a global parameter by assessment of material resistance with respect to brittle fracture.

The results for principal stresses distribution shown that highest maximum principal stress is reached just under the HAZ crack tip in direction of BM. Higher stresses are observed in the hard HAZ than in the softer WM. The stress will reach its peak value at a distance less than two times the local CTOD.

Therefore, presence of the overmatched weld root pass effects to stress-strain distribution at the vicinity of a crack tip. It can be expected that an increasing of stresses in HAZ can increase risk of brittle fracture at the HAZ which may have a low fracture toughness. If the brittle fracture in HAZ does not occurs, the initiation and growth of stable crack propagation are governed by local plasticity in the base metal. Analysis confirmed that overmatching of 13 percent in the root pass, it is not enough to ensure the crack path deviation towards ductile base metal, while the overmatching of 22 percent it does. The yielding is directed from the HAZ toward base material, but HAZ with its high strength restricts further plastic deformation and locally raises the stresses.

Numerical analysis shows that changing of crack tip position has a significant effect on fracture behavior in elastic and plastic loading range. Significantly low effect on fracture behaviour has changing of amount of overmatching weld metal in root layer. Obtained results give principles for idealization of finite elements modelling of fracture behavior of welded joints.

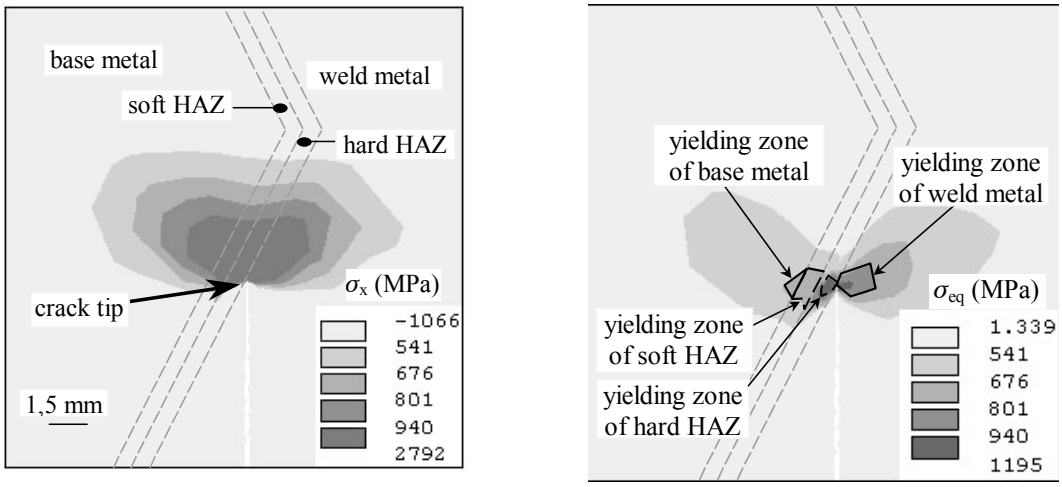

Fig. 2 Stress opening σ_x and equivalent stress σ_{eq} fields in the vicinity of the crack tip

References

[1] Fairchild, D.P., "Fracture Toughness Testing of Weld Heat-Affected Zones in Structural Steel, Fatigue and Fracture Testing of Weldments", ASTM STP 1058, H. I. McHenry and J. M. Potter, Eds., American Society for Testing and Materials, Philadelphia, 1990, 117-142

[2] Gubeljak, N.,"Fracture behaviour of specimens with surface notch tip in the heat affected zone (HAZ) of strength mis-matched welded joints", International Journal of Fracture 100, 1999, pp 155-167

[3] Matejicek, F., Gubeljak, N., Kozak, D. and Koçak. M., "Stress-Strain State at the Vicinity of the Crack Tip in Strength Mis-match Welded Joint", 13th European Conference on Fracture, San Sebastian, Proceedings on the CD-Rom, 1U.6, 2000

[4] BS 7448, "Fracture mechanics toughness test, Part 2. Method for determination of K_{IC}, critical CTOD and critical J-values of welds in metallic materials", TWI Abingdon Hall Cambridge, 1997

Dr Nenad Gubeljak, Assistant Prof., Faculty of Mechanical Engineering, University of Maribor, Institute for Structures and Machine Design, Smetanova ulica 17, SI-2000 Maribor, Slovenia, Tel. +386 2 220 7661, Fax: +386 2 220 7990, E-mail: nenad.gubeljak@uni-mb.si

Dr Dražan Kozak, Assistant Prof., Mechanical Engineering Faculty in Slavonski Brod, University of Osijek, Department of Mechanical Design, Trg Ivane Brlić-Mažuranić 18, HR-35000 Slavonski Brod, Croatia, Tel. +385 35 446 188, Fax: +385 35 446 446, E-mail: dkozak@sfsb.hr

Dr Franjo Matejiček, Professor, Mechanical Engineering Faculty in Slavonski Brod, University of Osijek, Department of Mechanical Design, Trg Ivane Brlić-Mažuranić 18, HR-35000 Slavonski Brod, Croatia, Tel. +385 35 446 188, Fax: +385 35 446 446, E-mail: fmatej@sfsb.hr

Dr Maks Oblak, Professor, Faculty of Mechanical Engineering, University of Maribor, Institute for Mechanics, Smetanova ulica 17, SI-2000 Maribor, Slovenia, Tel. +386 2 220 7800, Fax: +386 2 220 7990, E-mail: maks.oblak@uni-mb.si

4th International Congress
of Croatian Society of Mechanics
September, 18-20, 2003
Bizovac, Croatia

TESTING THE TIMBER – EPS CONCRETE COMPOSITE STRUCTURES

M.Haiman, M.Rak, J.Krolo, Lj.Herceg, V.Čalogović

Keywords: timber, lightweight EPS concrete, composite structures, lab tests, FE analysis, sheared connections

Abstract

This paper presents the results of the numeric and laboratory tests of the «T» section of EPS concrete-timber composite ceiling structures. Sheared connections of EPS concrete board and timber girder elements have been tested in several different ways by means of mechanical connectors. Shearing forces in the connection plane were assumed by means of dowels, then by means of nails, and by gluing the connection of EPS concrete and timber with epoxy glue.

All the tests were numerically modelled by means of FEA software COSMOS/M 2.8 and the results were compared with those of the laboratory tests.

Application of these structures in civil engineering practice is multiple, particularly in reconstruction of old timber girder floor structures or manufacture of new ones at the reconstruction of old buildings in areas exposed to frequent earthquakes.

1. Introduction

At the reconstruction of ceiling timber structures, they can be strengthened with reinforced concrete board composed with the existing timber girder. The new lightweight EPS concretes weighting 1200 to 1400 kg/m^3 provide new possibilities of application in composite structures.

In efforts to test and determine the rules of behaviour of such structures at static loads, several types of dowels were tested in the laboratory. The tests were carried out within the framework of the scientific research program supported by the Ministry of Science and Technology of the Republic of Croatia.

2. Lab tests

Sheared connections of a timber beam and an EPS concrete board were done for four different cases of connections in the connection plane, see Fig. 1.

In Type 1, the connection was done with Ø25 mm steel dowels placed, two of them in a single section.

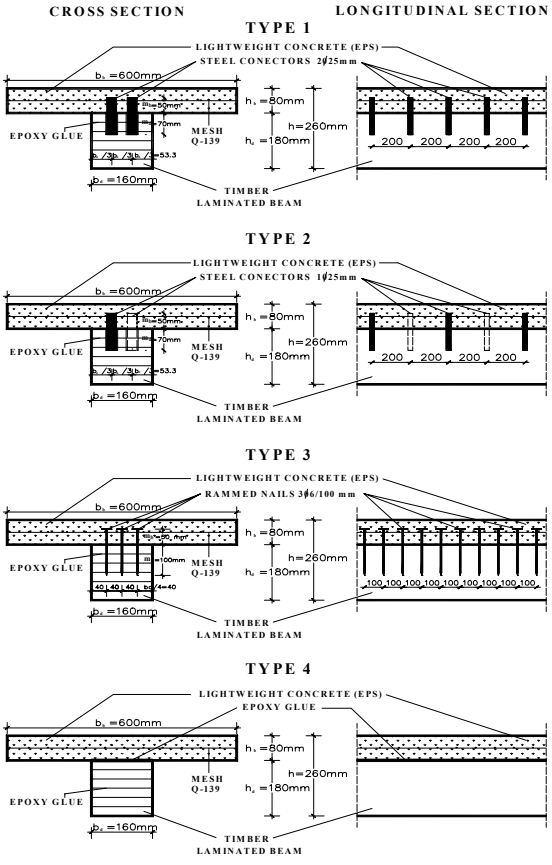

Fig. 1. Types of Timber-EPS concrete composite beams

The distance between the dowels in longitudinal direction was 200 mm. In Type 2, the same Ø25 mm steel dowels were used, but they were placed alternatively, 1 dowel in section, at distances of 200 mm. In these two types, the holes for dowels were of a slightly larger diameter than dowel diameter. Epoxy glue was placed in the holes and then the dowels were installed.
In Type 3, Ø6 mm nails were used for connection. In a single section, three nails were driven in up to the depth of 100 mm. Mutual distance between the nail groups was 100 mm.

Type 4 was tested with the connection by means of epoxy glue placed on timber beam elements directly before placement of EPS concrete.

Very high differences were obtained by laboratory test of each of the aforesaid types until failure as presented on diagram (Fig. 2). Types 1 and 4 have shown the best bearing capacity characteristics until breaking, while Type 3 with the nails yielded the worst test results.

Failure of all the tested types occurred by exceeding the tensile strength of the laminated timber beams.

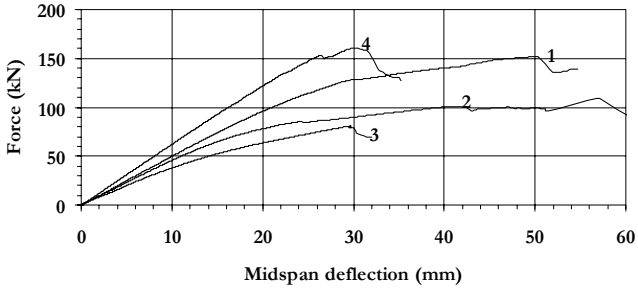

Fig. 2: Force – deformation ratio until failure, for tested types 1 to 4

3. Conclusion

Timber – EPS concrete composite structures account for relatively simple and inexpensive structures usable in repair or reconstruction of old timber beam ceilings. Such a combination is very advantageous for use in areas exposed to frequent earthquakes, where as lightweight structure as possible needs to make sufficiently solid and strong solution of floor structure strengthening. These solutions contribute to the general stability and solidity of buildings where such structures are applied.

By composite timber – EPS concrete structures, the floor structure bearing capacity is increased, and deformations for maximum exploitation loads are reduced.

The laboratory tests have shown that the use of epoxy glue as connection between EPS concrete board and timber beam is the best connecting solution.

Use of nails in connection plane for transfer of shearing forces of connection has brought the worst results and is not recommended for use in civil engineering practice.

All the numerical tests have shown very good compliance of the results with the results obtained in the lab. This provides additional certainty to the results of this scientific research.

Reference

[1] H. J. Blass, Mario. L.R. Van Der Linden, M. Schlager: «Timber Floors Strengthened with Concrete», Saving Buildings in Central and Eastern Europe – IABSE Colloquium Berlin 4-5 June, 1998.

Miljenko Haiman,Ph.D.Civ.Str.Eng.
Faculty of Civil Engineering Zagreb, Department for Structures, Kačićeva 26, 10000 Zagreb, HR
+385 1 4639-302, fax. +385 1 4828-052, mhaiman@grad.hr
Docent Mladenko Rak,Ph.D.Civ.Eng.; Joško Krolo,M.Sc.Civ. Eng.;
Docent Ljudevit Herceg,Ph.D.Civ.Eng.; Vladimir Čalogović, B.Sc.Phys.Eng., all from
Faculty of Civil Engineering Zagreb, Department for Technical Mechanics, Kačićeva 26, 10000 Zagreb, HR
+385 1 4639-289; fax. +385 1 4828-049; rak@grad.hr, krolo@grad.hr, vladimir@grad.hr
WEB page: www.grad.hr

4th International Congress
of Croatian Society of Mechanics
September, 18-20, 2003
Bizovac, Croatia

4thICCSM

A CONTRIBUTION TO THE STUDY OF PLASTIC STATE EVOLUTION IN BEAM STRUCTURES OF RECTANGULAR CROSS-SECTION

Miroslav HALILOVIČ, Boris ŠTOK

Keywords: beam bending, elasto-plasticity, deflection curve, plastic propagation, collapse

1. Introduction

Bending of beam structures is rather frequently addressed in technical practice. Despite being adequately and thouroughly analysed, a very limited number of analytically deduced solutions are known considering elasto-plastic bending. In this paper, however, elasto-plastic bending of beam structures, with rectangular cross-section area and elasto-plastic material with no hardening assumed, is investigated. The particular solutions derived under the assumption of at most parabolic bending moment distribution enable fully analytic tracing of the elasto-plastic state evolution in structural components by proportional application of loads to a structure.

2. Formulation of elasto-plastic beam bending problem

Considering the Bernoulli-Navier assumptions, material elasto-plastic properties constant and isotropic, with no hardening, but equal yield stress in tension and compression, the following differential equations

$$\frac{\mathrm{d}^2 w}{\mathrm{d}x^2} = \begin{cases} -\dfrac{3M(x)}{2Ebh^3} & \ldots \quad x \in \Omega_\mathrm{e}\,; \Omega_\mathrm{e} = \{x : |M(x)| \le M_\mathrm{e}\} \qquad (1a) \\ \dfrac{K}{\sqrt{M_\mathrm{p} - |M(x)|}} & \ldots \quad x \in \Omega_\mathrm{p}\,; \Omega_\mathrm{p} = \{x : M_\mathrm{e} < |M(x)| < M_\mathrm{p}\}\ , \qquad (1b) \end{cases}$$

governing deflection of a beam, can be deduced for a beam of rectangular cross-section. M_e and M_p are respectively values of the limit elastic and fully plastic bending moment.

3. Elasto-plastic solution of governing differential equation

Particular solutions to the above equations can be explicitly derived for at most quadratic moment distribution assumed. By enforcing the obtained general form solutions to fulfil boundary conditions and continuity conditions between elastic and elasto-plastic regions, analytical solutions specific to particular structural loading cases can be readily obtained.

4. On mechanical response properties by elasto-plastic loading

With the stress resultants known the plastic domain Ω_p as well as spreading of the plastic zone through the beam height are uniquely defined. For statically determinate structures it is also characteristic that neither distribution nor magnitude of the internal forces along the structure are influenced by the presence of plastic strains in the structure. Regardless of the material behaviour and non-linear stress distribution across a cross-section the internal forces are increased proportionally by a proportional increase of the applied loads. On the contrary, the described

property is not valid for statically indeterminate structures. With ongoing of the plastic deformation the bending stiffness is actually subject to a continuous variation, affecting thus reaction forces to vary in a non-proportional way in spite of the proportional application of external loads. In consequence, the internal forces are changed non-proportionally as well.

5. Numerical example

Mechanical response of a simply supported overhanging beam, subject to a concentrated force F ($F \geq 0$) at the free end and to a uniformly distributed load q ($q \geq 0$) between the supports is considered in detail. Of importance for the evolution of the plastic strains, along with the increase of the loading parameter λ, is as well the given ratio ψ between the two loads. It is actually this ratio that defines, by fixing location of a maximum bending moment, the position of the first plastic yield. Gradually increasing loadings for three characteristic load ratios, yielding different patterns of plastic zone propagation, were considered until the structure´s collapse. In Fig. 1a the respective plastic strain evolution, as the load level is increased within interval $\lambda_e < \lambda \leq 1$ is plotted for such a load ratio $\psi = \psi_2$ that leads to occurrence of two plastic hinges at the same time. From the graphical representation of the respective deflection curves in Fig. 1b, considered for the limit elastic and fully plastic load levels $\lambda = \lambda_e$ in $\lambda \to 1$, degradation of the structure´s functionality can be qualitatively visualized, with asymptotic approaching to the state of collapse clearly indicated.

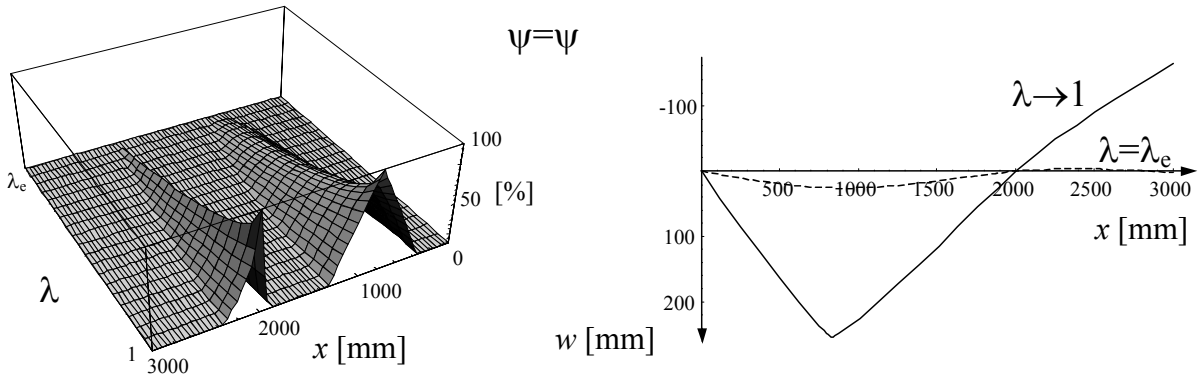

Figure 1: Elasto-plastic state evolution for the characteristic value of load ratio $\psi = \psi_2$
(a) plastic zone propagation with regard to the increasing load level λ ($\lambda_e < \lambda \leq 1$),
(b) deflection curves at limit elastic ($\lambda = \lambda_e$) and fully plastic load levels ($\lambda \to 1$).

References

[1] Saje, M., "Mešan variacijski princip za neomejeno velike deformacije ravninskih nosilcev in uporaba v metodi končnih elementov", Zbornik Kuhljevi dnevi '89. SDM, Ljubljana, 1989.
[2] Prager, W., Hodge, P.G., "Theory of Perfectly Plastic Solids", Dover Publications Inc., New York, 1951.
[3] Kaliszky S., "Plasticity, Theory and Engineering Applications", Akadémiai Kiadó, Budapest, 1989.
[4] Życzkowski M., "Combined Loadings in the Theory of Plasticity", PWN-Polish Scientific Publishers, Varšava, 1981.
[5] Smith J.O., Sidebottom O.M., "Inelastic Behavior of Load-Carrying Members", John Wiley & Sons Inc., New York, 1965.
[6] Goodier J.N., Hodge P.G., "Elasticity and Plasticity", John Wiley & Sons Inc., New York, 1958.
[7] Štok B., Kosel F., "Določitev potrebne geometrije orodja pri elastoplastičnem krivljenju nosilcev ob pogoju M=const." Zbornik del. 4. Jugoslovanski simpozij plastičnosti, Tuheljske toplice, 1985.
[8] Kosel F., Petrišič J., Bremec B., "Nesimetrični upogib v elasto-plastičnem področju". Zbornik Kuhljevi dnevi '99. SDM, Ljubljana, 1999.

M.Sc. Miroslav Halilovič, Assistant, Faculty of Mechanical Engineering, University of Ljubljana, Aškerčeva 6, Ljubljana, Slovenia, +386-1-4771-440, miroslav.halilovic@fs.uni-lj.si
PhD. Boris Štok, Professor, Mechanical Engineering, University of Ljubljana, Aškerčeva 6, Ljubljana, Slovenia, +386-1-4771-425, boris.stok@fs.uni-lj.si

4th International Congress
of Croatian Society of Mechanics
September, 18-20, 2003
Bizovac, Croatia

4thICCSM

OPTIMIZATION OF STATICALLY LOADED SKELETAL STRUCTURES

Boštjan Harl, Marko Kegl and Maks M. Oblak

Keywords: *skeletal structures, statically loaded, shape optimization, design elements*

1. Introduction

An attractive approach to shape optimization is offered by combining the *design element technique* and suitable design elements, for example, *Bézier bodies*, [3]. By this approach the geometrical body defined by the hull of the structure is divided into simpler geometrical objects called the design elements (DE). These can be parameterized in a rather simple way and the finite elements are then defined in the domain of the design element (Figure 1) rather than directly in the real 3D space. In that way we get some kind of a 'convective' finite element mesh, following automatically the geometry changes of the structure.

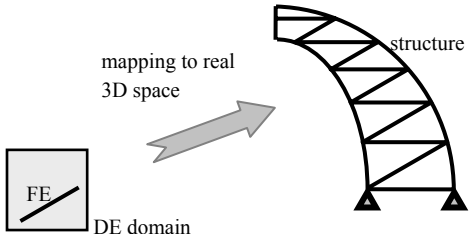

Figure 1. A FE is mapped from the DE domain to real 3D space

By this approach finite elements (FE) virtually of any kind can be employed. But, since the shape of the structure may vary significantly, it is a good idea to select an adequately accurate bar or beam element (see e.g. [2]) which accounts for kinematic nonlinearities. In that way possible structural stability problems are adequately captured and can be handled appropriately.

2. Shape parametrization and the design problem

Let us consider a skeletal structure S and let the hull of the structure be the surface of the geometrical body B (Figure 2).

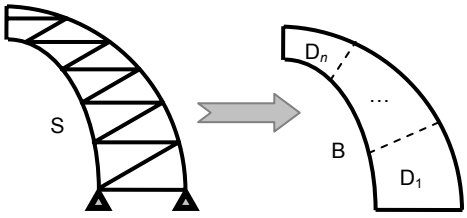

Figure 2. The hull of the structure defines the body B that is divided into design elements D_i

Depending on the complexity of the shape of S, B can be regarded as assembled of any number of design elements D_i. For several reasons described in more detail in [3], we take the design element D_i to be a Bézier body.

A Bézier body D can be regarded as the image of a unit cube U mapped into the real 3D space (Figure 3). The position and shape of D is fully determined by the position of its *control points* $\mathbf{q}_{ijk}$. A change of the position of $\mathbf{q}_{ijk}$ changes the position and shape of D.

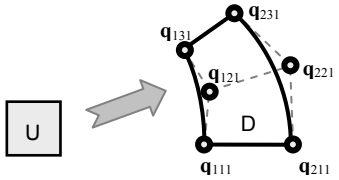

Figure 3. Shape and position of D is determined by the control points q_{ijk}

The coordinates of the control points $\mathbf{q}_{ijk}$ can be defined in dependence of a relative small number of parameters – the design variables assembled in the vector $\mathbf{b}$. Thus, by varying the values of the design variables $\mathbf{b}$, the shape of the whole structure is varied. Once this is done, it is not very hard to formulate the optimization problem in a standard form. Such a problem can then be solved by any suitable method (e.g. [1] and [4]).

3. Numerical example

As a numerical example let us just mention a shape optimization problem of the bridge shown in Figure 4. The shape of the bridge as well as the cross-sectional properties of beams and bars have been made dependent on 17 design variables. Displacement and stress constraints have been taken into account while minimizing the weight of the structure.

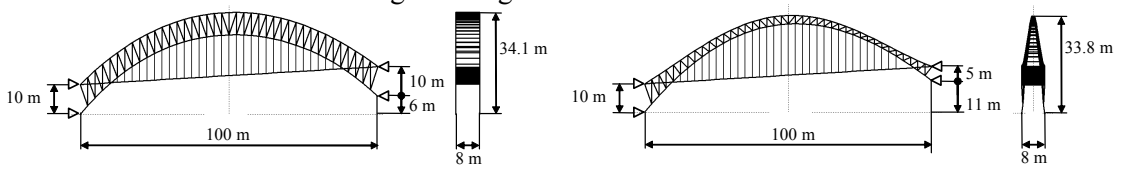

Figure 4. Initial (left) and final (right) design of the bridge

References

[1] Kegl, M. & Oblak, M.M., "Optimization of mechanical systems: on non-linear first-order approximation with an additive convex term", Communications in Numerical Methods in Engineering, Vol. 13, 1997, pp 13-20.

[2] Kegl, M. & Antes, H., "Shape optimal design of elastic space frames with non-linear response", International Journal for Numerical Methods in Engineering, Vol. 43, 1998, pp 93-110.

[3] Kegl, M., "Shape optimal design of structures: an efficient shape representation concept", International Journal for Numerical Methods in Engineering, Vol. 49, 2000, pp 1571-1588.

[4] Kegl, M., Butinar, B.J. & Kegl, B., "An efficient gradient-based optimization algorithm for mechanical systems", Communications in Numerical Methods in Engineering, Vol. 18, 2002, pp 363-371.

Boštjan Harl, Dr.
Faculty of Mechanical Engineering, University of Maribor, Smetanova 17, SI-2000 Maribor, Slovenia
bostjan.harl@uni-mb.si
Marko Kegl, Ass. Prof., Dr.
Faculty of Mechanical Engineering, University of Maribor, Smetanova 17, SI-2000 Maribor, Slovenia
marko.kegl@uni-mb.si
Maks M. Oblak, Prof., Dr.
Faculty of Mechanical Engineering, University of Maribor, Smetanova 17, SI-2000 Maribor, Slovenia
maks.oblak@uni-mb.si

4th International Congress
of Croatian Society of Mechanics
September, 18-20, 2003
Bizovac, Croatia

4thICCSM

CREEP DEFORMATION SUBSEQUENT TO PLASTIC STRAINING OF STAINLESS STEEL AT LOW TEMPERATURE

Kozo Ikegami

Keywords: Creep strain, Low temperature, Combined loading, Stainless steel, Hardening effect

1. Introduction

There are not so many experimental investigations on inelastic deformation at low temperature as reported by the author [1]. This paper reviews the several experimental results of stress-strain relations of stainless steel SUS 304 at low temperature for creep loading on the basis of the authors' experimental results [2] and [3]. The characteristic behaviour of creep deformation at low temperature is experimentally examined.

2. Experimental procedure

The testing machine has two hydraulic actuators which are mounted on the upper and lower parts of the machine. The upper and lower actuators give torsional and axial loads, respectively, to specimens through the double cylinders. Thin-walled tubular specimens are used in low temperature tests. A specimen is cooled by liquid nitrogen in the cooling bath. The low temperature states of 77 K are attained by liquid nitrogen. The strain of the specimens under loading conditions is measured by the image processing method of the grid patterns attached on the surface of the attachment of the specimens. The detailed testing system is previously reported by the authors [4].

3. Experimental results and discussions

Figure 1 is tensile creep strain curves at different stress levels against holding time. Large creep strain is observed in the range of 600 MPa to 800 MPa, but creep strain is small in 900 MPa to 1100 MPa. The creep deformation dose not depend on the magnitude of holding load, but the hardening rate of plastic deformation. Similar tendency is found in the results of compressive and torsional loading. The creep strain rate just after holding stress is approximately equal to the plastic strain rate at the holding stress. The creep strain stops after long holding time.

Creep strain has plastic hardening effect as plastic strain. The magnitude of plastic hardening by creep strain is denoted by $\Delta\sigma$ of the stress-strain curves. The relation between creep strain rate and plastic hardening magnitude $\Delta\sigma$ is represented by linear line as shown in Fig. 2. The relation is obtained by the following equation:

$$\ln \rho = \alpha^* - k\Delta\sigma \tag{1}$$

where the notation α^* is creep strain rate at the start point of holding stress and the notation k is the gradient of the linear relations. The value k depends on stress values.

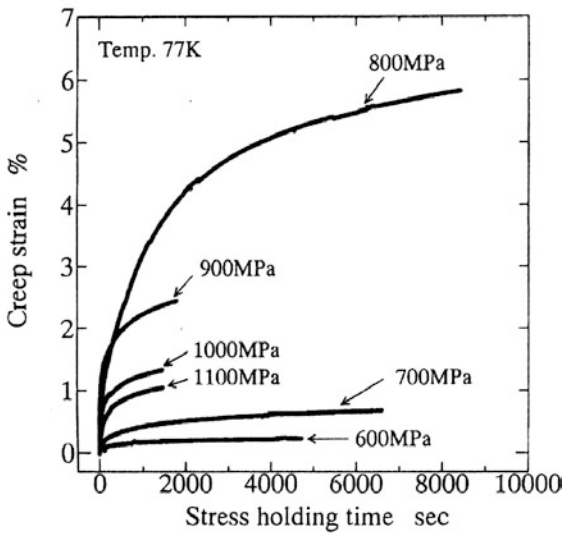

Fig. 1 Tensile creep strain curves at different stress level

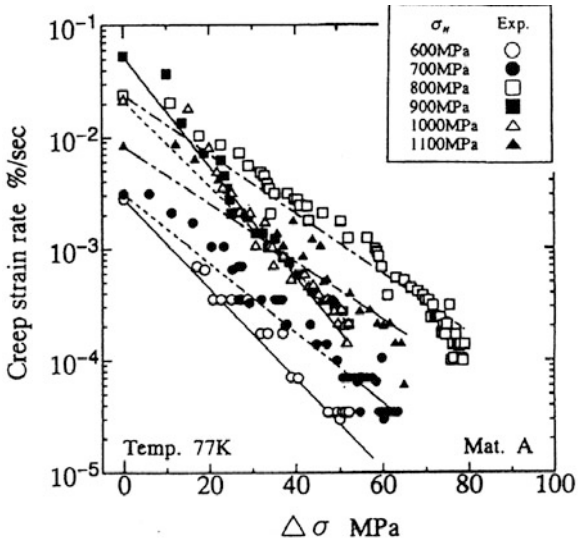

Fig. 2 Relations between plastic hardening rate and creep strain rate

4. Conclusions

Creep deformation of stainless steel in liquid nitrogen is experimentally investigated by subjecting thin-walled tubular specimens to axial and torsional loads.

(1) The creep strain gives rise to plastic hardening. The hardening magnitude by creep strain is the same as plastic strain.

(2) The creep strain induced by holding stress is related with the plastic strain rate at the holding stress.

(3) The creep strain rate has a linear relation with plastic hardening magnitude in logarithmic representation.

References

[1] Ikegami, K., "Experimental plasticity of metals at low temperature - A brief review -". In: Fan, J. and Murakami, S., editors. Advances in Constitutive Laws for Engineering Materials, Vol. II, Proc. Int. Conf. Constitutive Laws for Engineering Materials, Beijing: Int. Academic Pub,Beijing, 1989, pp 78-84.

[2] Tanaka, N, Shirasawa, Y, Nütsu, Y and Ikegami, K., "Experimental investigation of plastic deformation of SUS3O4 stainless steel at 77K", Transaction Japan Society of Mechanical Engineers, Vol. 57, No. 543,1991; pp 2775-2781.

[3] Kawai, I, Ikegami, K and Nütsu, Y, "Biaxial creep behavior of SUS 304 at low temperature" , Transaction of Japan Society of Mechanical Engineers, Vol. 62, No. 602, 1996, pp 2427-2434.

[4] Ikegami, K., "Experimental Studies of Plastic Deformation of Metal for Complex I.oading at Liquid Nitrogen", Proceedings of the 3~d international congress of Croatian Society of Mechanics, 2000, pp.375-382

Kozo Ikegami, Professor, Doctor
Tokyo Denki University, Department of Mechanical Engineering, 2-2 Kanda-Nishikicho,
Chiyodaku Tokyo 101-8457, Japan,
Tel. #81-3-5280-3370, Fax. #81-3-5280-3568, e-mail, kikegami@cck.dendai.ac.jp

4th International Congress
of Croatian Society of Mechanics
September, 18-20, 2003
Bizovac, Croatia

4thICCSM

EFFECT OF HARDENING RESPONSES ON ELASTOPLASTIC BEHAVIOUR OF SHELL STRUCTURES

Tomislav Jarak, Igor Karšaj and Jurica Sorić

Keywords: *finite strain, small strain, kinematic hardening, isotropic hardening, finite element analysis*

1. Introduction

In this contribution, the effect of isotropic and kinematic hardening responses on the load-displacement behaviour of shell structures is analysed. The basic equations for finite strain plasticity and the material model of small strain formulation are presented. The same isotropic hardening law is assumed for both formulations, while the Prager equation for kinematic hardening is used for the small strain model and the finite strain model employs free-energy based kinematic hardening formulation. Integration algorithms at material point level of a finite element formulation employ a closest-point projection scheme together with a consistent elastoplastic tangent modulus [1,2].

2. Material model

In order to describe the inelastic material behaviour, an elastic domain E described by convex yield function ϕ is assumed

$$E := \{(\boldsymbol{\tau}, \mathbf{q}, Y) : (\boldsymbol{\tau}, \mathbf{q}, Y) \leq 0\}, \tag{1}$$

where $\boldsymbol{\tau}$ is the Kirchhoff stress tensor, $\mathbf{q}$ is the back stress tensor describing kinematic hardening and Y is the internal variable, which describes isotropic hardening. As usual for metal plasticity, the von Mises yield criterion is assumed

$$\phi = \|\operatorname{dev} \boldsymbol{\xi}\| - \sqrt{\frac{2}{3}}(\sigma_{\mathrm{Y}} - Y), \tag{2}$$

$$Y = -HZ - (\sigma_{\infty} - \sigma_{\mathrm{Y}}) \cdot (1 - \exp(-\eta Z)). \tag{3}$$

H is the isotropic hardening parameter, Z is the internal variable energy conjugate to Y and σ_{∞}, σ_{Y} and η are the material constants. $\boldsymbol{\xi}$ is the relative stress deviator defined as $\boldsymbol{\xi} = \boldsymbol{\tau} - \mathbf{q}$.

There are certain differences between the small strain and the finite strain theory in definition of kinematic hardening. In the finite strain formulation a new internal variable $\mathbf{b}_{\mathbf{q}}$ is assumed in the following form

$$\mathbf{b}_{\mathbf{q}} = \mathbf{F}\mathbf{F}_{\mathbf{p}}^{-1}\mathbf{F}^{-1}, \tag{5}$$

where $\mathbf{b}_{\mathbf{q}}$ is the internal variable energy conjugate to the back stress tensor. By using the classical thermodynamical arguments the explicit expression for the back stress tensor is obtained

$$\mathbf{q} = -\rho \mathbf{b}_{\mathbf{q}} \frac{\partial \psi}{\partial \mathbf{b}_{\mathbf{q}}}. \tag{6}$$

The small strain theory model uses a linear kinematic hardening expressed by Prager equation

$$\dot{\mathbf{q}} = \frac{2}{3} k \dot{\lambda} \boldsymbol{\xi}, \tag{7}$$

where $\dot{\mathbf{q}}$ represents the back stress tensor rate, k the kinematic hardening modulus and $\dot{\lambda}$ the plastic multiplier rate.

3. Numerical examples

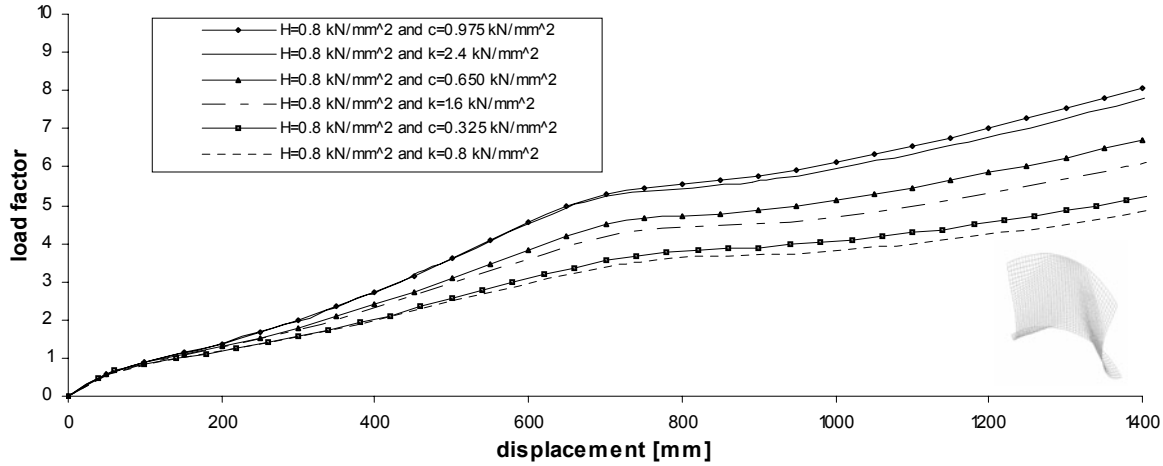

Figure 1. Scordelis-Lo roof: parametric analysis of the kinematic hardening parameters

4. Conclusion

This paper deals with a comparison of the small and finite strain formulation, especially with the influence of the isotropic and kinematic hardening responses on the elastoplastic behaviour of shell-like structures. Numerical examples show a relative good agreement of the results for the elastic ideal-plastic and the isotropic hardening responses. Special emphasis has been made to the comparison of the kinematic hardening responses at the small and finite strain formulation. It is evident that the similar elastoplastic behaviour can be found for both hardening formulations by adjustment of the kinematic hardening parameters. Although the aforementioned examples have mostly been used in the literature for large strain analyses, it is obvious that the presented examples do not exhibit large strain behaviour.

References

[1] Karšaj, I., Sansour, C. and Sorić, J. "An efficient free energy-based modelling of kinematic hardening in large strain elastoplasticity", Proceedings of the Seventh International Conference on Computational Plasticity (COMPLAS 2003), Barcelona, Universitat Politecnica de Catalunya, Spain.

[2] Sorić, J., Montag, U., Krätzig, W. B., "An efficient formulation of integration algorithms for elastoplastic shell analysis based on layered finite element approach", Comput. Methods Appl. Mech. Eng., 148, (1997), 315-328.

[3] Sansour, C., Wagner, W., "A model of finite strain viscoplasticity based on unified constitutive equations. Theoretical and computational considerations with applications to shells"., Comp. Meth. Appl. Mech. Engrg., 191, (2001), 423-450.

Tomislav Jarak, B.Sc., University of Zagreb, Faculty of Mechanical Engineering and Naval Architecture, Zagreb, Ivana Lučića 5, Croatia, +38516168514, tomislav.jarak@fsb.hr,
Igor Karšaj, B.Sc., University of Zagreb, Faculty of Mechanical Engineering and Naval Architecture, Zagreb, Ivana Lučića 5, Croatia, +38516168514, igor.karsaj@fsb.hr ,
Jurica Sorić, Ph.D., University of Zagreb, Faculty of Mechanical Engineering and Naval Architecture, Zagreb, Ivana Lučića 5, Croatia, +38516168103, jurica.soric@fsb.hr

th International Congress
of Croatian Society of Mechanics
September, 18-20, 2003
Bizovac, Croatia

4thICCSM

An Object Oriented Modelling Approach to Determination of Vibration Characteristics of Packaging Systems

V. Jaram and V. Damić

Keywords: *Object oriented modeling, Bond Graphs, packaging systems, distribution packaging, vibration characteristics, natural frequencies*

1. Introduction

A product-package system typically consists of an outer container, the cushion, the product, and a critical element. The critical element is the most fragile component of the product (e.g. electric boards). It is the part that is most easily damaged by a mechanical shock or by vibrations. The goal in distribution packaging is to provide a correct design for packaging so that its contents arrive safely at its destination. Vibration is associated with all transportation modes, although each mode has its own characteristic frequencies and amplitudes. The most troublesome frequencies are below 30 Hz because they are most prevalent in vehicles and it is difficult to isolate products from them.

2. Bond Graph Model development

A simple packaging system model was designed consisting of container body with a cantilever beam as the critical element carrying a device at its end. The package container plate was fixed on the table of a testing machine used for vibration testing of the package. The mathematical model of the package was developed using the bond graph methodology (Figure 1).

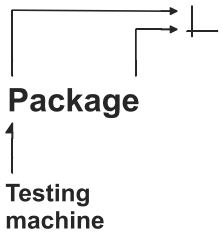

Figure 1. System level model of the Package system

It is shown how the bond graph model of typical vibration testing set-up can be developed within the bond graph programming environment. Using basic data from actual test performed on vibration table, a frequency response of the system was generated to simulate a typical laboratory vibration testing procedure. The goal was to predict the system's behaviour under vibration testing by simulation based on a model of the package system.

Further goals of this work were to show capabilities of Bond Graphs based approach in Computer Aided Total Packaging Distribution Design process. The complete design/testing process should be speeded up by continuous evaluation by simulation after each design/change step so that finished package design should meet design objectives, and enable that those expensive parts (products) are not destroyed during testing process (e.g. testing for resonant frequencies).

3. Results of Simulation

Based on the spectrum of input and output signals found by simulation the transmissibility (magnification factor) was calculated as $Q = 1 + (A_{output}/A_{input})$. It was done for the frequency range of 1 to 50 Hz and results are shown in diagram in Fig. 2 in log scale.

Comparing result (32,9 Hz) obtained by simulation and result obtained on vibration table (26,777 Hz) it can be seen that results are close to each other. It has to be emphasized and taken in consideration that simulation model applied was relatively simple (boundary conditions were simplified and it would be necessary to applied detailed model of boundary conditions). Nevertheless it can be concluded that results are very favourable and this work proves that method applied can be used for determination of dynamic properties during the product design process (computer aided total Packaging distribution design process) before specific product (part, component) is manufactured. On that way a need for intensive testing is reduced on those cases (except for) where and when it is absolutely necessary (e.g. because of security reasons and when hazardous situations are in question).

4. Conclusion

The ***BondSim***© system has been used for problem solving described in this work. It is designed as compact modelling framework based on the object-oriented approach in a visual environment. The functional model representation is based on bond graph methodology. The final system model is generated in symbolical form. Based on the model created ***BondSim***© produces mathematical model in the form of the system of differential algebraic equations. Simulation of the system behaviour is based on solving differential algebraic equation using suitable methods. Simulation results show close agreement with results of testing of the package on the testing machine.

The program BondSim is available from the second author.

References

[1] Brandenburg and Lee, "Fundamentals of Packaging Dynamics", 2nd Edition, MTS Corporation, Minneapolis, USA, 1985

[2] ASTM Standard D 5112 Test Method of Vibration (Horizontal Linear Sinusoidal Motion) Test of Products & ASTM Standard D 3580 Test Method of Vibration (Vertical Sinusoidal Motion) Test of Products

[3] Jaram V., "Evaluation of Bond Graph Based Object Oriented Approach to Determination of Natural Frequencies of Packaging System Elements", Master Deegre Thesis, RIT, Rochester, New York, USA, 2001.

[4] Shabana, A.A., "Dynamics of Multibody Systems", 2nd edition, Cambridge University Press, Cambridge, UK, 1998.

[5] Damić, V., Montgomery, J., "Mechatronics by Bond Graphs, An Object Oriented Approach to Modelling and Simulation", 1st edition, Springer-Verlag, Berlin Heidelberg, Germany, 2003.

[6] Cook R.D., Malkus D.S., Plesha M.E., "Concepts and Applications of Finite Element Analyis", John Wiley & Sons, 3rd ed., 1989.

Vladimir Jaram, Ms, The Polytechnic of Dubrovnik, Cira Carica 4, 20000 Dubrovnik, Croatia, tel. +20 445 700, fax. +20 435 590, vladimir.jaram@zg.hinet.hr

Vjekoslav Damić, Prof. Dr. sc., The Polytechnic of Dubrovnik, Cira Carica 4, 20000 Dubrovnik, Croatia, tel. +20 445 713, fax. ++20 435 590, vdamic@vdu.hr

4th International Congress
of Croatian Society of Mechanics
September, 18-20, 2003
Bizovac, Croatia

4thICCSM

THE ASSESSMENT OF STRUCTURED LIGHT AND LASER SCANNING METHODS IN 3D SHAPE MEASUREMENTS

Stjepan JECIĆ, Nenad DRVAR

Keywords: 3D scanning, structured light, laser, accuracy

1. Introduction

The development of optical 3D shape measurement methods is rapidly gaining importance as industry raises its demands in high technical performance of final products, short production times, low manufacturing costs and the overall product quality. This development can be clearly witnessed by the vast number of research papers published in the last 20+ years [1] as well as by the number of commercially available measurement sensors [3]. During that time, not all efforts were engaged in the inventions of new measurement technologies, but were mostly dedicated to the refinement of the existing knowledge thus improving the measurement accuracy of the existing sensors.

Nowadays, there are two mainstream non-contact optical measurement techniques that are well established with high technical and economic performance, based upon projected fringe and laser scanning methods.

In this paper, the assessment of the structured light and laser scanning methods in 3D shape measurements that are the core technologies of currently widespread 3D measuring sensors will be presented and critically observed. It will be done by analyzing basic principles of core technologies and potential sources of error of both mentioned methods, together with their current stage of application and achieved measurement accuracy on commercially available shape measuring sensors. Advantages and disadvantages with respect to various aspects are critically observed, like sensor types, method application, data acquisition conditions, measurement range, object reflectance, automation, accuracy, spatial resolution, method maturity, measurement planning and overall measurement costs.

2. Measurement principles overview

2.1 Laser scanner principle and error sources

Most of the laser scanner systems are based on the principle where one or more static detection units record projected coherent laser beam reflected off the object surface. Shape of the beam projected by modern sensors varies from a single spot, line (slit) or series of parallel lines. Provided that the geometry of relative orientation of optical components (obtained by previous sensor calibration) is known, the object coordinates of the projected laser beam can be easily calculated by the application of triangulation techniques.

The accuracy of calculated object points is affected by the errors introduced by the acquisition system geometry, reflectance of projected beam together with the ambient light changes, sharp corners and edges, sudden shape discontinuities with the respect to illumination, sensor occlusions, speckle noise and the inaccurate location of the projected line/point center.

2.2 Structured light scanner principle and error sources

Structured light sensors usually utilize visible non-coherent light sources for object point coding purposes that are projected on a whole camera field of view, thus being able to measure points in a range of a million within a single view measurement. Because of its non-coherent light source type, there is no speckle effect affecting the recorded images but its light intensity decreases rapidly with distance from the source.

Fundamental problem with structured light projecting technology is in the correspondence problem. It is being solved by projections of series of images consisting of some sort of structured pattern [2]. The motivation is to obtain the unambiguous point (or stripe) indexing in all illumination conditions, regardless of the size of the measurement volume, object shape, surface color and reflection properties. Phase shifting methods, namely Gray code-based, or heterodyne methods, are based on the multiple projections of various stripe patterns that provide continuous phase maps, thus solving the correspondence problem [2].

3. Comparison

Although both methods exploit the same triangulation principles, object coding is performed with light sources that have different effects on the measured results. Compared to non-coherent structured light scanners, the influence of speckles lowers the accuracy of the laser scanners, but provides superior measurement volumes under various illumination conditions.
It is often forgotten that measurement is just the initial part of the shape analyzing process, so it is also important to separately evaluate the quality of digitized data from the quality of measured point cloud together taking into account the amount of measured data.

4. Conclusion

Both presented methods judging by commercially available sensors proved competitive and have achieved robustness and accuracy sometimes better than 0.01mm that is required for current industrial needs, but with regards to size of the measurement volume structured light methods are more suitable for smaller objects of irregular surface geometry while lasers can successively measure objects several meters in range. If we extrapolate the preceding development pace, it becomes clear that the application of optical shape measurement will continue to expand.

References

[1] Blais, F., "A Review of 20 Years of Range Sensor Development", Proceedings of SPIE-IS&T, Vol. 5013.,2003,pp 62-76

[2] Gomerčić, M.,"Doprinos automatskoj obradi optičkog efekta u eksperimentalnoj analizi naprezanja",531.715-3:531.717.2, FSB Zagreb,1999

[3] Raindrop Geomagic, "3D Scanner Report", http://www.geomagic.com

Stjepan Jecić
Faculty of Mechanical Engineering and Naval Architecture, University of Zagreb, Chair of Experimental Mechanics, pp 102, 10002 Zagreb, Croatia, Tel. 38516168105, E-mail: stjepan.jecic@fsb.hr

Nenad Drvar
Faculty of Mechanical Engineering and Naval Architecture, University of Zagreb, Chair of Experimental Mechanics, pp 102, 10002 Zagreb, Croatia, Tel. 38516168447, E-mail: nenad.drvar@fsb.hr

4th International Congress
of Croatian Society of Mechanics
September, 18-20, 2003
Bizovac, Croatia

4thICCSM

ESTIMATION OF TOTAL BODY CENTRE OF MASS DURING HUMAN WALKING

Tanja Jurčević Lulić, Osman Muftić, Aleksandar Sušić

Keywords: *human walking, trajectory of the whole body centre of mass*

1. Introduction

The trajectory of the body centre of mass is often a parameter of interest when studying human walking, as it reflects the motion of the whole body. Since small displacements of the body centre of mass are important in balance control studies, it is essential to obtain valid estimates of the body centre of mass. The main aim of this study was to describe two methods of estimation of total body centre of mass during walking.

2. Methods

The first method of estimating the trajectory of the body centre of mass is the weighted average for each segment centre of mass, using appropriate kinematic and anthropometric data. This method is called a *Full-body model* method. However, it is difficult to apply this method for clinical gait analysis, because it requires accurate kinematic measurements of all segments of the body.

The other method of estimating the position of the body centre of mass is from force plate data. If it is assumed that the human body can be considered to be a system of rigid multisegments and air resistance and power loss within the link system are absent, the change in position in three dimensions can be calculated by the second time integral of the respective component of the ground reaction force.

The gait analysis equipment consisted of Elite system with two CCD cameras and a 9-m walkway with Kistler force platform located in the center. The measurement of ground reaction forces and recording of trajectories of characteristic body points on subjects was performed on 32 subjects at walking at normal speed ($0.95 \text{ m/s} \leq v \leq 1.7 \text{ m/s}$). The 24 reflective markers have been attached to palpable landmarks at human body. The model for calculating the total body centre of mass has been designed. The landmarks allowed the definition of a 15 segment whole body model which included foot, lower leg, thigh, upper trunk (thorax and abdomen), lower trunk (pelvis), head with neck, upper arm, forearm and hand segments. The joint centres and centres of mass of segments have been approximated using the data from literature [2, 3, 4]. Values of mass have been calculated using the regression method established by Donsky and Zatsiorsky [1]. An automatised method for determination of the total body centre of mass from full body kinematics has been established. 3D-coordinates of the marked points were the input data for a computer program written in Matlab, which calculates orientations of segments, joint centres and trajectories of the body mass centre.

Total ground reaction force was calculated from the data obtained by the use of one force plate. When the one foot made initial contact with the force plate, the other foot was still in contact with the ground, but its force were unrecordable. To achieve force data for a full gait cycle, the portion of data that was recorded when the other foot was still in contact at the end of the gait cycle was moved to beginning of the cycle.

In order to be able to compare trajectories of the body centre of mass, the determined data were

normalised by the subject height. The original data were averaged by normalising them to one hundred sample points per one walking cycle through spline interpolation. Ground reaction forces for both feet were normalised by body weight and shown as a function of duration of gait cycle. The constants in integration of ground reaction forces were defined as the values reducing the average of acceleration, velocity and displacement per one cycle to zero.

3. Results

Typical patterns of displacements of the body mass centre in three direction during gait cycle, calculated from two methods, have been established for every subject. *General patterns* and variation bandwidth of the standard deviation have been determined from *typical patterns* of all subjects for both methods. A *general pattern* represented the mean curve of the entire group of subjects studied.

Figure 1 shows comparison of *general patterns* of displacements of the body centre of mass in three directions calculated by using two different methods - weighted average for each segment centre of mass and twofold integration of ground reaction force data.

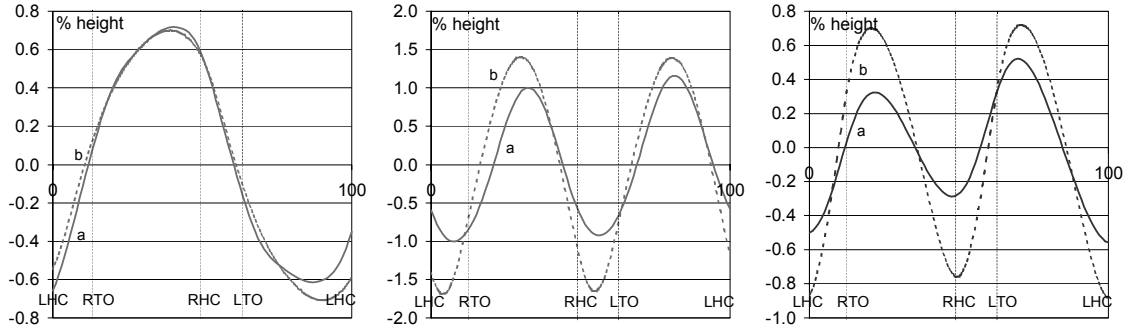

lateral direction *vertical direction* *fore-aft direction*

Figure 1. Comparison of *general patterns* of displacements of body centre of mass calculated by using two different methods: a - weighted average for each segment centre of mass (continuos line), b - twofold integration of ground reaction force data (dashed line)

4. Conclusion

In this study the 3D displacements of the human body mass centre during walking have been computed by using two methods: weighted average for each segment centre of mass and twofold integration of ground reaction force. We have developed a model and automatised procedure for determination of whole body centre of mass during human walking from full body kinematics. Using this technique we have found similar patterns and displacements of the body centre of mass as we have calculated using the force platform data.

References

[1] Donsky, D.D., Zatsiorsky, V.M., "Biomehanika" (in Russian), Fizkultura i sport, Moskva,1979

[2] Eng, J.J., Winter, D.A., "Kinetic analysis of the lower limbs during walking: What information can be gained from a 3D model?, Journal of Biomechanics, Vol. 28, No. 6, 1995, pp. 1223-1230

[3] Jurčević Lulić, T., Lulić, Z., Milčić, D., "Upper limbs influence on the trajectory of the body mass centre during human walking, Computer Methods in Biomechanics and Biomedical Engineering - 3, Gordon and Breach Science Publishers, 2001, pp. 269-274

[4] de Leva, P., "Adjustments to Zatsiorsky - Seluyanov's segment inertia parameters, Joint center longitudinal positions computed from a selected subset of Chandler's data", Journal of biomechanics, Vol. 29, No. 9, 1996, pp. 1223-1233

Tanja Jurčević Lulić, Osman Muftić, Aleksandar Sušić
tanja.jurcevic@fsb.hr; osman.muftic@fsb.hr; aleksandar.susic@fsb.hr
University of Zagreb, Faculty of Mechanical Engineering and Naval Architecture,
Institute of Applied Mechanics, Ivana Lučića 5, Zagreb, Croatia, + 385 1 6168549,

4th International Congress
of Croatian Society of Mechanics
September, 18-20, 2003
Bizovac, Croatia

4thICCSM

WIND TUNNEL APPLICATION OF AN INTELLIGENT PRESSURE SCANNER

P. Kesić, F. Majić

Keywords: *pressure measurement, airfoil, wind tunnel measurement, aerodynamic characteristics, pressure scanner*

Instead of using a large number of differential pressure transducers for pressure distribution measurement, an intelligent pressure scanner system was recently developed. The system consists of an array of silicon pressure transducers with a high performance microprocessor that provides measurement with low uncertainty, temperature compensation, *in situ* calibration and communication interfaces with the PC.

Two applications are considered in this paper: differential pressure (DP) transmitter calibration and the NACA 2421 airfoil aerodynamic characteristics measurement. The DP transmitter was efficiently calibrated and the effect of line pressure investigated. In the transmitter used, a small line pressure effect was found and the accuracy limits were within the manufacturer's specification. The airfoil characteristics were measured using a low aspect ratio wing model placed in the test section of a low speed wind tunnel. Using LabVIEW software, the program was developed for the speedy calculation of aerodynamic characteristics. The aerodynamic characteristics were determined for a selected airfoil at two Reynolds numbers ($Re=2\cdot10^5$ and $Re=4\cdot10^5$) in an angle of attack ranging from -5^0 to 25^0. Some discrepancies between the measured data and available data are caused mainly by the lack of two-dimensionality in the tunnel test section.

Figs. 1 and 2 show the pressure coefficient distribution around the airfoil at two Reynolds numbers.

Pressure distribution measurements were made at two relatively low Reynolds numbers $Re=2\cdot10^5$ and $Re=4\cdot10^5$. Consequently, the measured values of airfoil drag coefficient are greater than the values given in other literature for higher Reynolds numbers. Due to the lack of two-dimensionality, the lift curve slope shows a smaller value.

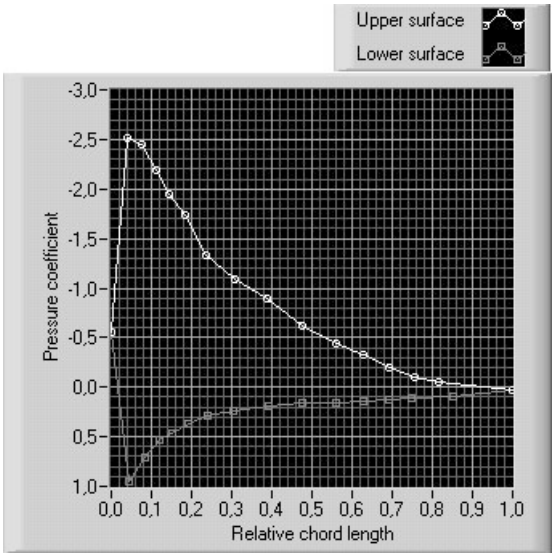

Figure 1. Pressure coefficient distribution along chord length (Re=2·10^5, α=16°35'10'')

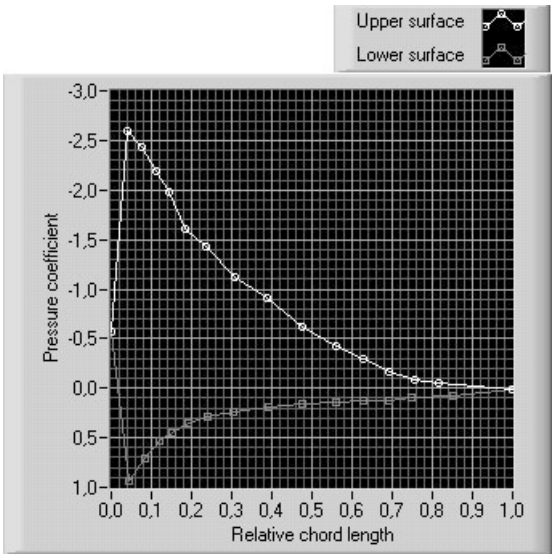

Figure 2. Pressure coefficient distribution along chord length (Re=4·10^5, α=16°35'10'')

In Figs. 3 and 4 the calculated lift coefficient and drag coefficient based on the pressure coefficient data are shown as a function of angle of attack at Re=2·10^5.

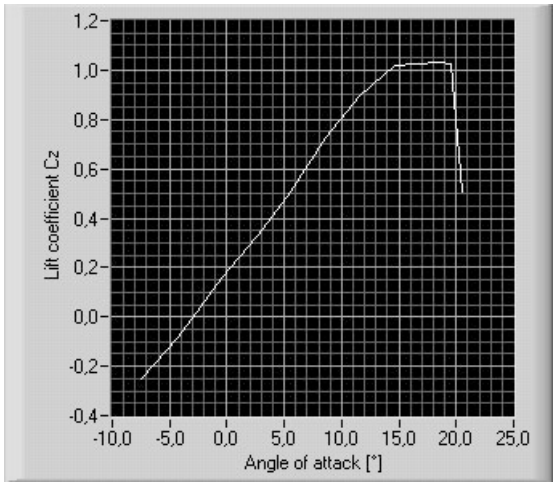

Figure 3. Lift curve at Re=2·10^5

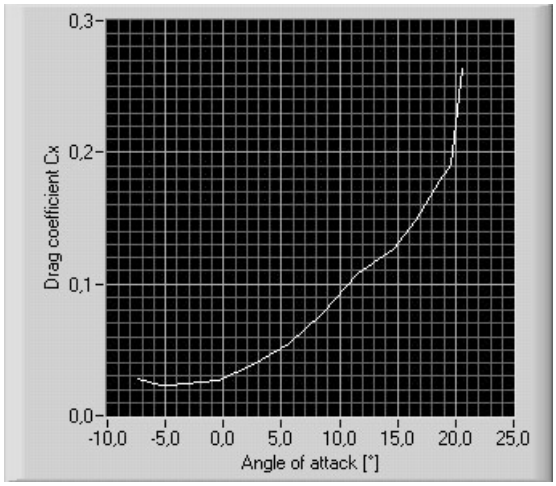

Figure 4. Drag curve at Re=2·10^5

References

[1] Matthews, C. A., "Intelligent Pressure Measurement in Multiple Sensor Arrays", Sensors, April 1996, pp 26-29.

[2] "Intelligent Pressure Scanners User's Manual (Model 9016, 9021, 9022) 9th edition", Pressure Systems Inc., Hampton, July 2001.

[3] Kesić, P., "Osnove Aerodinamike", Fakultet strojarstva i brodogradnje, Zagreb, 2003.

P. Kesić, F. Majić
Fakultet strojarstva i brodogradnje, Zagreb, Croatia; petar.kesic@fsb.hr
Fakultet strojarstva i brodogradnje, Zagreb, Croatia; frane.majic@fsb.hr

4th International Congress
of Croatian Society of Mechanics
September, 18-20, 2003
Bizovac, Croatia

4thICCSM

EFFECTIVE EVALUATION OF LOCAL CONTACT FIELDS

Vladimír Kompiš, Vladimír Dekýš

Keywords: Elastic contact; weak singular integrals; numerical integration & differentiation

If two elastic bodies with spherical surfaces with curvature differences in both directions and having much different curvature at least in one direction are in contact, then both displacement and stress fields have large gradients on the surface and subsurface regions. The contact area is very small and under normal loading the contact pressure may occur in order of several thousands N/mm^2. Maximum shear stresses, which are responsible for plastic deformations are localised in small volume under the contact surface. Accurate computation of the stress field is then responsible for correct evaluation of bearing capacity of both contacting bodies.

If both bodies in contact are massive and the contact area is small comparing to the radii of curvature of contacting bodies, then the contact can be considered as Hertz contact [1] and the problem can be solved analytically [2]. The solution is then described by elliptic integrals. However, more general problems are not possible to be solved in this way.

Both displacement and stress fields have large gradients localized on the small surface and subsurface regions and their accurate evaluation, requires large number of elements, if numerical methods like FEM, FVM, or even BEM are used.

The Boussinesq type solution can be used to describe the local fields. However, the expressions for both displacements and stresses require evaluation of singular integrals. Even more difficult is evaluation of quasi-singular integrals in the vicinity of the singularity point, which is the case of subsurface fields. Also the integration of Hertz type traction distribution, which correctly describes the local behavior, requires some special treatment.

Another possibility for solution of such local fields was introduced by Blokh [3], where the displacements $\boldsymbol{u}$ and stresses $\boldsymbol{\sigma}$ for the elastic isotropic upper half space with the normal $-\boldsymbol{e}_3$ in x_3 direction are expressed by weakly singular integrals

$$\begin{aligned}\boldsymbol{\sigma} = \frac{1}{2\pi}\Bigg[\nabla\left(\int_S \mathbf{q}\frac{dS}{\rho}\right)+\left(\int_S \mathbf{q}\frac{dS}{\rho}\right)\nabla\Bigg]+\frac{\nu}{\pi}\Bigg\{\nabla^3\cdot\int_S \mathbf{q}\left[x_3\ln\left(\rho+x_3\right)-\rho\right]dS+\\ +\mathbf{I}\nabla\cdot\int_S \mathbf{q}\frac{dS}{\rho}-\left[\nabla^2\cdot\int_S \mathbf{q}\ln\left(\rho+x_3\right)dS\right]\mathbf{k}-\mathbf{k}\left[\nabla^2\cdot\int_S \mathbf{q}\ln\left(\rho+x_3\right)dS\right]\Bigg\}-\\ -\frac{1}{2\pi}\nabla^2\cdot\int_S q_3\ln\left(\rho+x_3\right)dS-\frac{x_3}{2\pi}\nabla^3\cdot\int_S \mathbf{q}\ln\left(\rho+x_3\right)dS\end{aligned} \tag{1}$$

and

$$\mathbf{u} = \frac{1+\nu}{2\pi E}\left\{2\int_S \mathbf{q}\frac{dS}{\rho} + 2\nu\nabla^2\cdot\int_S \mathbf{q}\left[x_3\ln\left(\rho+x_3\right)-\rho\right]dS + \right.$$
$$\left. + (1-4\nu)\mathbf{k}\nabla\cdot\int_S \mathbf{q}\ln\left(\rho+x_3\right)dS - \nabla\int_S q_3\ln\left(\rho+x_3\right)dS - x_3\nabla^2\cdot\int_S \mathbf{q}\ln\left(\rho+x_3\right)dS\right\} + \tag{2}$$
$$+ \boldsymbol{\omega}\times\mathbf{r} + \mathbf{u}_0\ ,$$

in tensor notation. In these equations, ***q, I*** and ∇ are the vector of boundary tractions, identity tensor (= $\boldsymbol{e_i}\,\boldsymbol{e_i}$) and gradient vector, respectively. E and v are modulus of elasticity and Poisson's ratio, respectively and ρ is the distance from the source point (point where the traction is acting) to the field point (where corresponding field value is evaluated). ***ω, r*** and $\boldsymbol{u_o}$ are vector of rigid body rotation, radius vector of ρ and vector or rigid body displacement, respectively.

Two types of the weakly singular integrals are to be computed: the logarithmic and $(1/\rho)$. When the field point is inside the half space domain but close to the boundary, then quasi-singular integrals have to be computed. Moreover, the tractions are described by elliptic functions in Hertz contact and they have similar behavior also in more general contact problems.

Using local cylindrical coordinates with x_3 axis going through the field point, the singularities can be numerically removed. The expressions for stress and displacements contain the first and second derivatives of such integrals. They are computed then numerically in the presented approach.

The largest numerical errors are in the points near the contact boundaries. The integrals have higher order discontinuity. A numerical procedure is shown in the paper, which enables to obtain the displacement and stress fields with good accuracy also in such points.

The procedure enables to present the displacement and stress fields in the contact domain also for more general problems without necessity to use very fine meshes in numerical models.

References

[1] Hertz, H., "Miscellaneous Papers", McMillan, N.Y., 1896

[2] Hills, D. A., Nowell, Sackfield, D., A. "Mechanics of Elastic Contacts", Butterworth Heinemann Ltd., Oxford, 1993

[3] Blokh, B. I., "Theory of Elasticity", (in Russian), Univ. Press Kharkov, 1964

Prof. Dr.-Ing. Vladimír Kompiš, PhD.
University of Žilina, Faculty of Mechanical Engineering, Department of Mechanics, Veľký Diel,
010 26 Žilina, Tel: +421 41 5132950, e-mail kompis@mppserv.utc.sk

Ing. Vladimír Dekýš, PhD.
University of Žilina, Faculty of Mechanical Engineering, Department of Mechanics, Veľký Diel,
010 26 Žilina, Tel: +421 41 5132954, e-mail dekys@mppserv.utc.sk

4th International Congress
of Croatian Society of Mechanics
September, 18-20, 2003
Bizovac, Croatia

4thICCSM

Dynamic Analysis of Loads Moving Over Structures

Ivica Kožar, Ivana Štimac

Keywords: moving load, direct acceleration method

1. Introduction

Increase in traffic intensity and speed requires more complex analysis of structures than it was case before; today it is necessary to consider dynamic behaviour of structures that has been induced by loads moving over a structure. The simplest case of a moving load (dynamic) analysis is the case of a simple beam over which a concentrated load is moving, that is represented with a 4th order partial differential equation.

P.D.E. for moving load has been solved numerically with many benefits over closed solution (various boundary conditions, introduction of damping and discrete elements like springs and dashpots, additional supports and many more). Average acceleration method has been employed since direct use of finite differences had shown as being practically unusable. Numerical and analytical solutions have been compared.

2. Description of the problem

Problem of a mass less load moving on a beam is described with the known partial differential equation [2]

$$EI\frac{\partial^4 u}{\partial x^4} + m\cdot\frac{\partial^2 u}{\partial t^2} - P(t) = 0 \tag{1}$$

Analytical solution can be obtained most easily through use of harmonic series

$$u(x,t) = \frac{2\cdot P}{\rho\cdot L\cdot\omega(1)^2}\left[\sum_{k=1}^{50}\left[\frac{1}{k^2(k^2-\alpha^2)}\cdot\left(\sin\left(k\cdot\pi\cdot v\cdot\frac{t}{L}\right)-\frac{\alpha}{k}\cdot\sin\left(\omega(k)\cdot t\right)\right)\cdot\sin\left(k\cdot\pi\cdot\frac{x}{L}\right)\right]\right] \tag{2}$$

3. Numerical solution of the governing P.D.E.

Assuming that our acceleration is constant within the time interval (average acceleration method [1]) than we obtain this incremental equation

$$\boldsymbol{M}\Delta\ddot{\boldsymbol{D}}_j + \boldsymbol{C}\Delta\dot{\boldsymbol{D}}_j + \boldsymbol{S}\Delta\boldsymbol{D}_j = \Delta\boldsymbol{A}_j \tag{7.a}$$

In this equation we have unknown incremental accelerations, incremental speeds and incremental displacements but introducing the above assumptions their values can be deduced and substituted into eq.(7.a) what finally gives us

Average acceleration assumption can be replaced with the assumption that acceleration wearies linearly within the time interval, in which case we obtain linear acceleration method [1] with somewhat faster convergence and slightly better accuracy. On the other hand this method is only conditionally stable while the average acceleration method is unconditionally stable and is the method of choice for all subsequent numerical analysis.

Special care should be taken in discretisation in time of the external load ***A(t)*** since it is of great influence on the convergence of the numerical procedure.

Based on the above equations existing 2D finite element computer program OKVIRW has been extended to accommodate moving load analysis.

4. Examples

4.1 Periodic force influence

If the force is changing in time stable numerical methods could still give good answers. In this example there is no damping and load is varying by 5% eight times during its movement over the bema span (analysis is continued after the load had transferred the beam).

For numerical purposes concentrated force is represented as Dirak function varying in space and time.

As can be seen only 5% change in input load intensity gave us about 30% change in resulting beam forces since input load frequency is very close to the first eigenfrequency of the beam.

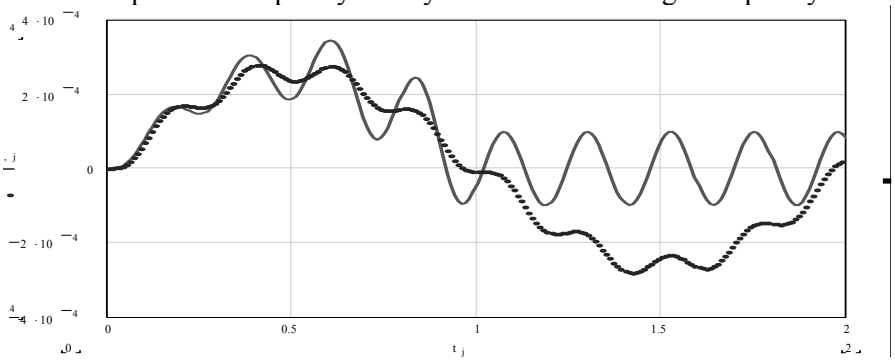

Figure 8. Comparison of the resulting displacement with the one produced by a constant force

5. Conclusion

As it can be seen through examples numerical approach to the problem of a moving load is quite suitable for engineering purposes: solutions are accurate and procedure based on average acceleration is robust. Further benefit of the numerical formulation is that various boundary conditions, damping, various ways of supports, changing forces can all be easily taken into analysis.

Acknowledgement

Work presented in this paper has been partially financed through technological project TP-02/0114-02 financed by the Ministry of Science and Technology.

References

[1] Weaver, W., Johnston,P. R.: *Structural Dynamics by Finite Elements*, Prentice-Hall, Inc., Englewood Cliffs, New Jersey 1987.

[2] Inglis, C.E.., Inglis, C.E., "Mathematical Treatase on Vibration in Railway Bridges", Cambridge University Press, London UK, 1934.

[3] Kožar, I.: *Kompleksno opterećeni štapovi(beam-columns)*, FRAK , 18/19, prosinac 1986.

[4] Štimac, , I., "ANALIZA MOSTOVSKIH KONSTRUKCIJA POBUĐENIH POKRETNOM MASOM", Magistarska radnja, Zagreb, 2003

Prof.dr.sc. Ivica Kožar
Faculty of Civil Engineering/ University of Rijeka, V. C. Emina 5, 51000 Rijeka, Croatia, +385 51 352 100, +385 51 332 816, ivicak@gradri.hr
mr.sc. Ivana Štimac
Faculty of Civil Engineering/ University of Rijeka, V. C. Emina 5, 51000 Rijeka, Croatia, +385 51 352 136, +385 51 332 816.

4th International Congress
of Croatian Society of Mechanics
September, 18-20, 2003
Bizovac, Croatia

4thICCSM

COMPARISON OF SOME IMPLICIT AND EXPLICIT SCHEMES FOR OPEN CHANNEL FLOW EQUATIONS

L. Kranjčević, L. Sopta and S. Vuković

Keywords: open channel flow, explici numerical scheme, implicit numerical scheme

Implicit and explicit numerical approaches in solving open channel flow equations are presented and compared regarding their performance, applicability and quality of results obtained. The one-dimensional St. Venant equations used in the modelling of open channel flow. They are based upon conservation of mass and conservation of momentum for unsteady flow in a a nonprismatic channel of arbitrary cross section, under assumption of a homogeneous, incompressible, viscous flow characterized by a hydrostatic pressure distribution.

Both explicit Q-scheme [1] and implicit [2] scheme analyzed in this paper, are based upon Roe's scheme [3] with approximate Riemann solver introduced. Having the same numerical origin and employing same numerical principles, chosen schemes are suitable for comparison. Physical domain is dicretised by finite difference method, with uniform computational mesh. Explicit method solves for one point at a time in certain time step - that is, one equation and one unknown. The main drawback of the explicit approach is that the unknown node must be within the zone of dependency of the nodes that are used to approximate the derivatives at the known time line – otherwise, the method will be unstable. Therefore, maximal time step is bound by Courant Friedrichs Lewy (CFL) condition. Implicit method solves for the unknowns in a domain simultaneously, requiring solution of simultaneous algebraic equations. The advantage is that matrix of a linear system to be solved at each time level has its arguments from the new time level $n+1$ and thus the unknown nodes are always in the zone of influence. Implicit scheme yields convergence in a smaller number of time steps, since the time step is no longer constrained by a stability limit, but on the other hand it requires more computational effort consequent upon the need to solve block tridiagonal system of equations per each time step (providing finite difference approximation is employed). Implicit procedure produces block tridiagonal linear system of equations with block matrices [2 x 2], that is to be solved in each time step:

$$\mathbf{A}\mathbf{w}_{i-1}^{n+1} + \mathbf{B}\mathbf{w}_{i}^{n+1} + \mathbf{C}\mathbf{w}_{i+1}^{n+1} = \mathbf{D}$$

where A, B, C are block matrices that are elements of a global matrix of the system and D represents RHS vector containing source term, some data from previous time level t^n and eventually imposed boundary conditions.

Numerical methods are tested on four benchmark test problems which have known analytic solutions, i.e., three steady and unsteady case test problems, subcritical flow; supercritical flow; transcritical flow; and unsteady dam-break test case.

Results of the first three steady test problems graphically show completely matching diagrams of calculated explicit, implicit and analytic water levels. Comparison of numerical data showed difference in calculated water depth of magnitude $10^{-3}\,m$, which is very satisfactory concerning high computational time gains, as given in Table 1.

The fourth test case is an idealized dam-break flow in a rectangular, frictionless channel with variable bottom topography. Dam break test problem was used to investigate the ability of methods to deal with propagating discontinuities. Propagating shock is tracked satisfactory with implicit

scheme, but it is obvious that shock front "smeares" as time steps and CFL numbers increase and numerical dissipation effects become significant. For implicit case, optimal CFL number proved to be approximately around CFL=2 with still significant gains in computational time.

Implicit scheme tested proved to be robust admitting very large steps in steady cases, resulting in high gains in computational time. In unsteady case implicit method also proved to be nondispersive, showing good shock tracking capability, and with moderate CFL numbers scheme produced acceptably dissipative results. Recent developments in computational science with new, time effective approaches in solving linear systems of equations resulting from implicit numerical shemes, make implicit methods even more attractive.

Table 1. Run times comparison

Test case	*Implic./explic. scheme*	*CFL*	*CPU TIME [s]*	*Test case*	*Implic./explic. scheme*	*CFL*	*CPU TIME [s]*
Test 1	*explicit*	*0.8*	*4.0*	*Test 4, time=0.1s*	*explicit*	*0.7*	*1.23*
	implicit	*10.6*	*0.44*		*implicit*	*3*	*0.55*
Test 2	*explicit*	*0.72*	*9.2*		*implicit*	*7*	*0.23*
	implicit	*9.4*	*1.7*	*Test 4, time=0.14s*	*explicit*	*0.7*	*1.73*
Test 3	*explicit*	*0.6*	*135.9*		*implicit*	*2*	*1.10*
	implicit	*8.1*	*44.7*		*implicit*	*7*	*0.33*
	implicit	*29.4*	*19*				

References

[1] Bermudez, A.,Vazquez,M.E., "Upwind methods for hyperbolic conservation laws with source terms", Comput.&Fluids 23(8),1049, 1994.

[2] Garcia-Navarro, P., Priestly, A., Alcrudo, F., "An Implicit Method for Water Flow Modeling in Channel and Pipes", Journal of Hydraulic Research, Vol. 32, No.5, 1994.

[3] Hudson, J., "Numerical Techniques for the Shallow Water Equations", The University of Reading, Dept. of Math., Numerical Analysis Report 2/99, 1999.

[4] MacDonald, I., "Analysis and Computation of Steady Open Channel Flow", Ph.D. thesis, University of Reading, Department of Mathematics, 1996.

[5] MacDonald, I., Baines,M.J.,Nichols, N.K., Samuels,.P.G. "Comparison of some Steady State Saint-Venant Solvers for some Test Problems with Analytic Solutions", Numerical Analysis Report 2/95, University of Reading, Department of Mathematics, 1995.

[6] Stoker, J.J., *Water Waves*, Inrerscience Publishers Inc., New York, 1957.

[7] Yee,H.C., "A Class of High-Resolution Explicit and Implicit Shock-Capturing Methods", NASA Ames Research Center TM-101088, USA, 1989.

Lado Kranjčević, M.S.
Faculty of Engineering/University of Rijeka, Department of Fluid Mechanics and Computational Engineering, Vukovarska 58, Rijeka, Croatia, Phone 00385 (0)51 651444, Fax 00385 (0)51 651490, lado.kranjcevic@riteh.hr
Prof. Luka Sopta, Ph.D., Professor
Faculty of Engineering/University of Rijeka, Department of Fluid Mechanics and Computational Engineering, Vukovarska 58, Rijeka, Croatia, Phone 00385 (0)51 651444, Fax 00385 (0)51 651490, luka.sopta@riteh.hr
Senka Vuković, Ph.D., Assoc. Prof.
Faculty of Engineering/University of Rijeka, Department of Fluid Mechanics and Computational Engineering, Vukovarska 58, Rijeka, Croatia, Phone 00385 (0)51 651444, Fax 00385 (0)51 651490, senka.vukovic@riteh.hr

4th International Congress
of Croatian Society of Mechanics
September, 18-20, 2003
Bizovac, Croatia

4thICCSM

EXPERIMENTAL AND MATHEMATICAL MODELLING OF SHORT OIL FILM BEARING

Petr Kučera, František Pochylý, Eduard Malenovský

Keywords: Reynolds equation of motion, Navier-Stokes equation of motion, oil film bearing, cavitated and noncavitated bearing, static position of the center of the shaft, comparison of experimental and mathematical modelling

1. Introduction

From general event of motion of body at real fluid I will specialize hereafter in planar event of motion with small celarances between the inner surface of body and the outer ring of bearing. From technical aplication's aspect oil-film bearings and long squeeze film dampers are general. The theoretical principle of almost analysis of oil-film bearings and long squeeze film dampers stem from Reynold's equation, what is in the main equation of motion of fluid. The circumferential course of motion of fluid between inner and outer ring of fluid film bearing is analysed at the one-dimensional flow on line with the length equal circumference of inner ring.

There are analysed events of short fluid film bearing, cavitation events of oil film bearings in this article. The solution, what propound F. Pochylý is more general. The main default equations of this event are Navier-Stokes's equation of motion of fluid and equation of continuity and boundary conditions. Hereafter there will be analysed three dimensional flow in this article, that corresponds to short oil-film bearing.

The new access is based on the separation of motion of body and fluid. The main algorithm of analysis of dynamic properties of rotor system is assembled of two discrete steps. At available software means, address to analysis system of fluid, is realized discrete coupler element at first. Follow-up work is realized at available software means, address to analysis dynamic properties of rotor systems, the analysis of rotor system with including results attached from previous result. By the advisable substitution we can separate and solve the motion of body and fluid. To analysis of motion of fluid is applied control volume method. To analysis of dynamic properties of fluid was applied Beziér's body. The solution is done by curvilinear coordinates. Beziér's body is applied for geometrical configuration and for aproximation speed and pressure functions. With changes of attitude of shaft is done the new generation of grid. This access make possible to separate solution of stationary and non-stationary part. On the base of this theory came around program system in the language Matlab.

2. Conclusion

In this article there are compared results of static equilibrium position of the center of the shaft under oil-film bearing on the rotary machine. There are compare results out going from Reynold's and Navier-Stokes equation of motion of fluid film in the oil-film bearing. At axess stem from Navier-Stokes equation there are compared two boundary conditions. At first we must prescribe on the ends of oil-film bearing the presure as a zero and the velocity function at the oil-film is calculated. At second we must prescribe the velocity of fluid film at the oil-film bearing and the pressure function at the oil-film is calculated. Mathematical modeling of static equilibrium position

of the shaft is also compared with experimental modeling. The results of experimental and mathematical modeling (Reynold's equation, Navier-Stokes equation – two boundary conditions) are almost the same. See figure no.1. At mathematical modeling there are calculated differences between external loading and internal forces from fluid for many points of the fluid of oil-film bearing. After that there is found the minimum (zero) of differences. The position with null force's differences is the static equilibrium position of the center of the shaft.

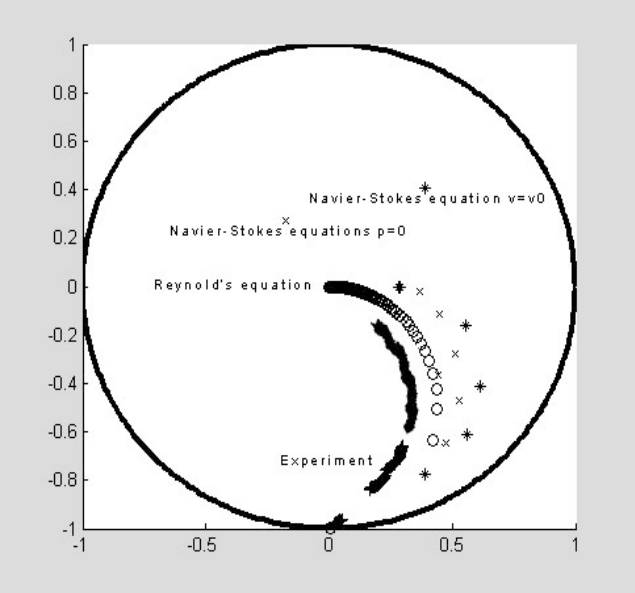

Figure 2. Static equilibrium position of the center of the shaft

Acknowledgement

The contribution is sponsored by the research task of Ministry of Education and Youth no. CEZ: MSM 262100001

References

[1] Muszynska, A.: "Rotor/bearings stability problems", BRDRC Minden, Nevada.

[2] Kramer, E.: "Dynamics of Rotors and Foundations", Springer-Verlag Berlin, 1993.

[3] Muszynska, A.: "Machinery dynamics short course", 1998.

[4] Gash, R., Pfutzner, H.: "Dynamics of Rotors", Springer Verlag Berlín, 1975.

[5] Vance, J., M.: "Rotordynamics of Turbomachinery", Wiley, New York, 1990.

[6] El-Shafei, A.: "Modeling Fluid Inertia Forces of short Journal Bearings for Rotordynamics Applications", Journal of Vibration and Acoustics, 1995

[7] Adiletta, G., Guido, A., R., Rossi, C.: "Chaotic Motions of a Rigid Rotor in Short Journal Bearings", Kluwer Academic Publishers, Netherlands, 1996

Ing. Kučera Petr
Institute of Mechanics of Solids, Faculty of Mechanical Engineering, Brno University of Technology, Technická 2, 616 69, Brno, Czech Republic, e-mail: kucera@umtn.fme.vutbr.cz
Doc. Ing. Malenovský Eduard, DrSc.
Institute of Mechanics of Solids, Faculty of Mechanical Engineering, Brno University of Technology, Technická 2, 616 69, Brno, Czech Republic, e-mail: malenov@umtn.fme.vutbr.cz
Prof. Ing. Pochylý František, CSc.
Institute of Power Engineering, Faculty of Mechanical Engineering, Brno University of Technology, Technická 2, 616 69, Brno, Czech Republic, e-mail: pochyly@khzs.fme.vutbr.cz

4th International Congress
of Croatian Society of Mechanics
September, 18-20, 2003
Bizovac, Croatia

4thICCSM

COMPARATIVE STRESS ANALYSIS AROUND AN ELLIPTIC OPENING IN THIN CYLINDER

Z. Kulenović

Keywords: *stress analysis, elliptic opening, thin cylinder*

1. Introduction

The components of modern thin-walled technical constructions for various purposes are very often shaped like cylindrical shells weakened by small openings. It is well known that these openings can in many cases essentially affect the load capacity, rigidity and stability of the constructions; therefore, it is an important problem in engineering. This paper is the result of research of stresses in an axially compressed thin cylinder weakened by small longitudinal elliptic opening. The suggested analytical solution is compared with the experimental solution, which has been obtained by 3D photoelastic frozen stress method.

2. Analytical solution

The state of stress around a small curvilinear opening with smooth contour in a thin, shallow, homogeneous and isotropic cylindrical shell can be described by a complex differential equation:

$$\Delta\Delta\Phi - 8i\beta^2 \frac{\partial^2 \Phi}{\partial y^2} = 0 \tag{1}$$

The solution of this equation which satisfying the boundary conditions in the infinity and expressed by polar coordinates (r, ϑ), may be written in terms of Hankel functions:

$$\Phi = \sum_{k=1}^{4} \sum_{n=0}^{\infty} a_n^{(k)} \Phi_n^{(k)} \tag{2}$$

Unknown complex constants $a_n^{(k)}$ are found from the boundary conditions of an opening. Since the opening contour is curvilinear the boundary conditions can be satisfied only with specially selected curvilinear orthogonal coordinates (ρ, γ) applying the method of conformal mapping. This problem has been solved by the application of analytic functions of complex variable, Cauchy integral formulas and the iteration method. The stress ratio k_ϑ along the edge of opening is:

$$\begin{aligned} k_\vartheta = \frac{\sigma_\vartheta}{\sigma_0} = \{\, 1 + 2\cos 2(\gamma+\alpha) - 2\varepsilon\cos 2\alpha - \varepsilon^2 + \frac{\pi\beta^2 r_0^2}{2} \{\, [\cos 2(\gamma+\alpha) + \varepsilon^2]\,(1-\varepsilon^2) + \\ + 2\varepsilon \sin 2\alpha\,[\sin 2(\gamma+\alpha) - \varepsilon \sin 2\alpha]\,\}\,\}\,(2\varepsilon\cos 2\gamma - 1 - \varepsilon^2)^{-1} \end{aligned} \tag{3}$$

where: $\sigma_0 = p/h = -F/2R\pi h$, $\gamma = \arctan\left[(1+\varepsilon)(1-\varepsilon)^{-1} \tan\vartheta\right]$.

The following values of the basic quantities, Figure 1, are: $a = 13,5$ mm, $b = 9$ mm, $R = 60$ mm, $h = 5$ mm, $r_0 = \frac{a+b}{2}$, $\varepsilon = -\frac{a-b}{a+b}$, $\alpha = 0^0$, $\nu = 0,48$ (Araldite B, t_Z = 150 ^{0}C).

3. Experimental solution

Model of cylindrical shell with elliptic opening have been made of photoelastic material Araldite B (Ciba). In a specially designed and precisely built device, the model was loaded axial-symmetrically to the compression. After the stress freezing procedure, model was diametrically cut along the generatrices into two parts, and the areas around the opening was photographed and analysed in monochromatic circularly polarized light. The stress ratio k_ϑ at the opening edge has been obtained by the expression, i.e.:

$$k_\vartheta = -\frac{2R\pi hf_\sigma N_\vartheta}{Fb_\vartheta} \tag{4}$$

where: f_σ = 0, 28 N/mm (Araldite B, t_Z = 150 ^{0}C), F = 170 N - loading force.

4. Conclusion

On the basis of analytical and experimental results, the curves of stress ratio k_ϑ at the edge of longitudinal elliptic opening depending on the polar angle ϑ have been comparatively drawn, Fig. 1.

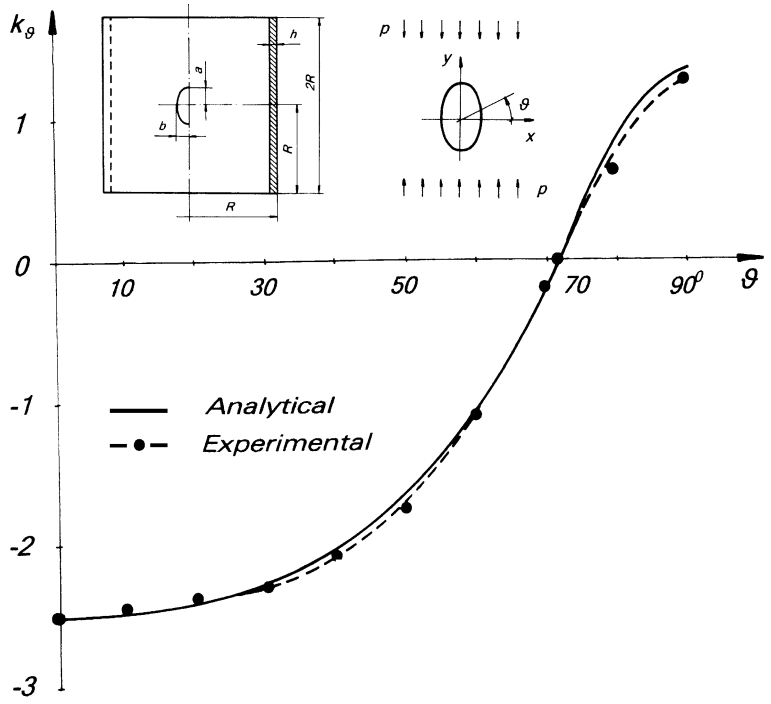

Figure 1. Stress ratio k_ϑ curves around elliptic opening in thin cylinder

It is noticeable that analytical and experimental value curves of the stress ratio around the observed longitudinal elliptic opening in thin cylinder are very similar in appearance and mutually agree well in all the analysed area. The analytically and experimentally obtained values of the stress concentration factor $K = |\max(k_\vartheta)|$ are equal. According to that, it can be asserted that the suggested and performed analytical solution is sufficiently accurate as well as appropriate for practical calculations of stress concentrations factors of thin cylinders with elliptic openings.

Zlatan Kulenović, Dr. Sc., Assoc. Professor
University of Split, College of Maritime Studies, Zrinsko-Frankopanska 38, HR-21000 Split, Croatia
Tel: +0385 (0) 21 380 762 , Fax: +385 (0) 21 380 759, e-mail: zlatan@pfst.hr

4th International Congress
of Croatian Society of Mechanics
September, 18-20, 2003
Bizovac, Croatia

NONLINEAR DISTORTIONS IN THE FIELD OF INTERACTING UNIDIRECTIONAL SH-WAVES IN CUBIC SYSTEM LAMINA

K. Kurennaya, V. Storozhev

Keywords: *Nonlinear waves propagation, crystal layer, anharmonic effects, combinative harmonics*

Introduction

Spreading, dispersions and localization regularities theoretical investigations of high-frequency nonlinear acoustic wave propagation in the hard crystalline waveguide are referred to modern problems of deformed hard bodies dynamics and ultraacoustics. The nonlinear elastic waves spreading regularity study problem remains comparatively little investigated for the present moment. The main interest of the free elastic waves spreading study is in the acoustoelectronic sphere application. Nonlinear effects in wave motions are used for the wave signals folding and integrating.

1. The mathematics model

In this paper the study technique of nonlinear distortion in the interacting unidirectional SH-waves field has been presented. Waves are propagating along the cubic system layer

$$V = \left\{ \left(x_1 , x_2 \right) \in R^2 , \left| x_3 \right| \le 1 \right\}. \tag{1}$$

The method of complex functions presentation by rows on small parameter degrees has been used. As a small parameter is the acoustic Mach number, wave amplitude to its length ratio.

Regularity study, defining spreading, cinematic and energy characteristics of nonlinear normal waves, has been conducted on the base of geometric exact three-dimensional model. In energetic potential expansion by deformation tensor components degrees the third order terms are present

$$U = \frac{1}{2} c_{ijkl} \varepsilon_{ij} \varepsilon_{kl} + \frac{1}{6} c_{ijklmn} \varepsilon_{ij} \varepsilon_{kl} \varepsilon_{mn} , \tag{2}$$

and in deformation tensor components representatives the nonlinear quadratic terms on displacement are present

$$\varepsilon_{ij} = \frac{1}{2} \left(u_{i,j} + u_{j,i} + u_{l,i} u_{l,j} \right). \tag{3}$$

This model allows to calculate the acoustoelectronic devices constructive parameters for processing the signals with a greater accuracy.

The stress tensor represents as a sum of linear $\sigma_{jq}^{(l)}$ and nonlinear $\sigma_{jq}^{(n)}$ parts

$$\begin{gathered} \sigma_{jq}^{(l)} = c_{jqik} u_{i,k} , \\ \sigma_{jq}^{(n)} = \frac{1}{2} c_{jqik} u_{l,i} u_{l,k} + c_{pqik} u_{j,p} u_{i,k} + \frac{1}{2} c_{jqiklm} u_{i,k} u_{l,m} . \end{gathered} \tag{4}$$

2. Numerical results

The non-uniform boundary problem for complex stress functions of anharmonic distortions has been formulated.

The representation for the complex stress functions $u_2^{(j)}$ of normal SH-wave, which belongs to the mode q of dispersion spectrum and has the circular frequency ω_j, follows from the spectral problem solution and is

$$
\begin{gathered}
u_{2q}^{(j)}(x_1,\, x_3,\, t) = F_q^{(j)} \cos(\alpha_q x_3)\, E(x_1,\, t,\, \omega_j,\, k_{jq}) \quad \left(q = \overline{0,\, \infty},\, j = \overline{1,\, 2}\right), \\
k_{jq} = \left(\left(\Omega_j^2 - c_{44}\alpha_q{}^2\right) \Big/ c_{44}\right)^{1/2}, \\
\Omega_j^2 = \rho\, c_*^{-1} R_*^2 \omega_j^2, \quad \alpha_q = q\pi, \\
E(x_1,\, t,\, \omega_j,\, k_{jq}) = \exp\left(-i\left(\omega_j\, t - k_{jq}\, x_1\right)\right).
\end{gathered}
\tag{5}
$$

The presentations for the nonlinear interacting SH-waves displacement functions follow from the problem solution. Under supposition, that P-SV-wave with such frequency and wave number combination as $(2\omega_{q_1},\, 2k_{q_1})$, $(2\omega_{q_2},\, 2k_{q_2})$, $(\omega_{q_1} + \omega_{q_2},\, k_{q_1} + k_{q_2})$, does not belong to any linear P-SV-waves spectrum mode for waveguide under consideration, the nonuniform boundary problem for anharmonic distortion solution has been obtained.

The results of nonlinear normal wave studies in geometric exact setting for finite thickness crystalline layer allow to give more correct qualitative and quantitative data about nonlinear wave motion forms, regularities of carrying the energy by signals in the nonlinear waves manner.

The combination type single-line normal waves second harmonics forms particularities have been described, comparative numerical analysis for monochromatic normal waves and their combination harmonics have been conducted.

Second harmonics intensity dependence on the frequency, energy flows distribution in normal waves second harmonics, forms of these flows, flows intensity dependence on the frequency have been explored.

Comparative numeric distribution analysis of amplitude characteristics of average for a period power flows in first and second harmonics of interacting SH-types waves, belonging to different modes of dispersion spectrum on the waveguide thickness have been conducted.

References

[1] Zarembo, L.K., Krasilnikov, V.A. “Nonlinear phenomena while elastic waves in solids propagation”, Sucsesses of Phys. scienses, Vol.102, No.4., 1970, pp 549-584.

[2] Kurennaya, K.I., Storozhev, V.I. “Nonlinear normal SH-waves second harmonics in monocrystal germanium lamina”, Theoret. and Appl. Mech., Vol.35, 2002, pp 131-138.

[3] Kurennaya, K.I., Storozhev, V.I. “Anharmonic effects while nonlinear normal P-SV-waves propagation in anisotropic elastic layer”, Theoret. and Appl. Mech., Vol.36, 2002, pp 116-124.

[4] Maugin, G., “Nonlinear Waves in Elastic Crystal”. London, Oxford Press, 1999.

Kristina Kurennaya, Post-Graduated Student
Donetsk National Universuty, Mathematics Department, 83055, Universitetskaya Street, 24, Donetsk, Ukraine, (38-0622) 93-46-28, (38-062) 335-50-21, kurennaya@univ.donetsk.ua
Valery Storozhev, Professor
Donetsk National Universuty, Mathematics Department, 83055, Universitetskaya Street, 24, Donetsk, Ukraine, (38-0622) 93-46-28, (38-062) 335-50-21, storozhev@matfak.dongu.donetsk.ua

4th International Congress
of Croatian Society of Mechanics
September, 18-20, 2003
Bizovac, Croatia

4thICCSM

THE STUDY OF BOUSSINESQ EQUATIONS FOR WAVE PROPAGATION FROM DEEP WATER TO SHALLOW WATER

Chi-Min Liu, Chin-Hwa Kong

Keywords: Boussinesq equations, linear kinematic properties, optimal wave model

1. Introduction

In present paper, we derive a fourth-order Boussinesq-type equations in terms of a velocity potential at an arbitrary water depth for wave propagation over an uneven bottom. An error function composed of five linear properties, which includes two dispersion characteristics and three kinematic properties, is introduced to evaluate the optimal wave equations. All linear properties of the optimal model are compared with those obtained by GKW model and the linear Stokes theory. We'll also demonstrate our $O(\mu^4)$ optimal model which can predict wave behavior in deep water more accurately than previous models.

2. Derivation of the $O(\mu^4)$ Boussinesq-type Equations

The Boussinesq equations can be expressed by the velocity potential Φ_m at arbitrary elevation. To simplify the present problem, the flat-bottom condition will be considered and the equations can be expressed as

$$\frac{\partial \eta}{\partial t}+\frac{\partial}{\partial x}\left[(h+\varepsilon\eta)\frac{\partial \Phi_m}{\partial x}\right]+\mu^2h^3H_1\frac{\partial^4\Phi_m}{\partial x^4}+\mu^4h^5H_2\frac{\partial^6\Phi_m}{\partial x^6}+\varepsilon\mu^2h^2H_3\frac{\partial}{\partial x}\left[\eta\frac{\partial^3\Phi_m}{\partial x^3}\right]=0$$

$$\frac{\partial \Phi_m}{\partial t}+\eta+\mu^2h^2H_3\frac{\partial^3\Phi_m}{\partial x^2\partial t}+\frac{\varepsilon}{2}\left(\frac{\partial \Phi_m}{\partial x}\right)^2+\mu^4h^4H_4\frac{\partial^5\Phi_m}{\partial x^4\partial t}+\varepsilon\mu^2\left[-h\eta\frac{\partial^3\Phi_m}{\partial x^2\partial t}+\frac{h^2}{2}\left(\frac{\partial^2\Phi_m}{\partial x^2}\right)^2\right]=0$$

where an important water-depth parameter m is defined as $m=\frac{z_m}{h}$

3. The Study of Linear Model Properties

In this section, five important linear properties of the present $O(\mu^4)$ Boussinesq-type equations are investigated to coincide with those of the exact linear solutions. Choosing the suitable water-depth parameter m, the corresponding optimal model can be applied within the range $0<\mu<5$. First, we neglect all nonlinear terms in (13) (14) and set the water-depth h to be unity, the Boussinesq-type equations can be represented as follows

$$\frac{\partial \eta}{\partial t}+\frac{\partial^2\Phi_m}{\partial x^2}+\mu^2H_1\frac{\partial^4\Phi_m}{\partial x^4}+\mu^4H_2\frac{\partial^6\Phi_m}{\partial x^6}=0 \tag{17}$$

$$\frac{\partial \Phi_m}{\partial t}+\eta+\mu^2H_3\frac{\partial^3\Phi_m}{\partial x^2\partial t}+\mu^4H_4\frac{\partial^5\Phi_m}{\partial x^4\partial t}=0 \tag{18}$$

The phase velocity and the group velocity can be expressed as

$$C(m,\mu)=\left[\frac{1-H_1\mu^2+H_2\mu^4}{1-H_3\mu^2+H_4\mu^4}\right]^{0.5}$$

$$C_g(m,\mu)=\sqrt{\frac{1-H_1\mu^2+H_2\mu^4}{1-H_3\mu^2+H_4\mu^4}}\cdot\left[\frac{1-2H_1\mu^2+(3H_2-H_4+H_1H_3)\mu^4-2H_2H_3\mu^6+H_2H_4\mu^8}{(1-H_1\mu^2+H_2\mu^4)\cdot(1-H_3\mu^2+H_4\mu^4)}\right]$$

And the parameters concerning the horizontal and vertical components of velocity of fluid particles are represented as

$$F_H(m,z,\mu)\equiv\frac{\Phi_x(m,z,\mu)}{\Phi_x(m,0,\mu)}=\frac{1-\left(H_3-\frac{z^2}{2}-z\right)\mu^2+\left(H_4+\frac{z^4}{24}+\frac{z^3}{6}-\frac{H_3z^2}{2}-H_1z\right)\mu^4}{1-H_3\mu^2+H_4\mu^4}$$

$$F_V(m,z,\mu)\equiv\frac{\Phi_z(m,z,\mu)}{\Phi_z(m,0,\mu)}=\frac{(z+1)\mu^2+\left(\frac{z^3}{6}+\frac{z^2}{2}-H_3z-H_1\right)\mu^4}{\mu^2-H_1\mu^4}$$

Similarly, the parameter indicating the particle trajectory at the free surface is

$$F_T(m,\mu)\equiv\frac{1}{\mu}\frac{\Phi_z(m,0,\mu)}{\Phi_x(m,0,\mu)}=\frac{\mu-H_1\mu^3}{1-H_3\mu^2+H_4\mu^4}$$

4. The Optimal Boussinesq-type Models

Considering all linear properties introduced in the previous section, an error function, $I(m,\mu)$, which is composed of five functions is defined as following

$$I(m,\mu)=E_C(m,\mu)+E_{Cg}(m,\mu)+E_H(m,\mu)+E_V(m,\mu)+E_T(m,\mu) \tag{34}$$

For any specific range of μ, one can obtain the corresponding optimal wave equations by minimizing the error function. Fig. 1 shows the comparison of error functions provided by various models from $\mu=4$ to $\mu=10$. As μ increases, our $O(\mu^4)$ model makes the error function much closer to the exact linear solution (i.e. the x-axis) than GKW $O(\mu^4)$ model. The difference of these two models occurring at large μ is that GKW model only makes its dispersion characteristic satisfy the Padé (4,4) approximation of the linear solution. On the contrary, our optimal model is obtained by a comprehensive survey corresponding to five properties of the linear solution. Therefore, our $O(\mu^4)$ model will behave a better phenomenon than GKW model for large μ. Moreover, the optimal value of *m* will remain almost steady as μ is large enough. To observe each linear property more lucidly, some evaluating functions respectively in Fig. 2 to Fig.4. It shows that some linear properties of GKW model, especially the particle trajectory in deep water, start to deviate intensely from the exact linear solution as μ increases.

5. Conclusions

In present study, the $O(\mu^4)$ Boussinesq-type equations are derived in terms of the velocity potential at an arbitrary elevation. Comparing all linear properties with those of the linear Stokes theory, the optimal model can be determined by choosing a suitable water-depth parameter m for any specific range of μ. An error function composed of five linear characteristics is also introduced to evaluate the optimal model. In deep water, the wave properties of the present optimal model are much closer to the exact linear solution than not only those obtained by the $O(\mu^2)$ optimal model but also GKW's results.

Chi-Min Liu, Assistant Professor,
Chien Kuo Institute of Technology,
1, Jieshou N. Rd., Changhua City,
TAIWAN.
Tel: +886-4-7111111 ext.2505
Email: jimmyliu@ms27.url.com.tw

Chin-Hwa Kong, Professor,
Department of Engineering Science and Ocean Engineering, National Taiwan University
73 Chow Shan Rd., Taipei,
TAIWAN.
Tel: +886-2-23625470 ext. 253
Email: chkong@ccms.ntu.edu.tw

4th International Congress
of Croatian Society of Mechanics
September, 18-20, 2003
Bizovac, Croatia

4thICCSM

TIME DOMAIN HYDRODYNAMIC SIMULATIONS USING THE FREQUENCY DOMAIN DATA

Šime Malenica, Jean Marc Orozco

Keywords: *frequency domain, time domain, Fourier transform, impulse response function, convolution, nonlinear hydrodynamics*

1 Introduction

The methodology for performing the time domain simulations using the frequency domain data is presented and applied to the problem of interactions of the floating bodies with water waves. The basic principles of the method are based on the well known procedure explained in [2]. The frequency dependent coefficients (added mass, damping, excitation) are first calculated using the 3D Boundary Integral Equations technique, and inverse Fourier transform is then applied to obtain the impulse response functions for each combination of motions. The motion equation is finally integrated in time using the Runge Kutta 4th order scheme. The method is first tested on the linear case both for regular and irregular excitaton, and is then applied for the nonlinear mooring simulations and for transient hydroelastic simulations.

2 Theory

Regardless of the method that is used to determine different hydrodynamic coefficients, the linear body motion equation in frequency domain takes the following form:

$$\left\{-\omega^2([\,\mathbf{M}\,]+[\,\mathbf{A}\,]) - i\omega[\,\mathbf{B}\,]+[\,\mathbf{C}\,]\right\}\{\boldsymbol{\xi}\} = \{\boldsymbol{F}\} \tag{1}$$

It's time domain equivalent is:

$$([\,\mathbf{M}\,]+[\,\mathbf{A}^{\infty}\,])\{\ddot{\boldsymbol{\xi}}(t)\} + +[\,\mathbf{C}\,]\{\boldsymbol{\xi}(t)\} + \int_0^t [\,\mathbf{K}(t-\tau)\,]\{\dot{\boldsymbol{\xi}}(\tau)\}d\tau = \{\boldsymbol{F}(t)\} \tag{2}$$

It can be shown (e.g. see [2]) that the different coefficients in the above equations are related to each other through the Fourier transforms. In particular it was shown that the impulse response function $K_{ij}(t)$ can be calculated from the following relation:

$$K_{ij}(t) = \frac{2}{\pi}\int_0^{\infty} B_{ij}(\omega)\cos\omega t \; d\omega \tag{3}$$

On the other hand, the excitation force vector (linear) for a given sea state, is calculated by summing up excitation from different wave components:

$$\boldsymbol{F}(t) = \sum_{i=1}^{N} \Re\{A_i \boldsymbol{F}(\omega_i) e^{-i(\omega_i t+\theta_i)}\} \tag{4}$$

3 Numerical results and discussions

In order to show the equivalence of two descriptions of the mechanical system, in figure 1 we show the results for pitch motion of an rectangular barge.

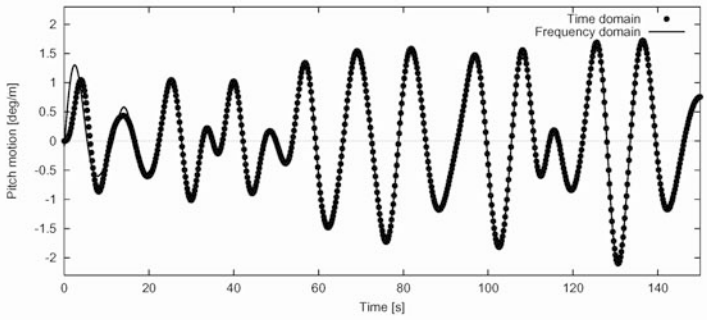

Figure 1: *Pitch motion by two methods for irregular wave excitation.*

Once the method has been validated for the linear case, the inclusion of non-linearities becomes relatively easy because the non-linear forces can simply be added in the right hand side of the equation (2). Two examples of application of the simulations in time domain, are presented in figure 2. First one concerns the nonlinear mooring simulations and the second one the transient hydroelastic behaviour of an elastic barge.

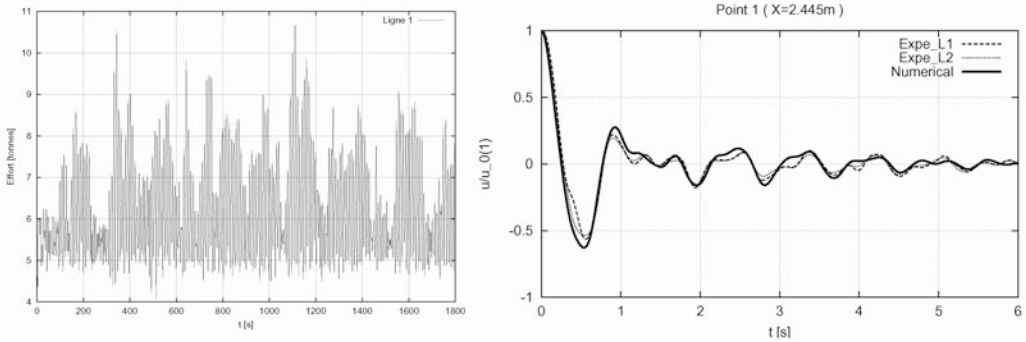

Figure 2: *Nonlinear mooring simulations and transient hydroelastic simulations.*

References

[1] Bingham W.E., 1994.: "Simulating ship motions in the time domain.", PhD Thesis, MIT.

[2] Cummins W.E., 1962.: "The impulse response function and ship motions", Schiffstecknik.

[3] King B., 1987.: "Time domain analysis of wave exciting forces on ships and bodies.", PhD Thesis, University of Michigan.

[4] Korsmeyer F.T., 1988.: "The first and second order transient free-surface wave radiation problems.", PhD Thesis, MIT.

[5] Kotik J. & Mangulis V., 1962.: "On the Kramers-Kronig relations for ship motions." Int. Shipbuilding Progress.

[6] Malenica Š, Molin B., Remy F. & Senjanović I., 2003.: "Hydroelastic response of a barge to impulsive and non-impulsive wave loads", Proc. 3rd Int. Conf. on Hydroelasticity, Oxford UK.

[7] Ogilvie T.F., 1964.: "Recent progress toward the understanding and prediction of ship motions." Proceedings of 5th Symp. on Naval Hydrodynamics, pp. 3-128.

Šime Malenica

Bureau Veritas - Research Department, 17 bis Place des Reflets, 92400 Courbevoie, France

Tel. +33142913379, Fax. +33142913395, e-mail : sime.malenica@bureauveritas.com

Jean Marc Orozco

Bureau Veritas - Research Department, 17 bis Place des Reflets, 92400 Courbevoie, France

Tel. +33142913397, Fax. +33142913395, e-mail : jean-marc.orozco@bureauveritas.com

4th International Congress
of Croatian Society of Mechanics
September, 18-20, 2003
Bizovac, Croatia

FRACTURE BEHAVIOUR OF HIGH-DUCTILE CCT SPECIMEN UNDER ELASTIC-PLASTIC CONDITIONS

Franjo Matejiček, Dražan Kozak, Pejo Konjatić

Keywords: *CCT Specimen, J-integral, crack growth, J-R curve, crack driving force, FE analysis*

Abstract

In assessing the integrity of structures containing cracks, it is important to quantify the relevant crack-driving force, so that its load carrying capacity can be predicted. For ductile materials permitting large-scale plasticity near the crack tip, this crack-driving force is frequently described as contour *J*-integral, which is one appropriate elastic-plastic fracture mechanics (EPFM) parameter (in absence of constraint effects) of low-strength and high-toughness materials. If there is excessive plasticity or significant crack growth, fracture toughness may depend on the size and geometry of the test specimen. Therefore, methodology for *J*-integral and crack length estimation of a CCT specimen made of high ductile stainless steel is presented in this paper. Estimation is conducted using results gained by experiments and it was confirmed using finite element analysis (FEA).

Research was conducted on specimens made of stainless steel X 5 CrNi 18 10, with yielding strength of $R_{p0,2}$=250 MPa and stress of 620 MPa by elongation of about 16%. First series of tests were conducted on specimens prepared for classic tension test (Figure 1 left) to determine real characteristics of material including σ-ε diagram, and after on standard CCT specimens shown right on Figure 1, with $2a/W = 10/30 = 0{,}3$.

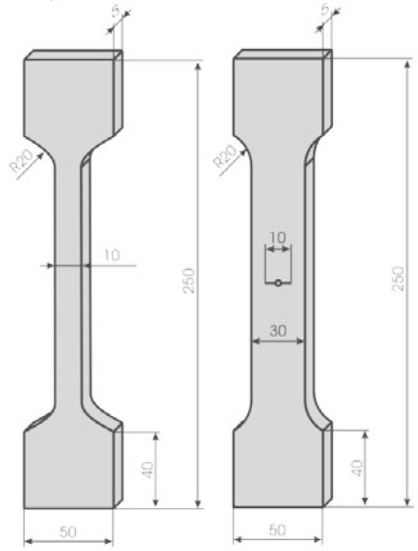

Figure 1. Tension test and CCT specimen

During testing, behind the force F, three characteristic displacements were measured: load line displacement (LLD), crack mouth opening displacement (CMOD) and crack tip opening displacement CTOD (δ_5). Single specimen method with loading-unloading compliance technique is used to determine compliance of material and hereafter crack extension Δa. It is often in engineering prac-

tice that only $J_{0,2BL}$ in crack resistance curve *J-Δa* could be determined corresponding to the fracture resistance at 0,2 mm of ductile crack growth.

J-integral for CCT specimen has been calculated measuring area under curve in *F-LLD* diagram representing plastic and elastic component of work and using expression:

$$J = \frac{\eta_e \cdot U_e}{B \cdot (0{,}5 \cdot W - a)} + \frac{U_p}{B \cdot (W - 2 \cdot a)} \tag{1}$$

A three-dimensional final element model of CCT specimen was prepared for finite element analysis in Ansys code. One eights of specimen is used for modelling to take advantage of symmetry (Figure 2). Finite element mesh consists of 16780 elements and 79392 nodes.

Finite element simulations show very good agreement between experimental and numerical results (Figure 3) and it can be applied to draw crack driving force, what is of great importance when the critical length of crack or critical applied stress should be determined.

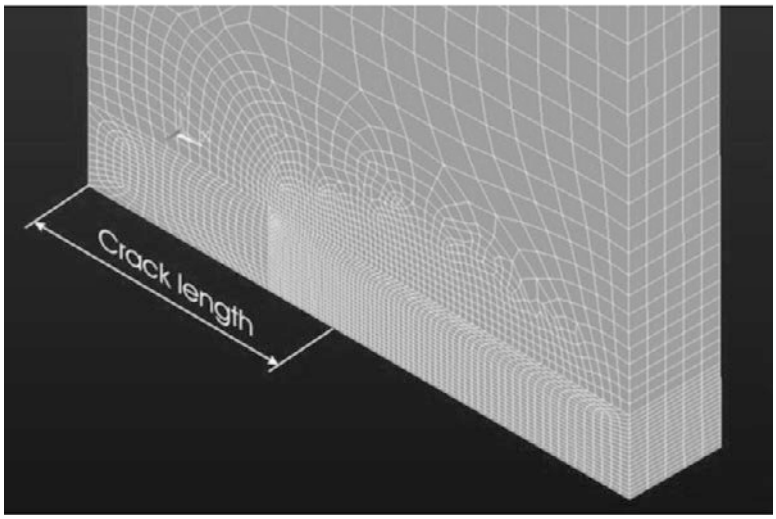

Figure 2. Finite element mesh

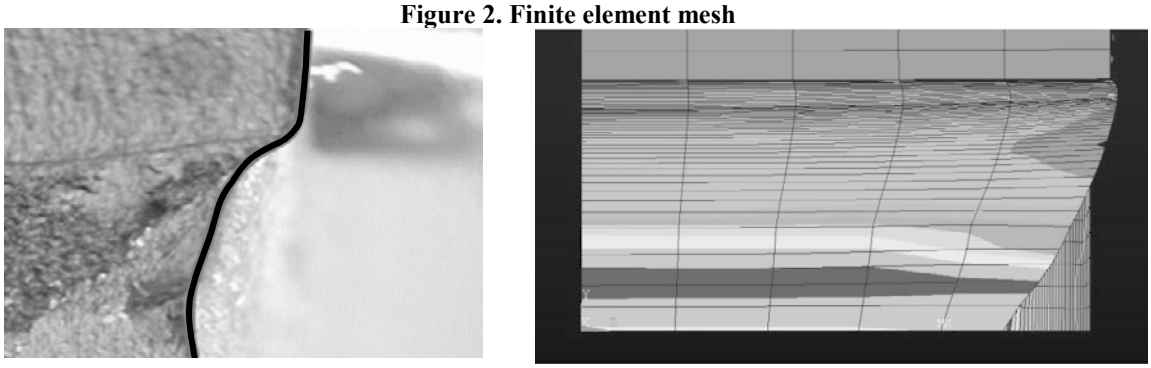

Figure 3. Crack mouth photo and FE simulation of dimple making

Dr Franjo Matejiček, Professor, Mechanical Engineering Faculty in Slavonski Brod, University of Osijek, Department of Mechanical Design, Trg Ivane Brlić-Mažuranić 18, HR-35000 Slavonski Brod, Croatia, Tel. +385 35 446 188, Fax: +385 35 446 446, E-mail: fmatej@sfsb.hr
Dr Dražan Kozak, Assistant Prof., Mechanical Engineering Faculty in Slavonski Brod, University of Osijek, Department of Mechanical Design, Trg Ivane Brlić-Mažuranić 18, HR-35000 Slavonski Brod, Croatia, Tel. +385 35 446 188, Fax: +385 35 446 446, E-mail: dkozak@sfsb.hr
Pejo Konjatic, BSc Mech.Eng., Mechanical Engineering Faculty in Slavonski Brod, University of Osijek, Department of Mechanical Design, Trg Ivane Brlic-Mazuranic 18, HR-35000 Slavonski Brod, Croatia, Tel. +385 35 446 188, Fax: +385 35 446 446, E-mail: pekon@sfsb.hr

4th International Congress
of Croatian Society of Mechanics
September, 18-20, 2003
Bizovac, Croatia

NUMERICAL ANALYSIS OF SINGLE-LAP ADHESIVE JOINT

Matejiček F., Raos P., Lucić M

Keywords: adhesive bonding, single-lap joints, modelling, physical characteristics

1. Introduction

Adhesive bonding technology is one of the most recent assembling techniques applied in industry and maintenance. Load bearing capacity (i.e. strength) of adhesively bonded joints depends on many various factors. These are characteristics of adhesive, properties of the materials to be bonded – adherends, bonding procedure, joint design and loading conditions [1].

Single lap adhesively bonded joint will be considered in the paper as one of the most applied joint design in engineering practice.

In experimental part of the paper, the testing is focused on determination of an optimum lap length. Joints are made of three types of adherends: aluminium, stainless steel and brass; and one type of adhesive: two component high-strength engineering adhesive. Simulation of stretching of joints with software based on FEM (Finite Element Method) is origin of researches in future.

2. Experimental research

The standard single lap specimens for evaluating the load bearing characteristics i.e. strength of adhesively bonded joint have been prepared accordingly Figure 1. Three types of adherends (materials to be bonded) have been considered; aluminium, stainless steel and brass. Dimensions of such prepared adherend plates were $a \times b \times s$=30×90×1,95 mm (30×90×1,50 for brass only*)* .The adherends are cleaned by an appropriate surface preparation method [2].

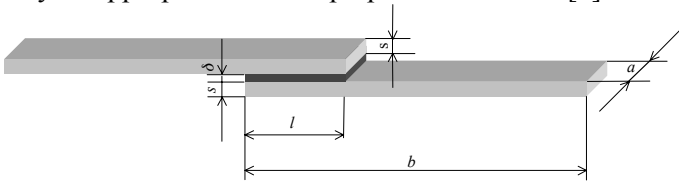

Figure 1. Single lap joint specimen

The thickness of the applied adhesive is maintain at 0,1 mm by using an appropriate fixture device and allowed to cure to reach maximum strength. The lap length has been varied in range from 15 to 60 mm. The all in this way prepared bonded joints have been stretched up to the break in the clamps of the tensile testing machine.

3. Numerical analysis

Simulation of stretching of joints with software based on FEM (Finite Element Method) is origin of researches in future. Numerical researches are based on one group of specimens made from two adherends: stainless steel and aluminium. Lap length which was used in numerical calculation was 30 mm (*l/a* ratio = 1).Thickness of adhesives has been used as 0,15 mm. Simulation of static load of query bodies was carried with software package ANSYS [3]. Comparison of numerical results with experiment shows Fig.2.

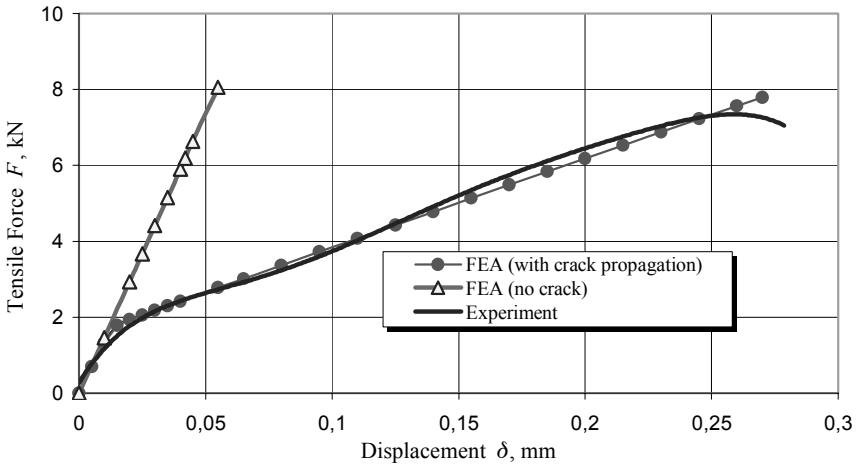

Figure 2. Numerical results compared with experimental (adherend: stainless steel)

6. Conclusion

One of the most decisive designing factors on strength of adhesively bonded joint is an overall lap length of the joint. It is necessary to find an optimum lap length aiming the bonded joint to be dimensioned properly. At the optimum lap length it is possible to reach a maximum load bearing capacity using a minimum quantity of applied adhesive.

In the experimental work it was researched the influence of the lap length on joint strength considering the joints made of three types of adherends (aluminium, stainless steel and brass). As expected, the experimental investigation confirmed very strong influence of lap length on strength characteristic of the joints. Obviously, the influence of the adherend deformational characteristics on joint strength is very significant, what was also confirmed in numerical investigation.

In the numerical part of this paper, the aim was to create appropriate model of adhesive joint. This is realised with good results. The model was used for both of aluminium and stainless steel as adherend, and all results are acceptable.

References

[1] Schindell-Bidinelli, E.H., Gutherz, W., "Konstruktives Kleben", VCH Verlag, Weinheim, 1988.
[2] N.N., "Technical Data Sheet, Product 3421", Loctite Corp., Dublin, 2000.
[3] N.N., "ANSYS Vers 6.0", ANSYS Inc. Canonsburg USA, 2000.
[4] Andruet, R. H., Dillard, D. A., Holzer, S.M., "Special Finite Elements for Analysis of Adhesive Joints", ECCOMAS 2000, 11-14 September 2000, Barcelona
[5] Pocius, A.V., "Adhesion and Adhesives Technology", Hanser Publishers, Munich-New York, 1997.
[6] Kralj, S., Kožuh, Z., " Designing of bonded joints", Proceedings HDTZ, Zagreb HR, 1994.
[7] Raos, P., Matejiček, F, Lucić, M.: "Experimental investigation on mechanical characteristics of adhesively bonded single-lap joints", 1st DAAAM International Conference ATDC 2002, Slavonski Brod, Croatia, 2002.
[8] Moaveni, S., "Finite Elemente Analysis", Prentice-Hall Inc., New Jersey, 1999.

Prof. Dr. Franjo Matejiček
Mechanical Engineering Faculty in Slavonski Brod, University of Osijek, Department of the Mechanical Design, Trg I.B.Mažuranić 18, HR-35000 Slavonski Brod, Croatia, Phone +385-35-446-188, Fax +385-35-446-446, fmatejicek@sfsb.hr,
Prof. Dr. Pero Raos
Mechanical Engineering Faculty in Slavonski Brod, University of Osijek, Department of Technologies, Trg I.B.Mažuranić 18, HR-35000 Slavonski Brod, Croatia, Phone +385-35-446-188, Fax +385-35-446-446, praos@public.srce.hr
Mirjana Lucić, B.Sc.Mechanical Engineering Faculty in Slavonski Brod, University of Osijek, Department of Technologies, Trg I.B.Mažuranić 18, HR-35000 Slavonski Brod, Croatia, Phone +385-35-446-188, Fax +385-35-446-446,mlucic@sfsb.hr

4th International Congress
of Croatian Society of Mechanics
September, 18-20, 2003
Bizovac, Croatia

LARGE DISPLACEMENT MODEL OF REINFORCED CONCRETE SPACE FRAMES

A. Mihanović, B. Trogrlić

Keywords: r/c space frames, large displacement, comparable body, null configuration

1. Introduction

The large displacement model of the material and geometrically nonlinear three-dimensional (3D) reinforced concrete frames follows incrementally small displacement theory presented in Ref. [1], and a conclusion about the quasi tangential stiffness matrix taken from Ref. [2]. The global 3D reinforced concrete structure consists of the beam-column straight members, each of them discretized by a few FE.

Updating the large translation displacement from increment to increment follows from simple summarising of the incremental translation displacement vector. Updating the large rotations is related to the FE and corresponds to the rigid body incremental rotations what is an approximate solution. This approximation shall be numerically tolerable if a length of the FE is small enough.

The geometrical updating of the predicted load and the internal forces depends on the differences of the tangent stiffness matrix between two increments. The mapping of the complete predicted load over the actual tangent stiffness matrix results in the new configuration called *null configuration*. In the same null configuration the predict load over new tangent stiffness matrix maps a new distribution of the internal force and strike out the additional displacement. The incremental loading, either follower or gravitational, follows the usual procedure.

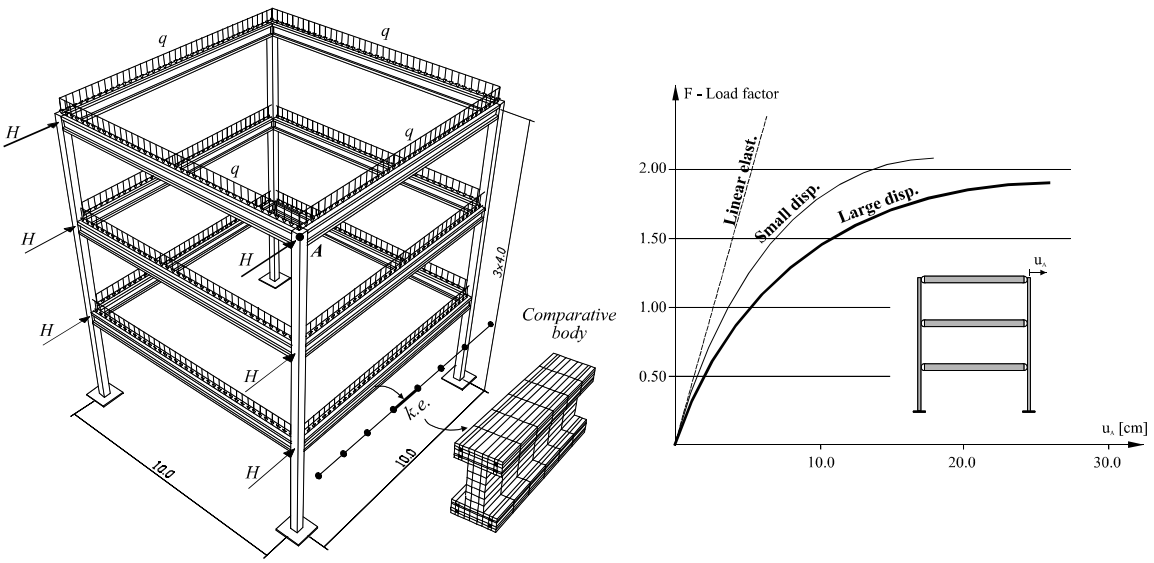

Figure. 1: R/C space frame, column-girder FE and 3D comparative body

The nonlinear beam-column FE adopts a decomposition approach for the cross-section to capture the uniaxial nonlinear behaviour of reinforced concrete. Filaments in section, see Ref. [3], are extended over the beam-column FE and form a prismatic body, which is discretized by brick FE, to capture the shear and torsional nonlinear behaviour of reinforced concrete. The model implemented flexural, lateral and torsional stability effects. The whole numerical procedure is incrementally-iterative. The direct iterative procedure was used at the frame level and at the cross-sections level.

The construction of the failure surface is applied and the equilibrium of the cross-section forces including plasticity of separate fibres is adopted in each incremental-iterative step. The failure of the structural system arises with the loss of the stability or with the step-by-step plastification of different cross-sections until the mechanism occurs. The results of the numerical analysis of frame from Fig. 1 and Fig. 2 for load q=19 kN/m and H=19 kN are reached for σ-ε uniaxial behaviour of concrete and steel shown on Fig. 3.

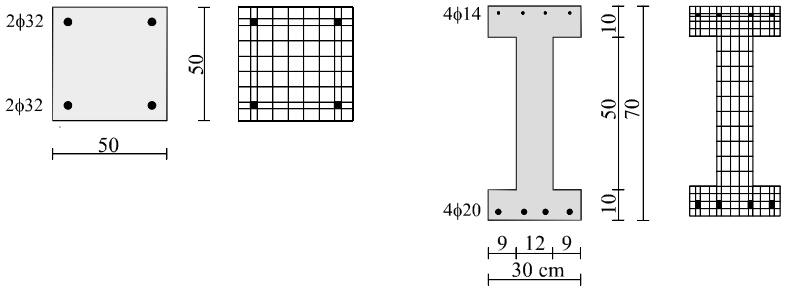

Figure 2. Discretization of reinforced concrete frame cross-sections, columns and girders

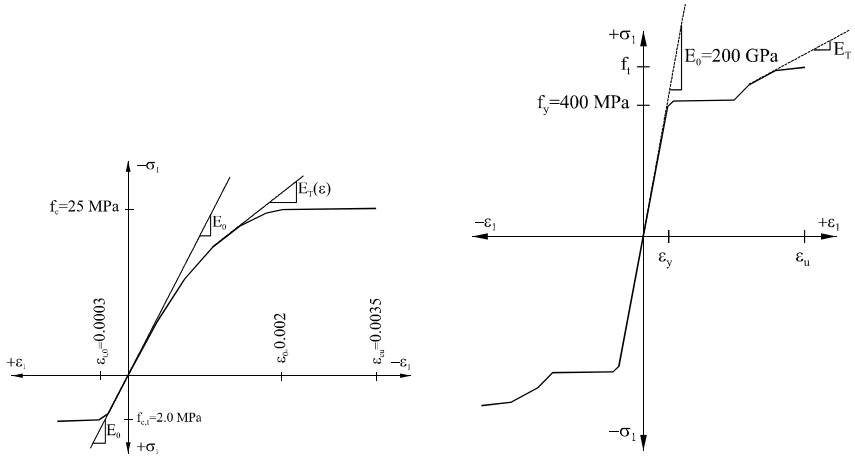

Figure 3. Uniaxial σ-ε diagram for concrete and reinforcing steel

2. References

[1] B.A. Izzuddin. Conceptual issues in geometrically nonlinear analysis of 3D framed structures, Comp. Meth. in Appl. Mech. and Eng., **191**: 1029-53, 2001.

[2] Y.B.Yang, S.R. Kuo, and Y.S. Wu. Incrementally small-deformation theory for nonlinear analysis of structural frames, Engineering Structures, **24**: 783-98, 2002.

[3] M. Romero, P.F. Miguel, J.J. Cano. A parallel procedure for nonlinear analysis of reinforcement concrete three-dimensional frames, Computers and Structures, **80**: 37-50, 2002.

Ante Mihanović, Prof. Ph.D., University of Split, Faculty of Civil Engineering, Matice hrvatske 15, phone: 021-303357, ante.mihanovic@gradst.hr

Boris Trogrlić, M.Sc., University of Split, Faculty of Civil Engineering, Matice hrvatske 15, phone: 021-303352, boris.trogrlic@gradst.hr

4th International Congress
of Croatian Society of Mechanics
September, 18-20, 2003
Bizovac, Croatia

STABILITY ANALYSIS OF STEEL SPACE FRAMES UNDER LARGE DISPLACEMENT

A. Mihanović, B. Trogrlić and V. Akmadžić

Keywords: space frames, large displacement, null configuration, comparative body

1. Introduction

The large displacement model of the material and geometrically nonlinear three-dimensional (3D) steel frames follows incrementally small displacement theory presented in Ref. [1], and a conclusion about the quasi tangential stiffness matrix taken from Ref. [2]. The global 3D steel structure consists of the beam-column straight members, each of them discretised by a few FE.

Updating the large translation displacement from increment to increment follows from simple summarizing of the incremental translation displacement vector. Updating the large rotations is related to the FE and corresponds to the rigid body incremental rotations what is an approximative solution. This approximation shall be numerically tolerable if a length of the FE is small enough.

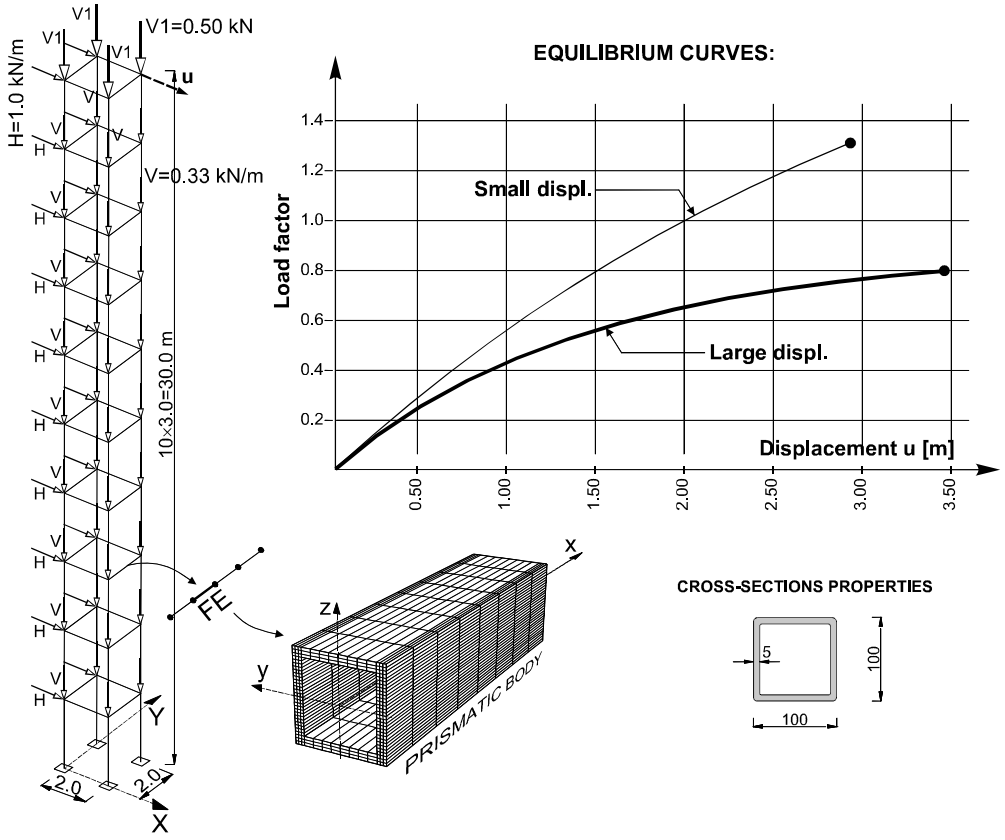

Figure 1. Steel space frame, column-girder FE and 3D comparative body

The geometrical updating of the predicted load and the internal forces depends on the differences of the tangent stiffness matrix between two increments. The mapping of the complete predicted load over the actual tangent stiffness matrix results in the new configuration called *null configuration*. In the same null configuration the predict load over new tangent stiffness matrix maps a new distribution of the internal force and strike out the additional displacement. The incremental loading, either follower or gravitational, follows the usual procedure.

The nonlinear beam-column FE adopts a decomposition approach for the cross-section to capture the uniaxial nonlinear behaviour of steel. Filaments in section, see Ref. [3], are extended over the beam-column FE and form a prismatic body, which is discretised by brick FE, to capture the shear and torsional nonlinear behaviour of steel. The model implemented flexural, lateral and torsional stability effects. The whole numerical procedure is incrementally-iterative. The direct iterative procedure was used at the frame level and at the cross-sections level.

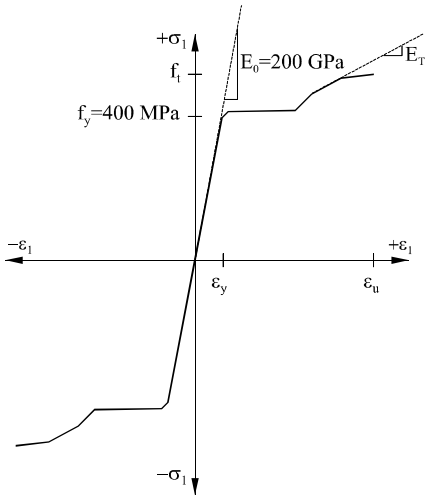

Figure 2. Steel uniaxial σ-ε diagram

The construction of the failure surface is applied and the equilibrium of the cross-section forces including plasticity of separate fibres is adopted in each incremental-iterative step. The failure of the structural system arises with the loss of the stability or with the step-by-step plastification of different cross-sections until the mechanism occurs. The results of the numerical analysis from Figure 1 are reached for σ-ε uniaxial behaviour of steel shown on Fig. 2.

2. References

[1] B.A. Izzuddin. Conceptual issues in geometrically nonlinear analysis of 3D framed structures, Comp. Meth. in Appl. Mech. and Eng., **191**: 1029-53, 2001.

[2] Y.B.Yang, S.R. Kuo, and Y.S. Wu. Incrementally small-deformation theory for nonlinear analysis of structural frames, Engineering Structures, **24**: 783-98, 2002.

Ante Mihanović, Prof. Ph.D., University of Split, Faculty of Civil Engineering, Matice hrvatske 15, phone: 021-303357, ante.mihanovic@gradst.hr

Boris Trogrlić, M.Sc., University of Split, Faculty of Civil Engineering, Matice hrvatske 15, phone: 021-303352, boris.trogrlic@gradst.hr

Vlaho Akmadžić, assistant, University of Mostar, Faculty of Civil Engineering, K. Tomislava 14, phone ++38766-319295, vlaho1@yahoo.com

4th International Congress
of Croatian Society of Mechanics
September, 18-20, 2003
Bizovac, Croatia

4thICCSM

PREPROCESSING UNITS FOR GENERATING MESH OF FINITE ELEMENTS DURING GENERATING MESH OF FINITE DIFFERENCES

Budimir Mijović, Elvir Abazović

Keywords: Finite differences, Finite element, Preprocessing, Simulation

1. Introduction

Program modules for generating, calculation and simulation of manufacturing and designing processes, as a rule can never completely cover requirements of all branches of industry so it is frequently necessary to effect adaptation or completion of the existing program modules for the purpose of their more effective use. Therefore it is possible to use some of the existing graphic preprocessing units for generating mesh of finite elements and develop modul for translating such generated moduls in format and syntaxis understandable to program package FLAC^{3D} [1]. A graphic preprocessor PATRAN 9.0 would suit better the requirements set by program package FLAC^{3D} since it has better geometric tools, openess of program for obtaining users subprograms, mobility and applicability even under Windows NT surface and price of the program [2].
2. Numerical modelling

Procedure of numeric simulation was performed from generating three-dimensional geometric model within CAD system, inputting of geometry in preprocessor unit PATRAN, adaptation of geometric entities and web generating, assigning of material properties and boundary conditions and at the end testing of incoming database for solver unit FLAC^{3D}. The results received by calculating by NASTRAN and FLAC^{3D} were compared. Wing of a blade has been equally loaded by surface pressure of 10 [MPa] which on its upper surface has pressure on a surface, and on a lower side the same underpressure has its effect which draw a blade normally from blade surface due to streaming of fluid round a blade. A blade was manufactured from alloyed steel with elasticity module E = 210 [GPa] and Poisson coefficient ν= 0.32. Steel specific density is ρ= 7850 [kg/m^3]. Material properties are awarded so that material is defined in accordance with name (steel), type (linear-elastic) and its properties (E = 210 [GPa], ν= 0.32, ρ= 7850 [kg/m^3]). Blade model contains 7980 knots and 11283 tetrahedron elements with 23467 degrees of freedom. The 20000 computational iterative steps were needed in program unit FLAC^{3D}.

3. Results

As verification of successfully carried out data transformation from graphic preprocessing made in program module PATRAN the analysis of results was used obtained by calculation by program module FLAC^{3D} and their comparison with results obtained by calculating with method of finite elements with NASTRAN program. Figure 1. gives a comparison of displacement in direction of global axis Y. The result of absolute displacement obtained by the analysis of finite differences produces maximum value of 133.27 [mm], while for the same model and same load the results calculated by solver NASTRAN unit produce maximum value of absolute displacement of 137 [mm]. Absolute deviation of the result of about 3.5 [mm] produces relative deviation of 0.36% and this can certainly be consequence of convergence parameter of calculation process. While FLAC^{3D}

analysis produce maximum positive value of displacement of 7.96 mm, the analysis by means of NASTRAN program produce value of 7.51 [mm].

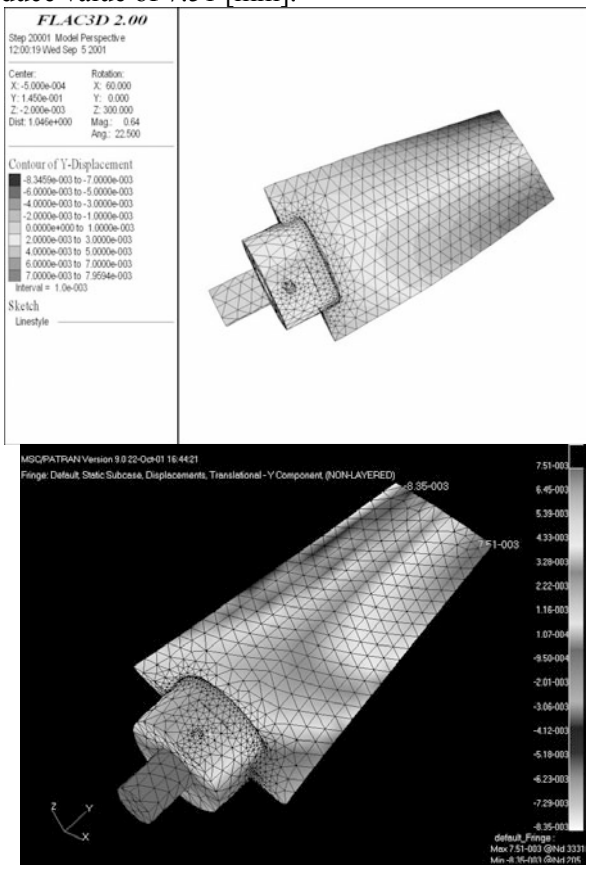

Figure 1. Contours of absolute displacement of blade by FLAC^{3D} and NASTRAN

In negative direction of displacement these values are closer to each other and produce value -8.346 mm (FLAC^{3D}) and -8.35 [mm] (NASTRAN).

4. Conclusion

Through the stated example of turbine blade, which has been calculated with two different numeric approaches, by method of finite elements and finite differences, it is possible to generate any form of threedimensional real model, and carry out its calculation by methods of finite differences and that its results are equally valuable. By defining known and requested sizes of numeric simulation decision are brought on the choice of way of simulation, finess of discreet model, relevant model of material, harnessing of boundary conditions which will simulate real working conditions and finally type and survey of the results on the basis of which correctness of the results will possibly be chacked as well as location of critical places for design of the considered example.

References

[1] Cundall, P. A., at all., FLAC Version 3.40 – Reference Manuel: ITASCA Consulting Group, Minessota-Mineapolis, USA, 1998

[2] MSN. Incorporation, MSC/PATRAN User Guide V.90, MSC Incorpotarion, 1999

Prof. Budimir Mijović Ph.D., Faculty of Textile Technology, University of Zagreb, baruna Filipovića30,Zagreb,Croatia,Tel.:++38513703154,Fax:++38513774029,E-mail:mijovic@hotmail.com. Elvir

Abazović dipl. Ing., GEOCONSULT ZT GmbH, Sterncksstrase 52, A-Salzburg, Austria, Tel.: ++43 662 65 96 50, Fax.: ++ ++43 662 65 96 510, E-mail: eab_64@hotmail.com

4th International Congress
of Croatian Society of Mechanics
September, 18-20, 2003
Bizovac, Croatia

4thICCSM

NUMERICAL PREDICTION OF AIRFOIL FLOW

Zoran Milas

Keywords: *airfoil, stall, lift/drag, modeling*

Abstract

Aerodynamic characteristics of the axial turbomachines, particularly of those with low rotor "solidity", are largely determined by their airfoil characteristics. Airfoil stall controls most of the blade stall smeared by 3D effects at the root and tip area.

Turbulent flow around NACA 0012 airfoil in the range of incidence angles from $0.^0$ up to stall angle at Re=2.8 10^6 is calculated by applying finite volume method with modified $k-\varepsilon$ turbulence model.

A grid independent solution is achieved on the C-type grid around airfoil with 1664*320 control volumes for the finest grid. Testing of various boundary conditions along open side boundaries at small incidence angles proves that they have negligible effect on calculated pressure and shear stress distribution along airfoil and airfoil lift/drag coefficients as well. Calculation of the flow at incidence angle $\alpha = 3^0$ with inlet boundary conditions along B-C-D ($\overline{u} = \mathrm{v}_0 \cos\alpha, \overline{\mathrm{v}} = \mathrm{v}_0 \sin\alpha, \overline{k} = \overline{k}_0, \overline{\varepsilon} = \overline{\varepsilon}_0$) and outlet boundary conditions along A-B diverged.

Inclusion of the laminar part by prescibing transition is required in order to bring the calculated data closer to the experimental ones. The computer programme is modified by suppressing turbulence, i.e. turbulent stress in the laminar region. Location of transition on the upper-lower part of airfoil x_{tr}/c is prescribed on the basisi of experimental data $[6]$. Zero value of turbulent viscosity $\mu_t = 0$ and very small value of turbulence kinetic energy $\overline{k}$ are imposed to all nodes in the laminar region in every step of the global iteration procedure.

Very good agreement is obtained between the calculated and the experimental values for the lift-drag coefficients and the pressure coefficient distribution at moderate incidence angles. Drag coefficient perfectly matches experimental values for smaller incidence angles. Underprediction of the lift coefficient is reduced. Maximum of the lift is more distinguished and analysis of the flow pattern indicates presence of separation bubble near the trailing edge at $\alpha \le 18^0$. Significant reduction of drag is due to smaller skin friction in the laminar part of the boundary layer that extends almost along entire lower part of the airfoil.

Increase of the lift is mainly because of higher (under) pressure along the airfoil suction side. Fig. 5 illustrates that increase in the peak pressure is quite discernible ($\Delta c_p \approx 0.5$ for $\alpha = 12^0$) and that calculated values no longer fall short of the experimental ones as much as before.

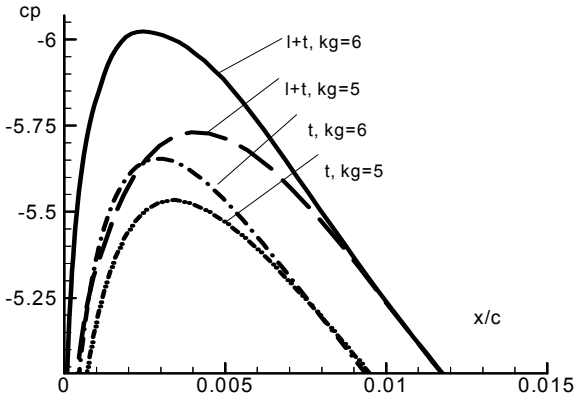

Figure 5 Pressure coefficient c_p along NACA 0012 airfoil leading edge (suction side) at Re=2.88 10^6, α=12^0 [7]: t- calc. assuming fully turbulent flow, l+t- calc. with prescribed transition laminar-turbulent, kg-grid finess index

References:

[1] Abbot, I.H., Doenhoff, A.E., "Theory of Wing Sections", Dover Publications, 1958.

[2] Angel, R.K., Musgrove, P.J., Galbraith, R.A., Green, R.B., "Summary of the Collected Data for Tests on the NACA 00 Aerofoils", University of Glasgow, ETSU WN 5072-P2, 1990.

[3] Eppler, R., "Airfoil Design and Data", Springer-Verlag, Berlin, 1990.

[4] Ferziger, J.F., Perić, M., "Computational Methods for Fluid Dynamics", Springer-Verlag, 1997.

[5] Lazauskas, L., "www.maths.adelaide.edu.au/llazauskas", 1997.

[6] Mehta, U.,Chang, K.C., Cebeci, T., "A Comparison of Interactive Boundary Layer and Thin Layer Navier Stokes Procedures", Numerical and Physical Aspects of Aerodynamic Flows III, Springer-Verlag, New York, 1985, pp. 198-215.

[7] Milas, Z., "Analysis of Turbulent Flow Around Airfoil", Faculty of Mechanical Engineering and Naval Architecture, PhD Thesis, University of Zagreb, Zagreb, 2001, p. 209.

[8] Perić, M., "A Finite-Volume for the Prediction of Three-Dimensional Fluid Flow in Complex Ducts", Thesis PhD, University of London, Imperial College, London, 1985.

[9] Rhie, C.M., Chow, W.L., "A Numerical Study of the Turbulent Flow Past an Isolated Airfoil With Trailing Edge Separation", AIAA-82-0998, AIAA/ASME 3rd Joint Thermophysics, Fluids, Plasma and Heat Transfer Conference, St. Louis, Missouri, 1982.

[10] Spalart, P.R., "Direct Simulation of a Turbulent Boundary Layer up to Re_θ=1410", J. Fluid Mechanics, Vol.187, 1988, pp.61-98.

Zoran Milas
University of Split
Faculty of Electrical Engineering, Mechanical Engineering and
Naval Architecture
R. Bošković, 21 000 Split, Croatia
E-mail: zmilas@fesb.hr

4th International Congress
of Croatian Society of Mechanics
September, 18-20, 2003
Bizovac, Croatia

EXPERIMENTAL ANALYSIS OF FREE DIVING FINS

G. Minak

Keywords: on field strain measurements, free diving fins, strain gages, polycarbonate

1. Introduction

Sport equipment performance analysis nowadays has a growing importance. In fact many sports are extensively equipment dependent and the overall athlete's performance is widely influenced by technical features. In free diving recently new materials have been adopted for fins like polycarbonates or carbon fibre reinforced composites and for monofins e.g. glass fibre reinforced composites. The choice of the geometry, of the material and of the lamination lay-up is based on experience and the experts feeling, not on quantitative measures. In this work, some experimental methodologies for the evaluation of physical parameters (dumping, hysteresis loop) and of the performances will be shown.

2. Materials and Methods

In order to establish a methodology we focused our attention on a very popular, but nowadays out of market free diving fin. It's an injection moulded fin, made with three different thermoplastic materials. The blade is in polycarbonate and four high range (± 10%) strain gages have been glued on the blade in different positions and have been protected with silicon coating. Data have been acquired by means of a Vishay portable system. The configuration has been a quarter of bridge and the acquisition frequency has been 1 kHz for dynamic measurements and 100 Hz for the static ones. Many kind of tests have been performed in laboratory and in swimming pool. The first and easiest to perform is the step response to determine the eigen frequencies and the dumping properties: prescribed strain has been imposed to the fin by means of a wire that has been cut instantaneously. Than utilizing an Italsigma servo hydraulic machine equipped with a 2 KN load cell the hysteresis loop has been drawn. The fin has been fixed to a beam, by mean of two bolts passing through the shoe and to the load cell and the actuator by a grip designed ad hoc in order to leave free the possibility of horizontal sliding. The machine has a displacement range of 100 mm, so different load levels have been obtained moving the fin in the direction of the actuator. Other test has been performed hanging up calibrated weights to find the load-strain function. This has bee done hanging up the weights directly on the edge of the blade or using a wire connected to the fin fixture and lying on the blade in order to simulate distributed load. Tests have performed in a swimming pool to determine the thrust impressed by the diver on the wall. The thrust has been correlated to fin deformation, and, through the calibration curve obtained in laboratory to the force exerted by the fin on the water. The thrust has been measured by means of two water resistant load cells suitable for low loads (<200 N). They have been designed as flexural beams equipped with four strain gages in full bridge configuration located in the maximum strain point determined by a finite element model. Many swimming stile and kicking rates have been tested, changing the position of the instrumented fin from one leg to the other to determine differences in the thrust. The testers have been an Apnea Academy free diving instructor, an experienced and an inexperienced free diver.

3 Results

In figure 1 an example of possible correlation between the force exerted by the fin on water, thick grey curve, and the thrust read by the load cells, thin black curve. Obviously a symmetric curve for the second fin shifted in phase could be added to the graph in order to obtain the total force on fins.
The mean force in this case can be valuated in 42 N while the mean thrust is 7 N. It is evident that only a small part of the force, nearly 16%, is transferred to the load cells due to hydrodynamic losses.

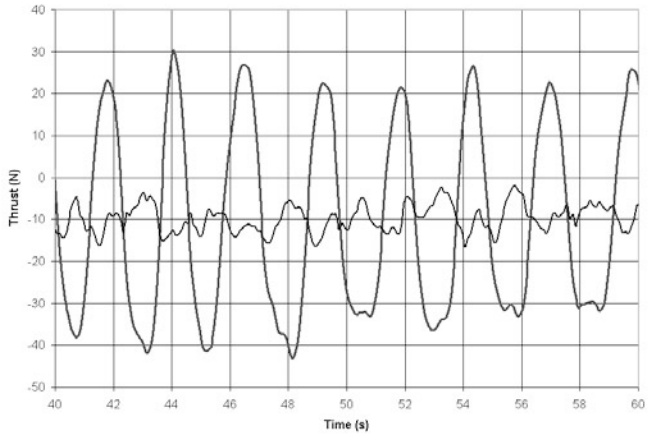

Figure1: Thrust and force on fin

From the figure a fatigue effect on the diver can be appreciated, since in the last four kicks the movement was not complete as in the previous ones. This suggest the possibility of using this methodology, together with image analysis in order to improve the biomechanics of fin swimming.

4 Conclusions and discussion

A simple methodology for the determination of the performances of free diving fins has been proposed. It is based on the use of strain gages and a submersible load cell and it could be utilized either for quantitative comparative testing or for biomechanical studies. The actual value for the thrust impressed by the fins is derived from the strain experimental data calibrating the instrumented fin in laboratory. Overall mechanical characterization of the fin has been performed, including material properties, hysteresis loop shape, first eigen frequency and dumping. In this work the approach described in [1] has been followed, even with different methodologies. Since the thrust is measured on a still diver it is not possible to take into account hydrodynamic effects in the analysis. For comparative test purposes this argument is not very important, but it would be for the determination of absolute fin efficiency. The next step will be the measure of the same quantities on moving divers by means of totally independent an submersible data acquisition systems.

References

[1] B. Atzori, N. Petrone, D. Zanatta, “Analisi bio-meccanica e simulazione numerica del movimento di pinneggiata subacquea” , XXXVI Convegno Nazionale AIAS, Catania, 1997
[2] ASTM sui materiali polimerici
[3] Christianson, R., Weltman, G. and Egstrom, G., “Thrust Forces In Underwater Swimming”, Human Factors, December, 1965.
[4] J. Picken, C. T. Crow , “Performance efficiency of swim fins”, Ocean Engineering, vol.2, pp. 251-258.

Giangiacomo Minak Ph.D.
Mechanichal engineering Department DIEM, Università degli Studi di Bologna, Via Risorgimento 2 40136, Italy +390512093266, +392093412, giangiacomo.minak@unibo.it

4th International Congress
of Croatian Society of Mechanics
September, 18-20, 2003
Bizovac, Croatia

MAXIMUM AIR POLLUTION SIMULATION USING GENETIC ALGORITHM

Z. Mrša, and Z. Čarija

Keywords: *air pollution modeling, Gaussian plume model, genetic algorithm, refinery plant SO_2 dispersion computer simulation*

1. Introduction

The region of the Rijeka municipality has very bad air. One of the main pollution sources is refinery plant near Rijeka. Its stacks emit significant amount of SO_2 pollutant. It is specially so when using high sulphor content fuel for power plant. Given the 17 point sources of SO_2 emission pollution resulting from high sulphur content in the fuel, the problem was to numerically simulate dispersion and distribution of SO_2 pollutant in the nearby surroundings for the worst possible meteorological data, with given topography of the terrain. Finally, different scenarios should be invented for pollution reduction, such as the alternative use of two different fuels with low and high sulphur content. The analysis of the height of the reconstructed power plant stacks on the pollution is carried out too. The Gaussian plume algorithm was used for the numerical simulation. The 17 sources were modelled at their real topographic locales with proposed SO_2 emissions. The stacks varied in height from 9.5 to 124 m, and were distributed through the whole refinery territory. The SO_2 emissions varied from 1 to 140 g/s coming from the sources such as refinery power plant, with highest emissions, to different refinery process plants. Here we used 120x131 = 15720 receptor mesh with 100 x 100 m resolution, covering 12 x 13.1 km area cantered at the power plant and including nearby urban areas. In the south-north direction (-15 to 60 deg) the terrain rises very steeply. We varied meteorological data in the chosen intervals that result in highest pollution. The input meteorological parameters used by Gaussian dispersion models are the wind speed, wind direction, isolation (during daytime) or temperature gradient (night), and the mixing height. We used genetic algorithm optimization tool [1],[2],[3]. Because of the varying terrain height and varying wind directions and speeds, even for the stationary pollution emissions multiple maxima of the surface pollution occur. Each individual set of meteorological data is represented by chromosome with different gene lengths; 8, 6, 5 and 1-bit string encoding wind direction, speed, mixing height and temperature gradient respectively. The search intervals for given four variables are input data.

2. Results analysis

In the genetic algorithm every individual produce input meteorological data for computer code for the simulation of distribution and dispersion of pollutants across the given terrain. Preliminary search resulted in following limits where maximum pollution occurs: wind speed 1-10m/s, direction 345°-60° (0 is north), mixing height 300 – 5000 m, temperature gradient –1 or 1. For given limits final detailed search with refined intervals gave maximum values. One population consisted of 20 individuals. The optimisation was achieved through 60 generations. The objective functional (fitness), is the SO_2 surface concentrations at any of given receptors for all possible variations of meteorological data in given intervals. The results show that worst pollution occures at night, with stabile atmospheric condition, class 5 or 6, and low speeds 1 – 2 m/s and south winds 15-45 degrees. In these conditions the plume hits the steep terrain nearest to the stack, while

difusion is still small, so that the concentrations are high.The highest values of fittness achieved after 20 generations.

Figure 1. shows maximal surface pollution distribution in given terrain for worst meteorological data: winds of 1 m/s, south-north direction 10°-12°, positive temperature gradient and high mixing heights 3880 – 5000 m. In order to estimate the influence of the stack height of the most influential stacks, these of the power plant, its variation is studied: original 35, 60 and 125 m. The linear regression of the maximum pollution concentration as a function of stack height, was established, showing that 80 m stack height would halve the maximum pollution concentration form 1600 to 800 $\mu g/m^3$.

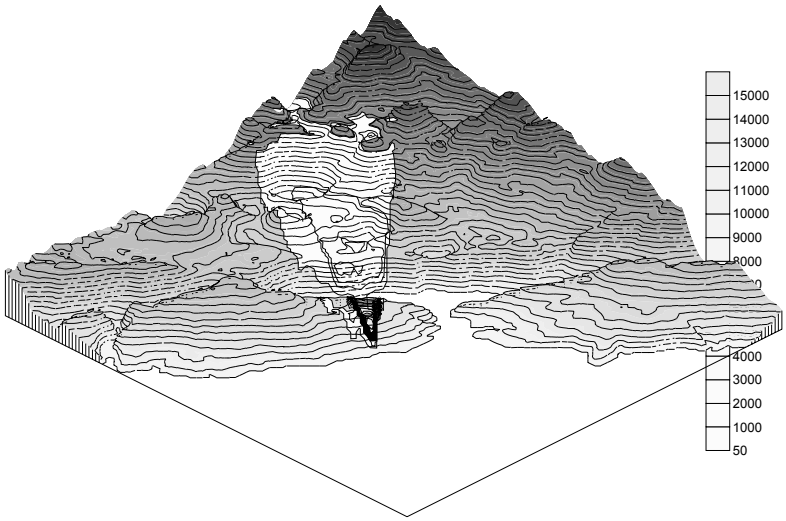

Fig. 1 The surface SO_2 concentration ($\mu g/m^3$) for worst meteorological conditions

3. Conclusion

The main conclusion is that proposed modelling of maximum pollution enables one to decide in which forecasted meteorological conditions the pollution would be above accepted values and therefore determine the time interval when cheap law sulphur fuel should be used instead of cheap high sulphur fuel. The linear regression of the maximum pollution concentration, as a function of stack height, was established.

References

[1] Čarija, Z., Mrša, Z. "Continuously variable intake manifold pipe length control using genetic algorithm", Proceedings of the 11th International DAAAM Symposium, Katalinic, Vienna Austria, 2000, pp 65-66.

[2] Goldberg, D.E. "Genetic Algorithms in Search, Optimization, and Machine Learning", Addison-Wesley, Reading, Massachusetts, 1989.

[3] Mrša, Z., Čarija, Z. "A turbulent flow shape optimization method for cascade profile design", Proceedings of the 3rd International Congress of Croatian Society of Mechanics, pp 443-450, ISBN 953-96243-3-9, Cavtat-Dubrovnik, September 2000.

Zoran Mrša, Prof. Dr. Sc.
Faculty of Engineering, University of Rijeka, 51000 Rijeka, Vukovarska 58, Croatia, Phone: 00385 51 651500 Fax: 00385 51 675818, e-mail: mrsa@riteh.hr
Zoran Čarija, Assist.
Faculty of Engineering, University of Rijeka, 51000 Rijeka, Vukovarska 58, Croatia, Phone: 00385 51 651500 Fax: 00385 51 675818, e-mail: zcarija@riteh.hr

4th International Congress
of Croatian Society of Mechanics
September, 18-20, 2003
Bizovac, Croatia

4thICCSM

MODELING OF DISPERSION AND DIFFUSION OF POLLUTANTS FROM INDUSTRIAL CHIMNEY STACKS IN RIJEKA REFINERY

Z. Mrša and M. Čavrak

Keywords: Atmospheric modelling, air pollution, ground concentrations, plume rise

1. Introduction

Environmental fluid mechanics is used to simulate the influence of pollutants to environment. Although it's not yet fully explained and usually every simulation in that field leads to discrepancy from a real physical system, it is necessary to have at least some air pollution dispersion scenarios to assess the influence of the humane born emissions. Numerical simulation of dispersion of pollutants from two chimneystacks situated in Rijeka's refinery were performed. Detection of ground-level concentrations of hazardous effluents (p.e. SO2, CO2) on a complex terrain around Bakar's bay (vicinity of Rijeka) was performed. Importance of conveying such a simulation is to ensure that pollutants are well dispersed and significant consequences on surrounding populated area detected. Geometry was made as 'box model' which bottom side was replaced with terrain topology. Unstructured tetrahedral mesh that consists of 250000 elements was generated. Five different south wind profiles (directed NW, N, NE, E and SE) with reference values of 2.5, 5 and 10 ms^{-1} were used as air velocity inlets . Combustion products from chimneys were set as effluent velocity inlets. Results that are depicted from set boundary conditions give an insight to behaviour of pollutants in a crossflow. Many simplified models (based on Gaussian plume model and Briggs plume rise equations) exist for fast calculation of pollutant concentrations, but they are not accurate enough. Their validity is superimposed just on the flat or linearly growing terrain with smooth roughness. Those limitations are the main reason that we adopted full 3D turbulence model for the better simulations on a complex terrain.

2. Problem definition

In order to perform the simulation we needed to define geometry for a domain of consideration, mesh it and finally define boundary conditions. IDEAS CAD software was used to make geometry based on terrain topology (Figure 1.) and to generate unstructured tetrahedral mesh. Geometry was made as a 'box model' (in atmospheric modelling one of the most used one [3]) which bottom side was replaced with terrain-shaped surface and it represent a control volume for the finite volume method, a numerical method we used.

Figure 1. Terrain topology

3. Results and discussion

Whenever dealing with air pollution we have to be careful with validating obtained data. Problems rise with terrain complexity and real-time meteorology. If meteorology is missing then it is not possible to evaluate emissions in any way. It is just an insight in how pollutants disperse with respect to the topology of terrain. Figure 2 shows ground concentration of SO2 for the south wind. It is seen from the picture that the smoke plume is leaded with the flow field and so curving the plume to the left so that it passes right through the town of Bakar.

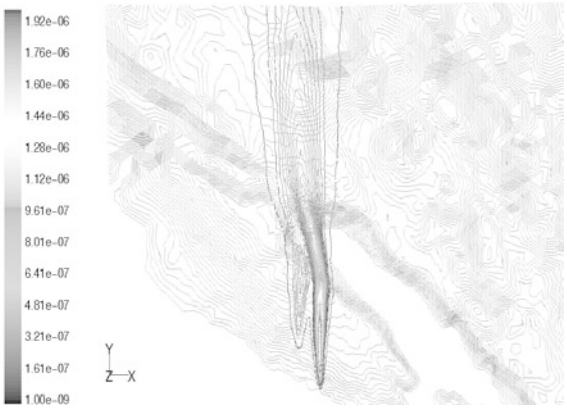

Figure 2. Ground concentrations of SO2 (kg/m^3) for South wind

4. Conclusion

Despite the lack of true meteorological boundary and initial conditions as it is accustomed in the field of atmospheric modelling, we obtained some useful and significant results. Ground concentrations of emissions from the chimneys have been investigated. The contour plots from figures shown before offer the insight on how flow field determines the path in which concentrations will be deployed on the ground. We haven't performed simulations for mainly jet dominated flows but we can guess that the plume will rise more and that concentrations measured on the ground need to be much lower.

References

[1] Westbrook, James A., Air Dispersion Models: Tools to Assess Impacts from Pollution Sources, American Bar Association, Natural Resources & Environment, Vol 13, No. 4, 1999. god.

[2] Zhang, X., Ghoinem, A. F., A computer model for the rise and dispersion of winf-blown, buoyancy-driven plumes – II. Linearly stratified atmosphere, United states Departement of Commerce, Technology Administration, National Institute of Standards and Technology, NIST-GCR-93-637, 1993.

[3] Zhang, Xiaoming & Ghoinem, Ahmed F., A computer model for the rise and dispersion of winf-blown, buoyancy-driven plumes – I. Neutrally stratified atmosphere, Pegamon Press Ltd., *Atmospheric Environment*, Vol. 27A, No. 15, str. 2295-2311, 1993.

Prof. dr. sc. Zoran Mrša, dipl. Ing.
University of Rijeka, Technical faculty, Department for fluid mechanics and computational engineering, Vukovarska 58, Rijeka, Croatia, +385 (0)51 651-500, +385 (0)51 651-290, mrsa@riteh.hr
Marko Čavrak, dipl. ing.
University of Rijeka, Technical faculty, Department for fluid mechanics and computational engineering, Vukovarska 58, Rijeka, Croatia, +385 (0)51 651-554, +385 (0)51 651-290, mcavrak@riteh.hr

4th International Congress
of Croatian Society of Mechanics
September, 18-20, 2003
Bizovac, Croatia

4thICCSM

ANTHROPODYNAMICAL STATUS OF THE CHILDREN SINCE THEIR BORN UP TO THE AGE OF TWO YEARS

Osman Muftić, Jasna Jurum –Kipke, Diana Milčić, Milivoj Novak

Keywords: *anthropometry, anthropodynamics, wire model, dynamical moments of inertia*

1. Introduction

Human measures, with this also at children, as a group of fundamental anthroplogical data, are widely elaborated in the specific literature. Unfortunately, there are mostly the data of adults and it is very seldom to find respective children's data and partially of the children since their born up to the two years. Knowing the values of these anthropometrical values are very important in a such examples when we use the biomechanics as the method of growing analysis.

2. Methods and materials

Harmonically constructed circle

The construction of harmonically circle is based according to Zederbauer on a regular triangle with hypo-tenuse a, and sides b, as it it shown in figure 1. After we draw over sides of triangle respective squares, we can finally draw the circle of radius R that passes through the peaks of a such geometrical construction. Mathematical relations between this geometrical values gives the harmonically numbers. Derived values of this relations are:

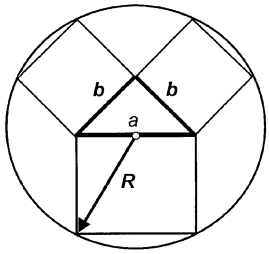

Figure 1. Harmonicall circle

$$a = 1; \quad R = \frac{\sqrt{5}}{2}; \quad b = \frac{\sqrt{2}}{2};$$

$$r = b - \frac{a}{2}; \quad d = R - \frac{a}{2}; \quad b + r.$$

which we call the harmonically determined numbers. This harmonically numbers were applied on a many natural and artistic examples showing surprised correlations between the dimensions of analysed objects or subjects.

3. Harmonically circle and the net of a body lengths canons

As the first step in children's dynamic anthropometry was in determination of the two main anthropometric characteristics as they are body length (standing height) and actual weight of the body as the functions of canonical and harmonically dependence. On the same way as we determined for adults so called eight head length canon, it is possible to apply four head length canon to the relations of the anthropomeasures at newborn babies as it is shown in the figure 2. Confirmation to this hypothesis we found in the relative relationships of the fundamental compositions of the newborns and adults, as it is shown in Table 1.

Table 1. Relative relationships of the body composition

Part	Newborn	Adult
Skin and fat	26%	25%
Intestines	16%	14%
Nerves	15%	3%
Muscles	25%	40%
Bones	18%	18%

According with the four head length canon of the newborn babies well as the children of two years, we established respective net in two directions. There are also obvious differences of the canons application to the children and the adult. Our research in the dynamical anthropomeasures of children resulted as first with prove of harmonically validity between the segmental and dimensional values. From the shape of the newborn baby in two directions located in the net of four squares we defined approximate ellipsoids respectively to the body parts, according to the Fig. 3. From this approximation we calculated out respective volumes of body parts as follows:

Head and neck - approximately: 655,0 cm^3
Trunk: 1962,5 cm^3
Hand: 226,9 cm^3
Leg: 250,0 cm^3.

Total volume, of a such body with lengths of 50 cm, is 3571,3 cm^3, what gives with specific density $\gamma = 1{,}09$ kg/dm^3 the new borne body mass of 3,9 kg.

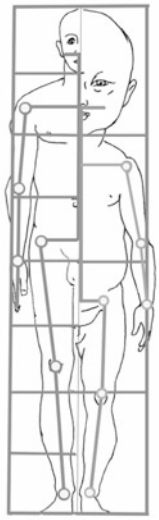

Figure 2. Comparative canons for an adult and newborn

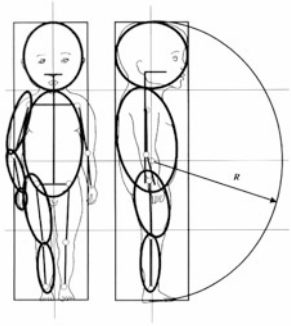

Figure 3. The contour of the newborn baby-4 head length canon

4. Conclusion

The established method of drawing the newborn's contours and wire model by the application of harmonically circle and four head length canon represents an easy and simple method with the use of which it is possible to determine the linear anthropomeasures of the new born baby of different height within normal limits directly from the knowledge of his height from head to heel. It is also shown a relative good correlation between harmonical values in different head length canons.

References

[1] Keros, P.: Temelji anatomije čovjeka, Zagreb: Medicinska Naklada, 1977.
[2] Muftić, O.: Harmonijska antropometrija kao osnova za primjenjenu dinamičku antropometriju, Zbornik radova Skupa o konstruiranju FSB, Zagreb: 1984.
[3] Muftić, O. Labar, J.: Sažeta formulacija dinamičkih antropomjera, Strojarstvo, 31: (4/6), pp 207 - 214, Zagreb, 1989.
[4] Muftić O.,:The Newborn Baby Anthropomeasures, Procc. of International Symposia Ergonomy 2001, Croatian Society of Ergonomics, Zagreb, Dec.2001.
[5] Zederbauer, E.: Die Harmonie im Weltal, in der Natur und Kunst, Orion Verlag, Wien und Leipzig, 1917.

Osman Muftić, Faculty of Mechanical Engineering, Univeristy of Zagreb, Ivana Lučića 5, 10000 ZAGREB, Croatia, +382-1-6168-222, osman.muftic@fsb.hr
Jasna Jurum–Kipke, Faculty of transportation, Zagreb; Diana Milčić, Faculty of Graphical Art, Zagreb
Milivoj Novak, Clinical Hospital Rebro, Zagreb

4th International Congress
of Croatian Society of Mechanics
September, 18-20, 2003
Bizovac, Croatia

4thICCSM

ANALYSIS OF THE NUMERICAL STABILITY IN THE SOLUTIONS OF THE SQUEEZE FILM DAMPER

J. Muller, E. Malenovský, F. Pochylý

Keywords: on field strain measurements, free diving fins, strain gages, polycarbonate

Abstract

This work is aimed at a movement of a stiff body in a real liquid, here is presented solid problem with small clearances between an inside body and outside bound. In the technical applications there are squeeze film dampers and hydrodynamics bearings. They are very often used in the rotor systems.

Squeeze film dampers together with roller bearings are used in the jet engines for reducing vibrations. Squeeze film damper is located between outer ring of roller bearing and engine frame. Radial clearance is rather small, only several decimals of millimeter. This hydrodynamics system added to a vibrating shaft additional effect, namely adding mass and adding damping. And this effect are very important and we can not neglect it.

In the literature is analysis of the squeeze film dampers very often publicize e.g. [1],[3]. Foundation all analyses is based on a Reynold‘s equation, it is motion equation of liquid. The liquid motion between inner and outer ring is assumed as one-dimensional flux by the straight line, whose length equals inner ring circumference, the pressure of the lubricant is constant in the radial direction. Are analyzed long and short, cavitatings and noncavitating squeeze film dampers and hydrodynamics bearings.

In this work is presented new access to analysis motion of the rigid body in the liquid. This access is based on a Navier-Stoke’s equation and was developed by F.Pochylý and E.Malenovský from VUT FSI, it is presented for example in [4]-[6]. The pressure in the radial direction is changeable, and the circumferential flow of the liquid is included. Using the suitable substitution, is possible to solve motion of the rigid body and the liquid separately. To analysis of the liquid motion is adopted control volumes method with Bézier body application.

The Bézier body is also used for description of a geometry configuration and also for approximation of speed and pressure function in curvilinear co-ordinates system [7]. Presented theory was pre-set in MATLAB programming code.

There are two approximation of the SFDs, namely long and short approximation. For a short damper $\partial p/\partial z >> \partial p/\partial \phi$, for a long damper $\partial p/\partial \phi >> \partial p/\partial z$. In this work is analyzed especially short SFD, which is a solid problem.

This is a new access to analysis, so we must compare this access and existing solutions based mostly on a Reynold’s equation. In this work are compared speed and pressure profiles and largely added effects. On the model examples are compared added effects for distinct geometrical dimensions and for distinct eccentricity of the outer ring of the journal in the squeeze film damper.

Important part is determination added effects depending on journal position in the damper. This effect must be included to the solution of the rotor system.

References

[1] El-Shafei A., Crandall S. H.: Fluid inertia forces in squeeze film dampers, ASME Rotating machinery and vehicle dynamics, DE-vol.35, 1991, pp.219-228

[2] Kramer E.: Dynamics of Rotor and Foundations, Springer-Verlag, Berlin, 1993

[3] El-Shafei, A.: Dynamics of rotor incomporating SFD, Ph.D. Thesis, Department of Mechanical Engineering, Massachusetts Institute of Technology, Cambridge, 1988

[4] Malenovský E., Pochylý F."The rigid body interaction with real liquid. Colloquium „DYNAMICS OF MACHINES 2000", Institute of termomechanics ASCR, Prague, 2000 Czech republic, pp 121-128

[5] Malenovský E., Pochylý F.: Computational Modeling of Velocity and Pressure Fields of Squeeze Film Dampers Using Navier-Stokes Eq., Proceedings Part III., Section No 9. Applied Mechanics, pp. 590-595

[6] Pochylý, F.,Malenovský, E., Hlavoň, P.: The nonstationary Motion of the Rigid Body in Real Liquid. 3rd Int. Conference Engineering Aero-Hydroelasticity, Prague, 1999, pp. 346-351

[7] Malenovský E.: Využití Bézierových entit v mechanice, Inženýrská mechanika , roč.7, 2000, č. 6, str 401-424

Acknowledgement:

The Grant Agency of the Czech Republic under grand no. CEZ: MSM 2600001 for which it is gratefully acknowledged supported this research work.

Ing. Jan Muller, VUT FSI Brno, Technická 2, 616 69 Brno, Czech republic, Tel.: +42054114 2335
e-mail: janmuller@centrum.cz

Doc. Ing. Eduard Malenovský, CSc.,VUT FSI Brno, Czech republic, Technická 2, 616 69 Brno,
Tel.:+420541142855,
e-mail: malenov@umtn.fme.vutbr.cz

Prof. Ing. František Pochylý, CSc., VUT FSI Brno, Technická 2, 616 69 Brno, Tel.: +42054114 2335,
e-mail: pochyly@khzs.fme.vutbr.cz.

4th International Congress
of Croatian Society of Mechanics
September, 18-20, 2003
Bizovac, Croatia

4thICCSM

QUADRILATERAL PLATE ELEMENT WITH INDEPENDENT ROTATIONAL D.O.F.

Ž. Nikolić and A. Mihanović

Keywords: thin plate, quadrilateral finite element, independent rotational d.o.f.

1. Introduction

The finite element models based on the displacement method are very popular in engineering. However, thin plate bending elements based on the Kirchhoff theory may cause unconvergence problems due to C^1 continuity requirement. Quadrilateral displacement element with 12 degrees of freedom and a polynomial expression does not satisfy the C^1 continuity requirement. Therefore, 12 d.o.f. plate element based on displacement method with the weaker continuity requirement, called non-conforming elements has become a challenge to many researches.

Many alternative ways for improving the behaviour of quadrilateral thin plate element in distorted mesh have been developed. The most significant of them are: hybrid stress element, discrete Kirchhoff element, generalized conforming element and refined non-conforming element.

An alternative way is modelling based on the Reissner-Mindlin theory instead of Kirchhoff theory. In this case only C^0 shape function continuity is required, hence an interpolation field is more easily constructed. In the most plate elements using Reissner-Mindlin assumptions, the interpolation used for the transversal displacements and the rotations involve the independent representation of each variable by its nodal values, usually with identical interpolations. To ensure a higher order of expansion for displacement, the concept of linked interpolation [1] of the displacement and rotations is introduced.

An independent representation of translational and rotational field and linking of them can be also used for improving the accuracy and convergence of quadrilateral thin plate element.

This paper presents a quadrilateral four-node thin plate bending element with a full compatibility of displacements and rotations at the nodes. The element has independent translational and rotational degrees of freedom at each node. This is in accordance with a unified approach to structural system modelling [2]. Similar element with independent translational and rotational d.o.f. and Hermitian shape functions has been developed in [3].

The shape functions for the approximation of the displacement field in this paper are determined from a polynomial of the fourth order. The different interpolation is used for translational and rotational part of the displacement field. The chosen shape functions satisfy the homogeneous differential equation of the thin plate bending and ensures a high order of interpolation for the plate displacement. The developed quadrilateral element has 12 degrees of freedom and posses very good performances.

2. Approximation of the displacement field

In this paper the finite elements with three degrees of freedom independent of each other are used, one translational displacement w_i perpendicular to the plate mid-plane and two rotational angles φ_i and θ_i around the two orthogonal axes located at the plate mid-plane. The unknown

displacement vector $\boldsymbol{u}_i$ at each node *i (i=1, ..., n)* of the plate element and the corresponding vector of the shape functions $\boldsymbol{N}_i$ can be represented as follows:

$$\boldsymbol{u_i} = [w_i, \varphi_i, \theta_i]^T, \qquad \boldsymbol{N_i} = \lfloor n_{iw}, n_{i\varphi}, n_{i\theta} \rfloor \tag{1}$$

where n_{iw} is the shape function with a unit translational displacement at the i-th node, while $n_{i\varphi}$ and $n_{i\theta}$ are the shape functions with a unit rotational angle around the local coodinate axes ξ and η, respectively. The shape functions at the first node are given with next expressions [4]:

$$\begin{aligned} n_{1w}(\xi,\eta) &= \frac{1}{8}\left(2 - 3\xi - 3\eta + 4\xi\eta + \xi^3 + \eta^3 - \xi^3\eta - \xi\eta^3\right) \\ n_{1\varphi}(\xi,\eta) &= \frac{1}{8}\left(1 - \xi - \eta + \xi\eta - \eta^2 + \xi\eta^2 + \eta^3 - \xi\eta^3\right) \\ n_{1\theta}(\xi,\eta) &= \frac{1}{8}\left(1 - \xi - \eta + \xi\eta - \xi^2 + \xi^2\eta + \xi^3 - \xi^3\eta\right) \end{aligned} \tag{2}$$

The shape functions satisfy the homogenous differential equation of the thin plate bending. Therefore, the equilibrium at the nodes is achieved without introducing the external forces.

The four-node plate element with independent translational and rotational d.o.f. is tested on few examples: a simply supported, clamped and corner supported square plate discretized by square and quadrilateral elements, a twisted ribbon and a skew simply supported plate. The results of computation are compared with analytical solution and also with those obtained with some other plate finite elements.

3. Conclusions

An arbitrarily quadrilateral thin plate finite element with independent translational and rotational degrees of freedom and different shape functions for the approximation of the displacement and rotations has been presented. The shape functions satisfy the homogeneous differential equation of the thin plate bending. The procedure for transforming the second-order derivatives of the shape functions from the local to the global coordinate system, which is necessary for evaluating a strain and stiffness matrix, is developed. Several examples analyzed to show a quality of the numerical solution. The numerical solution in the examples with a regular discretization (a square and a rectangular finite element) converges very fast to the exact solution. The increasing of the ratio of rectangular element sides has no influence on the numerical solution. The convergence of the numerical solution for discretization with parallelogram and arbitrarily quadrilateral finite elements is also achieved.

References

[1] Crisfield, M.A., "Non-linear Finite Element Analysis of Solids and Structures", Vol. 1, John Wiley, Chichester, Sussex, UK, 1991

[2] Ibrahimbegović, A., "A unified formulation for modelling of structural system: finite elements with rotational degrees of freedom", Int. Journal of Engineering Modelling, Vol. 3, No. 1-2, 1990, pp 21-27.

[3] A. Mihanović, A., Herak-Marović V. and Marović P., "The formulation of new fully compatible quadrilateral shell finite element", Int. Journal of Engineering Modelling, Vol. 6, No. 1-4, 1993, pp 1-11.

[4] Nikolić, Ž., "Contribution to the improvement of solutions on finite elements in frame structures and thin plates", Ph. D. Thesis, Faculty of Civil Engineering University of Split, Croatia, 1999

Željana Nikolić, professor
University of Split, Faculty of Civil Enginering, Matice Hrvatske 15, Split, Croatia,
tel: +385 21 303332, fax: +385 21 465117,
e-mail: zeljana.nikolic@gradst.hr

Ante Mihanović, professor
University of Split, Faculty of Civil Enginering, Matice Hrvatske 15, Split, Croatia,
tel: +385 21 303357, fax: +385 21 465117,
e-mail: ante.mihanovic@gradst.hr

4th International Congress
of Croatian Society of Mechanics
September, 18-20, 2003
Bizovac, Croatia

THE VIBRATIONS CYLINDER OF COMBINE HARVESTER

Pandurovic T.; Vujcic M. and Juric T.

Keywords: combine harvester, cylinder and flow load

1. Introduction

Combine harvesters are multiple machines composed of the harvesting and threshing machines, a grain tank, the driving motor with the energy transmitter and the steering and operating machine. All of these compose a technical whole lying on the solid construction frame with the cab for the driver. Both in Europe and in the rest of the world combine harvesters with tangential system of harvesting prevail. The grain mass (harvested grain crops) is brought in thin layer to the point between the cylinder and the grate concave. About 80% to 90% of the grain is separated from the grain mass by means of beaters within the rotating cylinder (Brkić, Kutzbach). The alternate rubbing of the grain mass layers creates friction forces and inertial forces (Meleg). The pressure generated is transmitted over the cylinder shaft onto the bearers, which is onto the construction frame of the combine (Pandurović). The experiments were performed in artificial conditions in order to get the cylinder load pressure quantitative assessment.

2. The Material and the Methods of Work

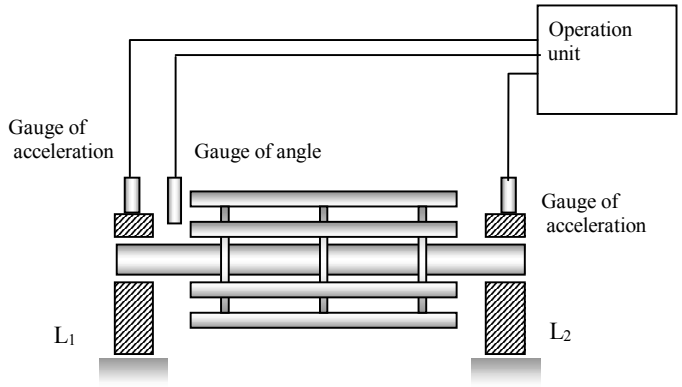

Figure 1. The Scheme of the vibrations on the bearers

To obtain the quantitative assessment of the threshing cylinder load pressure the vibrations (accelerations) were measured by means of an induction giver at B12/200 acceleration with frequency 200 Hz. Its signal is filtered in the operational unit - digital measuring amplifier DMC9012A, and with optical transducer OA1, so that the instruments display the amplitude values and the angle of the phase.

The HBM measuring equipment was used to measure the vibrations on the cylinder of Farm Liner Combine Harvester, produced by Đuro Đakovic – Županja who production was designed for family farms. The grain masses in different quantities were continually fed into the threshing unit.

Previously hand harvested grain mass was weighed for the mass flow, the spikes pointed forward were placed onto the 6.0 m long and 0.6 m wide conveyor.

3. Investigation Results

The obtained acceleration values depend on the grain mass flow and are approximated by a linear function as is:

$$a = 1.254 + 1.55 \cdot q \quad (1)$$

Where 1.254 = acceleration of empty work
q = the quantity of grain mass flow, kg/s
a = vertical acceleration of the bearer, m/s^2

Diagram 1. Graph showing the dependence of acceleration on the grain mass flow

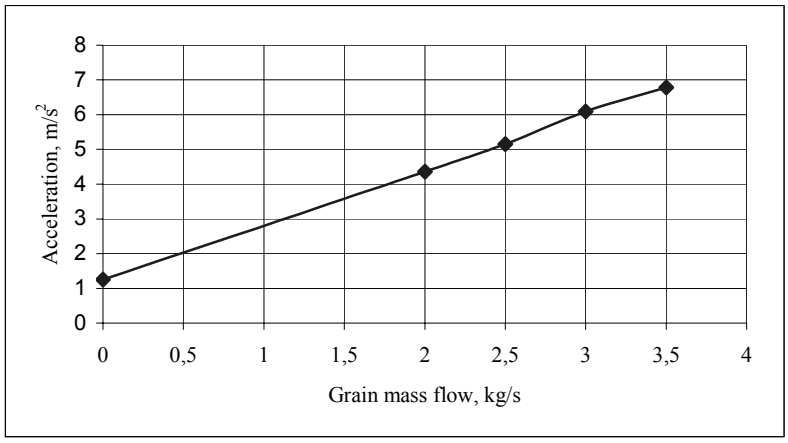

4. Conclusion

The grain mass flow is conveyed between the cylinder and the grate concave of the combine harvester. The beaters crash the ties between grains and wheat spikes generating friction and centrifugal forces by collision and rubbing the layers of grain mass. The experiment in artificial work conditions provided data of cylinder bearer vibrations. Statistics - mathematical analyses of the measuring results proved linear dependence of acceleration (and the load pressure) on the grain mass flow. The optimal mass flow of 3.5 kg/s increases the acceleration 4 times (and the load pressure) in comparison with the empty cylinder work. It means that work forces of grain separation (collision and friction force) are three times higher compared to idle centrifugal force. Low idle vibrations indicate quality balance whereas resonance lack show quality threshing cylinder construction.

References

[1] Brkić, D.; Vujčić, M. & Sebastijanović, S. "Razvojne tendencije univerzalnih žitnih kombajna", Proceedings of 5th International Research/Expert Conference, Brdarević, S., Mašinski fakultet Zenica, Zenica B&H, October 2000, pp 507-514.

[2] Kutzbach, D., "Efficient Crop Harvest", Proceedings of 28th Symposium Actual Tasks on Agricultural Engineering, Košutić, S. Zavod za mehanizaciju poljoprivrede Agronomskog fakulteta Zagreb (Ed), Opatija Hr, February 2000, pp 55-61.

[3] Meleg, J., "Analytické riešenie procesu mlátenia, separácie a poškodenia zrna mlátacími ústrojenstvami", *Acta technologica agriculture*, XXIV, Nitra 1983, pp 7-13.

[4] Pandurović, T., "Dinamička opterećenja bubnja vršalice žitnog kombajna", (magistarski rad), Fakultet strojarstva i brodogradnje Zagreb 2002.

Mr. sc. T. Pandurović, Dr. sc. M. Vujčić, Dr. sc. T. Jurić,
Faculty of Agricultural in Osijek - Dept. of Agricultural Engineering Vinkovci, Genscherova 16, 32000 Vinkovci, Croatia, Phone: 00385 32 306303, Fax: 00385 32 306304, E-mail: pando@pfos.hr; E-mail: vmate@pfos.hr: E-mail: pfmv@vk.tel.hr.

4th International Congress
of Croatian Society of Mechanics
September, 18-20, 2003
Bizovac, Croatia

4thICCSM

ON THE STRESS DISTRIBUTION IN THIN-WALLED BEAMS SUBJECTED TO BENDING WITH INFLUENCE OF SHEAR

Radoslav Pavazza and Branko Blagojević

Keywords: Thin-walled beams, bending, influence of shear, stresses

1. Introduction

The bending theory of thin-walled beams with influence of shear will be considered. The analytical solution for stress distributions will be investigated

2. Stresses in thin-walled beams subjected to bending with influence of shear

The shear stresses are

$$\tau_{x\xi}=\frac{Q_y S_z^*}{I_z t}+\frac{Q_z S_y^*}{I_y t};\quad A^*=\int_{s^*}\mathrm{d}A^*,\quad \mathrm{d}A^*=t\mathrm{d}s^*,\quad S_z^*=\int_{s_v^*} y\,\mathrm{d}A^*,\quad S_y^*=\int_{s_w^*} z\,\mathrm{d}A^*$$

where $Q_y=Q_y(x)$ and $Q_z=Q_z(x)$ are the shear forces with respect to y and z-axis.

The normal stresses are obtained as

$$\sigma_x=\frac{M_y}{I_y}z+q_z\frac{E}{GA_{rz}}z-q_z\frac{E}{GI_y}\int_0^{s_w}\frac{S_y^*}{t}\,\mathrm{d}s-\frac{M_z}{I_z}y+q_y\frac{E}{GA_{ry}}y-q_y\frac{E}{GI_z}\int_0^{s_v}\frac{S_z^*}{t}\mathrm{d}s+$$
$$+\frac{q_y E}{GA_{r,zy}}z+\frac{q_z E}{GA_{r,yz}}y+\frac{\tilde{N}_z}{A}+\frac{\tilde{N}_y}{A}+\frac{\tilde{B}_z}{I_\omega}\omega+\frac{\tilde{B}_y}{I_\omega}\omega$$

where $M_y=M_y(x)$ and $M_z=M_z(x)$ are the bending moments with respect to y and z-axis;

$$A_{ry}=\frac{A}{\kappa_y},\quad \kappa_y=\frac{A}{I_z^2}\int_A\left(S_z^*/t\right)^2\mathrm{d}A;\quad A_{r,yz}=\frac{A}{\kappa_{yz}},\quad \kappa_{yz}=\frac{A}{I_y I_z}\int_L\left[\left(S_z^*S_y^*\right)/t\right]^2\mathrm{d}s$$

$$A_{rz}=A/\kappa_z,\quad \kappa_z=\left(A/I_y^2\right)\int_A\left(S_y^*/t\right)^2\mathrm{d}A,\quad A_{r,zy}=A_{r,yz},\quad \kappa_{zy}=\kappa_{yz}$$

$$\tilde{N}_y=q_y\frac{E}{GI_z}\int_L\frac{A_y^*S_z^*}{t}\mathrm{d}s,\quad \tilde{N}_z=q_z\frac{E}{GI_y}\int_L\frac{A_z^*S_y^*}{t}\mathrm{d}s,\quad \tilde{B}_y=q_y\frac{E}{GI_z}\int_L\frac{S_z^*S_\omega^*}{t}\mathrm{d}s$$

$$\tilde{B}_z=q_z\frac{E}{GI_y}\int_L\frac{S_y^*S_\omega^*}{t}\mathrm{d}s,\ \tilde{M}_z=-q_y\frac{E}{GI_z}\int_L\left(S_z^*/t\right)^2\mathrm{d}A,\quad \tilde{M}_y=q_z\frac{E}{GI_y}\int_L\left(S_y^*/t\right)^2\mathrm{d}A$$

$$I_y=\int_A z^2\mathrm{d}A,\ I_z=\int_A y^2\mathrm{d}A,\quad A_z^*=\int_{s_1^*}\mathrm{d}A^*,\ \mathrm{d}A^*=t\mathrm{d}s_1^*,\ A_y^*=\int_{s_2^*}\mathrm{d}A^*,\mathrm{d}A^*=t\mathrm{d}s_2^*$$

In the case of the cross-sections with one axis of symmetry (for example, z-axis):

$$\sigma_x=\frac{M_y}{I_y}z+q_z\frac{E}{GA_{rz}}z-q_z\frac{E}{GI_y}\int_0^{s_w}\frac{S_y^*}{t}\,\mathrm{d}s-\frac{M_z}{I_z}y+q_y\frac{E}{GA_{ry}}y-q_y\frac{E}{GI_z}\int_0^{s_v}\frac{S_z^*}{t}\mathrm{d}s+\frac{\tilde{N}}{A}+\frac{\tilde{B}_z}{I_\omega}\omega$$

where due to the symmetry $A_z^*S_z^*=0$, $S_z^*S_y^*=0$, $S_z^*S_\omega^*=0$.

In the case of the cross-sections with two axes of symmetry:

$$\sigma_x = \frac{M_y}{I_y} z + q_z \frac{E}{GA_{rz}} z - q_z \frac{E}{GI_y} \int_0^{s_w} \frac{S_y^*}{t} \, \mathrm{d}s - \frac{M_z}{I_z} y + q_y \frac{E}{GA_{ry}} y - q_y \frac{E}{GI_z} \int_0^{s_v} \frac{S_z^*}{t} \mathrm{d}s \, .$$

where due to the symmetry $A_z^* S_z^* = 0$, $A_y^* S_y^* = 0$, $S_z^* S_y^* = 0$, $S_z^* S_\omega^* = 0$, $S_y^* S_\omega^* = 0$

3. Illustrative example

For bending in the vertical plane the normal stresses may be expressed as

$$\sigma_x = \phi \frac{M_y}{I_y} z \, , \quad \phi = \left(1 + \chi' - \chi'' - \chi'''\right)$$

$$\chi' = \frac{E}{G} \cdot \frac{q_z}{M_y} \cdot \frac{\int_A \left(S_y^* / t\right)^2 \mathrm{d}A}{I_y} \, , \quad \chi'' = \frac{E}{G} \cdot \frac{q_z}{M_y} \cdot \frac{\int_0^s \left(S_y^* / t\right) \mathrm{d}s}{z} \, , \quad \chi''' = \frac{E}{G} \cdot \frac{q_z}{M_y} \cdot \frac{\int_A \left(A_z^* S_y^* / t^2\right) \mathrm{d}A}{Az}$$

For the T-section $b_1 = h$, $t_1 = t$, for simply supported beam under uniformly distributed transverse load, $M_y = q_z l^2 / 8$, $E/G = 2{,}6$:

$\chi' = 5{,}512 \left(h/l\right)^2$; $\chi_1'' = 5{,}633 \left(h/l\right)^2$, $\chi_2'' = 3{,}910 \left(h/l\right)^2$; $\chi_1''' = -1{,}298 \left(h/l\right)^2$, $\chi_2''' = 0{,}433 \left(h/l\right)^2$,

where l is the beam length. Thus, for $s = -h_1$ and $s = h_2$, respectively:

$$\sigma_{1x} = \phi_1 \frac{M_y}{I_y} h_1 \, , \quad \phi_1 = 1 + \chi' - \chi_1'' - \chi_1''' = 1 + 1{,}177 \left(h/l\right)^2$$

$$\sigma_{2x} = \phi_2 \frac{M_y}{I_y} h_2 \, . \quad \phi_2 = 1 + \chi' - \chi_2'' - \chi_2''' = 1 + 1{,}169 \left(h/l\right)^2$$

4. Comparison with finite element method

The beam is modelled by quadrilateral membrane elements; the case $h/l = 1/5$ by 1440 elements, and the case $h/l = 1/3$ by 1536 elements; $E = 210$ GPa and $\nu = 0{,}3$.

Table 1. Comparison of the results of the analytic solution and FEA

	ϕ_1	FEA	Δ_1	ϕ_2	FEA	Δ_2
h/l=1/5	1,047	1,045	0,2	1,047	1,046	0,1
h/l=1/3	1,131	1,145	1,2	1,130	1,135	0,4

Here $\Delta = \left(\left|\text{FEA-}\phi_1\right| / \phi_1\right) \cdot 100$ and $\Delta = \left(\left|\text{FEA-}\phi_2\right| / \phi_2\right) \cdot 100$.

5. Conclusion

The stress distributions for bending with influence of shear of thin-walled beams are obtained in the closed analytical form. It is assumed that normal stresses in the transverse direction are small compared to the normal stresses in the longitudinal direction. The expressions are obtained for the beams with general thin-walled cross-sections.

The comparison with the results of the finite element analysis of a thin-walled beam with T-section subjected to uniform transverse loads has shown a high agreement of the obtained results.

Radoslav Pavazza, prof.
Faculty of Electrical Engineering, Mechanical Engineering and Naval Architecture, University of Split, Ruđera Boškovića bb, 21000 Split, Croatia, E-mail address: radoslav.pavazza@fesb.hr
Branko Blagojević, assis.
Faculty of Electrical Engineering, Mechanical Engineering and Naval Architecture, University of Split, Ruđera Boškovića bb, 21000 Split, Croatia, E-mail address: branko.blagojevic@fesb.hr

4th International Congress
of Croatian Society of Mechanics
September, 18-20, 2003
Bizovac, Croatia

4thICCSM

CONSTITUTIVE MODEL FOR TRANSIENT THERMAL CREEP IN CONCRETE

C.J. Pearce, N. Bićanić, C. Nielsen

Keywords: concrete at high temperature, transient thermal creep

When concrete is heated to several hundred degrees Celsius, its behaviour is altered significantly, becoming highly non-linear. This is an important issue to include when concrete is to be modelled and analysed under simultaneous loading and heating. The mechanical properties such as strength and modulus of elasticity are generally found to be decreasing with temperature, while high temperatures are found to significantly enhance the time dependent creep characteristics. Furthermore, a constitutive model also has to include the important experimental finding that alterations in strength, stiffness and creep depend on the combined load and temperature history. A simple constitutive model for concrete behaviour under transient temperatures has been proposed based upon a rheological model suggested by Thelandersson (1987). The total strain is decomposed into pure mechanical strain, free thermal strain and load induced thermal strain.

$$\dot{\boldsymbol{\varepsilon}} = \dot{\boldsymbol{\varepsilon}}^{m}\left(T,\boldsymbol{\sigma}\right) + \dot{\boldsymbol{\varepsilon}}^{ft}\left(T\right) + \dot{\boldsymbol{\varepsilon}}^{c}\left(T,\boldsymbol{\sigma}\right) + \dot{\boldsymbol{\varepsilon}}^{tm}\left(T,\boldsymbol{\sigma}\right) \tag{1}$$

where the last term is often termed transient creep and includes temperature dependent conventional creep and thermal-mechanical strain, whereas the conventional creep is ignored. The load induced thermal strain, corresponding to the last two terms of eq (1), is determined experimentally by measuring total strains during first time heating on a concrete specimen under sustained loading. The free thermal strain, recorded on an unstressed specimen, and the initial elastic strain are subtracted from the total strain to give the load induced thermal strain (or transient creep) as a function of temperature. The thermal-mechanical strain is irreversible and occurs only during first heating due to the combination of stress and temperature increase. During heating these strains relax the stresses arising from thermal gradients and incompatibilities between the aggregate and the cement paste. Significantly, however, the irreversibility of the thermal-mechanical strain leads to the build up of tensile restraining stresses during cooling. The model introduces a parabolic expression to describe the uniaxial thermal-mechanical response, whereby β^{-} is a bi-linear function of temperature. Here it is assumed that the load induced thermal strain is restricted to compression only

$$\dot{\varepsilon}_{ij}^{tm} = \frac{\beta^{-}}{f_c^{T_0}}\left(\left(1+\nu_c\right)\sigma_{ij}^{-} - \nu_c\sigma_{kk}^{-}\delta_{ij}\right)\dot{T}\,\mathrm{sgn}\left(\dot{\omega}\right) \tag{2}$$

where β^{-} is the coefficients of compressive and uniaxial thermo-mechanical strain respectively. $\boldsymbol{\sigma}^{-}$ is the negative projection of the stress tensor, and the $\mathrm{sgn}\left(\dot{\omega}\right)$ has been introduced to recognise the irreversible nature of thermo-mechanical strains. Furthermore, a transient creep Poisson's ration is introduced to describe the corresponding lateral thermal-mechanical response. Loss of strength

and stiffness due to mechanical processes is included via a coupled plasticity/damage formulation and thermal damage is included via the introduction of thermal damage parameter

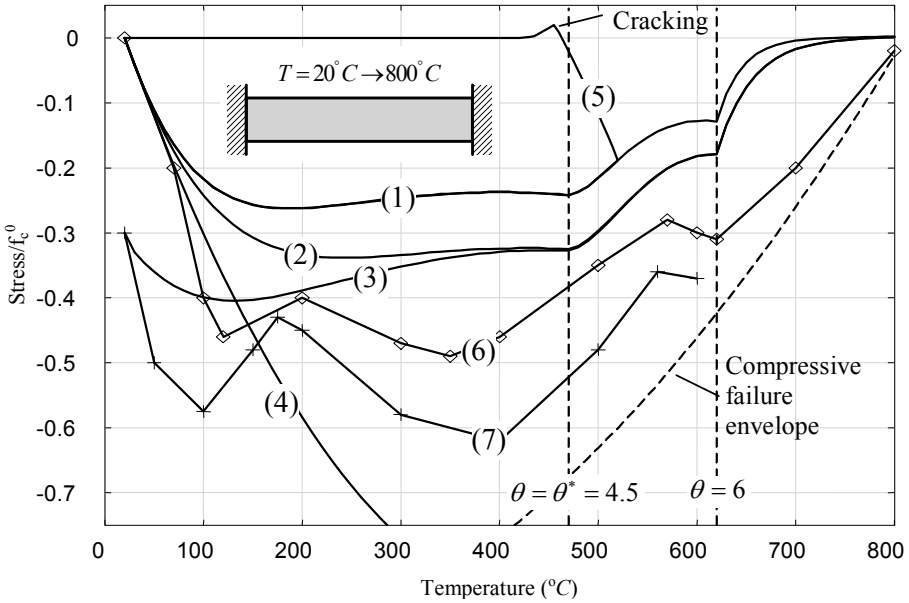

Figure 1. Load induced thermal strain. Numerical predictions compared to experimental results. (1) Set 1, Figure 3; (2) Set 2, Figure 3; (3) Set 2 plus initial prestress $\sigma = -0.3f_c^0$; (4) No thermo-mechanical strains; (5) Set 2 plus cooling from 480 ^oC; (6) & (7) Experimental results, Ehm (1986) and Schneider (1986). ($E_0/f_c^0 = 500$).

Figure 1 illustrates the effect that transient creep has on the response of the concrete member, whereby the stresses are significantly relaxed as compared to the response obtained when the thermal-mechanical strains were omitted. Moreover, Curve 5 illustrates the effect that transient thermal creep can have on such restrained structural concrete members; on cooling the thermal-mechanical strains are not recovered and therefore there is significant potential for cracking to occur (Rankine yield criterion adopted for the tensile response).

Acknowledgements

The third author was a Marie Curie Fellow funded by the European Commission under FP5, the Fifth Framework Programme (contract no. HPMF-CT-1999-0171).

References

[1] Bazant, Z.P. & Kaplan, M.F. 1996. Concrete at high temperatures, Material properties and mathematical models. Essex, England: Longman Group Ltd.

[2] Khoury, G.A., Grainger, B.N. & Sullivan, P.J.E. 1985. Transient thermal strain of concrete: literature review, conditions within specimens and behaviour of individual constituents. *Mag. of Concr. Res.* 37(132):131-144..

[3] Nielsen, C.V., Pearce, C.J. & Bicanic, N., 2002. Constitutive model of transient thermal strains for concrete at high temperatures. Submitted to *J. Engng. Mech.*

[4] Schneider, U. 1986. *Properties of materials at high temperatures, concrete, 2nd Edition,* RILEM Technical Committee 44-PHT, Technical University of Kassel, Kassel, Germany.

[5] Thelandersson, S. 1987. Modelling of combined thermal and mechanical action in concrete. J. Engng. Mech. 113(6):893-906.

Dr Chris Pearce
Department of Civil Engineering, University of Glasgow, Glasgow, UK, pearce@civil.gla.ac.uk
Dr Claus Vestgaard Nielsen
Danish Technological Institute, Copenhagen, Denmark
Prof Nenad Bićanić
Department of Civil Engineering, University of Glasgow, Glasgow, UK, bicanic@civil.gla.ac.uk

4th International Congress
of Croatian Society of Mechanics
September, 18-20, 2003
Bizovac, Croatia

INVESTIGATIONS OF WIND PROFILES AT THE DUBROVNIK LOCATION

Bernardin Peroš, Ivica Boko and Tihomir Šimunović

Keywords: Bora wind, second values, wind profile, turbulent characteristics

1. Introduction

Special profile measurements of the second values of the wind velocity and direction were performed in the period 14.03.2002. – 15.05.2001. at the construction site of the Dubrovnik bridge. The measurements were taken at the altitudes of 10, 52 and 140 m for one profile (cross-section) and at the elevation of 52 m at another profile, at a distance of 300 m from the first one. The investigations have shown that the 10-minutes averaging period is not sufficient to give a correct presentation of the turbulent characteristics of Bora in the Croatian coastal region and on the islands and that it is necessary to have the shortest possible averaging period the wind velocity with the required knowledge of the vertical change in the wind direction and velocity.

The paper deals with the data of the first second value profile measurements in Croatia performed in 2001 at the Dubrovnik location.

2. Profile measurements and turbulent characteristics of the Bora wind

The presented relationship between the maximum wind gusts and velocities averaged at intervals of 1, 10, 60 and 600 seconds (10 minutes) show that the Bora wind in the Dubrovnik region is a locally catabatic wind with a highly changeable intensity. This is particularly important considering the dynamic wind action upon the structures and it represents an entirely different load from those caused by stable winds with different directions (such as Jugo).

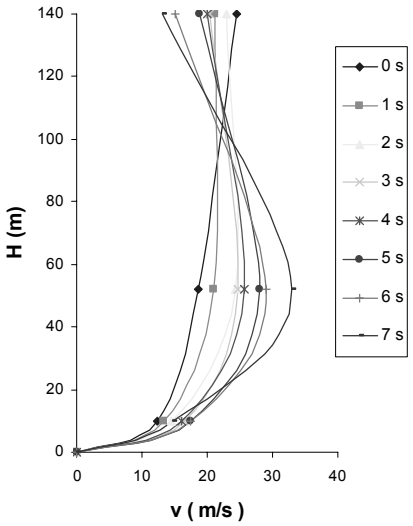

Figure1: Profile changes of the wind velocity

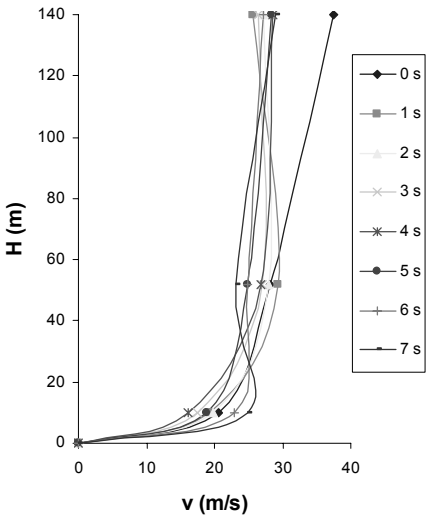

Figure 2: Profile changes of the wind velocity

Additional analysis of profile measurements points to the turbulent characteristics of the Bora wind where in the change of 1 second wind velocity were analyzed at the measurement points of the first profile for two characteristic cases (Figures 1 and 2).

It should be noted that the changes in the Bora velocity considering altitude significantly differ from the wind profile recorded in literature, which is especially evident when in our case the wind velocity constantly changes and in most cases the values decrease with the profile height.

Turbulent characteristics of the Bora are best described by the difference between the turbulence intensity (I_v) for specific wind velocities averaged at different time intervals and the value of the catabatic factor (F_M) which has been defined by the ratio between the maximum instantaneous wind velocity and the maximum average wind velocity at an interval.

In this paper the turbulence intensity was computed by using available data in two ways:

I_{vl} - as a ratio between the standard deviation of the average interval of wind velocity and the average interval wind velocity and as

I_{v2} - as the ratio between the standard deviation 1 sec, i.e. 1 min and the average minute, i.e. 10 minute wind velocity

According to the data available in Dubrovnik it is possible to compute the catabatic factor as:

F_{M1} - ratio between the maximum wind gusts and the average wind velocity

F_{M2} - ratio between the maximum gust and the maximum gusts at averaging intervals

3. Discussion and conclusion

The results of 1 second profile measurements of the Bora, a dynamic and locally catabatic wind, were analyzed.

Special attention was paid to the turbulence characteristics of the wind dependent upon the averaging interval of the measured wind velocity (1 second, 10 seconds, 60 seconds and 600 seconds) in order to determine the excitations (dynamic) action of the wind upon slender high structures.

The obtained values of the turbulence intensity I_v and the catabatic factor F_M (Table 2) and the recorded measurements of the wind velocities at each point (Figure 4-7) evidently prove that the turbulent component of the wind is better expressed for the wind with shorter averaging periods – second values of wind velocity.

Subsequently, it can be concluded that the 10 minutes averaging period recommended by Euronorms as a reference velocity for structures with a wind load is not sufficient to determine the real values of the turbulent characteristics of the Bora and they should be determined, in cases of high slender structures (with a dominant wind load) according to the second values measurements of the wind. These investigations represent meteorological basis for the development of the Croatian regulations for the dynamic wind load upon structures.

References

[1] B. Smith, Aerial Observations of the Croatian Bora, Collection Meteorological and Hydrologic Works, Vol. 10, pp. 127-129, Opatija, 1984.

[2] B. Peroš, Modelling of the Bora effects upon the lower layer, International Journal for Engineering Modelling, vol.7, No. 3-4, PP 81-95, 1994.

[3] B. Peroš, Reliability of Structures with a Dominant Wind Load, Ph. D. Thesis, Faculty of Civil Engineering, University of Zagreb, Zagreb, 1995.

[4] E. Shettini; G. Solari: Probability distribution and statistical moments of the maximum wind velocity, Wind and structures 1, 1998.

Bernardin Peroš, Prof. dr. sc., CEng, Full Professor
University of Split, Faculty of Civil Enginering, Matice Hrvatske 15, HR-21000 Split, Croatia,
tel: + 385 21 303331, fax: + 385 21 303331, e-mail: bernardin.peros@gradst.hr

Ivica Boko, Mr. sc., CEng, Assistent
University of Split, Faculty of Civil Enginering, Matice Hrvatske 15, HR-21000 Split, Croatia,
tel: + 385 21 303330, fax: + 385 21 303331, e-mail: ivica.boko@gradst.hr

Tihomir Šimunović, CEng, Assistent
University of Split, Faculty of Civil Enginering, Matice Hrvatske 15, HR-21000 Split, Croatia,
tel: + 385 21 303330, fax: + 385 21 303331, e-mail: tihomir.simunovic@gradst.hr

4th International Congress
of Croatian Society of Mechanics
September, 18-20, 2003
Bizovac, Croatia

4thICCSM

CONSTRUCTION OF BIFURCATION DIAGRAMS OF VAN DER POL – DUFFING OSCILLATOR

Rudolf R. Pušenjak, Maks M. Oblak

Keywords: *Van der Pol – Duffing oscillator, incremental harmonic balance, multiple time scales, bifurcation diagrams*

1. Introduction

The paper treats application of incremental harmonic balance method (IHBM) combined by multiple time scales for computing the steady-state periodic or almost periodic response of nonlinear dynamical system, which instead of the time domain applies the frequency domain. In this paper, IHBM with multiple time scales will be applied to treat a nonlinear dynamical system governed by van der Pol – Duffing equation:

$$\frac{d^2u}{dt^2} - \varepsilon\left(1-\mu u^2\right)\frac{du}{dt} + \Omega_0^2 u + \alpha u^3 = f\cos\left(\omega t + \varphi\right) \tag{1}$$

The time response of van der Pol – Duffing oscillator is formulated in terms of one time scale $\tau_1 = \eta\omega_1 t$ for periodic oscillations and by two time scales $\tau_1 = \eta\omega_1 t$ and $\tau_2 = \eta\omega_2 t$ for almost periodic oscillations. The periodic response is composed from harmonics of the fundamental frequency $\omega_1 = \omega$ so that all frequencies involved are commensurate. Opposite to this, an almost periodic response is composed from combination tones of noncommensurate frequencies ω_1, ω_2.

2. Method

By expanding all terms in Taylor series about the initial or guessed solution and keeping only expansions, which are linear in increments we first linearize equation (1) and then apply the Galerkin procedure to obtain linear algebraic system of equations for unknown Fourier coefficient increments:

$$\mathbf{H}\cdot\Delta\mathbf{a} = \mathbf{R} + \Delta\mathbf{F} - \sum_{k=1}^{M_S}\eta\Delta\omega_k\mathbf{Q}_k \tag{2}$$

Instead of parametrization with natural parameter, which fails in turning points, we introduce the parametrization by the arc lenght of the curve. The improved arc length continuation is used also to obtain equations of tangents in period doubling points. The stability of solutions is determined in terms of multiple time scales by using Floquet theory.

3. Computer simulation results

The paper presents construction of a bifurcation diagram for hinged – hinged beam. Small deflections $w(x,t)$ of the beam from the equilibrium are described by means of the dimensionless variables:

$$\frac{\partial^2 w}{\partial \bar{t}^2} + c\frac{\partial w}{\partial \bar{t}} + \left[\Gamma - K\int_0^1 \left(\frac{\partial w}{\partial \bar{x}}\right)^2 d\bar{x} \right] \frac{\partial^2 w}{\partial \bar{x}^2} + \frac{\partial^4 w}{\partial \bar{x}^4} = \bar{F}\left(\bar{x},\bar{t}\right) \tag{3}$$

With nondimensional bending force $\bar{F}\left(\bar{x},\bar{t}\right) = f\cos n\bar{\omega}\bar{t}\,\sin\pi\bar{x}$ and sinusoidal deflections w along the coordinate $\bar{x}$:

$$w\left(\bar{x},\bar{t}\right) = u\left(\bar{t}\right)\sin\pi\bar{x} \tag{4}$$

one obtains Duffing equation, which describes the time dependence of the beam deflections:

$$\frac{d^2u}{d\bar{t}^2} + c\frac{du}{d\bar{t}} - \pi^2\left(\Gamma - \pi^2\right)u + \frac{1}{2}K\pi^4u^3 = f\cos\left(n\bar{\omega}\bar{t}\right) \tag{5}$$

When nondimensional axial force takes the Euler critical value $\Gamma = \pi^2$, equation goes over on the form:

$$\frac{d^2u}{d\bar{t}^2} + c\frac{du}{d\bar{t}} + \frac{1}{2}K\pi^4u^3 = f\cos\left(n\bar{\omega}\bar{t}\right) \tag{6}$$

The beam bending in dependence on amplitude of exciting force is the basis for construction of bifurcation diagram with a very rich structure, which finally lead even to the chaotic oscillations. An example of such diagram is computed by IHBM with one time scale, $M_S = 1$ and is shown on the Fig.1, where is supposed, that beam is loaded by nondimensional bending force $\bar{F}\left(\bar{x},\bar{t}\right) = f\cos 2\bar{\omega}\bar{t}\,\sin\pi\bar{x}$.

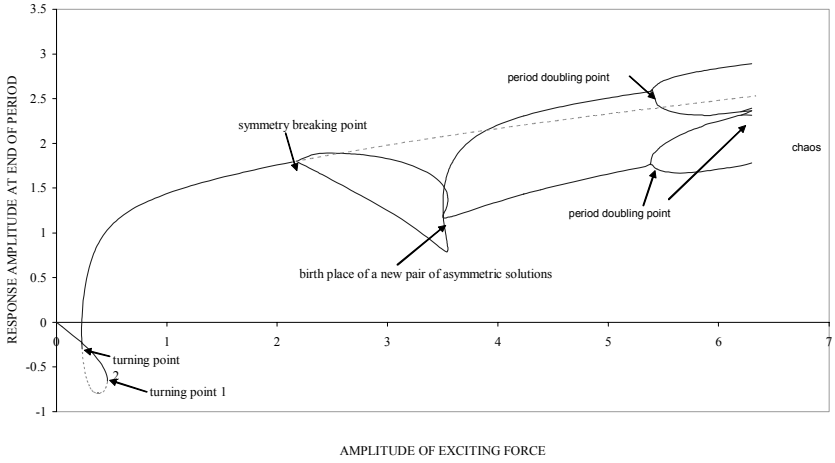

Figure1. Bifurcation diagram of beam bending response in dependence on exciting amplitude. —— stable solution, ----- unstable solution

As second example, the simulation results of amplitude curves of van der Pol-Duffing oscillator, which correspond to periodic and almost periodic oscillations are presented.

References

[1] Pušenjak,R., "Analiza nelinearnih oscilatorjev z več prostostnimi stopnjami – Analysis of Nonlinear Oscillators with Finite Degrees of Freedom". *Strojniški vestnik*. Vol.43,No. 5-6, 1997, pp.219-230.

[2] Pušenjak,R., Oblak, M., "Fundamental and Combination Resonances by Incremental Harmonic Balance Method and Multiple Time Scales". 3rd International Congress of Croatian Society of Mechanics, Cavtat, September 28-30,2000, pp. 499-506.

[3] Seydel, R., "Practical Bifurcation and Stability Analysis. From Equilibrium to Chaos". Second Edition; New York, Springer-Verlag, 1994.

[4] Friedmann, P., Hammond, C., E., and Woo, T.-H., "Efficient Numerical Treatment of Periodic Systems with Application to Stability Problems". International Journal for Numerical Methods in Engineering; Vol. 11, No. 7, 1977, pp.1117-1136.

4th International Congress
of Croatian Society of Mechanics
September, 18-20, 2003
Bizovac, Croatia

4thICCSM

AN ANALYTICAL ELASTIC - PLASTIC SOLUTION OF CRACK TIP OPENING DISPLACEMENT

Dragan Pustaić and Martina Lovrenić

Keywords: *Elastic-Plastic Fracture Mechanics, Dugdale Strip Yield Model, Plastic Zone, Crack Tip Opening Displacement, Analytical Methods of the Complex Variable*

1. Introduction

A thin plate with a straight crack is considered. The crack is loaded with two pairs of co-linear, concentrated compressive forces which act on the surface of the crack and open it, while the edges of the plate are free of loading. Two parameters of elastic-plastic fracture mechanics, i.e. the magnitude of the plastic zone around the crack tip r_p and the crack tip opening displacement δ_t are analyzed in this paper. Analytical methods of the theory of functions with complex variables are used in the analysis of these two parameters. The Dugdale plasticity model is used for modelling narrow plastic zones around the crack tips.

2. Definition of boundary conditions; loading and geometry of a plate

In this paper, we consider a thin, infinite plate ($z \in D$, D: $|z| \geq 0$) with a straight crack of a length $2a$, placed on the axis x ($z \in L$, L: $|\mathrm{Re}\, z| \leq a$, $\mathrm{Im}\, z = 0$). The boundary conditions on the free edges of the plate can be written as follows

$$\sigma_{xx} = 0 \ , \quad \sigma_{yy} = 0 \ , \quad \sigma_{xy} = 0 \ , \qquad \text{for} \qquad |z| \to \infty \ . \tag{1}$$

The additional boundary conditions for the crack surface are

$$\sigma_{xx} \neq 0 \ , \quad \sigma_{xy} = 0 \ \text{ and } \ \sigma_{yy} = 0 \ , \qquad \text{for} \qquad z \in L \tag{2}$$

except in the points $\mathrm{Re}\, z = \pm c$ and $\mathrm{Im}\, z = 0$ where the following condition must be satisfied

$$\lim_{A_0 \to 0} \int_{A_0} \sigma_{yy} \, \mathrm{d}A = F \ . \tag{3}$$

3. Equations of the plane theory of elasticity in a complex range

In this paper, equations, which give the basic combinations of stresses and displacements, will be transformed by introducing a new analytical function of a complex variable $Z(z)$, so that $Z(z) = 2\,\varphi'(z)$. The considered equations have assumed the following form

$$\begin{aligned} &\sigma_{xx} + \sigma_{yy} = Z(z) + \overline{Z(z)} \, , \\ &\sigma_{yy} - \sigma_{xx} + 2\mathrm{i}\sigma_{xy} = 2A - (z - \bar{z})\, Z'(z) \, , \\ &2\mu(u + \mathrm{i}v) = \frac{1}{2}\left[\frac{3 - \nu}{1 + \nu} \int Z(z)\mathrm{d}z - \int \overline{Z(z)}\, \mathrm{d}\bar{z} - (z - \bar{z})\, \overline{Z(z)} \right] - A\,\bar{z} \, . \end{aligned} \tag{4}$$

In the expressions (4), A is a real constant, μ is a shear modulus, and ν is Poisson's ratio.

4. Cohesive zone around a crack tip

According to the Dugdale model, the plastic zone is a narrow strip extending from the crack tip in the direction of the crack plane (Figs.1a and 1b). The Dugdale model considers, instead of a real,

physical crack, an *equivalent elastic crack* of length 2*b* (Fig.1c). Sections of this imaginary elastic crack $a \le x \le b$ are subjected to *constant cohesive stresses* σ_Y (Fig.1c).

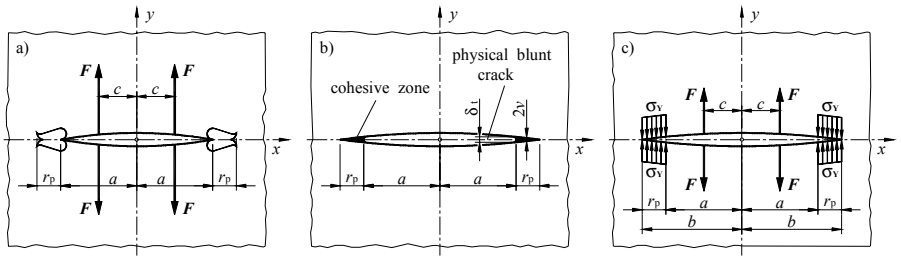

Figure 1. a) Loading on the crack, b) Plastic zones around crack tips, c) Constant cohesive stresses $\sigma_{yy}(x) = \sigma_Y$ on a section of an imaginary crack.

5. Derivation of Westergaard's complex function for the Dugdale model

In order to derive Westergaard's complex function for the Dugdale model, we consider the equivalent elastic crack of length 2*b* instead of a physical, blunted crack of length 2*a*. Westergaard's complex function for the Dugdale model will take the form [2]

$$Z(z) = \frac{2\sigma_Y}{\pi}\left[\frac{F\sqrt{b^2-c^2}}{\sigma_Y(z^2-c^2)} - \arccos\left(\frac{a}{b}\right)\right]\frac{z}{\sqrt{z^2-b^2}} + \frac{2\sigma_Y}{\pi}\operatorname{arcctg}\left(\frac{a}{z}\sqrt{\frac{z^2-b^2}{b^2-a^2}}\right). \qquad (5)$$

6.Determination of the displacements on the crack surface and of crack tip opening

In fracture mechanics, the most interesting issue is the analysis of displacements of the points on the surface of a physical crack, on its tip, and within the zone of plastification around the crack tip. Since these points belong to the axis *x*, it follows that $y = \operatorname{Im} z = 0$ and $z = x$, so, from the third equation of the set (4) simple equations for displacements are obtained

$$u(z) = \frac{1-\nu}{E}\operatorname{Re}\left[\int Z(z)\,\mathrm{d}z\right], \qquad v(z) = \frac{2}{E}\operatorname{Im}\left[\int Z(z)\,\mathrm{d}z\right], \qquad \text{for} \quad \operatorname{Im} z = 0. \qquad (6)$$

7. Conclusion

The analysis of some parameters of elastic-plastic fracture mechanics, such as the magnitude of the plastic zone around the crack tip r_p, the crack centre opening displacement δ_c, and the crack tip opening displacement δ_t (CTOD), has been carried out in this paper. The Dugdale model of plastic yielding has been used for modelling the narrow yield bands around the crack tips, under the assumption that the *cohesive stresses* σ_Y are *constant* in the yielded zone. The assumption of *elastic-perfectly plastic* model of the plate material has been introduced. Analytical methods based on the theory of functions of a complex variable have been used in the analysis of these parameters.

References

[1] Pustaić, D. and Štok, B., "Crack Tip Plasticity Investigations using Dugdale Strip Yield Model Approach", In: Proceedings of the 11th Biennial European Conference on Fracture – ECF 11, Engineering Materials Advisory Services, Poitiers – Futuroscope, France, 1996, Vol. I, 151-156.

[2] Pustaić, D., "Contribution to the Stress Analysis in the Thin Plates in Non-Linear Range", Ph.D. Thesis, University of Zagreb, Faculty of Mech. Engng. and Naval Arch., Zagreb, Croatia, 1990, [in Croatian].

Prof. Dragan Pustaić, Ph.D.
Faculty of Mech. Engng. and Naval Arch. / University of Zagreb, I. Lučića 5, Zagreb, Croatia,
Tel: ++385 (1) 6168 178, Fax: ++385 (1) 6168 187, e-mail: dragan.pustaic@fsb.hr
Martina Lovrenić, B.Sc.
Faculty of Mech. Engng. and Naval Arch. / University of Zagreb, I. Lučića 5, Zagreb, Croatia,
Tel: ++385 (1) 6168 514, Fax: ++385 (1) 6168 187, e-mail: martina.lovrenic@fsb.hr

4th International Congress
of Croatian Society of Mechanics
September, 18-20, 2003
Bizovac, Croatia

4thICCSM

MODELLING OF PLASTIC YIELDING MICROMECHANISM IN THE COHESIVE ZONE AROUND A CRACK TIP IN A STRAIN-HARDENING MATERIAL

Dragan Pustaić and Boris Štok

Keywords: *Dugdale Strip Yield Model, Variable Cohesive Stress, Strain-Hardening Material, Magnitude of the Plastic Zone, Crack Tip Opening Displacement, Analytical Methods*

1. Introduction

In this paper, we aim at creating a new and more reliable micromehanism of plastic yielding in the cohesive zone, which would better describe the real elastic-plastic state of the material around crack tips. The assumption of *variable cohesive stresses* σ_Y within the plastic zone is introduced. It is necessary to carry out an iterative procedure in order to establish a law of cohesive stresses distribution. The improved micromechanical model has been applied in the analysis of the elastic-plastic fracture mechanics parameters such as: the magnitude of the plastic zone around the crack tip r_p, the crack tip opening displacement δ_t, the displacements on the crack surface, etc.

2. Definition of boundary conditions; the loading and the geometry of the plate

A thin, infinite plate ($z \in D$, D: $| z | \geq 0$) with a straight crack of the length $2a$, lying on the axis x ($z \in L$, L: $| \mathrm{Re}\, z | \leq a$, $\mathrm{Im}\, z = 0$) is considered. Boundary conditions can be written in the form of

$$\sigma_{xx}(z) = \sigma_{xx}^{\infty} = k\sigma_{\infty}\,, \quad \sigma_{yy}(z) = \sigma_{yy}^{\infty} = \sigma_{\infty}\,, \quad \sigma_{xy}(z) = 0\,, \qquad \text{for} \qquad |z| \to \infty\,. \tag{1}$$

In expressions (1), the real constant k is the *biaxial load ratio.* It takes into account the dependence of the loading parallel with the crack plane on the loading perpendicular to it. The surface of a real, physical crack is free of loading, therefore, additional boundary conditions can be written

$$\sigma_{yy}(z) = \sigma_{xy}(z) = 0\,, \quad \text{for} \quad z \in L\,, \quad \text{and} \quad \sigma_{yy}(z) = \sigma_{Y}(z)\,, \quad \sigma_{xy}(z) = 0\,, \quad \text{for} \quad z \in L^{*}\,, \tag{2}$$

where L^*: $a \leq | \mathrm{Re}\, z | \leq b = a + r_p$, $\mathrm{Im}\, z = 0$. $\sigma_Y(z)$ stands for *variable cohesive stress* in the yielded zone. Allowing that cohesive stresses $\sigma_Y(z)$ in the plastic zone are changing, *hardening* of the material is modelled.

3. Tresca's and Mises' yield criteria

When the Dugdale strip yield model is applied, the cohesive zone around the crack tip is considered as a narrow strip of yielded material extending from the tip of the physical crack in the direction of the crack plane. Since the plate material has the property of hardening, it means that the increased loading will cause the increments of stresses and of elastic-plastic strains. The equivalent stress σ_{equ} will then be equal to the *current yield stress* of the material σ_{Yc}, where $\sigma_{Yc} > \sigma_{Y0}$. The *equivalent stress* σ_{equ} can be determined from *Tresca's* or from *Mises' yield criteria* which can be written in the analytical form as

$$\left[(\sigma_{xx} - \sigma_{yy})^2 - \sigma_{Y0}{}^2\right]\left[\sigma_{xx}{}^2 - \sigma_{Y0}{}^2\right]\left[\sigma_{yy}{}^2 - \sigma_{Y0}{}^2\right] = 0\,, \tag{3}$$

$$\sigma_{xx}{}^2 - \sigma_{xx}\sigma_{yy} + \sigma_{yy}{}^2 = \sigma_{Y0}{}^2\,. \tag{4}$$

4.Cohesive stresses in the plastic zone in the case of isotropic hardening of a material

It is assumed that the plate material has the property of hardening, to be more precise, either of *linear hardening* (E_T = const.), or of *non-linear hardening* where $E_T = E_T(\bar{\varepsilon}_p)$. E_T stands for the *tangential elastic-plastic modulus*, and $\bar{\varepsilon}_p$ stands for plastic strain. Hardening of the material is *isotropic*. According to the *work hardening hypothesis*, the *parameter of hardening* κ is equal to the work of plastic deformation. According to another one, this parameter is equal to the *equivalent plastic strain* $\bar{\varepsilon}_p$. The latter hypothesis is known under the name of *strain hardening hypothesis*.

5. Magnitude of cohesive zone around the crack tip

The magnitude of plastic zone r_p around the crack tip is determined under the assumption of *linear* distribution of *cohesive stress* $\sigma_Y(x)$ in the yielded zone, Fig.1b.

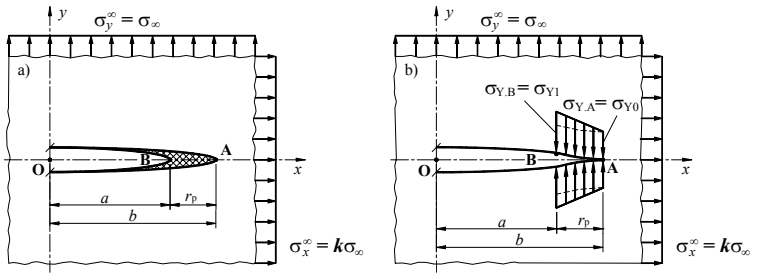

Fig. 1. a) Plastic zone around the crack tip, b) linear distribution of cohesive stress in the yielded zone

We get a transcendent equation from which we can determine, numerically, the length of the fictitious elastic crack b, and $r_p = b - a$

$$\frac{\pi}{2}\sigma_\infty\left(1-\frac{a}{b}\right)-\left(\sigma_{Y1}-\sigma_{Y0}\frac{a}{b}\right)\arccos\left(\frac{a}{b}\right)+\left(\sigma_{Y1}-\sigma_{Y0}\right)\sqrt{1-\left(\frac{a}{b}\right)^2}=0\ . \tag{5}$$

6. Conclusion

In this paper, we have tried to form a more reliable micro mechanism of plastic yielding in the yielded zone around the crack tip, which would better describe the real elastic-plastic state of the material. Dugdale strip yield model has been used for describing yielded zones. Our aim has been to model cohesive stresses in a plate made of a *linearly hardening material.* Isotropic hardening of the material has been assumed. A hypothesis of variable cohesive stresses $\sigma_Y(x)$ within the plastic zone has been introduced. It would be possible to determine the magnitude of the cohesive zone around the crack tip r_p, as well as the crack tip opening displacement δ_t using analytical methods.

References

[3] Štok, B. and Pustaić, D., "On the Influence of Loading Parallel to the Crack Plane on the Crack Opening and on the Magnitude of the Plastic Zone around a Crack Tip", Strojarstvo, Journal for the Theory and Application in Mechanical Engineering, 38 (2/3), (1996), 73-87 [in Croatian].

[4] Pustaić, D. and Štok, B., "Some Critical Remarks on the Dugdale Strip Yield Model for the Crack Tip Plasticity", In: Proceedings of the 12th European Conference on Fracture – ECF 12 – Fracture from Defects, Engineering Materials Advisory Services, Sheffield, United Kingdom, 1998, Vol. II, 889-894.

Prof. Dragan Pustaić, Ph.D.
Faculty of Mechanical Engng. and Naval Architecture / University of Zagreb, I. Lučića 5, Zagreb, Croatia,
Tel: ++385 (1) 6168 178, Fax: ++385 (1) 6168 187, e-mail: dragan.pustaic@fsb.hr
Prof. Boris Štok, Ph.D.
Faculty of Mechanical Engineering / University of Ljubljana, Aškerčeva 6, Ljubljana, Slovenia,
Tel: ++386 (1) 47 71 425, Fax: ++386 (1) 25 18 567, e-mail: boris.stok@fs.uni-lj.si

4th International Congress
of Croatian Society of Mechanics
September, 18-20, 2003
Bizovac, Croatia

DYNAMIC ANALYSIS OF NUCLEAR SPENT FUEL CONTAINER

J. Radnić and A. Harapin

Keywords: *dynamic response, rectangular fluid container, concrete shell, material and geometric nonlinearity*

1. Introduction

Seismic response of reinforced concrete nuclear spent fuel containers has been studied intensively in recent years. These studies were motivated with many heavy damages caused by strong earthquakes, like Alaska (1964.) or Parkfield (1966.). Some of results can be found in [1], [2] and [3]. In many of this studies, the flexibility of the structure with main nonlinear effects is not fully taken into account. This may be due to the fact that containers are usually made of reinforced or prestressed concrete and dominantly was analysed independent of the surounding liquid. Nevertheless, the flexibility of the containers must be taken into account in their dynamic analysis, together with liquid-structure dynamic interaction.

This paper shortly presents the results of seismic analysis of open rectangular reinforced concrete nuclear spent fuel container. Adopted model includes dynamic interaction of coupled liquid-structure system, as well as material and geometrical nonlinearity of the structure and material nonlinearity of the liquid.

2. Numerical model

Adopted numerical model for dynamic analysis of 3D fluid-structure coupled problems can be found in [4].

Applied model for dynamic analysis of shells can be found in [5], [6], [7], [8] and [9]. The 8 and 9 node curved shell element, without so-called shear and membrane "locking", have been used. Material model of structure is relatively simple and at the same time it includes dominant nonlinear effects of the reinforced concrete structures behaviour, such as:

- concrete yielding under compression,
- cracks development in concrete under tension,
- cracks opening and closing,
- tensile stiffness of cracked concrete,
- shear stiffness of cracked concrete,
- nonlinear behaviour of the steel,
- influence of strain rate on mechanical characteristics of steel and concrete.

Concrete properties can vary for each layer of the shell. The reinforcement is modelled as a special layer of respective thickness, with strength and stiffness in the direction of the steel bars. Geometrical nonlinearity (large displacement) of the structure can be also included.

For the fluid discretization, 20 or 27 node "brick" isoparametric finite elements have been used. Pressure formulation for linear, or displacement potential formulation for nonlinear fluid (cavitation) are adopted [4]. A fluid can be considered compressible and viscous. The Eulerian formulation have been used to define the fluid motion, assuming small displacements. Explicit-implicit Newmark's time integration is employed to predict the hydrodynamic pressures change.

3. Example

The Figure 1 depicts a typical open flexible container, wich is analised in this work, with length L=50 m, width W=20 m, height H=10 m, and the wall thickness t. The analysis is provide for thickness t=1.0 m and t=0.5 m. Liquid is partially filled up to the depth H_w. Finite element meshes are shown in Figure 2.

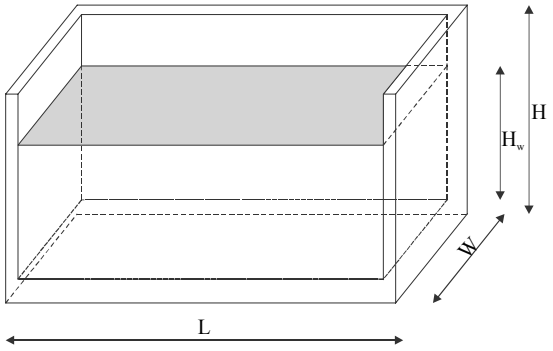

Figure 1. Geometry of analysed rectangular container

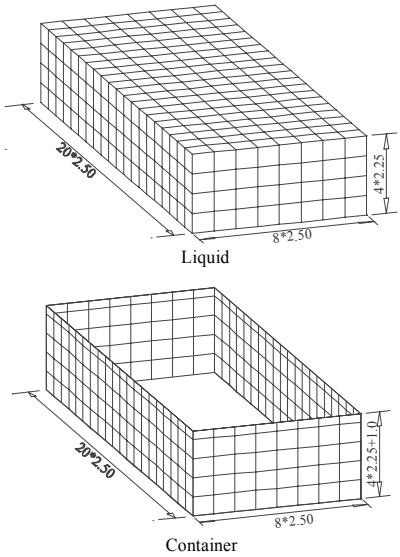

Figure 2. Finite element meshes of liquid-container coupled system

References

[1] Rammestorfer, F.G., Sharf, K. and Fisher, F.D., "Storage tanks under earthquake loading", Appl. Mech. Rev., Vol. 43, 1990., pp 261-282

[2] Kim, J.K., Koh, H.M. and Kwahk, I.J., "Dynamic Response of Rectangular Flexible Fluid Containers", Journ. of Eng. Mech., Vol. 122, No. 9, 1996., pp 807-817

[3] Koh, H.M., Kim, J.K. and Park, J.H., "Fluid-Structure Interaction Analysis of 3-D rectangular tanks by a variotionally coupled BEM-FEM and comparison with test result", Earthquake Eng. Struct. Dyn., Vol. 27., 1998., pp 109-124

[4] Harapin, A., "Numerical simulation of dynamic interaction between fluid and construction", Ph.D. Thesis, Faculty of Civil Engineering, University of Split, Split, 2000. (in Croatian)

[5] J. Radnić, A. Harapin, D. Matešan: "Static and dynamic analysis of concrete shells - shell element and models", Građevinar 53, 11, pp 695-709, 2001. (in Croatian)

[6] J. Radnić, A. Harapin, D. Matešan: "Numerical procedure in the static and dynamic analysis of concrete shells", Građevinar 53, 12, pp 759-771, 2001. (in Croatian)

[7] Radnić, J., Matešan, D. and Harapin, A., "Model for static analysis of concrete shells", Engineering Modelling, Vol. 13, No. 3-4, 2000., pp 93-99

[8] Huang, H.C. and Hinton, E., "A nine node Lagrangian Mindlin plate element with enhanced shear interpolation", Engineering Computations, Vol. 1, 1984, pp 369-379

[9] Figueras, J.A., "Ultimate load analysis of anisotropic and reinforced concrete plates and shells", Ph.D. Thesis, University College of Swansea, C/Ph/72/83, 1983.

Jure Radnić, Prof. dr. sc., CEng, Associated Professor
Faculty of Civil Engineering University of Split, Matice hrvatske 15, HR-21000 Split, Croatia,
tel/fax:+385(0)21 303-336, e-mail: Jure.Radnic@gradst.hr

Alen Harapin, Doc. dr. sc., CEng
Faculty of Civil Engineering University of Split, Matice hrvatske 15, HR-21000 Split, Croatia,
tel:+385(0)21 303-358, fax:+385(0)21 303-362, e-mail: harapin@gradst.hr

4th International Congress
of Croatian Society of Mechanics
September, 18-20, 2003
Bizovac, Croatia

4thICCSM

TIME-DEPENDENT ANALYSIS OF CONCRETE SHELLS

Jure Radnić, Domagoj Matešan

Keywords: Concrete, Shells, Time-dependent analysis, Creep, Shrinkage

Numerical model for time-dependent analyses of concrete shells will be presented. The model is based on the one given in [1], [2] for simulation of concrete shells exposed to short-term static loading, including the creep, shrinkage and aging of concrete as well as temperature effects. Therefore, presented model includes dominant non-linear effects of concrete structures behaviour such as:

- non-linear behaviour of concrete:
  - yielding and crushing in compression
  - opening and closure of cracks
  - tensile stiffness between cracks
  - shear stiffness of cracking concrete
  - creep
  - shrinkage
  - aging
  - temperature changes
- non-linear behaviour of reinforcement
  - yielding in tension and compression
  - strain hardening in tension and compression
  - temperature changes
- influence of the change in geometry (large displacements)
- influence of structure's construction/development in time

Detailed description of the model could be found in [3], [4].

Eight- and nine-node elements of degenerated curved shell with the layered material model across the shell thickness have been used [5]. Each node has five degrees of freedom: three translation displacements in the direction of global axes and two rotations about the axes in the shell middle surface. Concrete properties can be different for each layer across the shell thickness. It is adopted that each concrete layer is in the plane stress state. The reinforcement is modelled as a separate layer of an adequate thickness, with the strength and stiffness defined only in the direction of the reinforcement bars.

Linear-elastic behaviour of concrete is assumed until its tensile strength is achieved. Cracks can develop only in planes perpendicular to the middle surface of a shell. A smeared cracks model is adopted. The model of so-called fixed orthogonal cracks has been used. Partial and complete cracks closure in unloading is modelled as well as reopening of previously developed cracks at reloading. The increase in tensile stiffness of non-cracked concrete between the cracks has been simulated in a usual manner, indirectly via "descending curve" of the $\sigma - \varepsilon$ diagram of concrete in tension.

Shear stiffness of cracked concrete (the effects of aggregate "interlock" and dowel action) has also been simulated in a usual manner by reduction of the shear modulus (G_{12}, G_{13}, G_{23}) in dependence on the value of tensile strain perpendicular to the crack plane.
The theory of plasticity has been used for modelling of concrete behaviour in compression. At the beginning of loading, a linear-elastic behaviour of concrete is assumed until the yield condition is satisfied. After that, plastic behaviour of concrete is adopted. The associated flow rule i.e. the assumption of plastic strain vector perpendicular to the yield plane has been adopted. The condition of concrete crushing in compression is defined through strain components. In unloading, an elastic behaviour is assumed. After crushing, concrete stiffness is disregarded.

The reinforcing bars are modelled as separate steel layers of equivalent thickness at respective distance from the middle surface of a shell. Stress can occur only in the direction of reinforcement bars. Full compatibility of the displacement of reinforcement and surrounding concrete is taken into account. Steel behaviour is described by a bi-linear $\sigma - \varepsilon$ relationship, equally in compression and tension.

A Glanville-Dischinger method was used for calculation of uniaxial creep strain, which is based on the assumption that the creep rate is the function of current uniaxial stress of concrete σ and the elapsed time t since loading. The creep coefficient values are used according to the EUROCODE 2 [3]. Uniaxial shrinkage of concrete has been also described according to EUROCODE 2 [3]. The aging strain is taken into account indirectly, by an increase in the initial modulus of elasticity and concrete strength in time.

Step by step time integration is carried out, in which the incremental-iterative solutions are added to the preceding ones in order to obtain the current solutions.

Based on the presented model, the "TACS" computer program for time-dependent analyses of concrete shells has been developed. Since the date on some experimentally tested concrete shells or plates exposed to long-term loading were not available, the model has been verified on an analysed of reinforced concrete plate.

References

[1] Radnić, J., Harapin, A., Matešan, D., *"Static and Dynamic Analyses of Concrete Shells" – Shell Element and models"*, Građevinar, Vol.53, No. 11, Zagreb, 2001, pp 695-709. *(in Croatian)*

[2] Radnić, J., Harapin, A., Matešan, D., *"Numerical Procedure at Static and Dynamic Analyses of Concrete Shells"*, Građevinar, Vol.53, No. 12, Zagreb, 2001, pp 001-013. *(in Croatian)*

[3] Radnić, J., Matešan, D., *"Concrete Shell Computation with determination of Rheological Properties of Concrete"*, Građevinar, Vol.55, No. 1, Zagreb, 2003, pp 001-013. *(in Croatian)*

[4] Radnić, J, Matešan, D., *"Computation Model for Time-dependent Analysis of Concrete Shells"*, VII International Conference on Computational Plasticity COMPLAS 2003, CIMNE, Barcelona, 2003

[5] Huang, H.C., "*Static and Dynamic Analysis of Plates and Shells"*, Bristol: Springer-Verlag,. 1989

[6] EUROCODE 2, "*Design of Concrete Structures, Part 1: General Rules and Rules for Buildings"*, Br˘ssel, 1990

Jure Radnić, Time-dependent analysis of concrete shells
University of Split, Faculty of Civil Engineering, Matice Hrvatske 15, Split, Croatia, +385 21 303336, jure.radnic@gradst.hr

Domagoj Matešan, Time-dependent analysis of concrete shells
Institute of Civil Engineering, PC – Split, Matice Hrvatske 15, Split, Croatia, +385 21 558643, dmatesan@st.igh.hr

4th International Congress
of Croatian Society of Mechanics
September, 18-20, 2003
Bizovac, Croatia

4thICCSM

STATIC EQUILIBRIUM POSITION, VELOCITY AND PRESSURE FIELDS AT STATIC ANALYSIS OF LONG NONCAVITATING ELLIPTICAL AND OFFSET JOURNAL BEARINGS

V. Rak, E. Malenovský, F. Pochylý

Keywords: *Journal bearings, Computational modelling, Navier-Stokes eq., Bézier body application.*

1. Introduction

New approach to the analysis of coupled vibrations of rigid body and real liquid is presented in this contribution. Journal bearings are the special types of these coupled mechanical systems very often used in rotor dynamic systems. The radial clearance is in order of tenths of millimeters. This dynamic system causes additional effects (mass, damping and stiffness) relatively to the rotating shaft. This contribution is focused on static analysis problem only.

In technical experience is distinguished between long and short journal bearings. In long bearings, the pressure distribution around the bearing is invariant along the length of the bearing. Physically, this means that there is no flow in the axial direction. J. M. Vance considers short bearing if ratio L/D ≤ 0,25*, where* L *is the axial length of the bearing and* D=2R *is the bearing diameter. In this case the film pressure turns out to be a parabolic function of the axial coordinate* z*. This contribution is consider with computational modelling of long noncavitating journal bearings.*

Theoretical analysis

Basic Navier-Stokes equation for laminar flow has form

$$\rho \frac{\partial \vec{c}}{\partial t} + \rho \left[rot\, \vec{c} \times \vec{c} + \frac{1}{2} grad \left| \vec{c} \right|^2 \right] + \eta\, rot\, rot\, \vec{c} + grad\ p = \vec{0} \qquad (1)$$

Continuity equation

$$\rho\, div\, \vec{c} = 0 \qquad (2)$$

If we suppose the same liquid and shaft velocity on inner ring (shaft surface) and zero velocity on the outher ring (the bearing), the boundary conditions have form

$$\begin{aligned} &\text{S:} \quad \vec{c} = \vec{\omega} \times \vec{y} + \vec{z}^{\bullet} \\ &\Gamma: \quad \vec{c} = \vec{0} \end{aligned} \qquad (3)$$

Let we suppose, that shaft-centre position, velocity and pressure are given as sum of stationary and nonstationary parts of solution such as

$$z_j = z_{0_j}(x_i) + v_j(x_i, t)$$
$$c_j = c_{0_j}(x_i) + w_j(x_i, t)$$
$$p = p_0(x_i) + \sigma(x_i, t) \qquad (7)$$

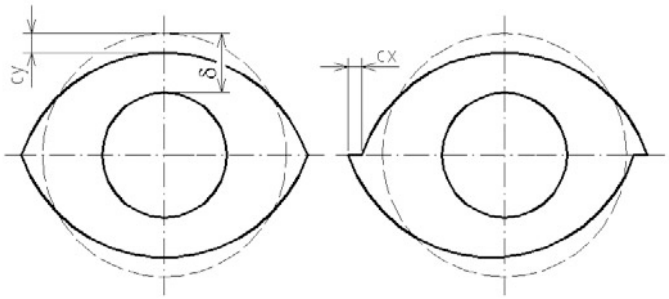

Fig.1 Lemon and offset journal bearing

By comparison items of stationary part we obtained equation system for stationary body motion analysis. By comparison items of nonstationary part we obtained equation system for nonstationary body motion analysis.

Acknowledgement

The Ministry of Education of the Czech Republic under experimental intention CEZ: MSM 2600001 is gratefully acknowledged for support of this research work.

Personal informations

Vladimír Rak
Brno University of Technology, Faculty of Mechanical Engineering, Institute of Solid Mechanics, Technická 2, 616 69 Brno, Czech Republic.
Tel.: +420.54114 7871; *e-mail:* rakvla@post.cz

Eduard Malenovský
Brno University of Technology, Faculty of Mechanical Engineering, Institute of Solid Mechanics, Technická 2, 616 69 Brno, Czech Republic.
Tel.: +420.54114 2855, *fax:* +420.54114 2876; *e-mail:* malenov@umtn.fme.vutbr.cz

František Pochylý
Brno University of Technology, Faculty of Mechanical Engineering, Institute of Energetics,
Technická 2, 616 69 Brno, Czech Republic.
Tel.: +420.54114 2335, *fax:* +420.54114 2329; *e-mail:* pochyly@umtn.fme.vutbr.cz

4th International Congress
of Croatian Society of Mechanics
September, 18-20, 2003
Bizovac, Croatia

4thICCSM

A NEW METHOD IN THE THEORY OF PLASTICITY OF PLATES

Riko Rosman

Analyzed is a rigid-plastic plate bounded by an arbitrary convex closed curve, laterally supported and either hinged or clamped along its boundary. In the ultimate limit state the middle plane of the laterally loaded plate becomes a zero-Gaussian curvature, i.e. a developable surface. When applying the virtual work principle to the corresponding mechanism, the work of the plate's internal forces within the plate's boundary is expressed through a double integral of the deflection's Laplacian extended over the plate's interior. To facilitate the analysis, the Green's theorem of the integral calculus is used to transform the double integral into a line integral along the plate's boundary of the deflection's normal derivative. Concretely, the work of the plate's internal forces during the deformation is found to be

$$V = m(1+\mu)\int \varphi \,\mathrm{d}u\,, \tag{1}$$

where m is the plate's positive plastic moment per unit length, or flexural strength, μ the ratio of the negative and the positive plastic moments usually chosen in advance, φ the slope of the normal of the boundary curve with respect to the undeformed plate's surface and u the coordinate oriented along the boundary curve. In the special cases of the circular and convex polygonal plates the evaluation of Eq. (1) is quite simple, much simpler as with the usual cinematic or mechanism analysis procedures.

For plates of a more involved form Eq. (1) for the work of the internal forces is transformed. In the polar coordinates θ and $R = R(\theta)$ of the boundary curve and $R' = \mathrm{d}R/(\mathrm{d}\theta)$ it takes the form

$$V = m(1+\mu)W\int_0^{2\pi}\left[1+\left(\frac{R'}{R}\right)^2\right]\mathrm{d}\theta\,, \tag{2}$$

in the corresponding Cartesian coordinates x and y, with $x' = \mathrm{d}x/(\mathrm{d}\theta)$ and $y' = \mathrm{d}y/(\mathrm{d}\theta)$,

$$V = m(1+\mu)W\int_0^{2\pi}\frac{x'^2+y'^2}{xy'-yx'}\,\mathrm{d}\theta\,, \tag{3}$$

where W is the plate's maximal deflection.

The work of the load is determined as usual.
As an example the new approach is applied to an elliptic plate subjected to an uniform load and a concentrated load at its mid- point, a favorable system for many engineering structures, and a simple result is obtained for the plate's required flexural strength.

With a and b as the ellipse's major and minor semi-axes, respectively, and t as a parameter defined in the region (0, 2π), the Cartesian coordinates of the plate's boundary curve are

$$x = a\cos t\,, \quad y = b\sin t\,. \tag{4}$$

The plate's required positive and negative plastic moments are found to amount

$$m = \frac{1}{1+\mu}\frac{ab}{a^2+b^2}\left(\frac{Q}{3}+P\right),\ m' = \mu m\,, \tag{5}$$

where Q denotes the total uniform distributed load and P the concentrated load.
In the special case of the plate hinged along its boundary μ must be set equal to zero, in the special case the plate is subjected only to the distributed load P must be set equal to zero and in the special case the plate is subjected only to the concentrated load Q must be set equal to zero in Eqs. (5).

REFERENCES

[1] Kreyszig, E.: Advanced Engineering Mathematics. Wiley, New York, 1999
[2] Rosman , R .: Beitrag zur plastostatischen Berechnung zweiachsig gespannter Platten, Bauingenieur 60 (1985), 151-159
[3] Rosman, R.: Beitrag zur plastostatischen Berechnung von Deckentragwerken aus auf Balken gelagerten zweiachsig gespannten Platten. Rad JAZU, Knjiga 432, 135-148, Zagreb, 1987
[4] Harris, J., Stocker, H.: Handbook of Mathematics and Computational Science. Springer, New York, 1998

Acad. Prof.em.Dr. Riko Rosman
University of Zagreb, Faculty of Architecture, Kačićeva 26, 10000 Zagreb, Croatia, Tel. +385/1/463 93 48
Fax:+385/1/482 80 79

4th International Congress
of Croatian Society of Mechanics
September, 18-20, 2003
Bizovac, Croatia

CONSERVATION LAW OF J INTEGRAL TYPE FOR MULTI-MATERIAL BODY

Aleksandar Sedmak, Drazan Kozak, Gorgi Adziev, Franjo Matejicek, Nenad Gubeljak

Keywords: J integral, welded joint, multi-material body, finite element method

1. Introduction

The *J* integral, as defined by Rice [1], has been used extensively as the fracture mechanics parameter. It was proved by Rice [1] that the *J* integral is path independent, can be identified with crack driving force, and describes stress and strain fields around crack, making it a valid fracture mechanics parameter. Anyhow, as stated in the Rice's original paper, besides other limitations, *J* integral is valid only for the homogeneous material, at least in crack direction.

In this paper, the influence of weldment heterogeneity is of primary interest and will be analyzed both theoretically and numerically. Theoretical analysis is applied in order to show that the *J* integral is not path independent for a generally shaped weldment. Anyhow, its path independence can be recovered if the modified *J* integral is introduced, comprising the original *J* integral and line integrals along weldment interfaces.

2. The modified J integral for multi-material body

The modified *J* integral for a weldment is introduced as for a multi-material body, represented by four regions of different material properties, Fig. 1: base metal (BM), weld metal (WM) and two regions in heat-affected-zone (HAZ) - one with fine grain structure (FG) and the other one with coarse grain structure (CG), as follows:

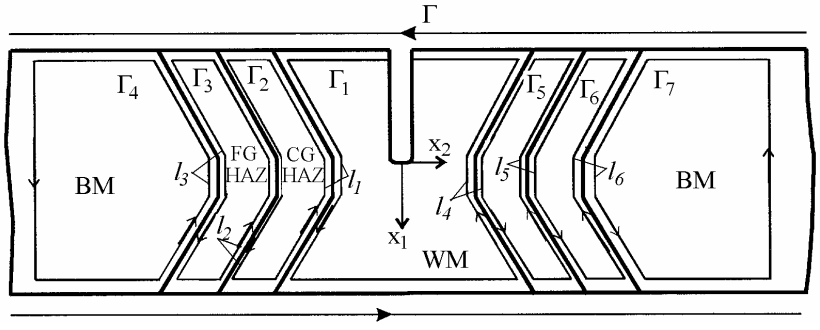

Figure 1. Integration paths for multi-material body

$$J = \int_{\Gamma}(Wn_1 - \sigma^{ij} n_j \frac{\partial u^i}{\partial x^1})ds - \sum_{a=1}^{6} \int_{\ell_a} (Wn_1 - \sigma^{ij} n_j \frac{\partial u^i}{\partial x^1})ds \qquad (1)$$

where l_a denote the closed contour around material interface. The modified *J* integral is path independent, as shown by Savovic [2], and has the following physical meaning: the first integral term represents the force acting on both the crack tip and material interfaces (discontinuities of stress and strain), whereas the second one eliminates the force on the boundaries.

3. Numerical procedure and results

Numerical analysis of elastic-plastic material behaviour is performed using elastic-plastic analysis of two-dimensional problems by the finite element method. Collapsed isoparametric eight-noded element around the crack tip are used, producing r^{-1} singularity.

In order to check a weldment heterogeneity influence on the *J* integral value the finite element method was applied to 2D plane strain problem. Both integral terms in eqn (1) were numerically evaluated on different paths. Results are shown in Tab. 1, showing the average value of *J* integral for six inner paths, J_{ave}, not intersecting material boundaries, the values of first integral term in the modified *J* integral for the remote paths intersecting the material boundaries (*J1*, *J2* and outer path *J3*), and the values of second integral term in the modified *J* integral along the boundaries between WM and CG HAZ (*J4*), between CG HAZ and FG HAZ (*J5*), and between FG HAZ and BM (*J6*).

Table 1. Results for *J1-J6* and J_{ave}

J1	J2	J3	J4	J5	J6	J_{AVE}
41.3062	42.2782	44.6796	-0.79005	0.34121	-0.3501	39.7158
100.481	95.6042	106.957	-5.58250	5.80860	-4.1670	92.5672
136.271	127.582	142.554	-8.46372	9.49186	-7.5983	125.372
202.666	187.190	206.002	-16.3222	16.4976	-14.327	188.772
247.370	225.526	247.658	-21.4016	23.0434	-20.973	232.632

As can be seen from Tab. 1 the finite element results confirm theoretical analysis of material interface effect on the *J* integral value. Namely, for all load levels, the Rice's *J* integral is path dependent because its values for different paths differ out of the limits of numerical error.

4. Conclusions

From the results and their discussion the following conclusions can be made:

- Directly measured J integral for weldments is generally not equal to the crack driving force because of path dependence problem caused by material interfaces between BM, HAZ and WM.
- The effect of material interfaces can be evaluated using the modified J integral, i.e. the additional line integral, obtained by theoretical analysis in order to regain the J integral path independence.

References

[1] Rice, J.R. "A path independent integral and the approximate analysis of strain concentration by notches and cracks". J. Appl. Mechanics, Trans. ASME E35, 1968, pp. 379-386.

[2] Savovic, N. "Theoretical, experimental and numerical analysis of weldment fracture mechanics parameters" (in Serbian). Doctoral thesis, Faculty of Mechanical Engineering, University of Belgrade, 1994

Prof. dr Aleksandar Sedmak
Faculty of Mechanical Engineering, University of Belgrade, 27. Marta 80, 11000 Belgrade, Serbia and Montenegro, phone 381-11-3370352, fax 381-11-3370364, asedmak@mas.bg.ac.yu
Doc. Dr Drazan Kozak
Mechanical Engineering Faculty, University of Osijek, Trg I.B. Mazuranic, HR-35000 Slav. Brod, phone 385-35-446188, fax 385-35-446446, dkozak@sfsb.hr
Assis. mr Gorgi Adziev
Faculty of Mechanical Engineering, University of Skopje, Karpos bb, 91000 Skopje, Macedonia, phone 389-2-399290, fax 389-2-363180, gadziev@ereb1.mf.ukim.edu.mk
Prof. dr Franjo Matejicek
Mechanical Engineering Faculty, University of Osijek, Trg I.B. Mazuranic, HR-35000 Slav. Brod, phone 385-35-446188, fax 385-35-446446, fmatej@sfsb.hr
Doc. dr Nenad Gubeljak
Faculty of Mechanical Engineering, University of Maribor, Cesta Proleterskih brigada 59, 2000 Maribor, Slovenia, phone 386-62-2207661, fax 386-62-2207990, nenad.gubeljak@uni-mb.si

4th International Congress
of Croatian Society of Mechanics
September, 18-20, 2003
Bizovac, Croatia

4thICCSM

APPROACH TO THE ANISOTROPIC BODY CONTACT BY THE OPTICAL METHOD OF CAUSTICS

D. Semenski, A. Bakić

Keywords: *optical method of caustics, contact force, anisotropic material*

1. Introduction

Experimental optical method of caustics is established in fracture mechanics through the stress intensity factor determination. Recently, the task of experimentation is to analyze the deformations of material surface and to assess the structural damage. An objective is the force determination and the analysis of the isotropic body contact. The extension to anisotropy introduces the procedure, which enables the treatment of composites that are mainly of orthotropic structure.

2. Theoretical background of the anisotropic body contact

Stress distribution in a homogeneous body with rectilinear anisotropy is dependent on only two co-ordinates in x-y plane, which is coincident with the plane of any one cross-section. The presumptions of theoretical approach to anisotropic body contact are:

1. The equations for the stress-strain state in the region near the point of force application are taken into account.
2. The elastic constants in composites for the usual orthotropic mechanical structure have significant mismatch in the directions of the principal axes of orthotropy *L* and *T*.

There are several conditions assumed in the analysis:

a) material is characterised by the coefficients $S_{ij} = S_{ji}$ of a compliance material matrix;

b) field of analysis of strains and stresses is near the crack-tip but outside the plasticity region;

c) material is a homogeneous continuum from macromechanical point of view;

d) body is in a state of plane stress.

3. Caustics analysis of the contact point vicinity

In the reflection method of caustics to the non-transparent specimen is loaded and illuminated by the concentrated field of light in the zone of high deformation gradients. The light beams are reflected and transferred from the specimen surface to the virtual plane at the distance z_0 behind the specimen, e. g. from the initial curve into the singular caustic curve. The result on the screen is a dark spot, surrounded by the concentrated light on its edge. Light beams conditions are described through *m* as a scale factor (parallel light beams $m = 1$, convergent light $m < 1$, and divergent light $m > 1$), *h* is a thickness of the specimen. The position of one light beam on the screen, at the distance z_0 behind the specimen, is described by the equation of the light beam components on the screen:

$$x' = mr\sin\varphi - z_0 h\frac{F}{\pi r^2}\left[B\,D(\varphi)\sin\varphi - B\frac{\partial D(\varphi)}{\partial\varphi}\cos\varphi\right],$$
$$y' = -mr\cos\varphi - z_0 h\frac{F}{\pi r^2}\left[B\,D(\varphi)\cos\varphi + B\frac{\partial D(\varphi)}{\partial\varphi}\sin\varphi\right]. \quad (1)$$

The introduced functions are:

$$A(\varphi) = S_{13}\cos^2\varphi + S_{23}\sin^2\varphi + S_{36}\sin\varphi\cos\varphi,$$
$$B = (u_1 + u_2)\sqrt{S_{11}S_{22}},$$
$$C(\varphi) = \cos\alpha\cos\varphi + \sqrt{\frac{S_{11}}{S_{22}}}\sin\alpha\sin\varphi, \quad (2)$$
$$L(\varphi) = S_{11}\sin^4\varphi + 2(S_{11} + S_{66})\sin^2\varphi\cos^2\varphi + S_{22}\cos^4\varphi,$$
$$D(\varphi) = \frac{C(\varphi)}{L(\varphi)}A(\varphi),$$

where $u_1 = -i\mu_1$, $u_2 = -i\mu_2$, may be real or conjugate complex numbers. They contain the information about the mechanical characteristics of material in x and y direction in the form of μ_k as the complex roots of characteristic material equation.

4. Simulations of the optical effects and experimental procedure

The dark spot will appear, surrounded by the concentrated light on the edge. The shape of singular caustic curves that are dependent on different angles of force inclination while the size of caustics is proportional to the force intensity. Evaluation of the experimental optical effects is based on the properly simulated unit caustics for each position of the principal axes of orthotropy. The simulations are performed by using the MATLAB functions. Graphical interface has been programmed to be used interactively and user friendly in order to change a kind of material (isotropic or anisotropic) and shadow illumination parameters. The measuring procedure will be established when the experimental optical effects will be taken, processed and compared to the simulated ones.

5. Conclusion

The amount of the applied force as well as its inclination (e.g. in the case of friction normal and tangential component of the force) can be identified from the optical effect (dark spot) on the screen. The experimentation will provide the development of procedure of contact force determination and will fulfil the extension of the method of caustics to mechanically anisotropic materials. Evaluation of the experimental optical effects should be done on the basis of properly simulated unit caustics for each specific position of the principal axes of orthotropy.

References

[1] Kalthoff, J.F., "Shadow Optical Method of Caustics", chapter in "Handbook on Experimental Mechanics" (ed. A.S. Kobayashi,), Prentice-Hall, Engelwood Cliffs-New York, 1987, pp. 430-500.

[2] Lekhnitskii, S.G. "Theory of Elasticity of an Anisotropic Body," Mir Publishers (transl.. from Russian), Moscow, 1981.

[3] Rossmanith, H.P.,Zhang, J., Knassmillner R.E., "Kontaktenkaustiken in orthotropen Werkstoffen", Österreichische Ingineur-und Architekten-Zeitschrift (ÖIAZ), 136. Jg., H. 6, 1991, pp. 214-218.

[4] Semenski, D., Jecić, S., Goja, S., Mažar, L., "On the Method of Caustics in Contact Problem", Proc. of 3rd Congress of Croatian Soc. of Mechanics, Cavtat-Dubrovnik, 2000, pp. 389-396.

4th International Congress
of Croatian Society of Mechanics
September, 18-20, 2003
Bizovac, Croatia

4thICCSM

DYNAMIC BEHAVIOUR OF DEEP WATER MARINE RISER

Ana Maria Ljuština, Joško Parunov, Ivo Senjanović

Keywords: *marine riser, hydroelasticity, sea current, regular waves, analytic solution, finite element method.*

Extended Abstract

The rapid growth of world's demands for larger amounts of energy and continued pursuit for new resources of oil and natural gas extended drilling operations to the offshore sites. In the down of marine technology, half of century ago in the Gulf of Mexico, the first offshore drilling facility was installed and the marine riser concept was applied. In the following decades varies of offshore structures, mostly explorational and exploitation, were installed not only in the calm costal waters of Mexico and Brazil, but also in the extremely harsh environment of the North Sea. One third of current world's oil production comes from beneath the sea, and most of the drilling operations take place at water depths up to 500 m, though some drilling is performed at water depths up to 2000 m. Vital part of all offshore productions and explorations structures, drill ships, submersible and semisumersible platforms is a marine riser. The marine riser is a conductor pipe connected between a fixed or a floating offshore structure and the wellhead at the seabed. Marine riser can be fixed at both of its ends, but it may be also supported by the articulated tower or tower buoy.
The sources of environmental excitations, which may influence the marine riser directly or indirectly by exerting forces on other components of the riser system, can be divided into two groups: the significant sources like a sea current, surface waves and wind gusts, that exert dominant hydrodynamic and aerodynamic forces on the riser and the supporting structure, and the less significant ones like internal waves, microseismic waves, tides, tidal and volcanic waves, that are usually ignored in dynamic analysis of marine riser. The configuration of the marine riser system varies depending on the type of the supporting structure, the site of operations and the environmental conditions, but the concept of the riser design hardly changes.

The present paper is concerned with the analysis of static and dynamic behaviour of the drilling marine riser. Marine riser is a specific slender offshore structure simply supported on its ends, exposed to the sever environmental conditions. Among varies influence factors that can exert the loads on the structure only the most significant ones are taken into account. The first level of marine riser analyses is static response due to a sea current and a platform offset, and the second level of riser analyses is dynamic behaviour due to the regular waves and platform surge motion.

The riser structure is modeled as a simple beam column with variable cross section and the axial force acting on the top of the riser. Static axial force consists of effective tension force, weight and buoyancy of the riser with sea water and drilling mud inside. The transverse load on the riser, due to a sea current, is determined according to the simplified current profile. The tidal part is assumed to be constant along the riser, and the part of the current caused by the winds is linearly varying with the depth. Regular waves are described in accordance with the theory of progressive sinusoidal wave. Horizontal wave load on the riser is specified by the Morison equation that takes into account inertia and drag force, but neglects the diffraction component.

Considering the equilibrium of transverse forces and bending moments, and using the beam theory of elasticity, problem of the elastic deformation of the riser exposed to steady sea current, riser tension force and platform offset is mathematically modeled by partial differential equation of static equilibrium.

For the beam column model of riser exposed to the regular waves and platform surge motion, partial differential equation of vibration is obtained. Axial force consists of static part, i.e. difference between buoyancy, tension force and weight, and dynamic part due to buoyancy variation in a progressive wave. Wave load on the marine riser is modeled by the modified Morison equation that takes into account relative motion of the fluid and the riser joint. Complete differential equation is transformed in pseudo-linear form and solved by an iteration procedure. Nonlinear problem of marine riser response to a regular wave is reduced to a set of coupled modal equations written in a pseudo-linear form and solved by harmonic acceleration methods and FEM in time and frequency domains, respectively.

In order to determine an approximate solution of riser response, the equation may be simplified. The linearisation of the equation of vibration and Morison equation comprises following assumptions:

a) Dynamic part of axial forces is neglected.
b) Convective part of acceleration is omitted.
c) Coupling between the «large amplitudes» of riser motion and excitation force is ignored.
d) Linearisation of nonlinear drag force.

Linearised drag coefficient is obtained from the equivalence of work of nonlinear and linearised drag force and depends on relative velocity between the fluid and a riser joint. Linearised transform of partial nonlinear differential equation of marine riser is solved in frequency domain by finite element method. Coupled linear modal equations are obtained and the problem is solved iteratively.

Following the established algorithms, static and dynamic behaviour of marine riser is determined for the particular riser. The riser is modeled by a 470 meters long finite element system, with the constant cross section properties and using 38 beam column elements. The analyses of marine riser static and dynamic behaviour are performed by computer programs developed for the slender, simply supported structures and adopted for the marine risers. Computational distributions of the deflection and bending moments showed the regions on marine riser with highest bending moments and largest deflection amplitudes. The largest deflection is at the riser top corresponding with the surge motion amplitude. Rotation angle amplitudes, bending moments and shear forces determined in time domain show good agreement with the linearised solution. Comparison of the results of static and dynamic analyses shows that the vessel motion and waves are the dominant source of riser bending stress. Riser displacement, rotations, axial forces, bending moments and natural modes and frequencies of free vibration are evaluated for the riser in air and in water. The tension force on top of the riser is determined with respect to the maximum allowable static rotation angle at the marine riser lower ball joint.

Mr. sc. Ana Maria Ljuština, research assistant
Faculty of Mechanical Engineering and Naval Archuitecture Departement of Naval Engineering and Marine Technology Chair of Marine Structures Design Ivana Lucica 5, Zagreb, Croatia
Tel: +385 1 6168164; e-mail: ana-maria.ljustina@fsb.hr

Dr. sc. Joško Parunov, senior assistant
Faculty of Mechanical Engineering and Naval Archuitecture Departement of Naval Engineering and Marine Technology Chair of Marine Structures Design Ivana Lucica 5, Zagreb, Croatia
Tel: +385 1 6168226; e-mail: josko.parunov@fsb.hr
Academic Ivo Senjanović, full professor
Faculty of Mechanical Engineering and Naval Archuitecture Departement of Naval Engineering and Marine Technology Chair of Marine Structures Design Ivana Lucica 5, Zagreb, Croatia
Tel: +385 1 6168142

4th International Congress
of Croatian Society of Mechanics
September, 18-20, 2003
Bizovac, Croatia

4thICCSM

CALCULATION MODELS OF THREE LAYERED ”SANDWICH” PANELS"

Vladimir Z. Sigmund, Darko Z. Sigmund and Jurko Zovkić

Keywords: r/c sandwich panels, experimental tests, nonlinear and linear analysis, design

1. Introduction

The "TVD process" has been developed for cheaper and faster building, reduction in required number of different operations, combination and integration of several building phases, lowering of montage and transport costs and lowering of energy costs in a finished building. Basic building element in the process is the "TVD thermo-panel" that has two spaced reinforcement meshes adequately connected with an insulating Polystyrene foam in-between thus forming a space truss. Its construction is simple and does not require high-energy consumption as it is made of standardized materials. Thermal element, held in place with the space truss, serves as a caisson for spraying of concrete and eliminates the need of formworks. The sandwich walls are completed „in-situ“ by spraying of concrete in several layers. Resulting TVD house is purely monolithic structure with interconnected walls and slabs that unite load carrying, energy conservation and sound insulation functions. Thickness of the finished insulated walls varies depending on its use (bearing and non-bearing outer- and inner-walls, slabs and base plate).

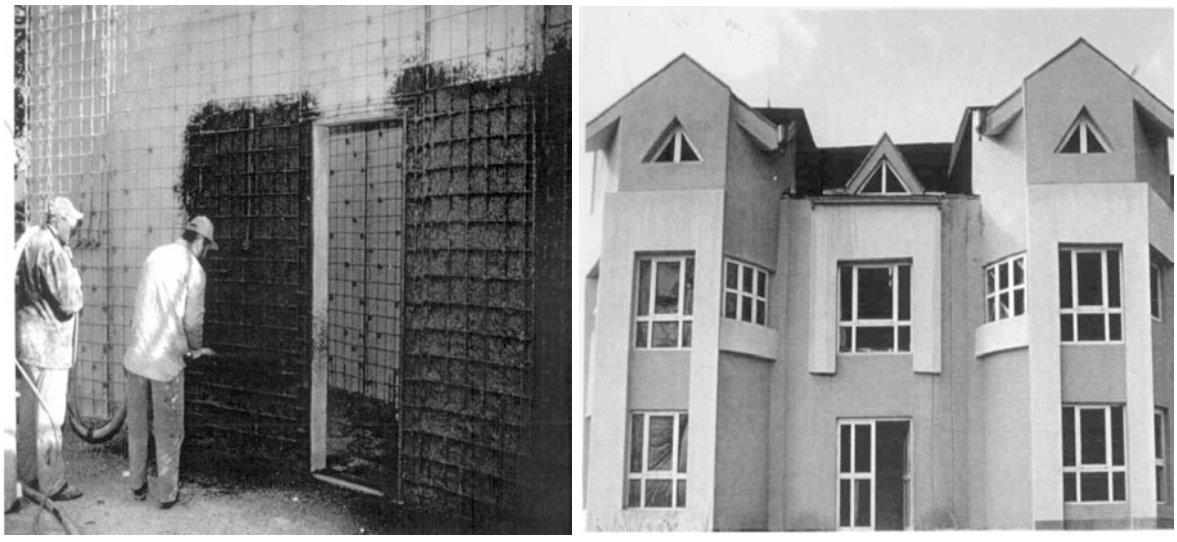

Figure 1 "Sanwich" wall production

The load bearing part of the composite “sandwich” walls are concrete withes spaced by the insulation in-between. Characteristic loading situations are: axial vertical loading, eccentric vertical loading, in-plane shear loading and wind lateral loading.

2. Experimental testing

The experimental tests were needed for studying of the achieved composite action and behavior of the "sandwich" walls under various loading situations. Known problematical areas are in material quality and characteristics and in achieved composite action of the finished wall. Sprayed concrete usually has about 20% of voids, has lower modulus of elasticity (40%-70% of the regular concrete with bigger value perpendicular to the spraying direction). "Sandwich" wall has small compressive area and is not suitable for concentrated loadings, problematical shear transfer among the withes, etc. Tested were homogeneous and composite short walls under axial loading and long "sandwich" panels, under axial loading and moment, lateral and in plane loading. Their results are shortly presented here.

Table 1 Basic geometrical and material characteristics of the tested model walls

TVD20-8	d	L	di	b	As	fys	Ac	g	MB	Fu	FT
	(cm)	(cm)	(cm)	(cm)	(cm2)	(Mpa)	(cm2)	(kN/m3)	(MPa)	(kN)	
M1	23.0	270	8.0	62	2.3	500	840.0	20.5	30.4	450.0	CR
M2	23.0	271	8.0	61	2.3	500	840.0	20.3	29.1	32.5	SS
M3	23.0	271	8.0	62	2.3	500	840.0	20.4	25.8	109.0	BS

3. Analytical modeling of the "sandwich" walls

Modeling of the experimental results by nonlinear mathematical models proved to be complicated as many parameters influenced the results. It was possible to simulate observed behavior by adjusting parameters in various manner although some of them had no physical meaning. Optimal and most logical combination of parameters has been chosen for further behavior and close to failure analysis. As nonlinear modeling is unsuitable for design purposes, proposed is the use of uniform concrete sections with higher safety factors. Modifications of analytical formulas were based on the results of experiments and non-linear analysis.

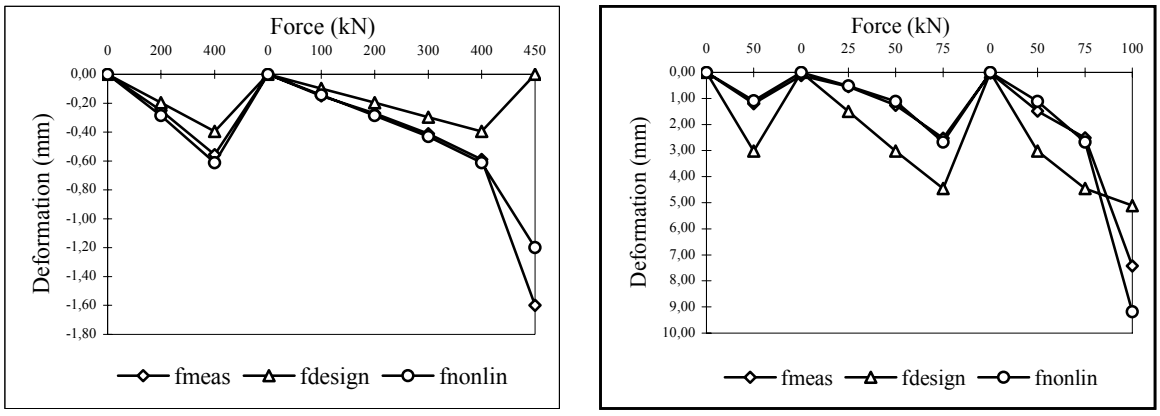

Figure 2 Comparison of the measured and calculated deformations for Model 1. and Model 3.

References

[1] Sigmund V., Herman K.,Sigmund, D., "Experimental and Analytical Investigation of Sandwich Panels", IABSE Symposium,Rio de Janeiro, 1999.

[2] Sigmund, V. Sigmund, D., Brana, P., "Adoptable building by use of «sandwich» panels", 1st DAAAM ICATDC, 12.-14. september 2002., Slavonski Brod, Croatia, pp. 233-239.

Prof.dr.sc. Vladimir Sigmund & Jurko Zovkić, CE
University J.J.Strossmayer in Osijek, Faculty of Civil Engineering, Crkvena 21, 31000 Osijek, Croatia, Telephone: +385.31.540-070; Telefax, +385.31.540-071; e-mail: sigmund@gfos.hr; jzovkic@gfos.hr
mr.sc. Darko SIgmund, BA, "Sigmund" d.o.o., Ljubinkovac st. 3, 10000 Zagreb, Croatia

4th International Congress
of Croatian Society of Mechanics
September, 18-20, 2003
Bizovac, Croatia

4thICCSM

ON NUMERICAL PREDICTION OF DAMAGE IN LAMINATED COMPOSITE SHELLS SUBJECTED TO LOW VELOCITY IMPACT

Ivica Smojver and Ivo Alfirević

Keywords: *finite element analysis; layered composite shells; impact damage; delaminations; matrix cracks*

1. Introduction

The paper addresses the problem of damage in layered composite shells by computational model that starts from the basic assumption that appearance of matrix cracks, in the case of low velocity impact, is interrelated and precursor to the appearance of delaminations, Collombet [2], Razi [6]. The numerical procedure elaborated in the paper employs 3D finite elements with reduced integration in the computation of stress field in the vicinity of the impact point. All calculations have been performed within the frame of ABAQUS software as it is possible to implement specially devised subroutines in it.

2. Formulation of damage modeling procedure and numerical example

The presented computational model is an extension of numerical procedure developed for laminate plates, therefore basic principles and assumptions remain the same as stated in [7]. Composite shell is assumed to be symmetrically loaded and supported. One layer of solid 8-noded elements is used in discretization of each shell lamina. Elements with reduced integration have been applied in order to better capture the flexural behavior of the shell. Material is assumed to be linearly elastic, and only cross-ply laminates have been modelled, leading to material symmetry. The material model previously defined through user subroutine UMAT in plate analysis has been applied in the shell analysis after the appropriate tensor transformations have been performed. Impactor is defined as rigid analytical surface that exactly describes the geometry of hemispherical tip, with its velocity and mass defining the loading through initial conditions. Only the case of low mass/low velocity impact has been studied, where the internal damage in form of barely visible impact damage is of particular significance. Material properties of the laminate have been calculated using averaging stress approach together with Eshelby's equivalent inclusion method [4]. The mechanical properties of the composite are calculated using averaging scheme devised by Mori and Tanaka [4] and defined in the ABAQUS user subroutine UMAT [1] where it is necessary to define the material matrix. More elaborate description of material model can be traced in [7]. Matrix cracking has been detected applying Hashin's tensile criterion [5] and degradation of mechanical properties in the case of the appearance of matrix tensile cracks is defined through the model by Tsai [8]. At the beginning of the analysis, coincident nodes are tied together with kinematic links defined with multi-point constraints [1] and if delamination is indicated in those nodes, altered kinematic relation is established through new multipoint constraints, where separation of nodes is allowed [1,7]. Usage of general purpose software ABAQUS made possible application of multi point constraints in coincident nodes of shell areas supposed to delaminate, and visualization of delaminated areas.

The impact of rigid impactor on the simply supported graphite/bismalemide $[0_4/90_4]_s$ cylindrical shell has been examined. The shell is subjected to the impact loading with constant kinetic en-

ergy of 0.8 J by the impactor with hemispherical tip of 3.175 mm radius. In addition, the mass of the impactor has been varied, as well as corresponding initial velocity. Matrix cracks projection area obtained by Ganapathy and Rao [3] has been compared with the present numerical model and excellent correlation confirmed. Dependence of matrix cracks area in the topmost layer of the laminate on the mass of the impactor has been examined and similar research has been performed in the analysis of interlaminar delaminations. Figs. 1 and 2 show the typical pattern of impact damage.

3. Conclusion

The numerically efficient computational model is proposed for prediction of matrix cracks and interlaminar delaminations in layered composite shells. Solid elements used in discretization of composite structure, together with appropriate local shell coordinate system and tensor transformations, enabled application of similar numerical models in the analysis of plate and shell structures. The insensitivity of damage area to the variation of mass/velocity of the impactor at the constant kinetic energy has been demonstrated.

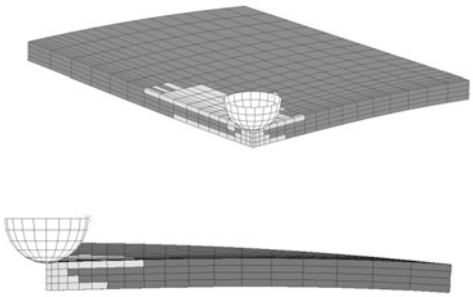

Figure 1. Matrix cracks ; $m = 2\ M$, at $t = 1.20$ ms

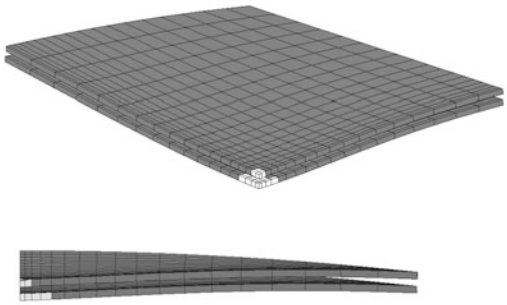

Figure 2. Delaminations; $m = 2\ M$, at $t = 1.20$ *ms*

References

[26] "ABAQUS Theory Manual, ver. 6.2-1", Hibbit, Karlsson and Sorensen, 2000.

[27] Collombet, F., Bonini, J., Lataillade, J.L., "A three-dimensional modelling of low velocity impact damage in composite laminates", Int. J. Num. Meth. Eng., Vol.39, 1996, pp 1491-1516.

[28] Ganapathy, S., Rao, K.P., "Failure analysis of laminated composite cylindrical/spherical shell panels subjected to low velocity impact", Computers and Structures, Vol.68, 1998, pp 627-641.

[29] Gavazzi, A.C., Lagoudas, D.C., "On the numerical evaluation of Eshelby's tensor and its application to elastoplastic fibrous composites", Computational Mechanics, Vol.7, 1990, pp 13-19.

[30] Hashin, Z., "Failure criteria for unidirectional fibre composites", J. Appl. Mech., Vol.47, 1980, pp 329-334.

[31] Razi, H., Kobayashi, A.S., "Delamination in cross-ply laminated composite subjected to low-velocity impact", AIAA Journal, Vol.31, 1999, pp 1408-1502.

[32] Smojver, I., Sorić, J., Alfirević, I., "Computational prediction of matrix cracks and delaminations in layered composites", Proc. 2nd European Conference on Computational Mechanics 2001. Cracow Poland, 2001, CD-ROM Edition

[33] Tsai, S.W., "A survey of macroscopic failure criteria for composite materials", J. Reinf. Plast. Comp., Vol.3, 1984, pp 40-62.

Ivica Smojver, Assistant Professor

Faculty of Mechanical Engineering, University of Zagreb, Department of Aerospace Engineering, I. Lučića 5, Zagreb, Croatia, (1) 6168 267, (1) 6168 187, ismojver@fsb.hr

Ivo Alfirević, Professor

Faculty of Mechanical Engineering, University of Zagreb, Department of Engineering Mechanics, I. Lučića 5, Zagreb, Croatia, (1) 6168 240, (1) 6168 187, ivo.alfirevic@fsb.hr

4th International Congress
of Croatian Society of Mechanics
September, 18-20, 2003
Bizovac, Croatia

4thICCSM

NONLINEAR MODELLING OF FLEXIBLE MATERIALS IN PLANE STRESS WITH APPLICATION TO STRESS CONCENTRATION IN TEXTILE

Željko Šomođi, Anica Hursa and Dubravko Rogale

Keywords: Flexible materials, numerical modelling, plane stress

1. Introduction

In this paper we present a part of the initial efforts at our Faculty of textile technology to introduce numerical modelling and computational mechanics to the field of textile and clothing engineering. Ignoring for the time being some other mechanical features of textile as a complex structure, such as anisotropy, non-homogeneity, non-linearity in extension and hysteretic behaviour in cyclic loading, we focus our attention to the description of non-linearity related to the flexibility, or in other words to the lack of compressive carrying capacity. In doing so, we explore some computational experience gained elsewhere in the context of metal plasticity [1] – in fact in the iterative numerical procedure, section 2, the step of stress reduction to the compressive limit is very similar to the return mapping algorithm in computational plasticity [2].

Finally, an emphasis is given to the examples, section 3. On one side, they illustrate some possibilities of our home-developed computer programme, and on the other they show an analysis of a selected problem relevant for the practical case of stress concentration in clothing

2. The iterative procedure for flexible material in plane stress

In this work we adopt the iterative approach, leaving a possible comparison with the incremental, or the combined incremental – iterative computation for later.

In the initial step (in the present context we refer to it as solid body prediction) the material is assumed to be linearly elastic. If in some point (finite element, Gauss point) the state of strain and stress is found to be on the non-existing compressive part of the assumed linearly elastic material characteristic, the correction needs to be done. In this work we adopt the model of a constant compressive limit. The impossible negative principal stress is simply reduced to the compressive limit. After this correction, the overall equilibrium no longer holds. The nodal forces exerted on a finite element are computed from the state of stress $\{\sigma\}^*$ inside this element following [3], and if for every node the corresponding contributions from the finite elements connected to that node are accumulated, the *out-of-balance residual nodal forces* $\{R\}$ are obtained. The residual forces give rise to the incremental displacements $\{\delta\}^{inc}$ via the global equation system $[K]\{\delta\}^{inc} = \{R\}$. The proper modification of the global stiffness matrix [*K*] has to be done prior to the solution of the global system. In our computations at this stage the initial stiffness method is in use – once computed global matrix [*K*] is applied in every iteration step, and not the tangent stiffness matrix. This of course means less programming effort and less computational time per iteration step, but on the other side poor convergence rate.

Once the incremental displacements are computed, they are accumulated to the previous state, as well as the appropriate incremental strains and stresses. The new state is again checked for the

violation of the compressive limit and the iteration progresses until the prescribed termination criterion is met.

On the basis of the described iterative concept, a PC programme is made using MS Visual Basic. Common constant strain triangular finite elements (CST) are used, with the global system solution by the Gauss elimination method. The programme has some user-friendly features in interactive definition of finite element mesh, boundary conditions and loading, and especially in the visualisation of results.

3. Example: tension strip with transverse perforation

In many numerical studies the computational model has been tested in a common example of a perforated strip in tension [1,2,4]. In our paper [5] we also analyse the strip with a circular hole. Here we consider a tension strip with transverse perforation, figure 1a. The material constants are taken as approximately corresponding to a previously tested textile material [6]: E=60MPa, ν=0.2, t=0.1mm (thickness).

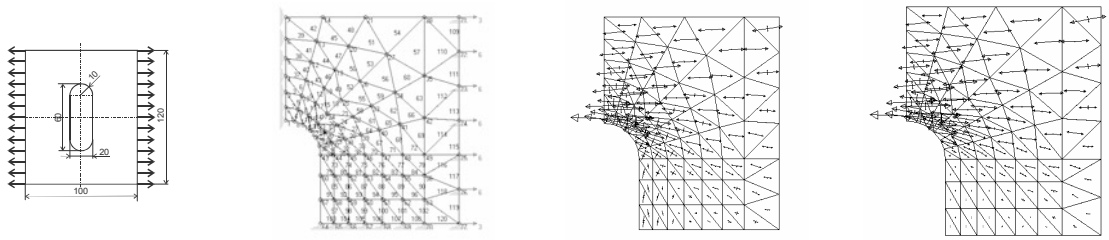

a) b) c) d)

Figure 1. Example: Geometry of the strip (a), finite element mesh with boundary conditions and loading (b), principal stresses in solid body prediction (c) and after iteration (d)

For reason of double symmetry only one quarter of the strip is modelled, the mesh consisting of 77 nodes and 120 elements, figure 1b). We also analysed the reinforcement of the critical zone with the aim of reduction of the stress concentration.

4. Conclusion

The proposed iterative model is suitable for the analysis of stress concentration in critical zones of clothing or technical textiles. It is our intention to apply this model in numerical optimisation of reinforcements of button-holes and similar critical places in clothes.

References

[34] Hinton, E., Owen, D. R. J., "Finite elements in plasticity", Pineridge Press, Swansea, 1980

[35] Nikolić, G.; Šomođi, Ž., Franulić Šarić D., "Mechanical Properties of Sewing Stitch performed in Frozen State", Book of Proceedings of the International Textile, Clothing & Design Conference "Magic World of Textile", ed. Dragčević, Z., Faculty of Textile Technology University of Zagreb, Zagreb, 2002, pp 380-38.

[36] Simo, J. C., Taylor, R. L., "A Return Mapping Algorithm for Plane Stress Elastoplasticity", International Journal for Numerical Methods in Engineering, Vol.22, 1986, pp 649-670.

[37] Sorić, J., Montag, U., Kraetzig, W. B., "On the increase of computational algorithm efficiency for elasto-plastic shell analysis", Engineering Computations, Vol.14, 1997, pp 75-97.

[38] Šomođi, Ž., "A Contribution to Elastic-plastic Analysis of Structural Elements", Ph D thesis, University of Zagreb (in Croatian), 1998

[39] Šomođi, Ž., Hursa, A., Rogale, D., "Finite Element Modelling of Textile in Plane Stress", submited for 4th International Conference *Innovation and Modelling of Clothing Engineering Processes – IMCEP 2003,* ed. Geršak, J., University of Maribor Faculty of Mechanical Engineering, Maribor, Slovenia, 2003

Asisst. Prof. Željko Šomođi, Ph.D.,Anica Hursa, M. Sc., Prof. Dubravko Rogale, Ph.D. Faculty of Textile Technology, University of Zagreb, Prilaz baruna Filipovića 30/III, HR-10 000 Zagreb, Croatia
Phone ++385 1 37 00 544, fax ++385 1 37 74 029,
e-mail: zeljko.somodji@zg.hinet.hr; anica.hursa@ttf.hr; dubravko.rogale@ttf.hr

4th International Congress
of Croatian Society of Mechanics
September, 18-20, 2003
Bizovac, Croatia

4thICCSM

THEORETICAL AND PRACTICAL PROBLEMS OF UP-TO-DATE STABILITY ANALYSIS OF STEEL STRUCTURES

Marta Sulyok

Keywords: *load and resistance factor design criteria, the general principles of Eurocode 3, flexural members, bending, shear, bending and shear, lateral-torsional buckling, target*

Abstract

It is shown that the reliability indices of the steel beams and plate girders in AISC Load and Resistance Factor Design Specification and in ECCS Eurocode-3, are neither uniform nor are they equal to the anticipated target values of β, which are for LRFD criteria β=3.0 and for EC-3 β=3.80. New resistance factors (ϕ and γ) are derive in order to achieve this aims.

1. Introduction

The purpose of this paper is to report the values of the reliability indices of beams and girders which are designed according to the new Load and Resistance Factor Design (LRFD) criteria of AISC and Eurocode-3 of ECCS. The method of the First-order probabilistic basis will be illustrated by the examples of the stability of steel beams with the selection of the load and resistance factors under dead and live loading for both mentioned design criteria.
New research work, done in connection with the application of EC-3 and EC-4 in our National standards, is analysed due to our design meteorological loads such as snow and wind loading on steel structures in Croatia in the procedure of calibration. The verification of the stability of steel structures is evaluated by FOSM comparing by test results in connection with the limit state design.

2. Theoretical models for lateral-torsional buckling in AISC and EC-3 specifications

It is evident that there are the differences in the design requirements for various specifications. The differences and similarities are compared for two code-rules which are based on the essentially the same theoretical background and the purpose of this section is to compare these methods and to draw the conclusions about the impact of the differences between them. These divergences are due to the different perceptions of the effects of initial imperfections. For specifications ECCS and AISC many variability arise especially in the inelastic range. The most general equation is the one adopted in Western Europe: $M_u = M_p\left(\frac{1}{1+\bar{\lambda}_M^{2n}}\right)^{1/n}$, with the exponent, which takes on values 2.5 for rolled, and 2.0 for welded beams. The variation of the buckling strength with $\bar{\lambda}_M$ for the various values of "n" and "α" is shown in Eq.1. The advantage of this method is its simplicity and generality but has its disadvantage as the implied reduction in flexural and torsional stiffness due to the partial plastification of the cross section.
The selected model is based on the buckling curves of the compression members with five different parameters of the initial imperfections, which are now in the use of Eurocode-3 (*Rondal&Maqui)* as follows:

$$\frac{\sigma_{cr}}{\sigma_y} = \frac{1}{2\bar{\lambda}^2}\left\{1+\alpha\left(\bar{\lambda}-0.2\right)+\bar{\lambda}^2-\sqrt{\left[1+\alpha\left(\bar{\lambda}-0.2\right)+\bar{\lambda}^2\right]^2-4\bar{\lambda}^2}\right\} \quad (1)$$

where is $\sigma_{cr}/\sigma_y=\chi$ for all five buckling curves.

3. Evaluation of web buckling test results for welded beams and plate girders in shear and combine bending and shear

The limit state design requirements for welded beams and plate girders in shear, and combined bending and shear, are analysed and criteria for two codes (AISC and Eurocode 3) are compared. As the differences in the design requirements are substantial, the comparison of the achieved reliability indices is made in order to find out the model, which is closer to the target reliability level. The statistical parameters of the experimental results are evaluated and the FOSM method is used for the procedure of the calibration. The results vary for two examined models and it is necessary to achieve target values of reliability by correction of the models by the resistance factors.

4. Results of calibration for the flexure (ECCS and AISC) and shear (by two models)

The analysis of laterally unsupported steel beams for various design models is obtained, by which the ultimate limit state of the lateral-torsional buckling strength is evaluated for the purpose of the calibration of the rolled beams under the snow loads from the measured data in Croatia. The results of the calibration varies with applied snow loads and slenderness ratio for three examined designed models, and for *ECCS* criteria they are in the range from realised reliability indices β= 3.20 to 5.19, for *AISC* Specifications indices are lower, such as β=3.10 to 4.80, and for the model of proposed system factor "n" is quite on the target safety side with β=4.20 and 6.20. For the combined bending and shear the resulting reliability index from the applicable tests is evaluated as β=2.50 , which is not the desired target value and the single value of the resistance factor ϕ=0.90 is inadequate to insure uniform reliability.

5. Conclusion

The calibration is performed with the designed models by global and by partial safety factors and the differences are the result of the basic formulations of the buckling curves. It is evident that there is the necessity to change the system factor "n" or "α" of buckling curves, or to correct the evaluation model by model and resistance factors with the target reliability level in order to achieve uniform reliability with the proposed loads factors, concerning the applied loads in certain cases. The reliability indices are not uniform, nor are they always close to the desired target value of β=3.8 for EC-3 or β=3.0 for LRFD of AISC. The reason for this disparity is that the single value of the resistance factor is inadequate to insure the uniform reliability. In order to adjust the curve from Eq.(2) with the experimental results, non-linear regression analysis is performed with new coefficient of imperfection α=0.247 for 95% fractile, and reliability index will be close to the target reliability level.

It is concluded that large discrepancies exist between codes, even those using essentially the same design methodology and the same experimental data base. This emphasizes the case for harmonization to arrive at a higher degree of uniformity of code design procedures and more rational safety margins.

References

[1] American Institute of Steel Construction*, Load and Resistance Factor Design,* AISC, 1986

[2] Eurocode 3. *Design of Steel Structures-Part 1-1: General rules and rules for buildings,* 1987

[3] Sulyok, M. and Galambos, T.V.*: The Evaluation of Resistance Factors for the Laterally Unsupported Rolled and Welded Beams and Plate Girders Designed by LRFD of the AISC,* Steel Structures: Advances Design and Construction, Elsevier Applied Science, London and New York, 1987, ISBN 1-85166-120-4

Prof.dr.sc. Marta Sulyok, e-mail: marta.sulyok-selimbegovic@arhitekt.hr

University of Zagreb, Faculty of Architecture, Kačićeva 26, 10000 Zagreb, Croatia, Tel. +385/1/463 93 48

4th International Congress
of Croatian Society of Mechanics
September, 18-20, 2003
Bizovac, Croatia

LUMBAR SPINE SYSTEM: BIOMECHANICAL MODEL EVALUATION

Mr.sc. Aleksandar Sušić, Dr.sc. Tanja Jurčević-Lulić

Keywords: *Lumbar spine functionality*

1. Extended abstract

Considering lumbar spine injuries, investigations were pointed in many different directions. Many are pointed in direction of establishing acceptable loads for analyzed task, while others are occupied with answering how and why injuries occur. Our approach in case of lumbar spine under external mechanical load is to propose approach that can offer better understanding of lumbar spine functionality. For this purpose, this paper describes hypothetic model of lumbar spine mechanism, reduced on sagittal mid plane. As found in our previous investigations, there is principle that can explain response of lumbar spine to applied external mechanical load. Our findings are compared with experimental results. Beside comparison of our findings, comparison with other authors shows even more similarities. Conclusion of this paper comes through noticeable dependence of lumbar spine extension torque and trunk inclination. Connection between lumbar spine responses and applied external mechanical load can be defined as regulative system, providing most efficient way to protect its functionality and health. Evidence for such a statement is in fact that every subsystem of lumbar spine system has its role, described as follows:

1. intra-abdominal pressure should help in providing mechanical stability and stiffness of the spine;
2. back muscles, besides inducing back muscle pressure, should produce force to overcome applied load and complete designed task;
3. back muscle pressure should offer support for the spine as well as contribution to mechanical stability and stiffness of the spine;
4. abdominal wall muscles are intended to create intra-abdominal pressure, but also indirectly to stiffen the spine.

Since some of the data is still hard to collect, exact interrelation is missing. Used approach can have implications in further biomechanical modelling. For evaluation of reliable relations between lumbar spine responses and applied external mechanical load further investigations are needed.

References

[1] Cholewicki, J., Juluru, K. and McGill, S. M. "Intra- abdominal pressure mechanism for stabilizing the lumbar spine", Journal of Biomechanics, (1999) 32, 13-17

[2] Cholewicki, J., Simons, A. and Radebold, A., "Effects of external trunk loads on lumbar spine stability", Journal of Biomechanics, (2000) 33, 1377-1385

[3] Cresswell, A. G., Grundström, H. and Thorstensson, A., "Observations on intra-abdominal pressure and patterns of abdominal intra-muscular activity in man", Acta Physiol Scand, (1992) 144, 409-418

[4] Gardener-Morse, M., Stokes, I., A. F., "The effects of abdominal muscle co activation on lumbar spine stability", Spine, (1998) 23 (1), 86-91

[5] Garg, A., Mital, A. and Asfour, S. S., "A comparison of isometric strength and dynamic lifting capability", Ergonomics, (1980) 23(1), 13-27

[6] Granata, K. P., and Marras, W.S., "An EMG- assisted model of trunk loading during free- dynamic lifting", Journal of Biomechanics, (1995) 28(11), 1309-1317

[7] Graves, J. E., Pollock, M. L., Carpenter, D. M., "Quantitative assessment of full range of motion isometric lumbar extension strength", Spine, (1990) 15 (4), 289-294

[8] Hodges, P. W., Cresswell, A. G., Daggfeldt, K. and Thorstensson, A., "In vivo measurement of the effect of intra- abdominal pressure on the human spine", Journal of Biomechanics, (2001) 34, 347-353

[9] Marras, W. S., Ferguson, S. A. and Simon, S. R., "Three dimensional dynamic motor performance of the normal trunk", International Journal of Industrial Ergonomics, (1990) 6, 211-224

[10] Marras, W. S., King, A. I., Joynt, R. L., "Measurements of loads on the lumbar spine under isometric and isokinetic conditions", Spine, (1984) 9 (2), 176- 188

[11] Marras, W.S., "Predictions of forces acting upon the lumbar spine under isometric and isokinetic conditions: a model-experiment comparison", International Journal of Industrial Ergonomics, (1988) 3, 19-27

[12] Pytel, J. L. and Kamon, E., "Dynamic strength test as a predictor for maximal and acceptable lifting", Ergonomics, (1981) 24(9), 663-672

[13] Sušić, A.: "Magistarski rad: Statičko i dinamičko utvrđivanje mehaničkog kapaciteta slabinske kralješnice", Fakultet strojarstva i brodogradnje, Zagreb, 2002.

Mr.sc. Aleksandar Sušić
Faculty of Mechanical engineering and naval architecture,
Ivana Lučića 5, 10000 Zagreb, Croatia, tel: 016168570, fax: 016168187, e-mail: aleksandar.susic@fsb.hr
Dr.sc. Tanja Jurčević-Lulić
Faculty of Mechanical engineering and naval architecture,
Ivana Lučića 5, 10000 Zagreb, Croatia, tel: 016168549, fax: 016168187, e-mail: tanja.jurcevic@fsb.hr

4th International Congress
of Croatian Society of Mechanics
September, 18-20, 2003
Bizovac, Croatia

4thICCSM

STRUCTURE OF THE INTEGRAL EXPERT SYSTEM FOR THE WORK AND CREATION OF THE KNOWLEDGE DATABASE

T. Svaguša, D.Radić, J.Wharram

Keywords: *expert system, models development, experimental testing, knowledge database, internet environment, civil engineering*

1. Introduction

The research and development are two basic hallmarks in Civil Engineering Institute of Croatia (IGH) that are put in practice through activities of construction design and laboratory testing. Numerous analytic, numeric and experimental methods are used in engineering mechanics for the purposes of construction design and testing of structures.
Reinforced concrete, prestressed structures and metallic structures applied for construction of buildings, bridges, viaducts and tunnels are some of examples of engineering practice in the field of technical mechanics in IGH.

Crucial step in solving the problem of knowledge management is made by the Implementation project of computational systems launched in January 2001. For the development of the Integral Expert System the newest computational technology of the world's leading supplier of software and hardware has been used: A/ e-Work workflow management system, B/ e-ViewWise document management system, C/ Oracle 8i relational database management system, D/ Hewlett Packard computational equipment and E/ Cisco Systems network equipment.

The most important characteristic of the Integral expert system is its use in Internet and Intranet environment because units of IGH are organised all over the Republic of Croatia.

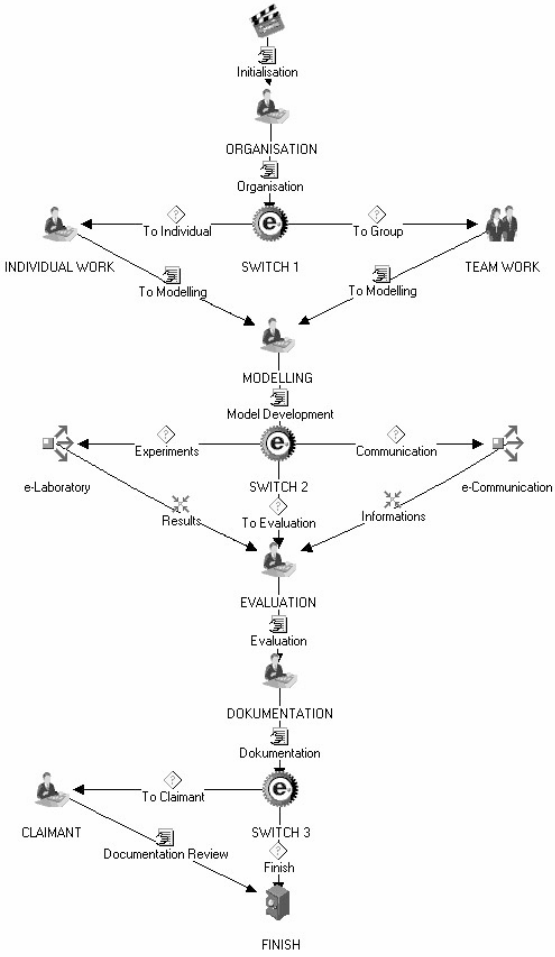

Figure 1: The e-Modelling system workflow

2. e-Work System

Workflow management system e-Work is the base of the Integral Expert System which consist of three parts: A/ The e-Modelling system, B/ The e-Laboratory Expert System and C/ The e-Communication system.

The e-Modelling system is surrounding for computer aided organisation, performance and control of the work in the field of scientific and expert research and development processes (See Figure 1). The e-Laboratory Expert System for the Laboratory Testing of Materials is the system for the computer aided performance and control of laboratory business processes with the aim of creation the Expert Knowledge Database within the fields of testing materials.

3. Knowledge Database

Knowledge Database is using the e-Work and e-ViewWise system for the management and Oracle database for data storage.
Knowledge Database has three levels.

A/ The Working Knowledge Database represents first level which is directly involved in the working process. It consists of database structure and data generated through the working processes.

B/ The Expert Knowledge Database is second level and consists of composing the catalogues and preparing them for the usage in the working process.

C/ The Scientific Knowledge Database presents third level and serves to elaborate the Knowledge Database and to extract scientific knowledge from the data in the Knowledge Database.

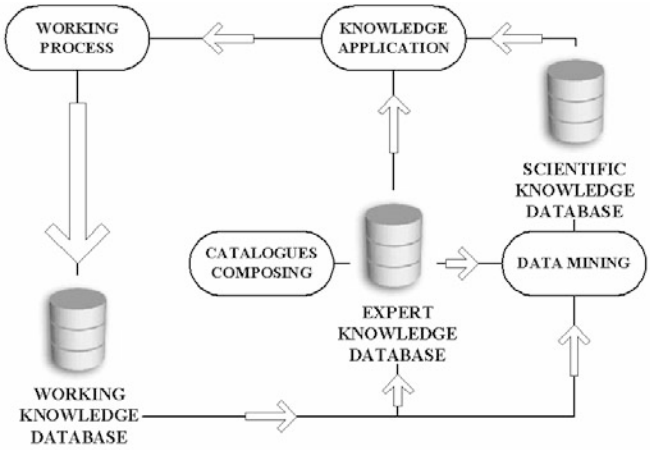

Figure 2. The Knowledge Database principal scheme

4. Conclusion

The Integral Expert System enables performance of the expert and scientific working processes in daily, research and development tasks within the field of technical mechanics, soil and rock mechanics and other expert and scientific areas in the field of civil engineering and creation od the Knowledge Database. Working surrounding of Internet environment enables access to Knowledge Database from all locations and to all users in the system. Dynamic structure and possibilities of extension of the system follows business organisation of IGH enabling extension and collaboration with other institutions and subjects interested for shearing expert and scientific resources and computational technology capacities. Integral ES generated solid foundations for further development of Knowledge Management and application of Artificial Intelligence and Decision Support Systems.

References

[1] Svaguša T., Radiæ D., Juriæ S., Wharram, J., "Structure of the Expert System for the Laboratory Testing of Materials e-Laboratory", Proceedings MATRIB 2003., Croatian Society for Materials and Tribology.
[2] Metastorm e-Work, "Designer User Manual - Version 5", Metastorm Co., London UK, 2001
[3] Computhink e-vW, "Training Manual - User & Advanced User", Computhink Inc., Chichago USA, 2002
[4] Q.Dong Q., Yan X, Chirco R.D., Wilhoit R.C., Frenkel M., "Database Infrastructure to Support Knowledge Management in Physicochemical Data - Application in NIST/TRC SOURCE Data System", Proceedings 18th CODATA Conference, Montreal, Canada, September 2002

Tomislav Svaguša, B.Sc.Mech.Eng.
Civil Engineering Institute of Croatia, Department for Steel Structures, Janka Rakuše 1, Zagreb, Croatia, Phone: ++385 1 6144 111, Fax: ++385 1 6144 756, e-mail: tsvagusa@zg.igh.hr
Dragan Radiæ, Dr.Sc.Civ.Eng.
Hermes-Consulting, Nehruov trg 42, Zagreb, Croatia, e-mail: hermes-consulting@zg.tel.hr
Joseph Wharram, Executive Vice President
Computhink Inc., 860 Parkview Blvd, Lombard, IL 60148, U.S.A., jwharram@computhink.com

4th International Congress
of Croatian Society of Mechanics
September, 18-20, 2003
Bizovac, Croatia

4thICCSM

ADAPTIVE TECHNIQUE IN NONLINEAR PROBLEMS

Ladislav Svoboda, Daniel Rypl, Zdeněk Bittnar

Keywords: adaptivity, plasticity

1. Introduction

Recently the authors have discussed error estimation procedures and adaptive mesh design based on recovery of stresses, strains and other gradients for linear problems. Application of such methods to practical engineering analysis is widely available today. Presently we are engaged in the extension of the methodology to nonlinear problems. At first glance, it appears simple because the solution is generally obtained by successive linearization, however several difficulties arise which we shall discuss here. The applications in this paper are focused on static problems of elasto-plasticity, common in engineering.

Generally, due to path dependency of the solution in materially nonlinear analyses, the loading is applied in an incremental manner with an iterative linearization, using the Arc-length method in each increment. The iteration is usually continued until a suitable norm of variables falls under a prescribed tolerance. Depending on the tolerance used in the termination of Arc-length iteration, an additional error to that due to discretization will occur in the computational process. This paper mainly focuses on the discretization error by assuming that the magnitudes of the increments and tolerance used are sufficiently small to make the iteration errors secondary.

The observed error is function of the loading and the decision of remeshing, while the nonlinear computation is being carried out, requires important engineering judgement. An appropriate norm of variables must be devised to monitor the accuracy of the solution helping to recognize the necessity of remeshing.

Various measures of error are adapted by investigators. The majority use either the L_2 norm of displacements or the energy norm. Some, however, use local indicators i.e. values of plastic strain or gradients of total displacement. This kind of criterion is usually used in localization problems and can only indicate the existence of error but not its magnitude. In this paper we will use energy norm computed from recovered stresses, which have proved to be the best in linear problems. The norm will be slightly adapted to suit plasticity problems. Obviously, success of this error estimation is depended on exactness of recovery method used and therefore we shall take the advantage of SPR (Superconvergent Patch Recovery) method, which has shown excellent performance in linear problems.

The majority of investigators compute error on the whole domain, it means also in plastic zones. Therefore they use incremental energy norm. In n-th increment the corresponding error is computed and added to the total error reached in increment $n-1$. The total error is stored at integration points and after generating a new mesh, corresponding values must be constructed for the new integration points. In this paper, however, the accuracy is controlled in elastic zones only. Therefore, in every increment the total error is computed again, thus it is not necessary to store the values. Then the error is compared with the prescribed limit, which is not, however, constant over the domain. The highest accuracy is required on elements close to plastic zones.

In this paper, after a short overview of general formulation of plastic problems, we explain the error norm used in the error estimator. The problem of updating the state variables after remeshing is discussed in some details too. Finally, we conclude our paper by some numerical examples.

Acknowledgement
Financial support was provided by IGS grant No. 0301011.

References
[1] Bittnar, Z. and Šejnoha, J., "Numerické metody mechaniky 1", ASCE Press Prague, 1992
[2] Bittnar, Z. and Šejnoha, J., "Numerické metody mechaniky 2", ASCE Press Prague, 1992
[3] Boroomand, B. and Zienkiewicz, O.C., "Recovery procedures in error estimation and adaptivity Part II: Adaptivity in nonlinear problems of elasto-plasticity behaviour", Comput. Methods Appl. Mech. Engrg., Vol.176, 1999,pp 127-146
[4] Zienkiewicz, O.C. and Zhu, J.Z., "Adaptivity and mesh generation", Int. J. Numer. Methods Eng., Vol.32, 1991,pp 783-810

Ing. Ladislav Svoboda
Czech Technical University, Department of Structural Mechanics, Thákurova 7, 166 29 Praha 6, Czech Republic, ladislav.svoboda@fsv.cvut.cz
Doc. Dr. Ing. Daniel Rypl
Czech Technical University, Department of Structural Mechanics, Thákurova 7, 166 29 Praha 6, Czech Republic, drypl@fsv.cvut.cz
Prof. Ing. Zdeněk Bittnar
Czech Technical University, Department of Structural Mechanics, Thákurova 7, 166 29 Praha 6, Czech Republic, bittnar@fsv.cvut.cz

4th International Congress
of Croatian Society of Mechanics
September, 18-20, 2003
Bizovac, Croatia

4thICCSM

EXPERIMENTAL METHOD OF MEASUREMENTS IN MULTIBODY DYNAMICS

Aco Šikanić, Sadko Mandžuka, and Dario Seferović

Keywords: filming, spatial movement, kinematics measurements, double somersault

1. Introduction

In spatial movement of dynamical systems in general case, the symmetrical distribution of masses changes with respect to the main plane of symmetry, as well as with respect to other referent planes. Typical examples of such systems are propulsion robots, and the human body as well.
Due to the complexity of the system of differential equations, set by the methods of spatial movement dynamic analysis, it is assumed that the additional kinematics parameters necessary for its solving will be determined by measuring characteristics parameters on the basis of taken motion pictures of the analysed movement, and that it will be possible to define a pattern of asymmetric multiple system spatial movements.

In other words, a number of equations will be eliminated by applying the measurement results obtained by the described method. As an example of the system to be analysed and measured, the right lower leg of a gymnast performing a double somersault will be taken.

2. Description of the System

The basic equipment of a photogrammetric system includes the following:
- PC with adequate graphics and video processor and appropriate software support, which make the core of the system.
- Black and white digital monitor for the selection of particular operations and as interface for the input of data necessary for carrying out analysis.
-High resolution colour monitor which besides being used for the viewing of the recorded material from the video recorder, is primarily used for the digitisation of each of body's reference points, for the presentation of particular phases of data processing and for the presentation of the results of the analysis.
- Video cameras are necessary to film the movement which is to be analysed. In order to reconstruct the movement in three-dimensional space at least two cameras are needed. In order to ensure the precision of filming, the cameras should be placed on adequate tripods.
- Video recorder is necessary for viewing recorded material and selection of the sequences which are to be analysed. It is directly connected to the central computer, which enables the transfer of video recording into the memory of the computer.
- Calibration frame is needed to transform digital recordings of two or more cameras into real three-dimensional images.

3. Filming

For the needs of three dimensional (3D) analysis at least two video cameras are necessary. The cameras should be positioned so that each of them can film the complete movement, special attention should be paid to the possibility of high quality filming of relevant joints and points of the body at the most crucial moments of the analysed movement. Also, the cameras should be positioned so that they mutually close an angle of 90 degrees, with a possible deviation as allowed by the software.

4. Digitisation of Video Recording

After high speed movies are taken, the first step in the analysis of spatial movement is the transformation

of the video recording into a number of frozen images in digitised format, which are then being input into the computer memory. The data stored in this way enable multiple manipulation of the recording, depending on the needs imposed by the characteristics of the analysed movement.

5. Digitisation of the Reference Points of Human Body

To achieve that, on each digitised image of the video recording, which is separately for each camera, one by one retrieved from the computer memory to the high resolution monitor, it is necessary to identify and locate anatomic points that describe human body. On the basis of digitisation of these referent points, that is by defining numerical co-ordinates of their position, applying suitable mathematical model, it is possible to locate and orientate each of the body's segments, and thus also the whole body while performing the analysed spatial movement. Since during the digitisation of referent points these points are also connected, in every image of the recording stick figures are created. The stick figures are described by lines running through the centres of gravity of particular body segments.

6. Three-Dimensional Transformation

Transformation in the process of converting two or more two-dimensional digital recordings into three-dimensional images. The process is computer controlled by means of specially developed software.

7. Measuring and Filtering of Kinematics Parameters and Data Presentation

Digitised referent points of the human body represent a series of measurements that have the number of repetitions that corresponds to the number of images in a recorded sequence. Their digitised values consist of their precise co-ordinates and of the amount of error resulting from the impossibility to locate precisely on the monitor anatomic points of the body. Data filtering is the procedure during which from the three-dimensional recording of the movement, noise and errors occurring during digitisation are being removed.

Data presentation is the final stage in data processing for the needs of spatial movement analysis. The majority of the existing systems enable data presentation in three basic manners: animation, graphs, numerical readout.

9. Conclusion

On the basis of the previous considerations, it may be concluded that the presented method of characteristic kinematics parameters measurements for the purpose of solving asymmetric multiple mechanical system spatial movements might be used with sufficient accuracy for the study of similar movements.

The method enables the determination of qualitative and quantitative influence of asymmetric mechanical system spatial movements on the positional changes of the motion curve of the centre of masses, and determination of optimal paths of the system, as well as the changes in the values of central dynamic moments of inertia in propulsion motion.

Applying the method, additional knowledge is gained, which enables a more successful approach to spatial movement optimisation.

References

[1] Ariel Performance Analysys System, Inc. California

[2] Hraski, Ž., Mejovšek, M., Primjena sustava za kinematičku analizu sportskih tehnika. Zbornik radova: Trener i suvremena dijagnostika, Zagreb, 1999.

[3] Šikanić, A., Istraživanje dinamike nesimetričnih višečlanih mehaničkih sustava, Disertacija, Fakultet strojarstva i brodogradnje, Sveučilište u Zagrebu, 2000.

[4] Terze, Z., Muftić, O., Dinamička analiza rotacijskog dijela gibanja čovjekova tijela u gravitacijskom polju sile teže. Kineziologija 27, (3-10), 1995.

Aco Šikanić, PhD, Brodarski institut, Av. V. Holjevca 20, Zagreb, Croatia,
Phone:+385 1 6504 105, Fax: +385 1 6504 360, e-mail: aco.sikanic@hrbi.hr
Sadko Mandžuka, PhD, Brodarski institut, Av. V. Holjevca 20, Zagreb, Croatia,
Phone:+385 1 6504 104, Fax: +385 1 6504 440, e-mail: sadko.mandzuka@hrbi.hr
Dario Seferović, BSc, Brodarski institut, Av. V. Holjevca 20, Zagreb, Croatia,
Phone:+385 1 6504 348, Fax: +385 1 6504 440, e-mail: dario.seferovic@hrbi.hr

4th International Congress
of Croatian Society of Mechanics
September, 18-20, 2003
Bizovac, Croatia

4thICCSM

WELL BALLANCED Q-SCHEME FOR NOZZLE FLOW EQUATIONS

Jerko Škifić, Luka Sopta and Senka Vuković

Keywords: *nozzle flow, Q-scheme, exact conservation property*

1. Introduction

Hyperbolic systems with geometrical source terms arise in various applications. One such application is fluid flow with cross section area variations, which arise naturally in the study of fluid flow phenomena in ducts, pipes, shock tubes, and nozzles. In such applications the source term may have low regularity, which causes numerical difficulty particularly when steady state solutions are computed. The fix for this numerical difficulty is to approximate the source term using decomposition and upwinding, thus creating balance between numerical flux gradient and numerical source term. In this paper we introduce extension of the Q-schemes proposed in [1] to nozzle flow equations, i.e., Euler equations with geometrical source term.

2. Mathematical model of nozzle flow equations with geometrical source term

Let us consider unsteady flow of compressible fluid. The appropriate governing partial differential equations form a balance law system:

$$\mathbf{u}_t + \mathbf{f}(\mathbf{u})_x = \mathbf{g} \tag{1}$$

where vectors for the conserved variables, flux, and source term are as follows:

$$\mathbf{u} = \begin{pmatrix} A\rho \\ A\rho v \\ AE \end{pmatrix},\ \mathbf{f} = \begin{pmatrix} A\rho v \\ A(\rho v^2 + p) \\ Av(E+p) \end{pmatrix},\ \mathbf{g} = \begin{pmatrix} 0 \\ pA_x \\ 0 \end{pmatrix} \tag{2}$$

Here t is the time, x is distance along the domain, ρ is fluid density, $A = A(x)$ is cross-sectional area, p is pressure in the fluid, v is fluid velocity, and E is fluid internal and kinetic energy.

3. Numerical methods for nozzle flow equations

General form of first-order Q-scheme is given by:

$$\mathbf{u}_i^{(n+1)} = \mathbf{u}_i^{(n)} - \frac{\Delta t}{\Delta x}\left(\mathbf{f}_{i+1/2}^{(n)} - \mathbf{f}_{i-1/2}^{(n)}\right) + \Delta t \mathbf{g}_i^{(n)} \tag{4}$$

$$\mathbf{f}_{i+1/2}^{(n)} = \frac{1}{2}\left(\mathbf{f}_i^{(n)} + \mathbf{f}_{i+1}^{(n)}\right) - \frac{1}{2}\left|\mathbf{Q}_{i+1/2}^{(n)}\right|\left(\mathbf{u}_{i+1}^{(n)} - \mathbf{u}_i^{(n)}\right) \tag{5}$$

$$\mathbf{g}_i^{(n)} = \mathbf{g}_{i+1/2}^{(n),L} + \mathbf{g}_{i-1/2}^{(n),R} \tag{6}$$

$$\mathbf{g}_{i+1/2}^{(n),L} = \frac{1}{2}\left(\mathbf{I} - \mathbf{R}_{i+1/2}^{(n)}\boldsymbol{\Lambda}_{i+1/2}^{(n)\ -1}\left|\boldsymbol{\Lambda}_{i+1/2}^{(n)}\right|\mathbf{L}_{i+1/2}^{(n)}\mathbf{R}_{i+1/2}^{(n)\ -1}\right)\mathbf{G}_{i+1/2}^{(n)} \tag{7}$$

$$\mathbf{g}_{i+1/2}^{(n),R} = \frac{1}{2}\left(\mathbf{I} + \mathbf{R}_{i+1/2}^{(n)}\boldsymbol{\Lambda}_{i+1/2}^{(n)\ -1}\left|\boldsymbol{\Lambda}_{i+1/2}^{(n)}\right|\mathbf{L}_{i+1/2}^{(n)}\mathbf{R}_{i+1/2}^{(n)\ -1}\right)\mathbf{G}_{i+1/2}^{(n)} \tag{8}$$

Here $\boldsymbol{G}_{i+1/2}^{(n)}$ is the numerical term related to the source term and its formulation is balance law dependent. In the nozzle flow case we choose:

$$\boldsymbol{G}_{i+1/2}^{(n)} = \begin{pmatrix} 0 \\ p_{i+1/2}^{(n)}\left(A_{i+1} - A_i\right) \\ 0 \end{pmatrix}. \tag{9}$$

and for such a version of the Q-schemes the exact conservation property is valid.

4. Numerical results

The achieved property of the proposed upwind schemes is the obtained correct balancing of the flux gradient and the source term. In order to illustrate the quality and the achieved improvement of these schemes we compare them with their versions with pointwise evaluated source term.
Several tests were conducted. Test with quiescent flow in a nozzle with irregular geometry showed that pointwise version produced unacceptably large errors, while balanced version showed exceptionally good results. Test with subsonic flow in a nozzle with irregular geometry showed equivalent results with the test with quiescent flow in a nozzle with irregular geometry, while test with a subsonic flow with shock showed that due to smooth nozzle geometry, pointwise and balanced schemes produced almost identical results.

5. Conclusion

The proposed new schemes for nozzle flow equations in the general case, i.e. for pipes and nozzles with irregular geometry, are based on the approach developed by Bermudez and Vasquez in [1]. As it is proved in the article the new schemes have the exact conservation property, i.e., they preserve exactly the quiescent flow. The numerical results in three test problems illustrate the superiority of the proposed approach when compared to the pointwise version of the same schemes.

References

[1] A. Bermudez, M.E. Vasquez, *upwind methods for hyperbolic conservation laws with source terms*, Computers And Fluids 23, 1049-1071 (1994).

[2] A. Harten, P.D.Lax, B. Van Leer, *On upstream differencig and Godunov-type schemes for hyperbolic conservation laws,* SIAM Review, Vol. 25, 35-61 (1983).

[3] J. D. Anderson Jr., *Computational fluid dynamics*, McGraw-Hill, New York 1995.

[4] A. J. Chorin, J. E. Marsden, *A mathematical introduction to fluid dynamics*, Springer-Verlag, New York, 1992

[5] R. J. Leveque, *Finite volume methods for hyperbolic problems*, Cambridge University Press, 2002.

[6] E. F. Toro, *Riemann solvers and numerical methods for fluid dynamics*, Springer-Verlag, Berlin, 1999.

Jerko Škifić, Young Assist.
Faculty of Engineering University of Rijeka, Department of Fluid Mechanics and Computational Engineering, Vukovarska 58, Rijeka, Croatia, 00385 (0)51 651497, 00385 (0)51 651490, jerko.skific@riteh.hr
Luka Sopta, Prof, Ph.D.
Faculty of Engineering University of Rijeka, Department of Fluid Mechanics and Computational Engineering, Vukovarska 58, Rijeka, Croatia, 00385 (0)51 651493, (0)51 651490, luka.sopta@riteh.hr
Senka Vuković, Asc. Prof, Ph.D.
Faculty of Engineering University of Rijeka, Department of Fluid Mechanics and Computational Engineering, Vukovarska 58, Rijeka, Croatia, 00385 (0)51 651494, 00385 (0)51 651490, senka.vukovic@ri.htnet.hr

4th International Congress
of Croatian Society of Mechanics
September, 18-20, 2003
Bizovac, Croatia

4thICCSM

DYNAMIC SIMULATION OF TRANSPORT AIRCRAFT LANDING IMPACT

Z. Terze, H. Wolf, S. Janković

Keywords: *Dynamics of landing aircraft, Multibody system aircraft model, Non-linear landing gear dynamics, Landing aircraft dynamic simulation.*

1. Introduction

During landing and taxi, an aircraft landing gear and parts of the airframe can be exposed to high dynamical loading. In the extreme situations even damages and loss of the stability of an airplane may be expected. Since during more common tail-down two-point landing conditions all of dynamical loads are carried on the main gears first, dynamical characteristics of the main gear are of the most significant importance for the safe touchdown during which the airframe load factors will be kept in the prescribed range. Although the basic characteristics of a landing aircraft dynamical response can be determined by linear dynamic analysis, the more accurate time-simulation requires full-scale non-linear multibody approach. Since dynamical response of a landing aircraft includes some unsteady aspects, not only because of the external landing impact, but also with regard to highly non-linear phenomena within landing gear mechanism, utilization of MBS modelling principles is mandatory.

2. Landing aircraft dynamical model

The aircraft dynamical model that allows for non-linear dynamic simulation of planar landing and taxi is designed as a five rigid-body multibody system. The model has variable kinematical structure but basically possess 7 planar degrees of freedom (DOF). The upper and lower part of landing gear is connected *via* non-linear force coupler modelled according to the shock absorber dynamical characteristics. Because of its great influence on an aircraft ground dynamical behaviour, the dynamical model of the main landing gear shock absorber is considered in details. To model aircraft tire dynamics an another non-linear force coupler is added to the overall model. The applied tire dynamical model considers its dynamical behaviour (inertia effects, centrifugal growth of tire radius), but side-loads and hysteresis effects are neglected for this type of simulations.
The aerodynamic axial and normal forces as well as pitching moment for the airplane configuration with landing gear in extended down position and the arbitrary deployed flaps and slots have been considered. In order to determine the airplane touchdown flight parameters, that serve as initial conditions for aircraft landing dynamical simulations, a flight trajectory prior to touchdown has been studied in the vertical plane by 3 DOF model with longitudinal wind.

3. Landing impact dynamic simulations

On the basis of the presented aircraft dynamical model, the landing impact dynamic simulations, prior to the nose gear ground contact, were performed for five initial descent velocities. Generally, dynamic simulations based on the presented non-linear multiple-DOF dynamical model, reveal that an aircraft pitching dynamics and shock absorber dynamical characteristics should not be neglected or too simplified during estimation of main landing gear and airframe dynamical loads during land-

ing impact. As an illustration of the results the graph in Figure 1 presents total force in the shock absorber strut of one elastic leg as a function of time and different touchdown descent velocities. Since the main landing gear comprises two legs, the total dynamic load transferred by the gear to the airframe has doubled value. By rewieving the other simulation results presented in the paper, it can be concluded that the wheel-spin-up forces increase up to the significant values that are comparable to the vertical dynamical loads.

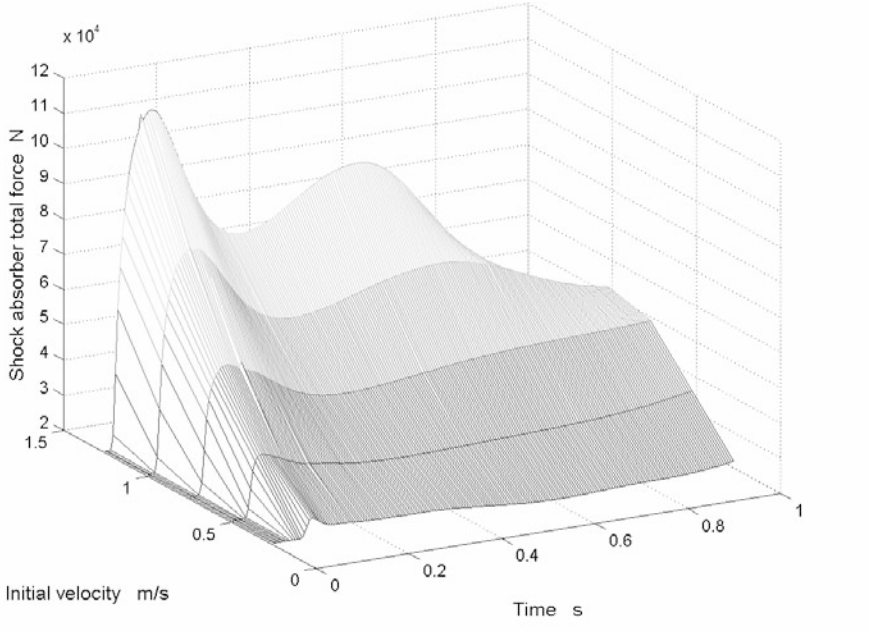

Figure1. Shock absorber total force *vs* time. Dynamic simulation results for five initial descent velocities $v_{z1} = 0.25\,\mathrm{ms}^{-1}$, $v_{z1} = 0.5\,\mathrm{ms}^{-1}$, $v_{z1} = 0.75\,\mathrm{ms}^{-1}$, $v_{z1} = 1.0\,\mathrm{ms}^{-1}$ $v_{z1} = 1.25\,\mathrm{ms}^{-1}$

References

[1] Chester, D. H., "Aircraft Landing Impact Parametric Study with Emphasis on Nose Gear Landing Conditions", Journal of Aircraft, 39, 2002, pp 394-403.

[2] Gerard van Es, W. H., "Pitching Moment Change Caused by High-Lift Devices on Wing-Body Configurations", Journal of Aircraft, 40, 2003, pp 391-393.

[3] Smiley, R. F., Horne, W. B., "Mechanical Properties of Pneumatic Tires with Special Reference to Modern Aircraft Tires", NACA Report No. 4110, 1958

[4] Terze, Z., et al, "Null Space Integration Method for Constrained Multibody System Simulation with no Constraint Violation", Multibody System Dynamics, 6, 2001, pp 229-243.

[5] Yadav, D., Ramamoorthy, R. P., "Nonlinear Landing Gear Behavior at Touchdown", Journal of Dynamic Systems, Measurement, and Control, 113, 1991, pp 677-683.

[6] Aircraft Maintenance Manual A319/A320, Airbus Industries, 2001

[7] Joint Aviation Requirements, JAR-25, Large Aeroplanes, 1996

Terze, Z., PhD, Assistant professor
Faculty of Mech. Eng. Nav. Arch./University of Zagreb, Dept. of Aerospace Engineering
Ivana Lucica 5, Zagreb, Croatia, tel: 6168476, e-mail: zdravko.terze@fsb.hr
Wolf, H., PhD, Assistant professor
Faculty of Mech. Eng. Nav. Arch/University of Zagreb, Dept. of Applied Mechanics,
Ivana Lucica 5, Zagreb, Croatia, tel: 6168168, e-mail: hwolf@fsb.hr
Jankovic, S., PhD, Professor
Faculty of Mech. Eng. Nav. Arch/University of Zagreb, Dept. of Aerospace Engineering,
Ivana Lucica 5, Zagreb, Croatia, tel: 6168267, e-mail: slobodan.jankovic@zg.tel.hr

4th International Congress
of Croatian Society of Mechanics
September, 18-20, 2003
Bizovac, Croatia

4thICCSM

ELASTOPLASTIC ANALYSIS OF CIRCUMFERENTIAL CRACKS IN PIPES

Z. Tonković, I. Skozrit and J. Sorić

Keywords: *elastoplastic fracture analysis, J-integral evaluation, pipes, through-wall circumferential cracks, off-centre cracks, combined internal pressure and bending*

Abstract

Elastoplastic fracture analysis of cracks existing in engineering structures is very important in assessing their structural integrity in nuclear power, chemical, civil and mechanical engineering. The crack opening displacement and *J*-integral of a through-wall circumferential crack in a pipe are the fundamental quantities for evaluating the reliability of a cracked component. The *J*-estimation for this crack configuration under various loading conditions, such as pure bending, pure tension and combined bending and tension, has been considered in References [2-4]. A postulated through-wall crack size is often calculated on the basis of its symmetric placement with respect to the bending plane [3,4]. However, in reality, the off-centre cracks can occur due to random imperfections around the pipe circumference. Elastic and elastoplastic finite element solutions for the *J*-integral for a pipe containing off-centre through-wall cracks under pure bending have also been presented and the special influence functions have been introduced [2]. A realistic evaluation of pipes fracture response demands consideration of more complex loading condition including combined bending and internal pressure. When fracture mechanics analysis is performed for through-wall cracked pipes subjected to internal pressure, it is a typical practice to transform the effect of pressure by the pressure-induced axial tension [3]. The hoop stress effect on the fracture response characteristics has been considered only in a limited number of studies [4]. Due to combined loading, a full parametric investigation of off-centre cracked pipes requires an enormous amount of FE computations, and thus only a limited set of solutions for non-proportional and proportional loading have been tabulated by authors in References [5,6].

The objective of the present paper is to provide additional reference data and to use it to obtain a new solution of the *J*-integral for pipes containing off-centre through-wall cracks subjected to combined internal pressure loads and bending, as shown in Figure 1. To achieve this goal, three-dimensional nonlinear finite element computations are performed within the finite element program ABAQUS [1]. The tension forces due to the pressure and pressure-induced hoop stresses are included. Under the assumption of small elastoplastic strain, the constitutive law characterizing the stress-strain response of mild steel is represented by the well-known Ramberg-Osgood model. Small, medium and large crack lengths with a variety of off-centre angles and radius-to-thickness ratios have been considered. In all tests, proportional loading approach is applied and the hoop stresses effect due to internal pressure is considered. Using finite element solutions, the effects of off-centred cracks and the loading on the *J*-integral are evaluated.

The computational results show that the *J* values for off-centre cracks are smaller than those for symmetric cracks. This statement is excepted for the offset crack angle of $\varphi = 15^{\circ}$ where the *J* values at the crack front I-II, which is farther away from the bending axis, are slightly higher than those for the symmetric centred crack. This demonstrates that for any crack size there is a limit-offset angle for which the *J*-integral values at the crack front I-II exceed those of the centred crack.

Those effects are also described in [2] for cracks under pure bending and in [5,6] for combined bending and internal pressure.

The proposed analytical approximation of elastic correction factors would reduce the computational effort in performing fracture analysis of pipes containing off-centre through-wall cracks subjected to combined internal pressure loads and bending. Further investigations should be directed towards the determination of the plastic correction factors and the limit-offset angles for the others typical crack lengths and their effects on the *J*-integral values.

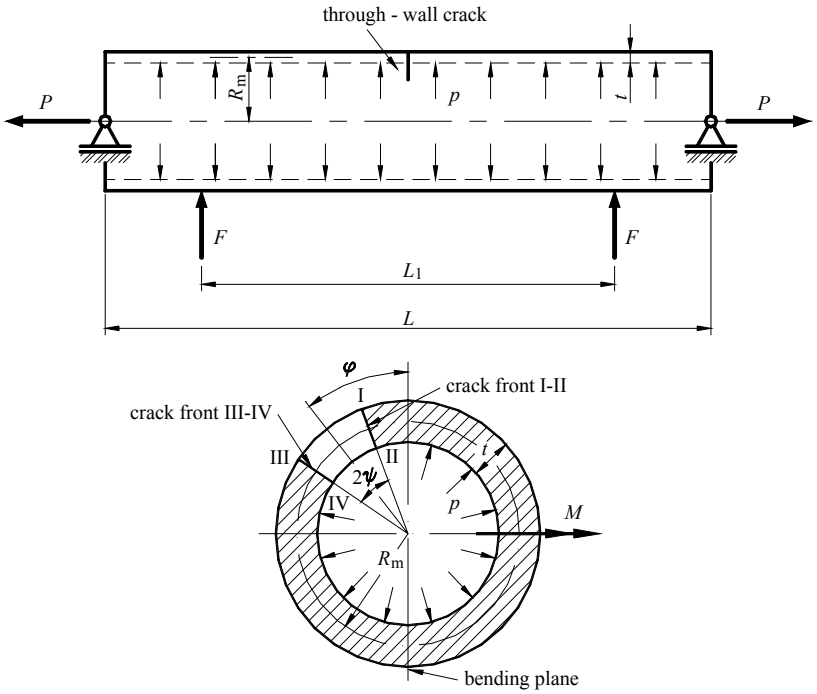

Figure 1. Off-centre through-wall crack in a pipe subjected to bending and internal pressure

References

[1] ABAQUS, "User's guide and theoretical manual", Version 6.3, Hibbitt, Karlsson & Serensen, Inc., 2003.

[2] Firmature, R. and Rahman, S., "Elastic-plastic analysis of off-center cracks in cylindrical structures", Engineering Fracture Mechanics, Vol. 66, 2000, pp. 15-39.

[3] Foxen, J. and Rahman, S., "Elastic-plastic analysis of small cracks in tubes under internal pressure and bending", Nuclear Engineering and Design, Vol. 197, 2000, pp. 75-87.

[4] Kim, Y.J., Huh, N.S. and Kim, Y.J., "Quantification of pressure-induced hoop stress effect on fracture analysis of circumferential through-wall-cracked pipes", Engineering Fracture Mechanics, Vol. 69, 2002, pp. 1249-1267.

[5] Tonković, Z. and Sorić, J., "Fracture analysis of cracked cylindrical shells under internal pressure and bending", Proceedings of The Sixth International Conference on Computational Structures Technology, Eds. Topping, B.H.V. and Bittnar, Y., Elsevier Science Ltd., Prague, Czech Republic, 2002, CD-ROM Edition .

[6] Tonković, Z., Sorić, J. and Skozrit, I., "Elastoplastic fracture analysis of through-wall cracked cylindrical shells", International Conference on Computational & Experimental Engineering and Sciences, Corfu, Greece, July 2003, accepted.

Dr. Zdenko Tonković, Assistant Professor, Tel ++385 1 6168 450, Fax ++385 1 6168 187, ztonkov@fsb.hr
Ivica Skozrit , Assistant, Tel ++385 1 6168 450, Fax ++385 1 6168 187, ivica.skozrit@fsb.hr
Dr. Jurica Sorić, Professor, Tel ++385 1 6168 103, Fax ++385 1 6168 187, jurica.soric@fsb.hr
Faculty of Mechanical Engineering and Naval Architecture/University of Zagreb, Institute of Applied Mechanics, Ivana Lučića 5, Zagreb, Croatia

4th International Congress
of Croatian Society of Mechanics
September, 18-20, 2003
Bizovac, Croatia

4thICCSM

FINITE VOLUME MODELLING OF ADHESIVE JOINTS AT SLOW AND IMPACT LOADING RATES

V. Tropsa, I. Georgiou, A. Ivankovic and A. J. Kinloch

Keywords: Adhesive joints, peel tests, fracture resistance, finite volume method.

1. Introduction

Understanding the high-rate fracture behaviour of adhesively-bonded joints is one of the key factors for their future application as a primary joining method in the automotive industry. This is due to the strain-rate sensitivity of such viscoelastic materials, which can lead to a premature failure of the joints under impact loading conditions, e.g. front-end car collisions. If such bonded joints fail prematurely (brittle fracture), the surrounding body-panels would not undergo substantial plastic deformation and the dissipated energy from the impact would be low.

Standard small-scale peel tests, such as T-peel and impact wedge-peel (IWP) tests are usually employed to describe the fracture behaviour of structural adhesives. In both tests, external loads are applied to fracture bonded portion of the peel specimen. In all tests, thin sheets of aluminium alloy substrates were bonded together using 'XD4600' and 'XD1493' structural, rubber-toughened epoxy adhesives. Although these tests are relatively easy to perform and thus popular in the industry, the analysis of the measured fracture resistance data needs extra care.

Finite volume (FV) models of above tests are developed to closely analyse mechanical and fracture processes. The specifics of each test are: a) T-peel is a quasi-static, bending dominated case with a very high geometrical aspect ratio; stress gradients in the region of neutral axis are very steep; only a smaller portion of the external energy is consumed for fracturing of the adhesive, b) IWP is a dynamic test with impact speeds typically between 1-2 m/s; with a thin substrate material the crack grows in a quasi-static manner with a substantial plastic deformations of the specimen arms; with a thick substrate material the crack tends to propagate rapidly, leaving specimen arms with a limited permanent deformation.

2. Experimental Procedures

The peel tests that are used to assess and evaluate the performance of adhesive joints and laminates can be broadly split into two categories, (a) those used in quasi-static loading conditions, (b) those employed to simulate impact loading conditions. The most representative tests in both categories are illustrated in Figure 1 (a) and (b).

2.1 Quasi-static test procedure (T-peel test)

The T-peel geometry is symmetrical and is mainly employed for testing flexible joints. The schematic of the test specimen is given in Figure 1(a). The peel force per unit width, P/b, is considered to be a measure of the strength of adhesion of the joint. However, the value of P/b is not solely dependent on the properties of the adhesive, but is also related to the test geometry, the thickness of the peel arms and their mechanical properties.

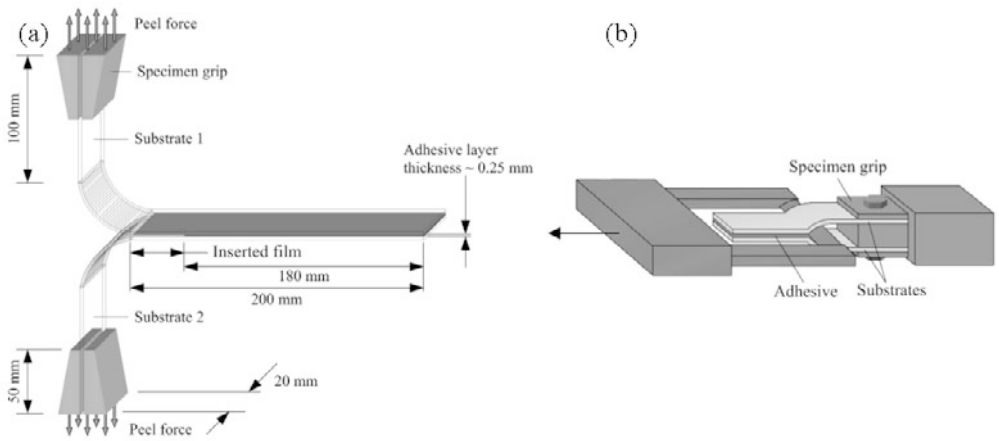

Figure 1: Schematics of the representative peel tests: (a) T-peel test; (b) Impact wedge peel test (IWP).

2.2 Impact test procedure (IWP test)

IWP tests are used to study the fracture behaviour of the structural adhesive joints at various loading rates. The test speed was varied between 0.4 and 11 m/s to investigate the effect of the rate on the cleavage force. In IWP test wedge is pulled through the adhesive joint (Figure 1(b)), which is shaped like a tuning fork. The substrates are cut out from aluminium sheets (1 and 2 mm thick).

3 Preliminary numerical results

A preliminary numerical simulation of the IWP tests was performed assuming linear-elastic behaviour for both the adhesive and the substrates. Two different geometries (i.e. 1 and 2 mm thick substrates) were modelled at an impact speed of 2 m/s. Although the analysis was limited to elastic materials, the numerical observations were qualitatively in a good agreement with the experiments. The numerical simulations predicted that in the case of thin specimens the crack was driven by the wedge at the test rate, whereas in the case of thick substrates the crack was predicted to propagate in a transient manner. The calculated crack speed was also correlating well with crack speeds measured from the high-speed photography. Examples of numerical results for both thin and thick specimens are shown in Figure 2.

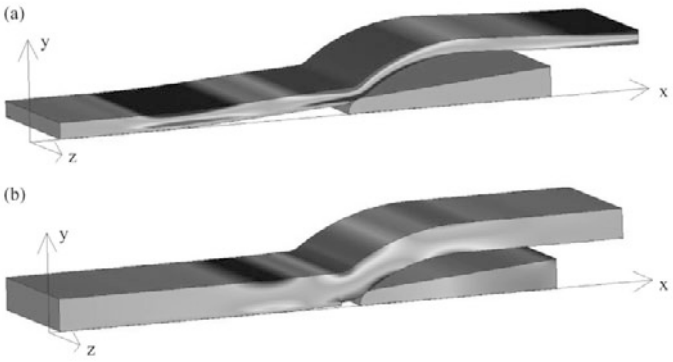

Figure 2: Normal stress σ_{xx} in IWP finite volume simulations: (a) 1 mm; 2 mm thick substrates.

Authors:

Dr. Vlado Tropsa, Imperial College, Mechanical Engineering Department, London SW7 2AZ, UK
Telephone: ++44 (0)207 594 7130, Fax: ++44 (0)207 823 8845, Email: v.tropsa@imperial.ac.uk
Dr. Ioannis Georgiou, Imperial College, Mechanical Engineering Department, London SW7 2AZ, UK
Telephone: ++44 (0)207 594 7130, Fax: ++44 (0)207 823 8845, Email: i.georgiou@imperial.ac.uk
Dr. Alojz Ivankovic, Imperial College, Mechanical Engineering Department, London SW7 2AZ, UK
Telephone: ++44 (0)207 594 7134, Fax: ++44 (0)207 594 7017, Email: a.ivankovic@imperial.ac.uk
Prof. A.J Kinloch, Imperial College, Mechanical Engineering Department, London SW7 2AZ, UK
Telephone: ++44 (0)207 594 7082, Fax: ++44 (0)207 594 7017, Email: a.kinloch@imperial.ac.uk

4th International Congress
of Croatian Society of Mechanics
September, 18-20, 2003
Bizovac, Croatia

4thICCSM

LARGE DISPLACEMENT FORMULATION FOR ELASTIC-PLASTIC SPACE FRAMES

Goran Turkalj, Josip Brnić and Domagoj Lanc

Keywords: *space frames, beam element, elastic-plasticity, non-linear displacement field, updated Lagrangian formulation, external stiffness approach, plastic hinges*

1. Introduction

In the field of structural engineering beams and frames constitute a very important class of load-carrying components, where they are applied both in their stand-alone forms and as stiffeners for some plate or shell assemblages. Because such structures, especially those of thin-walled cross-sections, could display very complex structural behaviour under a large displacement and rotation regime, the development of advanced non-linear beam models, which comprise both geometric and material inelasticity, has been a major activity of many structural engineering researchers in the recent years [1, 2].

The work presents a one-dimensional finite element formulation for non-linear analysis of space frames comprised of straight and prismatic beam members with solid and doubly symmetric cross-sections. Displacements and rotations are allowed to be large but strains are small. Using the updated Lagrangian (UL) incremental formulation, the assumption of isotropic and linear-elastic material behaviour and the non-linear displacement field of a beam cross-section based on inclusion of second-order terms of large rotations, a tangent stiffness matrix of a two-node space beam element is firstly developed. Due to the non-linear displacement field, all internal moments occurring in the geometric stiffness are obtained as those of semitangential behaviour. In this way the joint equilibrium of non-collinear elements is provided. External stiffness approach (ESA) is applied in the force recovery phase [4, 5]. Material non-linearity is introduced for an elastic-perfectly plastic material through the plastic hinge formation at finite element ends and for this a plastic reduction matrix of the element is determined. The interaction of element forces at a hinge and the possibility of elastic unloading are taken into account. The generalised displacement control method has been employed as an incremental-iterative solution strategy. After each iteration, the updating of nodal co-ordinates as well as orientations has been performed. In this, because of the non-commutative character of large incremental nodal rotations, the updating of nodal orientations for a new configuration has been performed using Rodriguez' large rotation formula.

2. Example

Figure 1a shows a framed dome loaded by a single concentrated load at the crown point. All dimensions are given in metres. Each frame member has a rectangular cross-section $b \times h$ = 0.76×1.22 m. Material moduli E = 20.69 GPa and G = 8.83 GPa. The yield strength σ_y = 80 MPa. Elastic and elastic-plastic cases are considered. In the analysis, each frame member is replaced by only one space beam element. In the elastic-plastic case, the yield function reported in Reference [2] is adopted. The obtained results for the vertical apex deflection are shown in Figure 1b, and compared with those reported by Park and Lee [3] applying three-dimensional elastic-plastic beam element being capable of incorporating large rotations and using the plastic zone approach. The significant deviation occurs after the vertical apex deflection of value 3.3 m, at which the present plastic hinge model becomes kinematically unstable due to the number of plastic hinges.

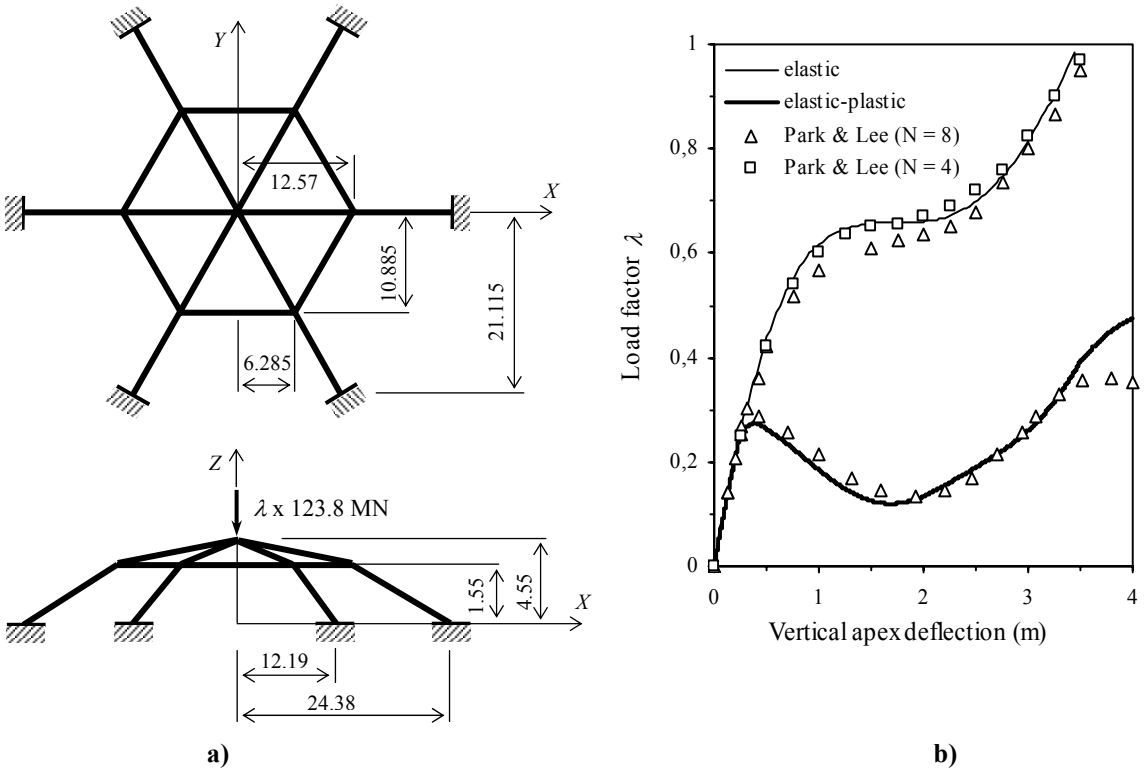

Figure 1. Frame dome

Acknowledgement

The research presented in this paper was made possible by the financial support of the Ministry of Science and Technology of the Republic of Croatia, under the project No. 0069-006.

References

[1] Gebbeken, N., "A Refined Numerical Approach for the Ultimate-Load Analysis of 3-D Steel Rod Structures", Engineering Computations, Vol. 15, No. 3, 1998, pp 312-344.

[2] McGuire, W., Gallagher, R.H., Ziemian, R.D. "Matrix Structural Analysis", John Wiley & Sons, New York, 2000.

[3] Park, M.S., Lee, B.C., "Geometrically Non-Linear and Elastoplastic Three-Dimensional Shear Flexible Beam Element of von Mises Type Hardening Material", Int. J. Numer. Meth. Eng., Vol. 39, 1996, pp 383-408.

[4] Turkalj, G., Brnić, J., Prpić-Oršić, J., "Large Rotation Analysis of Elastic Thin-Walled Beam-Type Structure using ESA Approach", Computers & Structures, 2003, in press.

[5] Turkalj, G., Brnić, J., Prpić-Oršić, J., "Updated Lagrangian formulation using ESA approach in large rotation problems of thin-walled beam-type structures", Proc. of the Eight Int. Conf. on Civil & Structural Engineering Computing, Topping, B.H.V. (ed.), Civil-Comp Press, Stirling, Scotland, 2001.

Goran Turkalj, Asst. Professor, Ph.D.
University of Rijeka, Faculty of Engineering, Department o Engineering Mechanics, Vukovarska 58, Rijeka, Croatia, Phone: ++385 51 651 499, Fax: ++385 51 651 490, e-mail: turkalj@rijeka.riteh.hr
Josip Brnić, Full Professor, Ph.D.
University of Rijeka, Faculty of Engineering, Department o Engineering Mechanics, Vukovarska 58, Rijeka, Croatia, Phone: ++385 51 651 491, Fax: ++385 51 651 490, e-mail: brnic@rijeka.riteh.hr
Domagoj Lanc, Assistant, M.Sc.
University of Rijeka, Faculty of Engineering, Department o Engineering Mechanics, Vukovarska 58, Rijeka, Croatia, Phone: ++385 51 651 495, Fax: ++385 51 651 490, e-mail: dlanc@rijeka.riteh.hr

4th International Congress
of Croatian Society of Mechanics
September, 18-20, 2003
Bizovac, Croatia

4thICCSM

COMPUTATIONAL EVALUATION OF ROAD RESTRAINT SYSTEM

M. Vesenjak, Z. Ren

Keywords: *roadside safety, road restraint system, distance spacer, finite element method, dynamic numerical simulations*

To provide appropriate safety levels for vehicle passengers the safety barriers on roads should be designed so as to absorb as much impact energy as possible in the case of vehicle impact and at the same time maintain their integrity. Practical observations of installed systems along Slovenian's highways indicate that the current design of the road restraint system is too stiff, especially in the initial phase of an impact, which results in unacceptable decelerations during vehicle impact. By adopting the European transportation legislation, it is necessary to re-evaluate the safety barriers and propose certain design changes. This requirement prompted a new research into ways how to evaluate the current road restraint system.

Traffic barriers are used to reduce severity of accidents that occur when an errant vehicle leaves the travelled way. Road restraint systems on public roads in the European Union have to fulfil the EN 1317 standard in terms of the vehicle containment level, the level of expected vehicle occupant decelerations during an impact and the consequent system deformation.

The current design of the road restraint system has been investigated with computational analyses in the framework of nonlinear dynamic finite element analysis (LS-DYNA). A 20-meter long segment of the road restraint system was modeled with the shell elements. The impacting vehicle was approximated as a rigid bumper. An elastic-plastic material model was used and failure criteria were set accounting the plastic strain in shell elements and force in bolt connections. The whole model was fixed at the posts. All surfaces of the model were defined as a single surface contact model.

The bumper was prescribed to have the initial velocity of 100 km/h at the impact angle of 20° with regard to the guardrail. The analysis time interval was set to 450 ms. The time step was set to 1,4 μs and the analyses run 85-95 hours on a PowerPC with 2 AMD 2000+ MHz processors and 2 GB RAM.

The results of computational simulations are shown in the figure 1.

Figure 1. Deformation of the road restraint system under applied load

In terms of safety, the "weakest" part of this design is the distance spacer. It can be seen that it is to stiff and does not deform as it should. In this way it does not absorb enough crash energy in order to lower accelerations and consequently the impact severity of the vehicle during its impact. With such a design it does not fulfill its main purpose and does not contribute to roadside safety.

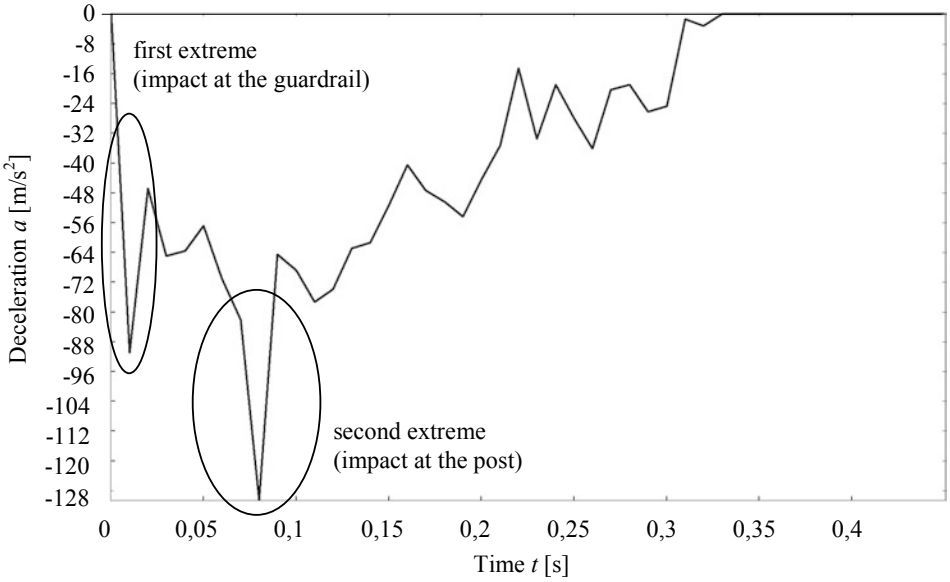

Figure 2. Lateral vehicle deceleration during impact at the road restraint system

The distance spacer has significant influence on the behavior of the road restraint system in the initial phase of an impact where it should act as an efficient energy absorber. With new distance spacer design it is possible to achieve better crash energy absorption and consequently lower the decelerations which the vehicle passengers have to withstand during an impact and thus decrease the impact severity.

The results of computational analyses prove that the current design does not deform as expected and does not absorb enough crash energy in order to lower the accelerations and consequently the impact severity during an impact. It is obvious that the current distance spacer was designed only according to the geometrical rules, regardless of its functionality.

However, it is possible to minimize the stiffness of the road restraint system and maximize the energy absorption ability of the system with new distance spacer designs. In this way the decelerations during an impact are reduced, and the roadside safety would increase rapidly.

The next phase of this research is concerned with a comparative parametrical analysis of a real vehicle impact into different road restraint system designs.

[1] Committee on Roadside Safety Figures. "Future Directions in Roadside Safety", [Online] available: http://www.nas.edu/trb/publications/ec002/part1.html [16. may, 2002].

[2] Engstrand, K. E. "Improvements to the Weak - Post W - Beam Guardrail", Worcester: Worcester Polytechnic Institute, 2000

[3] "European Committee for Standardization. European Standard EN 1317-1, EN 1317-2, Road Restraint Systems", 1998.

[4] Livermore Software Technology Corporation. "LS-DYNA Keyword User's Manual", 2001.

[5] Nafems. "Nafems – A Finite Element Dynamics Primer. Nafems Birniehill", Glasgow, 1992.

Matej Vesenjak, Dipl. Ing. Mech Eng.
University of Maribor, Faculty of Mechanical Engineering, Smetanova ul. 17, 2000 Maribor, Slovenia,
tel: +386 2 220 7717, fax:+386 2 220 7994, e-mail: m.vesenjak@uni-mb.si
Prof. Zoran Ren
University of Maribor, Faculty of Mechanical Engineering, Smetanova ul. 17, 2000 Maribor, Slovenia,
tel: +386 2 220 7702, fax:+386 2 220 7994, e-mail: ren@uni-mb.si

4th International Congress
of Croatian Society of Mechanics
September, 18-20, 2003
Bizovac, Croatia

4thICCSM

DYNAMIC ANALYSIS OF MULTIBODY SYSTEMS USING CONSTRAINT ELIMINATION METHODS

Frane Vlak, Vedrana Cvitanić and Željan Lozina

Keywords: flexible and rigid multibody systems, holonomic constraints, finite element method, time integration methods, large displacements/rotations

1. Introduction

The equations of motion for constrained flexible multibody systems can be derived by application of standard constraint elimination methods above Hamilton's principle. This leads to the following matrix form of dynamic equilibrium for systems with holonomic constraints of the type $\mathbf{\Phi}(\mathbf{q}, t) = 0$

$$\begin{aligned} \mathbf{M}\ddot{\mathbf{q}} + \mathbf{E}^{\mathrm{T}}\mathbf{S}\mathbf{e} - \mathbf{f} + \mathbf{B}^{\mathrm{T}}\left(k\boldsymbol{\lambda} + p\mathbf{\Phi}\right) = 0 \\ k\mathbf{\Phi} = 0 \end{aligned} \tag{1}$$

where $\mathbf{M}$ is symmetric mass matrix, $\mathbf{q}$ generalized displacement vector, $\ddot{\mathbf{q}}$ generalized acceleration vector, $\mathbf{e}$ deformation vector, $\mathbf{S}$ symmetric stiffness matrix, $\mathbf{f}$ external force vector, $\boldsymbol{\lambda}$ Lagrange multiplier vector and $\mathbf{E}$ and $\mathbf{B}$ are deformation and constraint gradients, respectively. Scaling factor $k = 1$ and penalty factor $p = 0$ denote the Lagrange multiplier method, $k = 0$ and $p \to \infty$ the penalty function method and $k = 1$ and $0 < p << \infty$ the augmented Lagrangian method.

Time integration of the motion equations is performed using the Newmark method without (N) and with numerical dissipation (ND), the Hilber-Hughes-Taylor algorithm (HHT) or the generalized-α method (α), that are based on Newmark kinematical hypotheses

$$\mathbf{q}_{t+\Delta t} = \mathbf{q}_t + \Delta t\dot{\mathbf{q}}_t + \left(0.5 - \beta\right)\Delta t^2\ddot{\mathbf{q}}_t + \beta\Delta t^2\ddot{\mathbf{q}}_{t+\Delta t} \qquad \dot{\mathbf{q}}_{t+\Delta t} = \dot{\mathbf{q}}_t + \left(1-\gamma\right)\Delta t\ddot{\mathbf{q}}_t + \gamma\Delta t\ddot{\mathbf{q}}_{t+\Delta t} \tag{2}$$

where β and γ are time integration parameters and Δt is time integration step.

System of equations (1) and (2) is solved iteratively using standard Newton procedure. In this article, based on the above formulations, linearized equations of dynamic equilibrium for two-node bar finite element undergoing large displacements/rotations but small strains together with imposed length constraint are derived. Developed procedures are examined and verified on single and double pendulum problem using MATLAB written code.

2. Numerical examples

Single pendulum motion, with horizontal initial position, is analysed and numerical results are compared with analytical solution in order to test efficiency of presented algorithms for dynamic analysis of constraint multibody systems. Obtained results are shown in Table 1.

Table 1. Mean number of iterations for single pendulum problem

	Time integration method			
Constraint elimination method	N	ND	HHT	α
Lagrange multiplier method (LMM)	3.290	2.840	2.574	2.762
Penalty method (PM)	3.692	3.898	3.694	3.838
Augmented Lagrangian method (ALM)	3.692	3.898	3.694	3.838

From the results shown in the paper it can be clearly seen that for Newmark method without numerical dissipation the penalty and augmented Lagrangian method (which give identical results for this problem), despite the larger number of iterations compared to Lagrange multiplier method, keep solution stability, while Lagrange multiplier method becomes unstable after cca. 380 time steps. On the other side, that instabilities are not so obvious if the displacement solutions are analysed. Displacement solution for all the analysed cases shows excellent agreement with analytical solution.

Similarly to the previous example double pendulum is analysed, too. The results shown in Table 2 are obtained using HHT time integration method with parameters $\alpha_f = 0.02$ and $\alpha_m = 0$.

Table 2. Numerical results for double pendulum problem

Problem	Mean number of iterations	Energy loss (%)	Min. penalty factor	Max. penalty factor
Unconstrained/Elastic	14.364	-0.02596460894	-	-
Constrained/LMM	4.091	-0.02598455102	-	-
Constrained/PM	3.277	-0.02596900313	50	500
Constrained/ALM	3.277	-0.02596900114	1	100

Obtained results shown in Table 2 indicate that the augmented Lagrangian method compared to the penalty method, with same mean number of iterations, gives almost similar result using smaller values of penalty factor. Relatively high mean number of iterations for unconstrained problem can be explained with rigorous convergence criterion used and it can be additionally decreased by using smaller time integration step.

4. Conclusions

A nonlinear finite element solution procedure for constrained multibody dynamic problems has been presented in this work. Four time integration schemes and three constraint elimination methods are implemented and compared on the problems of single and double pendulum. Obtained results show good agreement with theoretical solutions and thus give possibility to use these procedures for solving more complex problems.

References

[1] Geradin, M., Cardona, A., "Flexible Multibody Dynamics. A Finite Element Approach", Wiley UK, 2000

[2] Glowinski, R., Le Tallec, P., "Augmented Lagrangian and Operator-Splitting Methods in Nonlinear Mechanics", Society for Industrial and Applied Mathematics USA, 1989.

[3] Hill, R., "Aspects of invariance in solids mechanics", Adv. Appl. Mech., Vol.18, 1978, pp. 1-75.

[4] Wriggers, P., Simo, J.C, Taylor, R.L., "Penalty and augmented Lagrangian formulations for contact problems", Proceedings NUMETA 1985, Swansea UK, 1985, pp.97-106

Frane Vlak, Mr. sc., MechEng, Assistent
University of Split, Faculty of Electrical and Mechanical Engineering and Naval Arhitecture , Ruđera Boškovića bb, HR-21000 Split, Croatia, tel: + 385 21 305864, fax: + 385 21 463877, e-mail: frane.vlak@fesb.hr
Vedrana Cvitanić, Mr. sc., MechEng, Assistent
University of Split, Faculty of Electrical and Mechanical Engineering and Naval Arhitecture , Ruđera Boškovića bb, HR-21000 Split, Croatia, tel: + 385 21 305865, fax: + 385 21 463877, e-mail: vcvit@fesb.hr
Željan Lozina. Dr. sc., MechEng, Full Professor
University of Split, Faculty of Electrical and Mechanical Engineering and Naval Arhitecture , Ruđera Boškovića bb, HR-21000 Split, Croatia, tel: + 385 21 305890, fax: + 385 21 463877, e-mail: zeljan.lozina@fesb.hr

4th International Congress
of Croatian Society of Mechanics
September, 18-20, 2003
Bizovac, Croatia

4thICCSM

ABOUT THE PROPELLER INFLUENCE ON AIRCRAFT AERODYNAMIC CHARACTERISTICS

Milan Vrdoljak

Keywords: *aerodynamics, propeller wake, propeller – lifting surface interference*

1. Introduction

Flowfield at the lifting surface that is embedded in the propeller wake can significantly change as well as its aerodynamic characteristics. This influence can be of different effect depending on the aircraft configuration. Methods used in three dimensional analysis of the flow around the propeller are CFD and discrete vortex methods. Due to the problem of the numerical vortex dissipation hybrid methods of these two are also introduced. As for the propeller—wing interference calculations methods based on the propeller momentum theory are still used. In this work discrete vortex method, based on lifting line theory is used to describe propeller, its wake and its influence on the downstream lifting surface. The investigation considered in this paper is purely computational and it is assumed that the flow is subsonic and inviscid. The problem is clearly time—dependent but here it will be considered as quasisteady.

2. Propeller model

Propeller is modelled with the vortex system based on the lifting line method. Blade of finite span is described with n discrete elements each having horseshoe or Π vortex. This vortex of circulation Γ_k ($k=1 \ldots n$) consists of bound vortex placed at 1/4 chord line and trailing vortices leaving trailing edge on the element ends. Every element has a control point at 3/4 chord line in which surface boundary conditions must be satisfied

$$A_i^{\,k}\,\Gamma_k = a_i\,, \tag{1}$$

where coefficients a_i, $i=1 \ldots n$ are defined as

$$a_i = \left(-\vec{V}_\infty + \vec{\Omega}\times\vec{r}_i\right)\cdot\vec{n}_i\ .$$

Influence coefficients $A_i^{\,k}$ present induced velocity of k-th Π vortex of unit circulation on i-th control point and are determined using Biot—Savart's law. Solving equation (1) we can obtain unknown propeller blade spanwise circulation distribution Γ_k, $k=1 \ldots n$. At the beginning of calculation the propeller wake is unknown so the Goldstain's helicoidal wake is assumed.

Propeller vortex wake is formed of trailing vortices from all blades. Free—wake method is applied for propeller wake roll—up and its results are used to recalculate circulation distribution on the propeller blade in order to improve initial solution using helicoidal wake geometry.

3. Influence of the propeller wake on the lifting surface

Same vortex model used for propeller blade — rotating lifting surface and its wake is used in analysis of the fixed lifting surface — wing or tail. Lifting surface is divided into m elements each

having Π vortex of circulation Γ_j. Vortices Γ_k from vortex wake of the propeller blade ($k=1 \ldots n$) will induce velocity in control point P_i at lifting surface ($i=1 \ldots m$) with normal projection equal to $B_i^k \Gamma_k$. Influence coefficients B_i^k define influence of k-th vortex of unit circulation from the propeller wake on i-th control point of lifting surface. Circulation distribution for lifting surface under the influence of propeller can be determined using boundary condition

$$A_i^j \Gamma_j = a_i ,$$

with influence coefficients A_i^j defined as influence of j-th Π vortex of unit circulation from lifting surface ($j=1 \ldots m$) on i-th control point of the same lifting surface ($i=1 \ldots m$). Coefficients a_i are defined as

$$a_i = -\vec{V}_\infty \cdot \vec{n}_i + B_i^k \Gamma_k \ .$$

4. Results

Presented model was applied on the Purdue model propeller — two bladed propeller [1] with constant chord and given pitch $\beta(y)$. Tractor configuration was considered with propeller set in front of rectangular wing at a given angle of attack [2]. Results for wing local lift coefficient of presented model for the case of isolated wing and case of wing under the influence of propeller for one angle of referent blade ψ_0 (Figure 1) are compared with results of numerical method from [2].

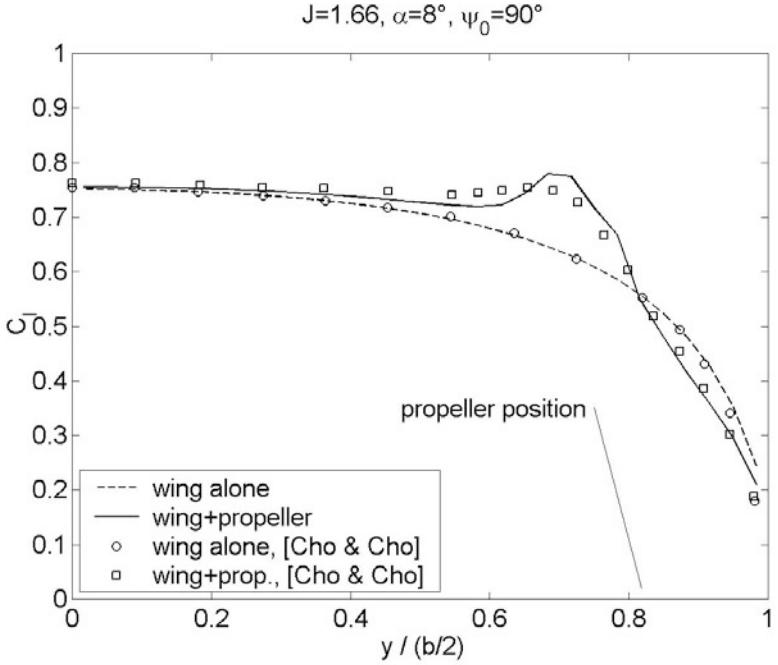

Figure 1. Wing local lift coefficient with propeller influence

References

[1] Dave P. Witkowski, Alex K.H. Lee, and John P. Sullivan, "Aerodynamic interaction between propellers and wings", Journal of Aircraft, Vol.26, No.9, 1989., pp.829–836.

[2] Jinsoo Cho and Jaeheon Cho, "Quasi–steady aerodynamic analysis of propeller–wing interaction", International Journal for Numerical Methods in Fluids, Vol.30, 1999., pp.1027–1042.

Milan Vrdoljak
Institute for Research and Development of Defense Systems, P.O. Box 252, HR-10002 Zagreb, Croatia
mvrdolja@jagor.srce.hr

4th International Congress
of Croatian Society of Mechanics
September, 18-20, 2003
Bizovac, Croatia

4thICCSM

ANALYSIS OF KINEMATICS AND FORCES IN ABOVE-KNEE PROSTHESIS DURING THE STAIR CLIMBING

A. Vučina

Keywords: kinematic analysis, above-knee prosthesis, hydraulic cylinder

1. Introduction

To date, the problem of climbing stairs for a transfemoral amputee has not been resolved. The underlaying reason for this unresolved problem of stair climbing for a person with an AK prosthesis lies in the need to introduce an external source of energy, which would provide the user with the energy required to lift the body when climbing stairs. This approach is ussually disregarded due to the presumption of a need for a robust external source of power, which would be unacceptable to the user. This paper is intended to prove the real possibility that a person with an AK prosthesis can climb stairs through a kinematic analysis of the movement of an AK prosthesis with a built-in hydraulic cylinder connected to an external source of power and analysis of forces in the AK prosthesis.

2. Analysis of kinematics and reaction forces of the stair

The recording and measuring of one transfemoral amputee are carried out (age 70, weight 70 kg, height 172 cm, amputation on right side). The AK prosthesis ENDOLITE type SFEUK with an Endolite Multiflex foot is fitted to the transfemoral examinee. The existing damper in the knee joint is substituted with a specially constructed hydraulic cylinder [1,2,3]. Five passive markers with 1 cm diameters were used for marking characteristic points on the AK prosthesis. They were placed laterally on the right side of AK prosthesis at the following points: hip, knee joint line, ankle joint line, heel and fifth toe of the prosthetic foot to study the motion of the hip, knee and foot of the prosthesis. Three staircases with different rise/run ratios were used (shallow (SH) 25º; moderate (M) 30º; steep (ST) 36º). Staircases had banisters on the left side. Two CCD cameras of ELITE system were used [4]. The movement of the AK prosthesis in a sagital plane was analyzed, from the moment of the first contact of the prosthetic foot with a step, until the moment of separation from the same step. The characteristic angles of the AK prosthesis in a sagital plane are chosen for analysis of the climb, these are the hip angle, knee angle and foot angle. Specific angles of the prosthesis in a sagital plane are defined. The analysis included the highest pressure of the hydraulic installation of the prosthesis achieved during the climbing, and also the knee moment generated by this pressure in order to make possible this stair-climbing. The period of climbing for the transfemoral amputee can be divided into four phases. The first phase is the first contact of the prosthetic foot with the stair when the examinee touches the stair with the front of his prosthetic foot. This initial phase lasted on the shallow staircase 34,386% of the total period of climbing, on the moderate staircase 40,319 % and on the steep staircase 11,820%. The initial foot angle to the surface of the stair was: on the shallow staircase 16,808°, on the moderate 9,641° and on the steep 5,422°. It was noted that as the ratio of the staircase increased the initial foot angle decreased and the lenght of the initial phase decreased. The second phase of climbing begins with the pulling of the manifold handle, in which the pulling out of the piston starts in the knee joint of the AK prosthesis.

The first reaction is that the prosthetic heel strikes and the almost simultaneous separation of the left leg from the ground, as the knee angle and hip angle decrease. Then begins the third phase of climbing, when the prosthetic foot is resting on the step and the healthy leg swings up in order to touch the second step and lift the body of the amputee. At this phase extension of the AK prosthesis in the knee joint continues until the extension is complete. The fourth phase begins at the moment when the foot of the left, healthy leg is resting entirely on the second step and prosthetic foot separates from the first step.

The average pressure in the hydraulic installation during climbing with the AK prosthesis was $86x10^5$ Pa. The maximal moment produced by the force of the hydraulic cylinder during climbing with the use of a banister was 54,28 Nm, and during the climbing with the use of both a banister on the left side and pulling on a horizontal rope with the right hand was 53,07 Nm.

For the analysis of the reaction force of a stair, detailed analysis of its vertical component for all samples of climbing was carried out. The curve of the vertical reaction force of a person with the AK prosthesis looks like the one for nonamputee [5].

During the stair-climbing with using a banister hand-hold on the left side, the first peak on vertical reaction curve was lower than the same peak for nonamputees for 27% (SH), 16% (M) and 38% (ST); The second peak was lower for 26% (SH), 24% (M) and 18% (ST); The valley was lower for 28% (SH), 22%(M) and 27% (ST) [5].

During the climbing of examinee with the AK prosthesis with the use of a banister hand-hold on the left side and horizontal pulling force by right hand, the vertical reaction force of the stair was little greather than the same force during the climbing with the use of a banister only.

3. Conclusion

It can be concluded that a hydraulic installation with $100x10^5$ Pa as nominal pressure can be used for stair-climbing with the use of a banister hand-hold. Analysing the vertical reaction force of the stair during the climbing of a person with the AK prosthesis with hydraulic cylinder built in the knee joint and connected with an external source of power, it is established that the vertical reaction force is smaller than the same force during the climbing for nonamputees. These results leed us to conclusion that it is feasible to create a drive for an AK prosthesis for stair-climbing with a unit whose weight and over-all dimensions would not interfere with the comfort of the prosthesis user.

References

[1] Dedic R., Vucina A.: One possibility for interpretation of the movement of human body. International Design Conference, Dubrovnik, Croatia, 1988.

[2] Dedic R., Vucina A.: New technical solution for improvement of movability of prosthesis for above knee amputees, International conference-RIM, Bihac, Bosnia and Herzegovina, 2000.

[3] Dedic R., Vucina A., Hudec M.: Simulation of climbing up the various types of stairs with above knee prosthesis. International Conference UPS Mostar, Bosnia and Herzegovina 2001.

[4] ELITE System Manual, BTS, Milano, 1994.

[5] Vucina A. The contribution to the research of kinematics and forces in the above-knee prosthesis during the stair climbing. Doctor thesis, University of Mostar, December, 2002.

Author: Adisa Vucina, PhD
Faculty of mechanical engineering, University of Mostar, Bosnia and Herzegovina,
Tel/Fax: 00 387 36/32 23 58, e-mail: adisa.vucina@tel.net.ba

4th International Congress
of Croatian Society of Mechanics
September, 18-20, 2003
Bizovac, Croatia

4thICCSM

A NUMERICAL ANALYSIS OF THE SHIP'S PROPELLER SHRINK-FITTING

Nenad Vulić, Lovre Krstulović-Opara

Keywords: ship, keyless propeller, shrink-fitting, nonlinear FEA analysis

1. Introduction

In merchant marine ships of nowadays, propellers play a significant role in their propulsion systems. Propellers are used to convert the shaft's rotation into the thrust force that is transmitted to the hull, causing the ship's motion. The most common junction between the propeller and the shaft is the conical keyless shrink-fit junction. This junction is of particular importance when applied on large merchant ships. Therefore, this shafting detail deserves a particular attention in design, construction, manufacture and assembly, as well as in the exploitation surveys.

Owing to the fact that there were many failures of this important junction part reported, the International Association of Classification Societies (IACS) dealt with this problem since 1978, establishing the common Unified Requirement UR K3. However, neither the all IACS societies have implemented this UR completely, nor the problem has completely been solved. This was the reason why this problem was assigned to the IACS Working Party on Machinery, with the main focus on improving the existing UR. The development of numerical tools, particularly the simulation of contact problems using the Finite Element Method, enabled more detailed analysis that was not possible in the early eighties.

The conical keyless shrink-fit junction of an 8,3 m diameter propeller of the 166.300 tdw oil tanker, presently being built in Croatia, was modelled by using the non-linear finite element package ADINA. The fitting process and the conditions met in exploitation were simulated for various operating temperatures that are strongly effecting the junction. Figure 1 shows a characteristic numerical modelling result.

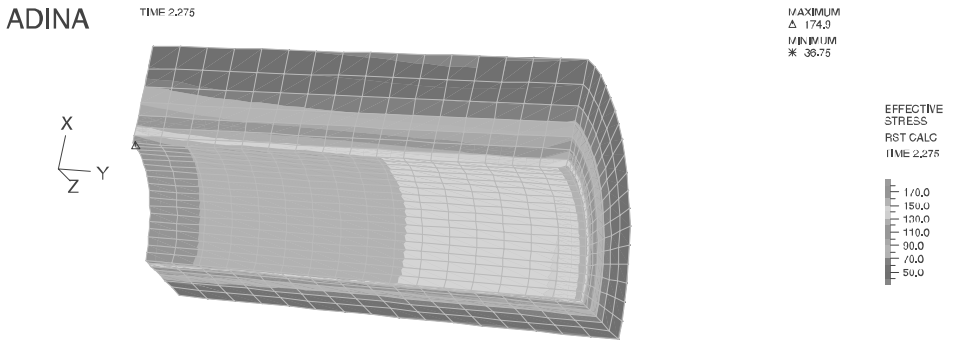

Figure 1. Effective stress distribution when cooling the junction from 18°C to 0°C

Analytical results are based on the pressure-axial displacement relation during the fitting process (1), the push-up force relation (2), and the relation describing the thermal pressure changes in exploitation (3):

$$\delta_x = p_x \cdot \frac{D_s}{2\theta}\left[\frac{1}{E_g}\left(\frac{K^2+1}{K^2-1}+\nu_g\right)+\frac{1}{E_o}\left(1-\nu_o\right)\right] \tag{1}$$

$$F_x = A \cdot p_x \cdot (\mu_0 + \theta) \tag{2}$$

$$p = p_x\left[1+\frac{D_s}{2\theta \cdot \delta_x}\left(\alpha_o-\alpha_g\right)\cdot\left(t-t_x\right)\right] \tag{3}$$

The obtained results are presented in tabular and chart forms and compared with the analytical ones obtained by the IACS UR. The analytical and numerical results show a very good agreement.

2. Conclusion

A simple analytical method and a numerical finite element approach have been implemented to the calculation of keyless shrink-fit of the propeller to its shaft. The analytical method is based on the simple analytical calculations, as stated in CRS rules [1] and IACS UR K3 [2]. The numerical modelling uses a rather complicated non-linear approach, especially when modelling the contact.

The most important conclusion is that the value of the simple analytical method has been proved, by comparing its results to the ones obtained by numerical modelling in the presented case of a real practical situation, i.e. the 166.300 tdw oil tanker. This fact is of great importance for the future development of the IACS UR K3.

Further work is going to be focused on the improvement of the analytical method, taking into account the unequal pressure distribution along the junction. Numerical results and feedback obtained during the assembly process in a shipyard will be used to evaluate the worth of the analytical approach. The final goal is to obtain a comprehensive, robust, fast and verified method, which may be easily implemented in a classification society surveyor's everyday work.

Acknowledgement

The financial support from the Croatian Ministry of Science and Technology (project No. 023023 *Fatigue strength of machines and constructions*) is gratefully acknowledged.

References

[1] -, "Rules for the Technical Supervision of Sea-Going Ships, Part 7-Machinery Installation", Croatian Register of Shipping, Split, 2002

[2] -, "Keyless fitting of propeller (without ice strengthening)", Unified Requirement K3, International Association of Classification Societies, London, 1978

[3] Internet site: www.adina.com

[4] K.J. Bathe, "Finite Element Procedures", Prentice Hall, 1996.

Dr.-Ing. Nenad Vulić
Croatian Register of Shipping, Machinery and Materials Department, Marasovićeva 67, Split, Croatia,
telephone: +385 21 408 163, telefax: +385 21 358 159, e-mail: Nenad.Vulic@fesb.hr
Dr.-Ing. Lovre Krstulović-Opara
University of Split, Faculty of Electrical Engineering, Mechanical engineering and Naval Architecture,
Ruđera Boškovića bb., Split, Croatia,
telephone: +385 21 305 891, telefax: +385 21 463 877, e-mail Lovre.Krstulovic-Opara@fesb.hr

4th International Congress
of Croatian Society of Mechanics
September, 18-20, 2003
Bizovac, Croatia

MULTISCALE MODELLING OF WOVEN COMPOSITES INCLUDING INTERFACES

Martin Wierer, Michal Šejnoha and Jan Zeman

Keywords: multiscale modelling, woven composites, homogenization, Hashin-Shtrikman variational

We pointed out in the previous works that a successful prediction of the macroscopic behavior of complex layered composite structures requires detailed modeling on various size scales [4, 6]. Bridging individual length scales is usually accomplished by introducing multi-scale or hierarchical modeling. A suitable method of attack then depends on the complexity of the problem under consideration. While an accurate coupled analysis that satisfies all the continuity and equilibrium conditions between individual scales and at the same time accounts for all the local phenomena, e.g. stress and strain gradients, is of the general interest, the computational feasibility of the problem often calls for a simplified uncoupled solution strategy. Such an approach then assumes that the analysis at individual scales is performed independently in the sense that output from one is used as an input to the second. Such a solution procedure is also adopted in the present study.

As suggested by the title the general goal of this contribution is to address an effect of imperfect bonding on the response of woven composites usually supplied in the form of complex multilayered structures. A typical example of such a structure is displayed in Fig. 1. In particular, the large macroscopic structural part is represented by the wound composite tube of the size of meters while the smallest scale to be considered is of the size of graphite fiber diameter, which is about 10μm, the graphite fiber being a part of the basic building block - the fiber tow (about 12 000 fibers). The present geometrical arrangement thus promotes the analysis to be carried out on three levels (micro - level of fiber tows, meso - single ply, macro - laminated tube). However, since the emphasis is on the modeling of interfacial behavior between individual tows within a single ply we limit our attention to two lowest scales only (micro and meso-scale).

It is well known that the essential part in the modeling of composites is the formulation of representative volume element (RVE). While the periodic nature of a fiber-tows arrangement, Fig. 1(a), reduces the basic geometrical model on meso-scale to a certain periodic unit cell, the distribution of fibers within individual tows (micro-scale) assumes random character, see Fig. 1(c). Analysis of material systems with periodic fields is now well understood and the interested reader may consult the work of, e.g., [2] among others. Analyses of material systems with disordered microstructures, however, are still a subject of ongoing research. Some promising directions are discussed in papers [7, 5]. In the present contribution, this difficulty is handled by employing a computational model based on the extended Hashin-Shtrikman variational principles [3] to provide estimates of the local fields on micro-scale. Numerical analysis on micro-scale is then followed by mesoscopic analysis of a certain periodic unit cell formed by individual fiber-tows. Standard homogenization technique based on periodic fields is implemented within the framework of the finite element method [2] and extended to account for the imperfect bonding along the fiber-tow interfaces.

The constitutive modeling on both scales is completed by including the time dependent behavior of individual phases using the concept of eigentresses. In particular, the generalized Leonov model is implemented to govern the nonlinear viscoelastic response of the matrix phase. In addition, the tensile brittle failure of the polymeric matrix at the fiber matrix interface is assesed with the help of plastic-damage model discussed in [1].

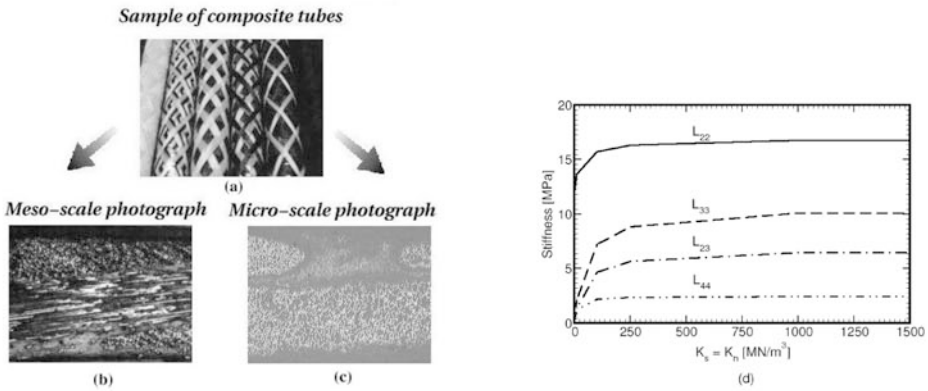

Figure 1. Multiscale model and effective properties of the two-ply composite tube

As an example we plot homogenized stiffnesses of the two-ply woven composite tube found with the present approch for various material properties of the interface between individual fiber-tows, see Fig. 1(d). Note that K_s and K_n represent the diagonal entries of the interface material stiffness matrix.

Acknowledgement

This work was sponsored by GAČR grants 106/03/0180 and GP103/01/D052 and by CTU project No. CTU030111.

References

[1] K. de Proft. *Combined experimental-computational study to discrete fracture of brittle materials*. PhD thesis, Vrije Universiteit Brussel, Brussel, 2003

[2] J.C. Michel, H. Moulinec, and P. Suquet. Effective properties of composite materials with periodic microstructure: A computational approach. *Computer Methods in Applied Mechanics and Engineering*, 172:109–143, 1999.

[3] P. Procházka and J. Šejnoha A BEM formulation for homogenization of composites with randomly distributed fibers *Engineering Analysis with Boundary Elements*, 27(2):137–144, 2003.

[4] M. Sejnoha and J. Sejnoha. Multiscale modeling in engineering. *Slovak Journal of Civil Engineering*, Accepted for publication, 2001.

[5] M. Šejnoha and J. Zeman. Overall viscoelastic response of random fibrous composites with statistically quasi uniform distribution of reinforcements. *Computer Methods in Applied Mechanics and Engineering*, 191(44):5027–5044, 2002.

[6] J. Šejnoha and M. Šejnoha Multi-scale modeling of composites with randomly distributed phases. Theoretical and Applied Mechanics, 141–152, 2001.

[7] J. Zeman and M. Šejnoha. Numerical evaluation of effective elastic properties of graphite fiber tow impregnated by polymer matrix. *Journal of the Mechanics and Physics of Solids*, 49:69–90, 2001.

Mgr. Ing. Martin Wierer
Czech Technical University in Prague, Faculty of Civil Engineering, Department of Structural Mechanics, Thákurova 7, 166 29 Prague 6, Czech Republic, Tel:+420-2-24354472, Fax:+420-2-24310775,
e-mail:martin.wierer@fsv.cvut.cz
Doc. Ing. Michal Šejnoha, Ph.D.
Czech Technical University in Prague, Faculty of Civil Engineering, Department of Structural Mechanics, Thákurova 7, 166 29 Prague 6, Czech Republic, Tel:+420-2-24354494, Fax:+420-2-24310775,
e-mail:sejnom@fsv.cvut.cz
Ing. Jan Zeman
Czech Technical University in Prague, Faculty of Civil Engineering, Department of Structural Mechanics, Thákurova 7, 166 29 Prague 6, Czech Republic, Tel:+420-2-24354482, Fax:+420-2-24310775,
e-mail:zemanj@cml.fsv.cvut.cz

4th International Congress
of Croatian Society of Mechanics
September, 18-20, 2003
Bizovac, Croatia

4thICCSM

ADAPTIVE TIME-STEP IMPLICIT METHODS FOR SOLVING CONTACT PROBLEMS IN ROTORDYNAMICS

Roberto Žigulić, Sanjin Braut, Ante Skoblar, Mirko Butković

Keywords: rotordynamics, contact problem, adaptive time step methods

1. Introduction

In the paper the determination of transient nonlinear multidisc rotor response, whirling with slip on the vibrating stator, is shown. Nonlinearities are taken in the mathematical model through the normal contact force, as a function of deformation, deformation velocity as well as contact angle, in the contact point. Some results in using HHT α, WBZ α and generalized α method, for numerical obtaining of response of run-down rotor during the contact with vibrating stator in the dry friction bearings, are given. The numerical stability and accuracy of these methods are compared. Special attention is paid to the possibility of using the adaptive time step calculation. For this purpose different numerical indicators, which detect the ranges where the time-steps have to be reduced or where they may be enlarged, are compared. Also the criteria for the recalculation with the smaller and larger step size are given.

2. Results of Calculations

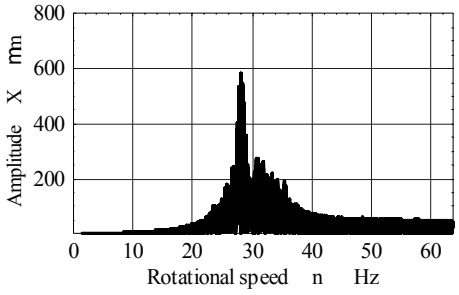

Figure 1. Horizontal displacement, α_f=0.1, α_m=0.08, variable time step, instantaneous dis-

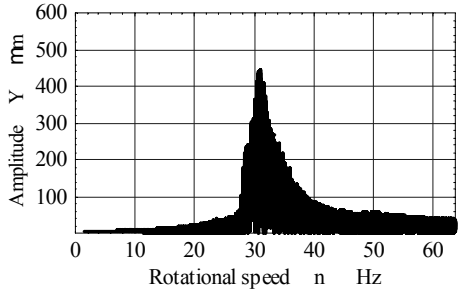

Figure 2. Vertical displacement, α_f=0.1, α_m=0.08, variable time step, instantaneous dis-

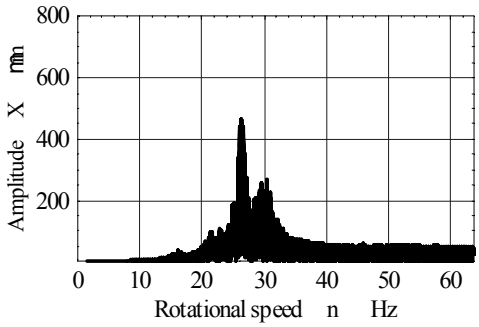

Figure 3. Horizontal displac., α_f=0.1, α_m=0.08, v.t.s., total displacement of a current step

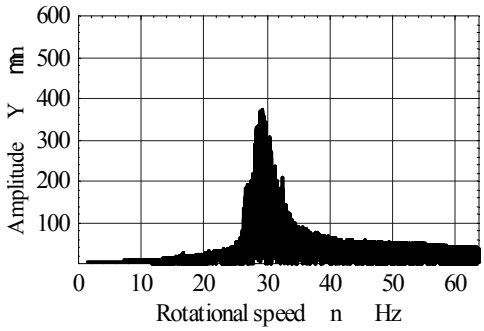

Figure 4. Vertical displac., α_f=0.1, α_m=0.08, v.t.s., total displacement of a current step

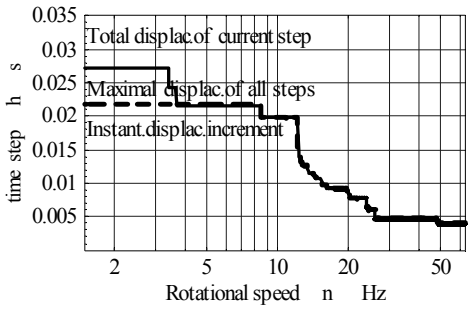

Figure 5. Time steps *h*, variable time step, instan-

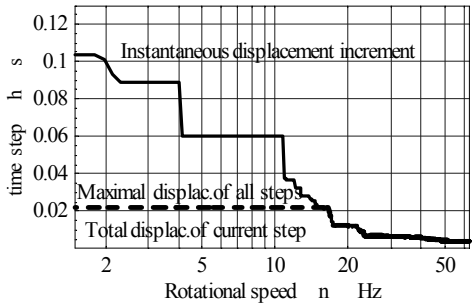

Figure 6. Time steps *h*, v.t.s., total

2. Conclusions

(1) Generalized α method represents a successful tool in solving of nonlinear contact problems of the rotor in the dry friction bearings. This method posses an optimal algorithm for the minimization of low-frequency dissipation while attain the high-frequency dissipation improving the convergence of iterative equation solver. Optimal parameters of generalized α method obtained in the paper, for contact problems of rotor in dry friction bearings, are α_f=0.1 and α_m=0.08.

(2) Adaptive time step procedure reduces computational cost and improves its accuracy. The limit parameters for adaptive time step procedure should be selected very carefully to obtain the accurate and true values of vibrational parameters. The method of a norm of the instantaneous displacement increment gives the best accuracy of the results (identical with the fixed time steps) while the method of total displacement of a current step is something faster but with the lower accuracy. The method of a norm of the maximal displacements of all steps should be avoided. After the passage through the critical speeds, in the area of small displacement magnitudes, different types of reference displacement can be combined. The highest savings in the computational time can be attained if the method of the instantaneous displacement increment is used after the method of a norm of the total displacement of a current step.

References

[1] Žigulić, R., Butković, M., Braut, S., Nonlinear Dynamics of Multi-disc Rotor in Dry Friction Bearings, *Proceedings of Sixth International Conference on Rotor Dynamics*, Sydney, Australia, 30th September-4th October, Vol. II, 960-967,2002

[2] Li, X. D., Zeng, L. F., Wiberg, N. E., A simple local error estimator and an adaptive time-stepping procedure for direct integration method in dynamic analysis, *Communications in Numerical Methods in Engineering*, 9:273-292, 1993

[3] Zienkiewicz, O. C., Xie, Y. M., A simple error estimator and adaptive time-stepping procedure for dynamic analysis, *Earthquake Engineering and Structural Dynamics*, 20, 871-887, 1991

[4] Rapolder, M., Parallele Finite-Element-Simulation der Bauwerk-Boden-Interaktion mit adaptiven Zeitintegrationsverfahren, *Dissertation*, Technische Universitaet Munchen, 2000

Assis. Prof. Roberto Žigulić, Ph. D.
Faculty of Engineering, University of Rijeka, Department of Engineering Mechanics, Vukovarska 58, 51000 Rijeka, Croatia, Tel: 00385 51 651502, Fax: 00385 51 651490, e-mail: zigulic@riteh.hr
Assist. Sanjin Braut, M. Sc.
Faculty of Engineering, University of Rijeka, Department of Engineering Mechanics, Vukovarska 58, 51000 Rijeka, Croatia, Tel: 00385 51 651498, Fax: 00385 51 651490, e-mail: sbraut@riteh.hr
Assist. Ante Skoblar, dipl. ing.
Faculty of Engineering, University of Rijeka, Department of Engineering Mechanics, Vukovarska 58, 51000 Rijeka, Croatia, Tel: 00385 51 651498, Fax: 00385 51 651490, e-mail: askoblar@riteh.hr
Prof. Mirko Butković, Ph. D.
Faculty of Engineering, University of Rijeka, Department of Engineering Mechanics, Vukovarska 58, 51000 Rijeka, Croatia, Tel: 00385 51 651492, Fax: 00385 51 651490,
Polytechnic of Karlovac, Ivana Meštrovića 10, 47000 Karlovac, Croatia,
ALSTOM, Mala Švarča 155, 47000 Karlovac, Croatia, e-mail: butkovic@riteh.hr

AUTHOR INDEX